THE ROLE OF RNA IN THE PACKAGING APOBEC3G INTO HUMAN IMMUNODEFICIENCY VIRUS TYPE 1 PARTICLES

By

Atuhani Seth Burnett

Dissertation

Submitted to the Faculty of the

Graduate School of Vanderbilt University

in partial fulfillment of the requirements

for the degree of

DOCTOR OF PHILOSOPHY

in

Microbiology and Immunology

December, 2007

Nashville, Tennessee

Approved:

Professor Mark R. Denison

Professor H. Earl Ruley

Professor Christopher Aiken

Professor James G. Patton

Professor Paul Spearman

Copyright © 2007 Atuhani Seth Burnett
All Rights Reserved

To my wonderful parents, Austin and Olive Burnett

who gave me everything that I have

taught me the value of hard work

inspired my imagination

then set me free

ACKNOWLEDGMENTS

This work would not have been possible without the financial support of the Vanderbilt Physician Scientist Training Program, and NIH grants R01 AI40338 and R01 AI67101. I would first like to express my deepest gratitude to Paul Spearman for his constant support, wise counsel, and taking the time to invest in my success. He was always kind and patient, treating me with the respect of a colleague. As my teacher and mentor I have come to value his advice highly and I consider it a privilege to have been trained by him. To all the members of the Spearman Lab, I will always be thankful for your friendship and support during my graduate years. In particular, I would like to recognize Jason Hammonds who has become a close friend and an invaluable source of advice. Much of the work found in chapter II could not have been done without his expertise and several experiments were done in collaboration with him. I would like to recognize Aaron Derdowski who has become a reliable friend, and upon whose work chapter II-IV were founded. The techniques that he developed and took the time to personally teach me have become the foundation for everything I have learned afterward. I thank Vasundhara Varthakavi, Xinhong Dong, Hua Li, and Lingmei Ding for teaching me the basics of good science. Your hands on help, many discussions, and your example were exactly what this growing scientist needed.

I would like to give thanks to the faculty, students, and staff of the Department of Microbiology and Immunology, but especially our chairman, Jacek Hawiger, for his energy and dedication to the students of the department. I greatly appreciate the efforts and advice of my thesis committee Mark Denison, Chris Aiken, Earl Ruley, and James

Patton. Their helpful suggestions and excellent scientific discussions have contributed significantly to my solid development as a scientist. I would like to thank the leadership in the Vanderbilt Medical Scientist Training Program for their belief in me particularly past Director David Robertson, and current Director Terence Dermody.

Finally, I would like to thank my family and friends for their love and steadfast support. I would especially like to thank the Leonce family, particularly my grandfather Evrad Leonce, for their support. I would like to thank the Burnett family also for their continued support. Words cannot express my gratitude to my parents, Austin George Burnett and Olive Eleanor Burnett, for their prayers on my behalf, their inexhaustible encouragement of my spirits, and their unqualified confidence in my abilities. I love them deeply and without them, I undoubtedly would have failed, even before beginning. I would like to thank my brother Tatnai for all the great discussions we had about medical research, thanks for keeping me sharp! I thank also my brother Dave and my sisters Tehani and Natasha for their emotional support and solidarity. I would like to give special mention to my aunt, Dr. Jacinta Leavell, who was kind enough to give me a place to live, provided a listening ear and sound advice, and served as a role model at an early stage in my career. I am fortunate to have developed friendships with several wonderful people during graduate school. These include Roy Barco, Sungjune Kim, Alex Stanic, and Kelie Reece for whose friendships I am truly grateful. My success in graduate school is an accomplishment in which many people have played a part and my gratitude extends beyond those whose names are mentioned here.

TABLE OF CONTENTS

Page

LIST OF TABLES

Table **Page**

LIST OF FIGURES

LIST OF ABBREVIATIONS

Å	Angstroms
A/T/G/C	Adenine / Thymine / Guanine / Cytosine
A3G	APOBEC3G
AID	activation-induced cytidine deaminase
AIDS	Aquired Immunodeficiency Syndrome
ALV	Avian Leukosis Virus
AP-3	Adaptor Protein Complex 3
APOBEC3G	Human Apolipoprotein B mRNA-editing enzyme, catalytic polypeptide-like 3G
ARV	AIDS Related Virus
BES	N, N-bis[2-Hydroxyethyl]-2-aminoethanesulfonic acid
BBS	BES buffered saline
CA	Capsid
CCR5	CC chemokine receptor 5
CD4	cluster of differentiation 4
CD8/CTL	cluster of differentiation 8 / Cytotoxic T Lymphocytes
CDC	Centers for Disease Control
Cer	Cerulean (a cyan fluorescent protein)
CMV	Cytomegalovirus
Crm-1	Chromosome Region Maintenance 1
CXCR4	CXC chemokine receptor 4

DNA	deoxyribonucleic acid
ECCDA	E. Coli Cytidine Deaminase
ELISA	enzyme-linked immunosorbent assay
EM	Electron Microscopy
ER	Endoplasmic Reticulum
ESCRT	endosomal sorting complex required for transport
FIV	feline immunodeficiency virus
FRET	Fluorescence Resonance Energy Transfer
Gag	Group specific antigen
GFP/CFP/YFP	Green/Cyan/Yellow Fluorescent Proteins
GRID	Gay Related Immunodeficiency Disease
GST	Glutathione-S-Transferase
HAART	highly active anti-retroviral therapy
HA	hemagglutinin
HBV	Hepatitis B Virus
HIV-1	human immunodeficiency virus type-1
hMPV	human metapneumovirus
HMW	high molecular weight
HTLV-3	Human T-Lymphotropic Virus type III
I domain	Interaction domain
IN	Integrase
kDa	kilodaltons
KS	Kaposi sarcoma

LAV	Lymphadenopathy Associated Virus
LMW	low molecular weight
LTR	Long Terminal Repeats
MA	matrix
MLV	murine leukemia virus
mRNA	Messenger Ribonucleic Acid
MVB	Multivesicular Body
N protein	nucleoprotein of hMPV
NC	nucleocapsid
NES	Nuclear Export Signal
NF-κB	nuclear factor immunoglobulin κ chain enhancer B-cell
NIH	National Institutes of Health
NLS	Nuclear Localization Signal
nm	nanometers
ORF	Open Reading Frame
P bodies	mRNA Processing Bodies
P protein	phosphoprotein of hMPV
PBMC	peripheral blood mononuclear cells
PBS	phosphate-buffered saline
PIC	Pre-Integration Complex
PR	Protease
RFU	Relative Fluorescence Units
siRNA	small interfering RNA

RNA	Ribonucleic Acid
ROI	Region of Interest
RRE	Rev Response Element
RSV	Rous Sarcoma Virus
RT	Reverse Transcriptase
SDS PAGE	Sodium Dodecyl Sulfate Polyacrylamide Gel Electrophoresis
SIV	simian immunodeficiency virus
SU	Surface glycoprotein also gp120
TAR	Trans-activating response region
TCID50	Tissue Culture Infective Dose
TEM	Transmission Electron Microscopy
TM	Trans-Membrane glycoprotein also gp41
Ven	Venus (a yellow fluorescent protein)
VLP	virus-like particle

CHAPTER I

BACKGROUND

Introduction

Human Immunodeficiency Virus Type 1 (HIV-1) infection is the cause of Acquired Immune Deficiency Syndrome (AIDS), a major source of morbidity and mortality worldwide. The ability of HIV to subvert natural human immune defenses has contributed highly to its success in infecting the over 40 million people globally who are currently living with the virus. Even more alarming is that since the discovery of AIDS in 1979, it has claimed the lives of over 30 million people. Fortunately, the development and use of Highly Active Anti-Retroviral Therapy (HAART) has significantly increased the life expectancy for a newly diagnosed HIV-1 patient from 8 years in 1980 to over 20 years in 2005 (62, 122). However, recent statistics demonstrate that efforts to curb the growing AIDS pandemic are only just beginning. In 2005 alone, 5 million people were newly infected with HIV-1 and 3 million deaths were reported. In addition, the number of infected people has been steadily rising with the greatest increases occurring in Sub-Saharan Africa and Asia. Therefore, while some advances have been made in the area of drug development, it is clear from these reports that in many ways, the struggle with HIV-1 is only just beginning (186).

The history surrounding the development of new retroviral inhibitors is a story that highlights the profound and vital role that basic research can play in improving human suffering at the bedside. The HIV-1 protease was first cloned and expressed by

Christine Debouck and colleagues as described in a 1987 basic science communication (45). Based on comparisons with known retroviruses and the results of her experiments, Debouck speculated that her work would pave the way for the development of a new class of anti-retrovirals that inhibited particle maturation and therefore lead to the production of non-infectious, replication deficient virions. The studies published by Debouck and colleagues led to the opening of a new field of research with a flurry of several hundred basic science papers on the subject. Furthermore, these were also followed by the release of the first HIV-1 protease inhibitor, Amprenavir, by Glaxo Wellcome Inc. in 1999. HAART, which involves combined use of combinations of potent HIV-1 inhibitors to prevent the emergence of drug-resistant virus mutants, has since revolutionized the treatment of HIV, and has resulted in greatly enhanced survival for those with access to these valuable medications. Despite this success, drug toxicities and viral resistance often limit the long-term therapeutic success. Additional targets for antiretroviral therapy are therefore being actively investigated. It is within this model of bench-to-bedside science that the studies described in this thesis gain their significance.

Presently, an understanding of the cellular and molecular events occurring during viral protein trafficking, viral RNA trafficking, and particle assembly is unclear. Particularly, the role that viral RNA plays in recruiting cellular retroviral inhibitors, and the extent of viral protein involvement in retroviral genomic RNA trafficking, require further study. Therefore, a detailed understanding of these events at the molecular and cellular level will facilitate the future development of inhibitors to specific steps in the viral life cycle, thus helping to curb the HIV pandemic at the global level.

AIDS History

In 1981, reports started to emerge describing homosexual men in America who were severely immuno-suppressed and therefore could not fight off infections from normally non-pathogenic organisms. These reports also described rare opportunistic infections found only in immunosuppressed individuals such as Pneumocystis carinii pneumonia (86) and Kaposi sarcoma (KS) (57). It was believed at the time that this disease was confined to the homosexual population and therefore given the name Gay Related Immunodeficiency Disease (GRID). Soon, groups of Haitians, intravenous drug users, and hemophiliacs began showing symptoms of the disease. Finally, two years after the first homosexual cases emerged, the Centers for Disease Control (CDC) reported the first case of heterosexual transmission in 1983. As a result the disease was renamed Acquired Immune Deficiency Syndrome or AIDS. While a cluster of symptoms had been assigned this name, the causative agent of this syndrome had not yet been identified (132).

Retroviruses were first suspected as the causative agent of AIDS when three separate laboratories isolated three separate retroviruses from AIDS patients. In 1983 in France, Lymphadenopathy Associated Virus (LAV) was isolated from the lymph node of a patient with AIDS as a collaborative effort between the laboratories of Jean-Claude Chermann and Luc Montagnier (3). In 1984, similar retroviruses were isolated from AIDS patients in the labs of Jay Levy at the University of California San Francisco and Robert Gallo at the National Institutes of Health (NIH). These retroviruses were called Human T-Lymphotropic Virus type III (HTLV-3) by the Levy group and AIDS Related Virus (ARV) by the Gallo group (123, 175). All three viruses were shown to be similar in

virion morphology to other lentiviruses by electron microscopy and were thus renamed Human Immunodeficiency Virus 1 (HIV-1) (97, 125, 160). It is interesting to note that since the discovery of HIV-1, corpses dating as far back as 1959 in China have been discovered to contain the virus (207). This verifies that HIV was circulating in human populations at least 20 years before its official discovery in 1983.

History of Retroviruses

The Retroviridae family of viruses exhibits a unique and fascinating replication strategy that involves converting their RNA genome to a DNA genome using an enzyme called reverse transcriptase (RT). This activity is contrary to all other organisms that use DNA to store genetic information and RNA to transport that information to ribosomes and serve as a template for protein synthesis. As a result, in all other organisms genetic information always flows from DNA to RNA to proteins. Even other RNA viruses use their RNA as a template for protein synthesis and direct RNA genome replication, thus, preserving this central dogma of cellular molecular biology. The name "retro" therefore comes from the fact that during one part of the retroviral life cycle genetic information flows in reverse, from RNA to DNA.

The first retroviruses, discovered in the early 20th century, were Avian Leukosis Virus (ALV) and Rous Sarcoma Virus (RSV). Vilhelm Ellermann and Oluf Bang discovered ALV in 1908 while Peyton Rous discovered RSV in 1911. Both are C type retroviruses discovered because of their ability to cause tumors in chickens. The discovery of these oncoretroviruses led to the development of the oncogene theory of cancer formation which became very important to the field of cancer biology. This theory

states that genes (called oncogenes) within some retroviruses actually cause cells to become cancerous or can influence certain cellular genes (also called oncogenes) to make a cell cancerous. Other retroviruses were discovered, many of which did not cause tumors, but some of which took a long time to cause disease. These "slow" viruses were called lentiviruses and include viruses like Bovine Immunodefficiency Virus (BIV), Simian Immunodefficiency Virus (SIV), Feline Immunodefficiency Virus (FIV), HIV-1 and 2. To date, seven genera of retroviruses have been categorized:

1. Mammalian type B retroviruses, example: mouse mammary tumor virus
2. Mammalian type C retroviruses, example: Moloney murine leukemia virus
3. Avian type C retroviruses, example: Rous sarcoma virus
4. Mammalian type D retroviruses, example: Mason-Pfizer monkey virus
5. HTLV/BLV-type retroviruses, example: human T-cell leukemia virus
6. Lentiviruses, example: human immunodeficiency virus
7. Spumaviruses, example: human foamy virus

Lentiviruses: Properties and Classification

Lentiviruses are a genus of retroviruses that contain three defining features. First, the morphology of the internal virion structure determined by electron microscopy has an unusual cylindrical or cone-shaped core in the mature virus particle. Secondly, they encode several accessory genes that are not present in other retroviral genomes. Lastly, lentiviruses are defined by a biphasic course of viral gene expression. The diseases caused by lentiviruses are characterized by long and variable incubation periods, persistent viral replication, neurological manifestations, and destruction of specific

hematologic or immunologic cells (49). HIVs and SIVs comprise the primate lentiviruses. They are all closely related, encode six accessory genes (*tat*, *rev*, *nef*, *vpr*, *vif*, and *vpu*, or *vpx* depicted in Figure 2A), and infect cells using CD4 as the primary cell surface receptor. HIV-2 is less prevalent than HIV-1 and is found predominantly in Guinea Bissau, Ivory Coast, and Senegal. There are two major subgroups of HIV-1; group M or main group and group O or outgroup with SIVcpz (chimpanzee) viruses clustering midway between them. Group O is rare and originally found only in Camaroon, Gabon, and France. Group M, however, is responsible for most HIV-1 cases and eight clades have been found (A through H) that cluster by geographic region. For instance, clade B is most prevalent in North America and Europe, clade E is common in northern Thailand, while a variety of clades is found in Africa. As a result, the majority of scientific studies of HIV utilize HIV-1 as the most clinically relevant virus (35).

HIV-1 Pathogenesis

HIV-1 is transmitted by sexual contact, by blood products, or vertically from mother to infant. Free and cell-associated virus is found in semen, vaginal fluids, blood, and breast milk (64). Infection follows three phases: Acute infection, clinical latency, and AIDS. The typical course of HIV infection is depicted in figure 1, which was modified from Pantaleo et al. 1993 (152). HIV infects hematopoietic cells expressing the viral receptor, CD4 (42). Initial engagement of the viral attachment glycoprotein, gp120, to the CD4 receptor is followed by a second interaction with one of two co-receptors, CCR5 or CXCR4 (2, 28, 46, 56, 66). Infection initiates the acute phase which is characterized by an acute mononucleosis-like illness which lasts for 3-6 weeks (184). An intense burst of

viremia, accompanied by a drop in CD4+ cells, peaks at 6 weeks post infection (30, 40, 77). Around this same 3-6 week period post-infection, antiviral immune responses can be detected that coincide with the ensuing decline in viremia and illness (103). This antiviral response is in the form of HIV-specific CD8+ cytolytic T lymphocytes (CTL) (116). Ten weeks post infection, antiviral cell mediated immune responses peak resulting in resolution of viremia and a partial rebound in CD4+ cells (116). The asymptomatic phase of the disease is referred to as clinical latency. Clinical latency lasts approximately 8 years but can be prolonged to over 20 years with HAART, cocktails containing combinations antiretroviral agents (62, 122). This stage of disease is characterized by persistent viral replication held in tight control by the immune system (32). During clinical latency several hundred rounds of viral replication, immunological pressure, and generation of escape mutants result in an increasingly heterogeneous population of viruses (32, 91). Acquired immunodeficiency syndrome (AIDS) is the last stage of HIV pathogenesis. AIDS commences when CD4+ T helper cell counts drop below 200 cells/mm^3 of blood and viremia begins to rise. Progressive AIDS disease is associated with a dramatic deterioration of clinical outlook including the acquisition of opportunistic diseases, malignancies, and disruption of lymphoid architecture. The death of massive numbers of lymphoid cells results in an inability to combat opportunistic pathogens. The patient then succumbs to these infections resulting in death (152, 184).

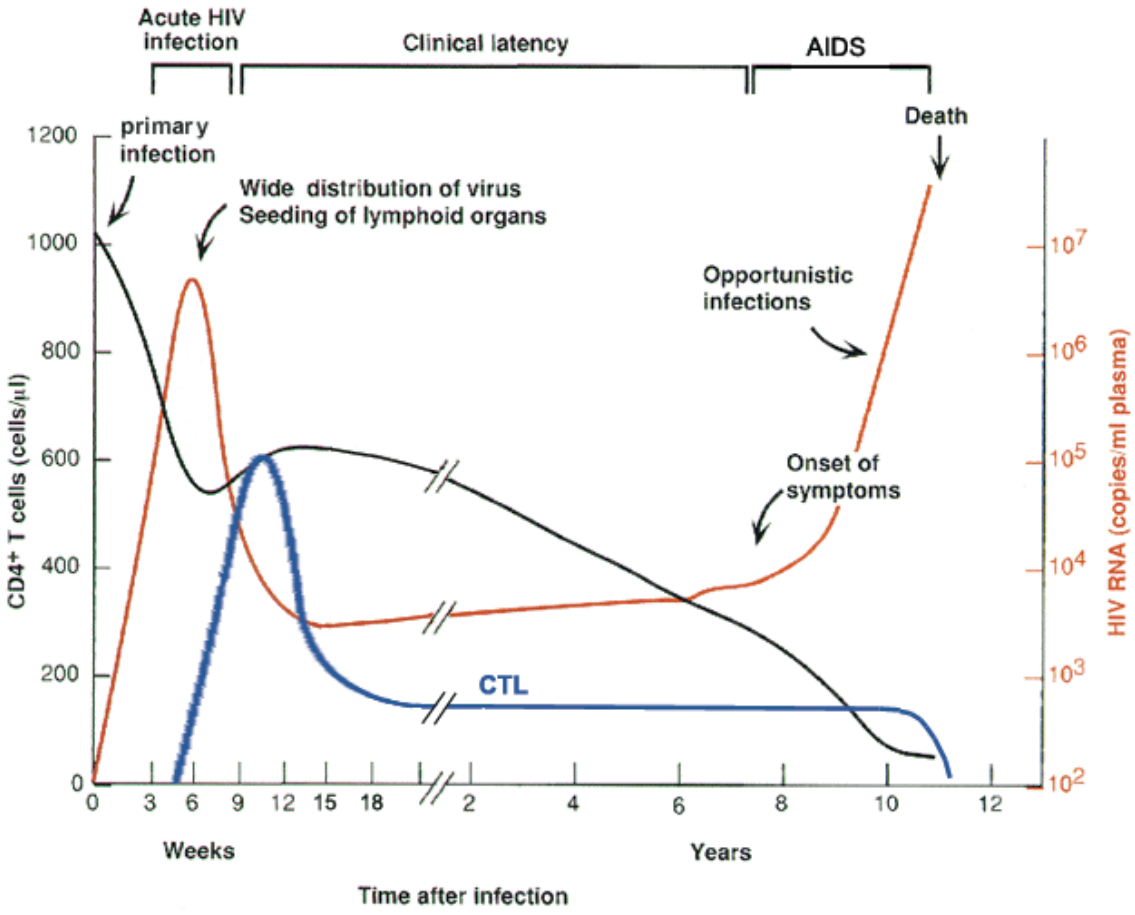

Figure 1. Typical course of HIV infection. Time courses of CD4+ T-cell counts (black line), viremia (red line), and cytotoxic T-cell (CTL) counts (blue line) during HIV infection and disease progression. Modified from Pantaleo et al. 1993.

Retroviruses and HIV-1: Structure and Genetic Organization

All retroviral genomes are flanked by non-coding sequences called Long Terminal Repeats (LTR). LTR sequences contain promoter elements, packaging signals, and transcription enhancement elements, which are critical to the process of reverse transcription and are thus essential to the virus life cycle. In addition, all retroviruses contain four essential genes *gag*, *pro*, *pol*, and *env* (Figure 2A). These genes encode multiple proteins on a single polypeptide chain: Pr55Gag (Figure 2B), Pr160Gag-Pro-Pol (Figure 2C), and gPr160Env (Figure 2D). Individual proteins are generated from each polypeptide following proteolytic cleavage by the viral protease in the case of Gag and Gag-Pro-Pol, or by cellular furin proteases in the case of Env (72, 88, 95, 143). Simple retroviruses require only these four genes to replicate, while complex retroviruses like HIV-1 contain additional assessory genes designated *tat*, *rev*, *nef*, *vpr*, *vif*, and *vpu*. These contribute to defending the virus against host proteins and the host immune system (Figure 2A).

Retroviruses are spherical particles approximately 100 nm in diameter (31, 33, 34). The surface of retroviral particles are covered with a phospholipid bilayer derived from the plasma membrane of the cell from which they were produced (34, 39). As a result, the viral membrane contains cellular membrane proteins such as cellular adhesion molecules (22, 112, 137). In addition, and perhaps more importantly, the viral membrane contains the viral attachment and entry glycosylated proteins which are encoded by the *env* gene. These *env* gene products are termed gp120 (SU) and gp41 (TM) for HIV (Figure 2D). Directly underneath the membrane, the viral Matrix (MA) protein forms a protein shell. Inside this MA shell resides the core, constructed from the Capsid (CA)

Figure 2. HIV-1 genes, proteins, and structure. A. Diagram depicting the HIV-1 genome and open reading frames (ORFs). Essential genes are depicted in white while assessory genes are in gray. B. Schematic depicting the 55 kDa Gag precursor gene product (Pr55 Gag). Cleavage products Matrix (p17 MA, green), Capsid (p24 CA, gray), Spacer Peptide 1 (p2 SP1, white), Nucleocapsid (p7 NC, yellow), Spacer Peptide 2 (p1 SP2, white) and p6 (p6, light blue). The N-terminal Interaction "I" domain is labeled in NC. C. Schematic depicting the 160 kDa Gag-Pro-Pol precursor gene product (Pr160 Gag-Pro-Pol). Cleavage products Protease (p10 PR, red), Reverse Transcriptase (p66/p51 RT, dark blue), Integrase (p32 IN, aqua blue). D. Schematic depicting the glycosylated 160 kDa Env precursor gene product (gPr160 Env). Cleavage products Surface protein (gp120 SU, orange), and Trans-Membrane protein (gp41 TM, gold). E. Schematic depicting the mature HIV-1 virus particle. The location of the proteins described above are depicted. Also depicted are the location of the viral membrane (lipid bilayer) and RNA genome.

A.

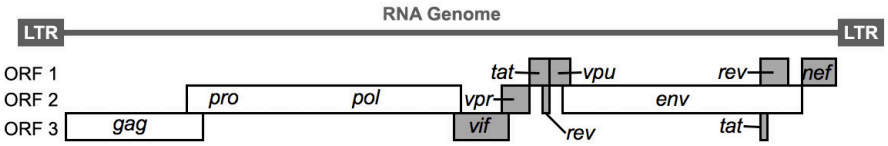
RNA Genome
LTR
LTR
ORF 1
ORF 2
ORF 3
gag
pro
pol
vif
vpr
tat
rev
vpu
env
rev
tat
nef

B.

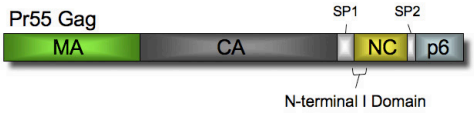
Pr55 Gag
SP1
SP2
MA
CA
NC
p6
N-terminal I Domain

C.


Pr160 Gag-Pro-Pol
PR
RT
IN

D.


gPr160 Env
SU (gp120)
TM (gp41)

E.

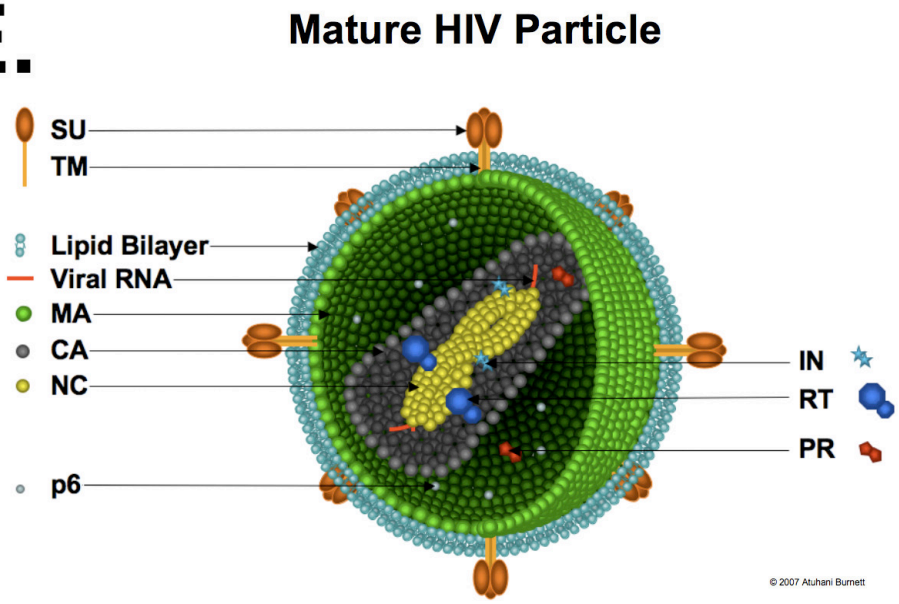
Mature HIV Particle
SU
TM
Lipid Bilayer
Viral RNA
MA
CA
NC
p6
IN
RT
PR
© 2007 Atuhani Burnett

protein, and which contains the genomic RNA of the virus in complex with the Nucleocapsid (NC) protein as depicted in Figure 2E. MA, CA, and NC are *gag* gene products (Figure 2B). The viral core also contains the enzymes Reverse Transcriptase (RT) and Integrase (IN), which are *pol* gene products that aide the virus in inserting its genetic material into the host cell genome (35).

The shape or morphology of a retrovirus' core is a distinctive feature that is clearly visible upon examination of a virus by electron microscopy (EM). There are four main types of mature virus particle morphologies, designated Type B, C, D, and lentivirus. Although there are four different morphologies there are only two main assembly patterns. Type C viruses and lentiviruses assemble and bud at the plasma membrane and exhibit cylindrical and conical mature core morphologies, respectively (Figure 4B) (34). Type B and D viruses first assemble in the cell cytoplasm as immature type A particles that lack a membrane. Type A particles then traffic to plasma membrane where they acquire a membrane during the budding process as they exit the cell and mature. The resulting mature core structures are spherical in shape and either eccentrically stuck to one side of the viral membrane (Type B particles) or centrally located in the virus (Type D particles). These designations are important because core morphology by transmission electron microscopy (TEM) has been used historically to classify retroviruses.

HIV-1 Life Cycle and Particle Assembly

All steps in the retroviral life cycle can be divided into two stages, early and late, as depicted in Figure 3 (71). The early stage spans the time between attachment of the virus

particle to the cell, and integration of the viral DNA into the host genome. The late stage begins with viral gene expression and culminates with assembly, budding, and particle maturation. Therefore, the viral life cycle begins with attachment of the virus to cell membranes. While this step has traditionally been thought to occur using the gp120 Env attachment protein of the virus, recent studies have provided evidence that initial contact between the virus and the host cell involves non-gp120-mediated interactions between cell adhesion molecules on both the viral and cellular membranes (92). Specifically, these studies show that neutralizing antibodies raised against gp120 attachment protein of the virus do not prevent viral attachment but instead neutralize viral infectivity by preventing membrane fusion. After approximately 20 minutes of attachment, the viral envelope protein gp120 locates and engages the viral receptor CD4 (92).

The interaction of gp120 with CD4 initiates the early phase of the viral life cycle. CD4-gp120 attachment results in conformational changes that allow gp120 to bind one of two co-receptors, CCR5 or CXCR4 (2, 28, 46, 56, 66). After receptor attachment, the transmembrane protein gp41 is responsible for causing the fusion of the viral membrane with the cellular membrane, resulting in the viral core being released into the cell cytoplasm. The core then disassembles, losing the capsid shell in a process referred to as uncoating. The uncoating process produces a high molecular weight complex containing the viral genome referred to as the Pre-Integration Complex (PIC) (13, 17, 59, 63). During the uncoating process the virus also begins to convert its single stranded RNA genome into double stranded DNA in a synthesis reaction called reverse transcription. In this process, the viral RT enzyme first uses the RNA coding strand, or plus (+) strand, of the viral genome to synthesize a complementary DNA minus (-) strand, creating an

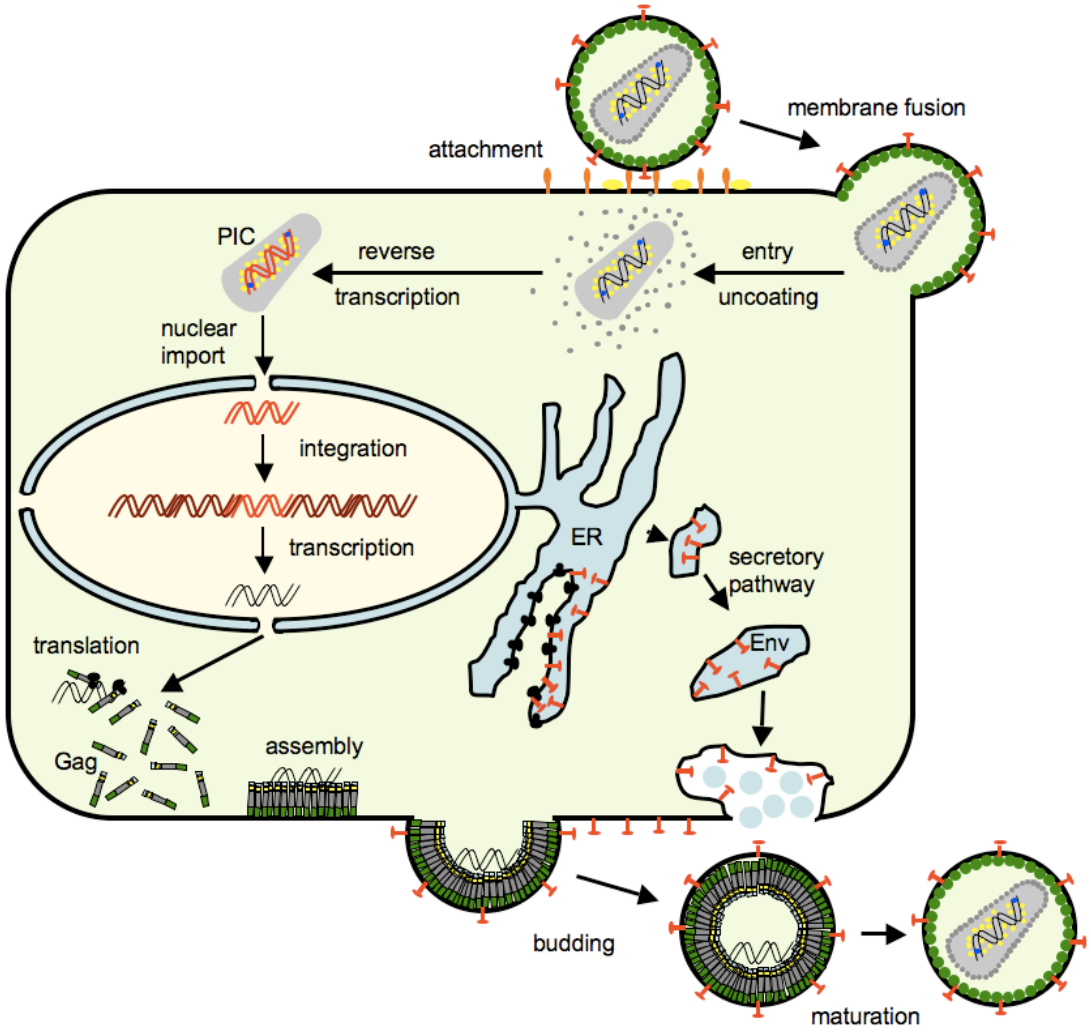

Figure 3. Retroviral life cycle. Early Phase. Attachment of gp120 with the CD4 receptor and CCR5/CXCR4 co-receptors leads to virus/cell membrane fusion. After entry of the core into the cytoplasm most of CA is lost during uncoating. Reverse transcription converts the viral RNA genome into a DNA provirus resulting in the creation of the Pre-Integration Complex (PIC) that enters the nucleus and integrates provirus into host genomic DNA. Late Phase. Viral mRNA transcribed producing viral proteins. Gag is made in the cytoplasm and traffics to the plasma membrane through a largely unknown route. Env is made in the endoplasmic reticulum (ER) and traffics to the plasma membrane through the secretory pathway. Particles assemble at the plasma membrane, bud off, and release from the cell as immature non-infectious particles. Proteolytic cleavage of Gag and Gag-Pro-Pol results in maturation and the rearrangement of the internal structure of the particle, which is now infectious.

RNA-DNA hybrid molecule. RT then degrades the RNA portion of this hybrid leaving an exposed single stranded DNA(-) molecule. Finally, the RT enzyme catalyzes the synthesis of the complemantary DNA(+) strand using the minus (-) strand as a template (35). It is important to note that this process creates a replication intermediate where the viral genome exists as a single stranded DNA molecule, thus making it susceptible to mutation by the viral restriction factor APOBEC3G. In the final steps of the early phase of virus replication, the PIC is transported into the nucleus where it integrates into the host genome, facilitated by the integrase (IN) enzyme. Once the virus has become part of the host cell genome, it is impossible to extricate and is called a provirus. The provirus then produces viral RNAs and proteins leading to events of the late phase of virus replication.

Late events of viral replication begin with the expression of viral RNA from the nucleus. The two main viral structural proteins, Gag and Env, utilize distinct mechanisms for expression and trafficking to the plasma membrane. These disparate mechanisms reflect the fact that Env is a transmembrane protein whose outer domain is on the external surface of the virus, while Gag is associated with the inner leaflet of the viral membrane. Therefore, Env is synthesized in the endoplasmic reticulum (ER) where it is inserted into the ER membrane with the external portions of the protein residing in the lumen of the ER (70). Env then traffics to the plasma membrane in vesicles of the secretory pathway where cellular furin proteases cleave it into the transmembrane gp41 and external gp120 fragments during transit (95, 143). Fusion of secretory vesicles with the plasma membrane allows luminal protein domains, such as the gp120 portion of Env, to reside on the external surface of the plasma membrane, while simultaneously allowing the release

of luminal contents into the extracellular media (Figure 3). In contrast, Gag is synthesized on free cytoplasmic ribosomes from genomic full-length mRNA. Gag molecules multimerize, attach to the cytoplasmic face of cellular membranes, and traffic to the plasma membrane using cellular protein trafficking pathways (70). Gag proteins are cotranslationally modified by the addition of myristic acid on the amino terminal glycine residue, following removal of the initiator methionine (101, 171, 194). This myristate modification is required for plasma membrane binding of Gag and particle formation (18, 107). Gag-Pro-Pol molecules, synthesized from the same mRNA as Gag, are the result of a -1 frame shift mutation which circumvents the *gag* stop codon and allows the ribosome to read through *pro* and *pol*. This event occurs when a ribosome that is near the end of the *gag* gene slips backward one base. It then begins to read the *pro* sequence that overlaps with the end of *gag* but exists in an alternate reading frame, producing the Gag-Pro-Pol fusion protein. The frame shift strategy is a way for the virus to package a reduced amount of Pro and Pol compared with Gag (1:20) (105), while using the same trafficking and targeting mechanisms to sites of assembly.

The exact pathway that Gag follows on its way to the plasma membrane remains largely unknown. However, recent studies from our lab showed that Gag trafficking relies heavily on cellular machinery. For example, en route to the plasma membrane, Gag traffics through the multivesicular body (MVB) which is a late endosomal compartment using the cellular adaptor protein complex 3 (AP-3) (53). In addition, the NC domain of the Gag protein specifically binds to and recruits the genomic mRNA into virus particles, however, it is unclear where and when this interaction occurs and therefore what particular role Gag plays in genomic RNA trafficking to sites of assembly. Finally, Gag

and Env meet at the plasma membrane where particles are formed. Immature particles then require cleavage of Gag by HIV protease to become infectious. The HIV-1 life cycle is depicted in Figure 3.

Gag Trafficking and Assembly Domains

During virus particle budding, Gag induces plasma membrane curvature, and cellular machinery is used to seal and release immature and non-infectious viral particles (Figure 4C) (80, 187). Immature retroviral particles contain all of the structural proteins of the virus in the precursor form (Pr55 Gag, Pr160 Gag-Pro-Pol) stuck to the underside of the viral membrane (10, 81, 85, 140). Examination of immature particles by Transmission Electron Microscopy (TEM) shows the electron dense protein material in the immature particle as a dark circle just inside the limiting membrane of the virus (Figure 4A) (53). During or after particle release, the HIV-1 protease cleaves Gag into MA, CA, spacer peptide 1 (p2), NC, spacer peptide 2 (p1), and p6 proteins. These products reassemble into the mature infectious particle exhibiting the distinctive lentivirus core structure (Figure 4B) (53, 87).

The HIV-1 Gag protein is responsible for directing the production and assembly of retroviral particles (71). Therefore, the expression of Gag alone in cell culture is sufficient to produce non-infectious virus-like particles of normal density (84). This process is depicted in figure 4D and is identical to HIV-1 budding, except this occurs in the absence of other HIV-1 gene products or RNA. To accomplish this, Gag molecules contain distinct functional domains that carry out essential tasks in the HIV-1 assembly process. These include the M domain in MA, the N-terminal and C-terminal CA domains,

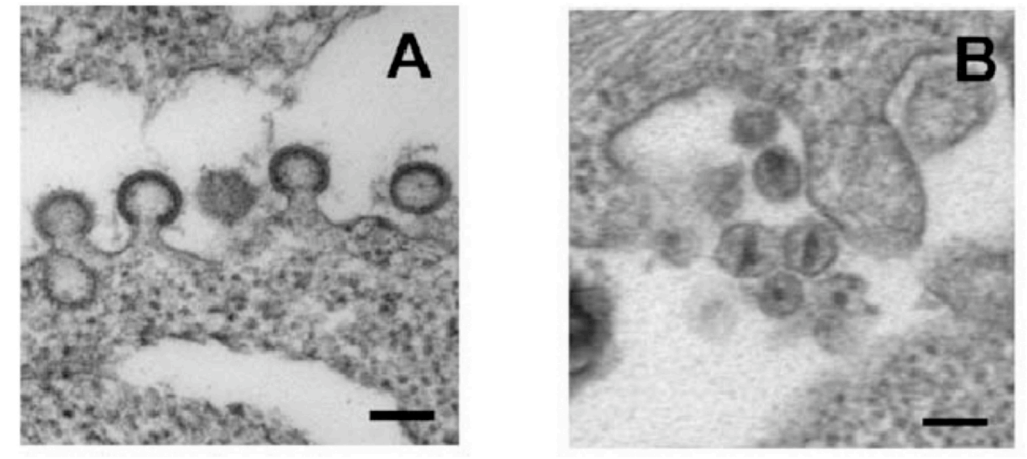

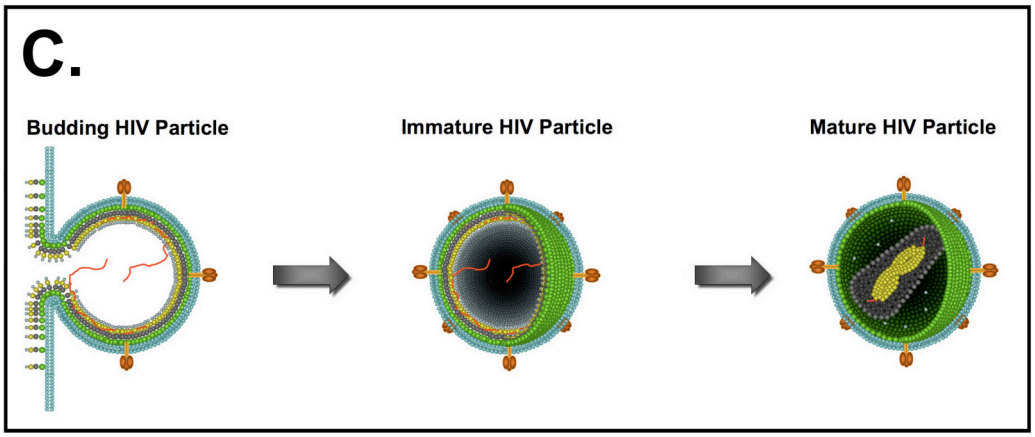

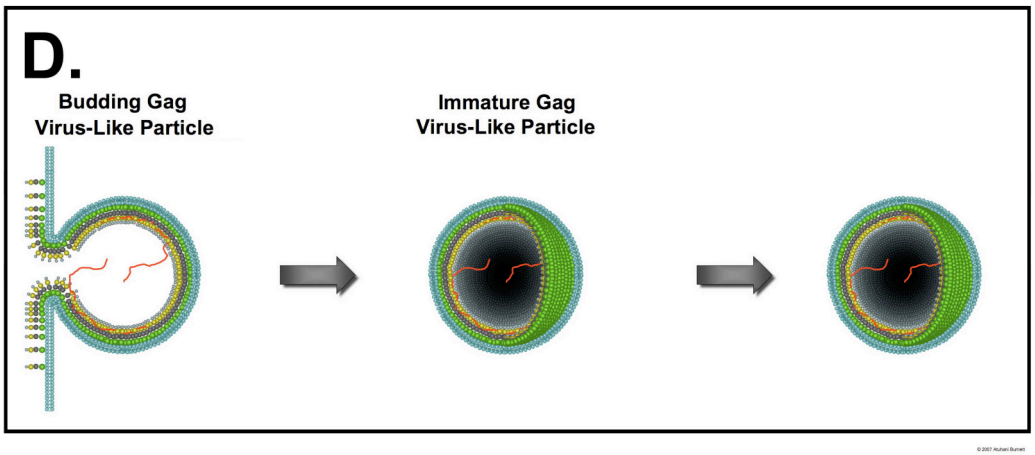

Figure 4. Stages in particle budding. A. Electron micrographs of HIV-1 budding and immature viral particles. B. Electron micrographs of mature HIV-1 viral particles. A-B adapted from Dong et al. 2006. C. Schematic diagram of HIV-1 budding and maturation. D. Schematic diagram of Gag virus-like particle budding.

the I domain in NC, and the L domain in p6. The M domain causes the localization of Gag to the plasma membrane through the insertion of myristic acid into the lipid by-layer and the interaction of basic matrix residues with the negatively charged membrane (206). Both interactions are necessary for efficient plasma membrane localization of Gag (179). The C-terminal domain (CTD) of CA contains sequences necessary for CA dimerization, Gag-Gag interactions, and particle assembly (168, 189). The CTD also contains a 20 amino acid region called the major homology region (MHR) that is highly conserved among retroviruses, however, the function of the MHR remains largely unknown (195). The I domain region within NC promotes Gag-Gag interaction (19). This region is also critical for Gag-membrane binding and proper retroviral particle density (164, 165). The assembly functions of the I domain are widely thought to work via the RNA binding properties of basic residues located in the N-terminal region of NC. The L domain is responsible for enabling the final separation of the budding viral particle from the cell by recruiting the Tsg101 protein which is a member of the vacuolar protein sorting pathway (80). Tsg101 recruits associated Endosomal Sorting Complexes Required for Transport (ESCRT) to sites of budding by binding to the PTAP motif located in the p6 region of Gag (187).

Viral RNA Trafficking

Retroviral mRNA synthesis requires host cell transcription machinery and transcription factors that bind promoter elements within the 5' LTR. The host RNA polymerase II complex and associated complexes perform basal transcription of HIV-1 RNA by binding to the TATA box region upstream of the Gag ATG start site. The

cellular transcription factors NF-κB and Sp-1 are the major promoters of viral RNA synthesis (155). NF-κB is significant because it is used by host immune cells during activation, thereby stimulating HIV-1 replication during immune cell activation. Host cell splicing of HIV-1 mRNA produces the early gene products *tat*, *rev*, and *nef*. The HIV-1 Tat protein binds to a stem loop structure known as TAR located with the first 59 RNA bases synthesized by the RNA polymerase II (99, 144, 163). This binding event promotes the elongation of HIV-1 RNA by hundreds to thousands of fold, thereby increasing early gene protein expression (44, 68). Once sufficient Rev protein accumulates, it is transported back into the nucleus and binds to a highly structured group of RNA stem-loops within the *env* gene referred to as the Rev Response Element (RRE) (115, 129, 201). The nuclear export factor Crm1 then binds to the Rev Nuclear Export Signal (NES) (9), causing the export of singly spliced and unspliced genomic mRNA, and increasing the expression of the HIV-1 late genes *vpu*, *env*, *vpr*, *vif*, *gag*, *pol* (198). Viral genomic RNA is recruited into virus particles through a specific interaction between the NC region of the Gag protein and the Psi (ψ) packaging signal, an RNA stem-loop structure located immediately upstream of the Gag ATG start site. However, little is known about how Gag locates the genomic RNA in the cell, and the site in the cell where this interaction takes places. The focus of Chapter V is the development of a robust method of labeling HIV-1 genomic RNA with fluorescent markers that will allow us to track its trafficking in live cells. The co-expression of fluorescent Gag molecules will then allow us to answer these important questions.

Cytidine Deaminases and APOBEC3G

APOBEC3G (A3G) belongs to the larger super-family of proteins called cytidine deaminases. This group of proteins contains several other well known proteins, including 1) E. Coli Cytidine Deaminase (ECCDA), the prototypic cytidine deaminase whose crystal structure is still used to predict the present structures of mammalian cytidine deaminases (8, 147), 2) human apolipoprotein B mRNA editing cytidine deaminase subunit 1 (APOBEC1), which deaminates ApoB mRNA to create a stop codon and thus regulates the differential expression of ApoB-100 to ApoB-48 (73, 120), and 3) activation-induced cytidine deaminase (AID) which produces somatic hypermutations in B lymphocytes by mutating the DNA that codes for B cell receptor proteins (145). Each of these enzymes replace the primary amine group of cytosine with a double-bonded oxygen, thus converting cytidine to uridine (89). Structurally, cytidine deaminases contain zinc finger domains that bind to DNA or RNA (26, 94). Based upon several crystal structures, coimmunoprecipitation assays, and yeast two-hybrid experiments, these cytidine deaminases have been shown to dimerize around nucleic acids in a head-to-tail fashion with their active sites opposing one another (147). It is therefore not surprising to find that A3G also forms dimeric or multimeric complexes in the presence of RNA (110, 193).

The cytidine deaminase A3G inhibits the replication of retroviruses including HIV, simian immunodeficiency virus (SIV_{mac}), murine leukemia virus (MLV), (98, 131, 176, 199), retrotransposons (180) and other viruses which undergo a reverse transcription step such as Hepatitis B Virus (HBV) (185). Insights into the mechanisms allowing A3G to accomplish this task can be gained by first considering some of its biochemical and

localization properties. A3G is expressed in peripheral blood leukocytes, spleen, testes and to a lower extent in the ovaries (110). It is a cytoplasmic protein that only hypermutates the single stranded DNA (ssDNA) of viruses that contain a cytoplasmic ssDNA intermediate (106). Therefore, cellular DNA is protected from attack by A3G, as it is double stranded and contained within the nucleus. However, retrovirus ssDNA is very susceptible to hypermutation provided A3G can obtain access to it during reverse transcription. This can happen if A3G, which can bind to both ssRNA and ssDNA (106), is packaged into virus particles in complex with the genomic RNA. A3G would then be in a position to attack ssDNA intermediates during the process of reverse transcription.

A3G becomes incorporated into retroviral particles as they exit an infected cell. Upon infection of a target cell by these particles and the initiation of reverse transcription, the incorporated A3G causes extensive deamination of cytidines on the exposed cDNA minus strand created during the reverse transcription process. This results in extensive and lethal G to A nucleotide substitutions in the proviral DNA (98, 121, 131, 204). For reasons not completely understood, APOBEC3G expressed in the cytoplasm of HIV target cells is unable to gain access to reverse transcription ssDNA intermediates. Thus, a critical aspect of the antiviral function of APOBEC3G is its ability to be packaged into assembling virions (113, 133, 177). As a result, the major focus of experiments in this thesis involves determining the precise mechanism by which APOBEC3G is packaged into virus particles. When I initiated these studies, it was known that APOBEC3G is packaged into particles in a NC dependent manner (124, 202). However, it was unclear whether RNA molecules were critical for APOBEC3G packaging. The experiments in Chapter II were designed to address this question.

The Viral Infectivity Factor and APOBEC3G

HIV-1 expresses a 23 kDa basic protein late in the replication cycle called Viral Infectivity Factor or Vif (78, 79, 173). Vif neutralizes A3G through a mechanism that ultimately leads to the exclusion of A3G from viral particles (113). Vif binds to both A3G and members of the cullin-ubiquitin ligase complex. These members, including Cullin5, Elongin B, Elongin C, and the RING protein Rbx, induce polyubiquitination of A3G leading to its degradation by the ubiquitin proteasome pathway (36, 65, 200). Elimination of cellular A3G by this mechanism prevents virion incorporation and thereby eliminates the antiviral activity of A3G. As a result, Vif is critical for producing infectious virus particles in APOBEC3G expressing cells referred to as non-permissive; these include primary cells and certain cell lines such as the H9 and CEM T cells (11, 37, 61, 74, 75, 178, 188). In contrast, permissive cell lines such as HeLa, HEK 293T, Jurkat T cells, and SupT1 T cells do not express A3G, therefore, HIV produced in these cells is infectious regardless of Vif expression (176).

Research Objectives

A3G is an RNA binding protein that is packaged into virus particles through its interaction with the NC region of Gag. Therefore, Gag-associated RNA may play a central role in facilitating APOBEC3G packaging into virus particles. This suggests that genomic RNA trafficking may play an important role in the assembly of retroviral particles. The overall goal of my research was to understand the molecular events surrounding APOBEC3G and retroviral RNA trafficking to the plasma membrane and

packaging into virus particles. To achieve this broad goal, experiments were performed according to the following four Specific Aims:

Specific Aim 1. ***To define the requirements for APOBEC3G packaging into virions.***

The I domain of Gag is an N-terminal region of the nucleocapsid, which is known to bind RNA, and is also known to contribute assembly functions to the Gag protein. Due to the fact that both A3G and NC are RNA binding proteins, I hypothesized that RNA is required for A3G interactions with the I domain of Gag. To this end, I tested a series of mutant Gag constructs spanning the I domain to determine if quantitative I domain function correlates with A3G packaging in Gag virus-like particles (VLPs). I also used membrane flotation studies to determine if I domain function correlated with the association of A3G to cellular membranes. Finally, I assessed RNA involvement by using Gag-GST pull down studies, and by comparing RNA and A3G levels in VLPs. The studies in specific Aim 1 contribute important information to the role of RNA in both I domain function and A3G packaging.

Specific Aim 2. ***To determine if RNA dependent A3G multimers are packaged into virus particles.***

The hypothesis tested in Aim 2 was that A3G exists in RNA containing complexes, and that Gag recruits these complexes into VLPs through RNA binding. FRET fluorometry has been used previously to detect Gag-Gag interactions. Therefore, in order to assess the first part of this hypothesis, I used this technique to determine if A3G complexes are RNAse sensitive which would prove that RNA is an integral component of these complexes. To address the second part of the hypothesis, determining if VLP

associated A3G is packaged as a monomer or a complex, FRET studies were used to assess whether A3G complexes are a component of VLPs. In addition, I subsequently examined if A3G complexes are packaged through Gag binding directly to the A3G or by Gag binding to the RNA in these complexes. To this end, I used FRET to analyze whether a direct Gag-A3G interaction could be detected in VLPs. These studies provide a mechanistic insight into the structural relationship between Gag, A3G, and RNA molecules involved in virus particle assembly. It was discovered that A3G was packaged into virus particles as homo-multimeric complexes known to contain RNA without a direct interaction between A3G and Gag.

Specific Aim 3. ***To define the subcellular localization of A3G-RNA complexes.***

Virus particle assembly occurs at the plasma membrane. Therefore, A3G molecules should traffic through this location in order to be packaged into VLPs. Fluorescent microscopic analysis using deconvolution techniques were used to evaluate the localization of A3G to the plasma membrane during particle assembly. The location of A3G interaction in cells was determined by confocal spectral analysis of A3G FRET using the acceptor photobleach method. While this assay was sufficient to assess A3G interactions in discrete cellular locations, a novel live cell FRET microscopy technique was developed to determine the overall subcellular localization of A3G complexes during particle assembly. These studies support the model developed in previous specific aims by showing the recruitment of A3G multimeric complexes to the plasma membrane by Gag for ultimate packaging into particles through a Gag-RNA interaction.

Specific Aim 4. ***Development of a system to track retroviral genomic RNA during trafficking and assembly.***

The trafficking of HIV-1 genomic RNA from the nucleus to the plasma membrane, where assembly occurs, is critical to the formation of infectious virus particles. The fourth specific aim involves the development of reagents necessary to observe this movement. Strategies included the creation of MS2-fluorescent proteins for RNA labeling, and the generation of reporter RNA by the engineering of MS2 binding sites into proviral expression constructs and over-expression constructs. I used fluorescent microscopy to determine that the reporter RNAs, containing MS2 binding sites, caused export of the MS2-fluorescent tags into the cytoplasm. The results presented in this Specific Aim form the foundation for future studies on retroviral RNA trafficking.

CHAPTER II

IMPORTANCE OF THE NUCLEOCAPSID BASIC LINKER FOR PACKAGING OF APOBEC3G INTO HIV-1 GAG VIRUS-LIKE PARTICLES

Introduction

The HIV-1 Gag protein is responsible for facilitating APOBEC3G incorporation into virions as evidenced by the fact that Gag virus-like particles (VLPs) efficiently incorporate APOBEC3G (55, 182, 202). In addition, *in vitro* binding experiments have shown that APOBEC3G binds efficiently to the nucleocapsid (NC) region of the Gag polyprotein (1, 24, 124, 169, 182, 202). Finally, Gag constructs in which a leucine zipper protein-protein interaction domain replaced the nucleocapsid region produced particles devoid of APOBEC3G (124, 202). When my studies were launched, the precise mechanism by which NC recruits APOBEC3G was unclear. In particular, the role played by RNA and distinct RNA binding regions within NC was controversial. *In vitro* binding experiments between NC and APOBEC3G that utilize RNA depletion by RNAse A treatment have been reported which support (124, 169, 182, 202) or refute (1, 24) the role that an RNA bridge may play in this interaction.

An essential retroviral assembly function is contained within the N-terminal region of nucleocapsid (6, 14, 191). This region, termed the interaction domain ("I" domain), is necessary for Gag-Gag multimerization, the formation of detergent-resistant Gag complexes, plasma membrane localization of Gag, and the formation of normal density retroviral particles (47, 164, 165). The I domain has been implicated in mediating RNA binding to NC through electrostatic interactions of basic residues with cellular or

viral RNA. Furthermore, in experiments using C-terminal NC truncations of Gag, the I domain phenotype correlated with the number of basic residues expressed (164). Therefore, it seemed reasonable to hypothesize that APOBEC3G incorporation might be linked to the assembly functions associated with the I domain.

In the studies described in this Chapter, I examined the requirements for APOBEC3G incorporation into HIV virus-like particles (VLPs). Surprisingly, I found that APOBEC3G incorporation did not correlate closely with the presence of the I domain. Rather, mapping of APOBEC3G incorporation and RNA revealed a key role for the basic linker region of Gag, located between the two zinc finger domains of NC. The amount of RNA incorporated into particles did correlate, however, with APOBEC3G recruitment to the plasma membrane and packaging into particles. Thus, taken together we conclude that the basic linker region in NC is essential for RNA-dependent APOBEC3G recruitment into virus particles.

Materials and Methods

Plasmid construction

This study employed Gag and APOBEC3G expression constructs fused to variants of the codon-optimized version of CFP and YFP (Clonetech, Palo Alto, CA). Some of the CFP and YFP expression vectors, and several of the Gag expression constructs were previously described (47). Briefly, the C-terminal CFP and YFP expression constructs were created by first replacing the EGFP gene in pEGFP-N3 (Clontech) with either the CFP gene from pECFP-N1 or the YFP gene from pEYFP-N1.

These new constructs were designated pECFP-N3 and pEYFP-N3, respectively (47). The N-terminal YFP expression construct was produced by replacing the EGFP gene in pEGFP-C1 (Clontech) with the YFP gene from pEYFP using an AgeI site located 5' to the ATG start site in both plasmids and a BsrGI site located in the 3' end of both genes prior to the stop codon. This new construct was designated pEYFP-C1. The Gag coding sequences for all constructs were derived from the codon-optimized version of HXB2 Gag in expression plasmid pVRC3900 (104). PCR cloning was then used to amplify the *gag* gene from the pVRC3900 vector, with a HindIII site at the 5' ATG and a BamHI site at the 3' end. The amplified *gag* gene was then ligated into both pEYFP-N3 and pECFP-N3 by digestion of the BamHI and HindIII sites located within the multiple cloning regions. A schematic diagram of the Gag expression constructs employed in this study is shown in Fig. 7B. The APOBEC3G coding sequences for all constructs were derived from the plasmid CEM15 that was obtained from Michael Malim along with a C-terminal HA-tagged version, both of which were previously described (176). These constructs are referred to hereafter as APOBEC3G and APOBEC3G-HA. PCR cloning was used to amplify the APOBEC3G gene with an EcoRI site prior to the 5' ATG and an SmaI site at the 3' end. The amplified APOBEC3G gene was then ligated into pEYFP-N3 by digestion of the EcoRI and SmaI sites located within the multiple cloning region. This new construct was designated A3G-YFP.

The oligonucleotides used in PCR amplifications for Gag-CFP constructs were GTCAAGCTTGTCGACATGG GCGCCCGCGCCAGC-(F) (forward oligonucleotide for all Gag-CFP constructs), CGGGATCCCTTCACGATCTT GCGCTG-(R) (Gag391-CFP), CGGGATCCGCAGTTGCGGGCGGTGTG-(R) (Gag405-CFP),

CGGGATCCCTTC TTGCGGGGGGCGCG-(R) (Gag411-CFP), CGGGATCCGCAGTCCTTCATCTGGTG-(R) (Gag426-CFP), CGG GATCCATTAGCCTGTCGCTCGGTG-(R) (Gag432-CFP). Oligonucleotides used in PCR amplifications for A3G-YFP construct were GGAATTCGCCACCATGAAGCCTCACTTCAGAAAC-(F), TCGCCCGGGTTTTCCTGATTCTG GAG-(R).

Cell lines and transfections

The human kidney cell line 293T was maintained in Dulbecco's modified Eagle medium with 10% fetal bovine serum and antibiotics at 37°C in 5% CO^2, and grown in 100-cm^2 tissue culture dishes. Transfections were performed by either the calcium phosphate-BBS transfection method or with Lipofectamine 2000 (Invitrogen, Carlsbad, Calif.), with 10 μg of total plasmid DNA unless otherwise stated.

Production and purification of immature Gag virus-like particles (VLPs)

Cell culture supernatants from transfected 293T cells were harvested 48 to 72 hours post-transfection, clarified by centrifugation, filtered through a 0.45-μm filter, and pelleted through a 20% sucrose cushion (100,000 × g for 2 h at 4°C). The pellets were resuspended in 1.0 mL of phosphate-buffered saline (PBS) and analyzed by scanning cuvette fluorometry using a tunable PTI cuvette fluorometer (Photon Tehnology International, Lawrenceville, NJ).

Gradient analysis of Gag VLPs

Gag VLPs, purified as described above, were analyzed by centrifugation on linear 20 to 60% sucrose gradients. Particles resuspended in PBS were overlaid on linear 20 to 60% sucrose gradients. Ultracentrifugation was performed at 100,000 × *g* overnight at 4°C in a Beckman SW41 rotor. Equal fractions were collected, and the density of each fraction was determined with a refractometer. Samples were subsequently diluted in PBS and pelleted at 100,000 × g for 2 h at 4°C in a Sorvall S45A rotor. Samples were resuspended in 100 μl of PBS. Protein content was analyzed by scanning cuvette fluorometry and RNA content was analyzed by RiboGreen dye incorporation after treatment with RQ1 DNAse according to the manufacturer's instructions. Briefly, 10 μl of each fraction was incubated with 0.1 units/μl of RQ1 DNAse and half the supplied reaction buffer (5 mM $MgSO_4$, 20 mM Tris-HCl, 0.5 mM $CaCl_2$) in PBS for 2 hours at 37°C. Samples were then incubated with 0.1% SDS at 65°C for 20 min to lyse particles. An equivalent volume of RiboGreen (Invitrogen, Carlsbad, CA), diluted 200 fold in TE, was then added and allowed to sit in the dark for 10 min. Samples were read on a VersaFluor (BioRad Laboratories, Hercules, CA) cuvette fluorometer along with RNA standards. The original concentration of RNA was then calculated.

Antibodies and Immunoblotting

Particle and lysate preparations were analyzed by SDS-polyacrylamide gel electrophoresis followed by transfer to a nitrocellulose membrane and immunoblotting. Gag was blotted with sera pooled from HIV seropositive patients. APOBEC3G antisera was provided by Warner C. Greene through the NIH AIDS Research and Reference

Reagent Program (181). Secondary horseradish peroxidase conjugated antibodies for ECL-film analysis were obtained from Promega (Madison, WI). Secondary fluorescent conjugated antibodies for detection on the LiCor Odyssey were obtained from LI-COR, Inc. (Lincoln, Nebraska).

Isolation of membrane fractions and analysis by scanning cuvette fluorometry

Cells were harvested for analysis 48 hours following transfection. Three 10 cm^2 dishes of nearly confluent 293T cells were included for each experimental sample. Cells were washed in phosphate-buffered saline, allowed to swell in hypotonic buffer (10 mM Tris-Cl pH 8.0, plus protease inhibitors) for 20 min on ice, and broken by dounce homogenization. The lysates were then adjusted to 0.1 M NaCl, and the nuclei and unbroken cells were removed by centrifugation at 1000 × g for 10 min. For isolation of membrane fractions, postnuclear supernatants containing cytosolic and membrane components were then adjusted to 50% iodixanol from a stock solution of 60% iodixanol (Nycomed Pharma, Oslo, Norway). Forty percent and ten percent solutions of iodixanol were layered on top of the 50% iodixanol layer. The preparation was centrifuged in a Beckman SW41 rotor at 41,000 rpm for 2 h at 4°C. The membrane fraction was taken from the 10%-40% iodixanol interface as a 1-mL sample. Each sample was kept at 4°C and analyzed by fluorometry in a PTI T-format scanning cuvette spectrofluorometer (Photon Tehnology international, Lawrenceville, N.J.). For analysis of CFP emission to compare the relative amount of CFP present, samples were excited at 433 nm, and an emission scan was performing ranging from 460 to 550 nm. For analysis of YFP emission to compare the relative amount of YFP present, samples were exited at 513 nm,

with an emission scan ranging from 524 to 534 nm. Data were collected from at least three different independent experiments for each expression construct.

Results

Specificity of APOBEC3G packaging into Gag VLPs

We first confirmed the findings of other groups that Gag alone is sufficient to package APOBEC3G into VLPs (1, 24, 55, 124, 169, 202). To this end, Gag VLPs were produced in 293T cells in the presence and absence of APOBEC3G-HA overexpression. When APOBEC3G-HA was expressed alone, it was not released into the cell culture media. However, Gag expression and VLP production were sufficient to release APOBEC3G into the cell culture media (Figure 5A). In order to facilitate quantitative studies of the specificity of APOBEC3G packaging into Gag VLPs, a fluorescent system of tracking the relative amounts of APOBEC3G and Gag was developed using an APOBEC3G-YFP fusion protein (hereafter referred to as A3G-YFP). Packaging of A3G-YFP into Gag VLPs was readily demonstrated (Figure 5B), indicating that APOBEC3G-fluorescent protein fusions may be useful in further characterizing the determinants of APOBEC3G packaging.

APOBEC3G-YFP is functional and potently restricts the replication of HIV

Prior to mapping the NC region critical for APOBEC3G packaging, it was necessary to verify that A3G-YFP behaves like untagged APOBEC3G in every way including its ability to dramatically reduce the infectivity of HIV particles. In addition,

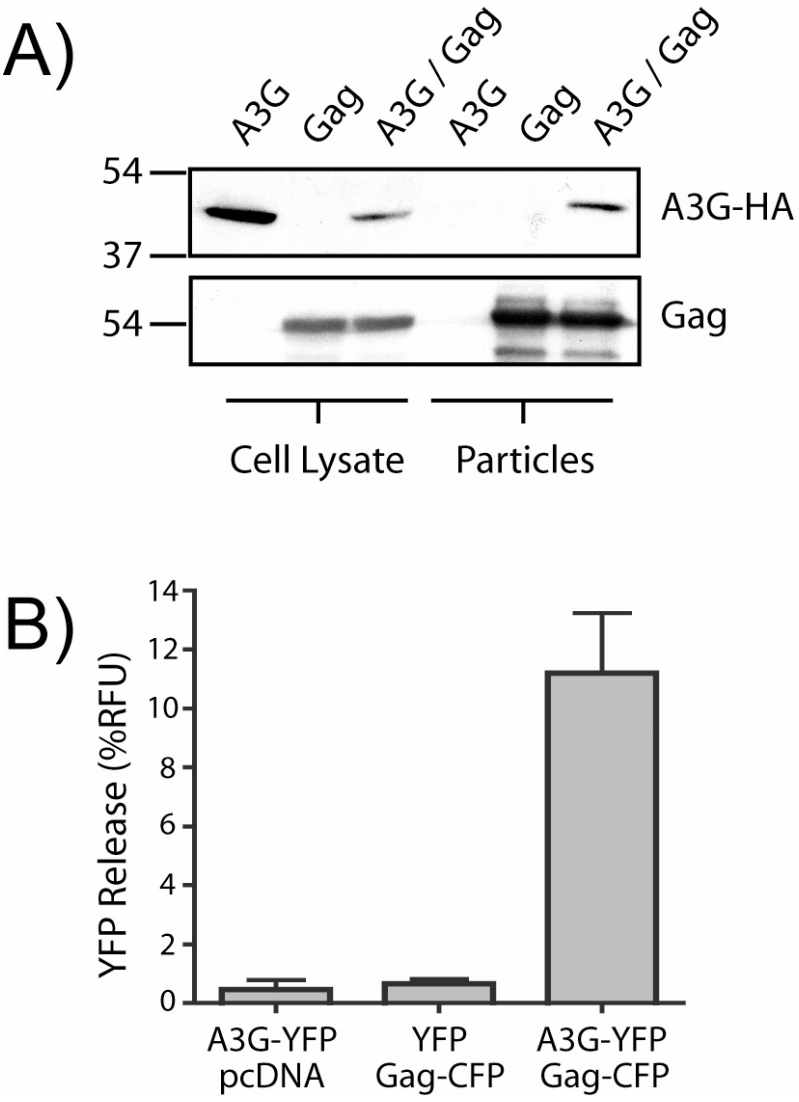

Figure 5. APOBEC3G incorporation into Gag VLPs. (A) APOBEC3G bearing an HA tag was expressed in 293T cells in the presence or absence of Gag. Shown are immunoblots probed with anti-HA antibody (top) and pooled HIV patients' sera (bottom). (B) A3G-YFP or YFP alone was co-expressed with Gag-CFP, and the amount of YFP incorporated into Gag-CFP particles and corresponding cell lysates were quantified using a scanning cuvette fluorometer. Results are shown as a percent of total Relative Fluorescence Units (RFU) released (supernatant/supernatant + cell).

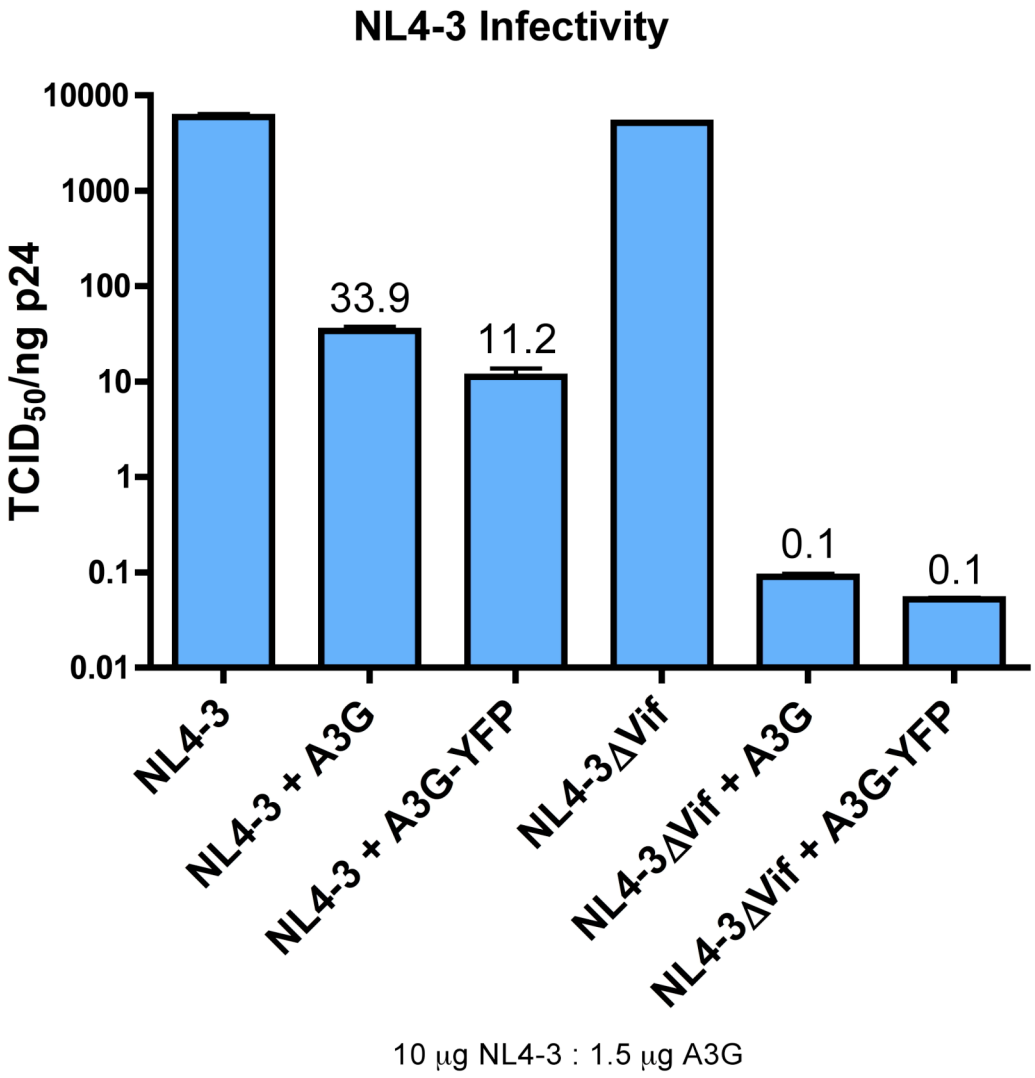

Figure 6. APOBEC3G-YFP potently restricts HIV-1 strain NL4-3. NL4-3 virus was produced from 293T cells co-transfected with 10 μg of the indicated provirus and 1.5 μg of either pcDNA3.1, APOBEC3G (A3G), or APOBEC3G-YFP (A3G-YFP). Infectivity of each virus (TCID50/ml) was assayed using a luciferase reporter gene in the TZMBL cell line. The infectivity is reported as normalized to virus concentration in nanograms of CA p24 per ml. Expression of either A3G or A3G-YFP was sufficient to reduce the infectivity of HIV-1 virus by 100 fold. However, an otherwise identical provirus lacking Vif expression produced virus that was reduced in infectivity by 100, 000 fold in the presence of both A3G and A3G-YFP expression.

the use of APO-YFP on a provirus lacking Vif such as NL4-3ΔVif should produce a more profound effect on the infectivity of the released particles due to the absence of Vif-induced A3G degradation. Therefore, NL4-3 and NL4-3ΔVif viruses were produced in the presence of pcDNA3.1 vector only, A3G, or A3G-YFP. The concentration of each virus was first determined by p24 ELISA. The infectivity of each virus was then determined using the Tissue Culture Infective Dose (TCID50/ml) method and infection of the HIV reporter cell line TZMBL. The results are illustrated in Figure 6 as infectivity normalized to virus content (TCID50/ng p24). Both A3G and A3G-YFP were able to reduce the infectivity of NL4-3 by 100 fold and of NL4-3ΔVif by 100, 000 fold. This indicates that A3G-YFP is just as potent as A3G in restricting virus infectivity and therefore virus replication. In addition, based on the more profound restriction effects of A3G-YFP on NL4-3ΔVif, I concluded that A3G-YFP is as susceptible to Vif degradation and neutralization as A3G. Together, these data confirmed that A3G-YFP is an appropriate and relevant tool to study A3G packaging into HIV particles. Most interestingly, however, was the observation that even wild type HIV-1 can be restricted quite effectively by the correct expression levels of A3G. This suggests that the studies presented in this thesis can be applied to clinical strains of HIV-1 in the unusual context of APOBEC3G over-expression.

Efficient APOBEC3G incorporation requires the NC basic linker region

The packaging of APOBEC3G into virions or VLPs has been shown by a number of groups to be dependent on the NC region of Gag (1, 24, 124, 169, 182, 202). We sought to more precisely delineate the region of NC required for APOBEC3G packaging,

and to determine if APOBEC3G packaging sequences directly correlate with the "I" or Interaction domain which localizes to NC (47, 164, 165). To this end, we utilized a panel of Gag protein constructs spanning the NC region fused to CFP (Fig. 7B). These constructs have been extensively characterized for their ability to produce particles of normal density, their membrane-binding properties, and their ability to interact with detergent-resistant membrane fractions (51, 164, 165). I reasoned therefore that these properties might be correlated with APOBEC3G packaging.

To test this, VLPs were collected and purified from 293T cells that were cotransfected with A3G-YFP and each of the Gag-CFP fusion constructs. Relative levels of Gag were determined by CFP fluorescence, and relative APOBEC3G levels were determined by YFP fluorescence. Approximately equivalent expression levels of APOBEC3G in each of the cell lysates examined was verified by YFP fluorescence (data not shown). Very small amounts of APOBEC3G were released in the absence of Gag (Fig. 5B), presumably in microvesicles that co-purify with the VLPs. The small amount of A3G-YFP released in the absence of Gag (always less than 5% of values in the presence of Gag) was subtracted from the fluorescence values in the presence of each of the Gag-CFP constructs, and the Gag-dependent packaging of A3G-YFP plotted (Fig. 7C). Values are expressed as YFP relative fluorescence units (counts/sec), divided by CFP relative fluorescence units (counts/sec).

Gag377-CFP expresses MA, CA, and SP1 of Gag, and the particles produced from this protein failed to package APOBEC3G (Fig. 7C). Gag384-CFP includes the minimal "I" domain(164), yet unexpectedly also failed to package APOBEC3G. Additional constructs that did not contain the basic linker region (between amino acids

Figure 7. Nucleocapsid determinants of APOBEC3G incorporation. (A) Schematic illustration of $Pr55^{Gag}$ and position of the N-terminal I Domain and selected amino acids. (B) Schematic representation of Gag-CFP constructs subdividing HIV-1 NC. Asterisks indicate the sites of Gag truncation and CFP fusion. The number represents the C-terminal amino acid residue expressed, with the Gag initiator methionine considered residue 1. Arrows represent HIV protease cleavage sites. (C) Gag-CFP fusion constructs illustrated above were cotransfected with A3G-YFP. Supernatants were concentrated through 20% sucrose cushion. A3G-YFP released in microvescicle contamination is estimated by the YFP fluorescence released when A3G-YFP is co-transfected with pcDNA control and represented less than 5% of the signal seen upon expression of full-length Gag. This value is subtracted and the resulting Gag-induced Relative Fluorescence Units (RFU) of A3G-YFP released is shown as a normalized value relative to the amount of Gag protein present. (D) Gag-CFP fusion constructs illustrated above were cotransfected with APOBEC3G. Supernatants were concentrated through 20% sucrose cushion. CFP fluorescence was used to normalize virus like particle concentration. Proteins were resolved by SDS-polyacrylamide gel electrophoresis followed by immunoblot analysis with APOBEC3G anti-sera and pooled HIV patient sera for Gag-CFP.

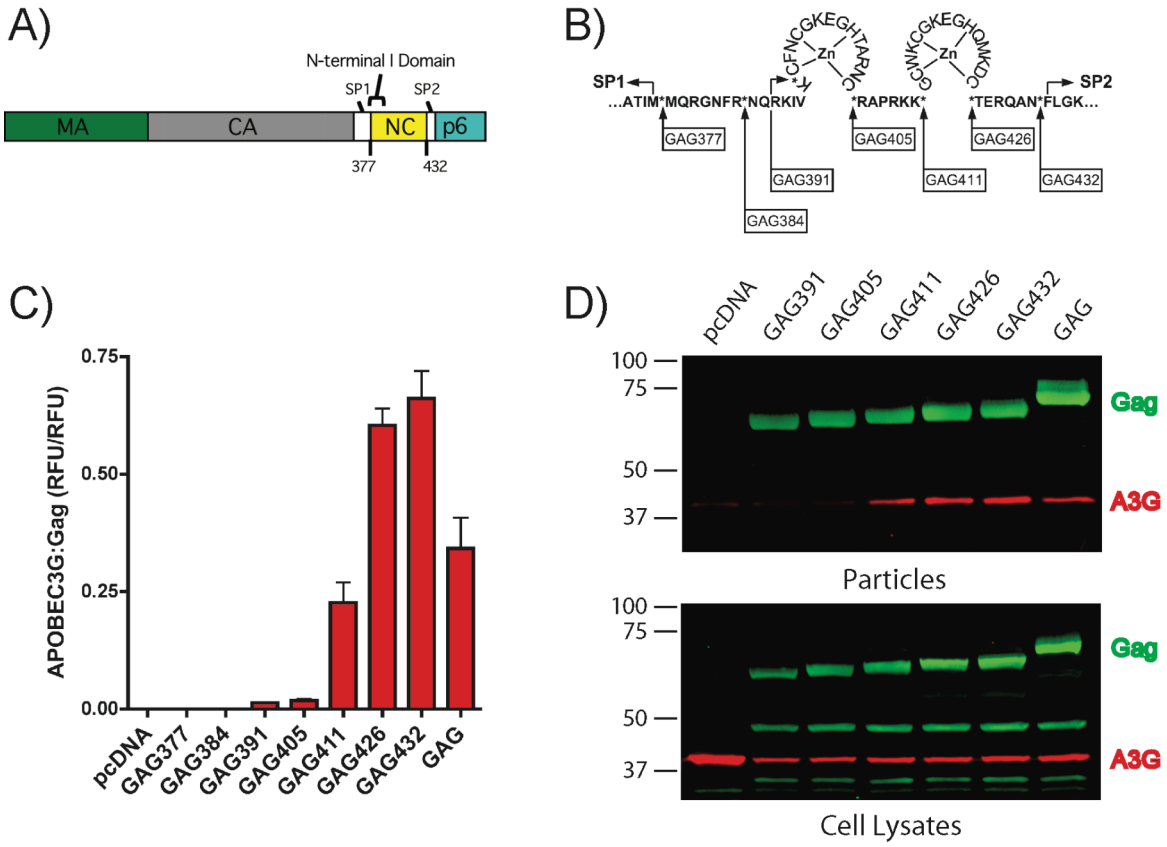
A)
N-terminal I Domain
SP1
SP2
MA
CA
NC
p6
377
432
B)
SP1
...ATIM*MQRGNFR*NQRKIV
RAPRKK
*TERQAN*FLGK...
SP2
GAG377
GAG384
GAG391
GAG405
GAG411
GAG426
GAG432
C)
APOBEC3G:Gag (RFU/RFU)
0.75
0.50
0.25
0.00
pcDNA
GAG377
GAG384
GAG391
GAG405
GAG411
GAG426
GAG432
GAG
D)
pcDNA
GAG391
GAG405
GAG411
GAG426
GAG432
GAG
100
75
50
37
Gag
A3G
Particles
Cell Lysates

405 and 411) were released into the media in the form of VLPs, but packaged very little APOBEC3G. This was also true for Gag405-CFP, a Gag-CFP fusion construct that includes the intact N-terminal zinc finger domain, which failed to package APOBEC3G above background levels (Fig. 7C). However, the addition of the six amino acid basic linker region represented in Gag411-CFP produced a sharp increase in packaging efficiency. Interestingly, constructs that contain the basic linker plus the second zinc finger region but lacking p6 incorporated an enhanced amount of APOBEC3G compared to wild type Gag using this assay.

To ensure that this packaging phenotype was not an artifact of the YFP fusion construct, these experiments were repeated with an untagged APOBEC3G construct. In this experiment, the VLP pellets were normalized for loading by measuring the amount of Gag as indicated by CFP fluorescence, and the incorporated APOBEC3G protein was detected by Western blotting on a LiCor fluorescence imaging system. Gag411-CFP, a construct containing the basic linker, demonstrated APOBEC3G packaging, as did constructs including the second zinc finger and the entire NC region (Figure 7D). Together, these results confirmed the dependence of APOBEC3G packaging on the nucleocapsid region, and suggested that the basic linker is required for incorporation. Strikingly, the packaging requirements of APOBEC3G were distinct from the minimal "I" domain, which has been mapped more proximally to the N-terminal domain of NC (164).

RNA content of particles correlates with APOBEC3G content

Both APOBEC3G and the nucleocapsid (NC) subunit of Gag are known to bind ribonucleic acids (RNA), however, the role of RNA binding in packaging has not been completely resolved. While some investigators report RNA-dependent packaging (169, 182, 202), others have reported a direct APOBEC3G-NC interaction (1, 24). If the ability of NC to bind to cellular RNA is the prime determinant of APOBEC3G packaging into HIV VLPs, then we would expect that the amount of RNA packaged in VLPs should correlate with the quantity of APOBEC3G packaged. Furthermore, truncated Gag constructs that lack subdomains of NC may package less cellular RNA. In order to test these hypotheses, VLPs from several of the constructs outlined in Fig. 7B were purified by equilibrium density sedimentation on a linear sucrose gradient. Equal fractions were collected, treated with DNAse, and analyzed for protein content by CFP fluorescence, and for RNA content by incorporation of the fluorescent dye RiboGreen (Molecular Probes). The RNA content of each construct expressed as an RNA/Gag fluorescence ratio present in the 1.16 g/ml particle peak is shown in Fig. 8A, and a representative curve demonstrating co-fractionation of total RNA and Gag is shown in Fig. 8B. We found measurable RNA incorporation in constructs representing the "minimal" I domain (Gag384, Fig. 8A), which did not increase substantially when the entire N-terminal domain was included (Gag405). Inclusion of the NC basic linker substantially increased the RNA/Gag ratio (Gag411), and inclusion of full-length NC enhanced this further (Gag432). The pattern of RNA incorporation that we observed closely mimicked the relative levels of incorporation of A3G-YFP (compare Fig. 8A and Fig. 7C). These data support a model in which APOBEC3G binds to the cellular RNA that is incorporated into

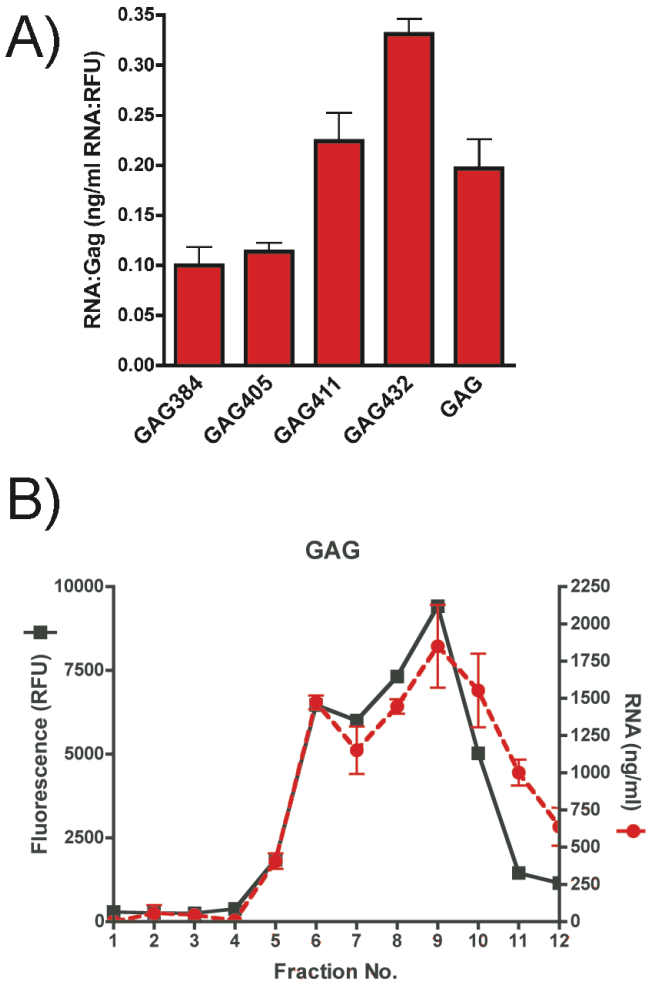

Figure 8. RNA content of particles correlates closely with APOBEC3G content. Gag-CFP fusion constructs were transfected into 293T cells. Supernatants were purified on linear 20 to 60% sucrose gradients. Fractions were collected from the top of the gradient, treated with RQ1 DNAse, stained with RiboGreen, and subjected to analysis by fluorometry. (A) RNA content of particles in peak fractions are shown normalized to Gag-CFP content (RNA/Gag ratio). (B) Sedimentation pattern of Gag-CFP VLPs (black squares) and associated RNA (gray circles).

the developing virion, and indicates that the quantity of APOBEC3G incorporated is greatest in those particles with the highest RNA content, which in this experiment was the result of non-specific interactions between NC and cellular RNA. Interestingly, the very low level of APOBEC3G packaged in the absence of the basic linker region (Fig. 7C), despite packaging of some cellular RNA by Gag384 and Gag405, argues that there may be either a specific contribution of the basic linker region of NC for packaging or a threshold level of RNA incorporation that dictates packaging.

NC basic linker is required for membrane recruitment of APOBEC3G

Particle budding is known to occur at the plasma membrane in both primary T cells and 293T cells (71). Therefore, we examined whether Gag constructs that packaged APOBEC3G also recruited it to membrane fractions. To this end, 293T cells were cotransfected with A3G-YFP and the panel of Gag-CFP truncation mutants, and membranes were isolated via flotation on iodixanol gradients. The membrane-enriched fraction was collected and assayed along with the cell lysates for APOBEC3G and Gag protein content by YFP and CFP fluorescence, respectively. Results are expressed as percent membrane fluorescence compared to total cell lysate fluorescence (Fig. 9). Marked recruitment of APOBEC3G to cellular membranes was observed upon expression of Gag (Fig. 9A). The recruitment of APOBEC3G to the membrane fraction largely mirrored the results described above for particle incorporation; those constructs lacking the basic linker failed to recruit APOBEC3G into membrane fractions. In parallel, we measured the membrane flotation of Gag (Fig. 9B). Remarkably, Gag membrane

Figure 9. Nucleocapsid determinants of APOBEC3G membrane recruitment. Gag-CFP fusion constructs illustrated in Fig. 2B were cotransfected with A3G-YFP. The protein content of membrane-enriched fractions generated by flotation on iodixanol step gradients was determined by fluorescence spectrophotometry. The percentage of protein present in the membrane fraction was calculated by dividing by the protein present in the total cell lysate. (A) YFP signal was used to determine the amount of APOBEC3G present in membrane fractions for each indicated construct. (B) CFP signal was used to determine the amount of Gag protein present in membrane fractions for each indicated construct.

A)

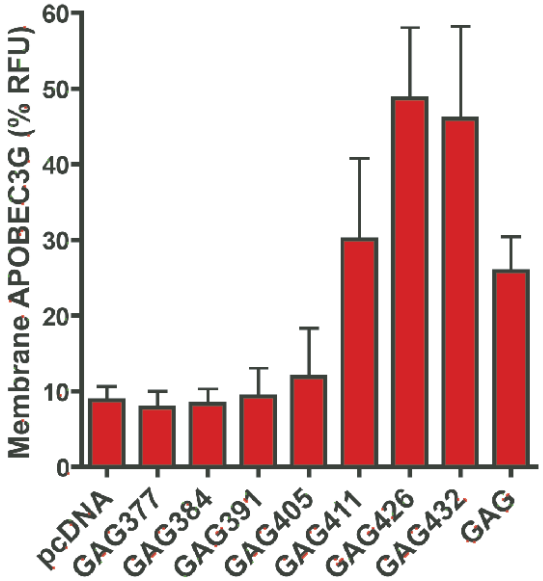
Membrane APOBEC3G (% RFU)
60
50
40
30
20
10
0
pcDNA
GAG377
GAG384
GAG391
GAG405
GAG411
GAG426
GAG432
GAG

B)

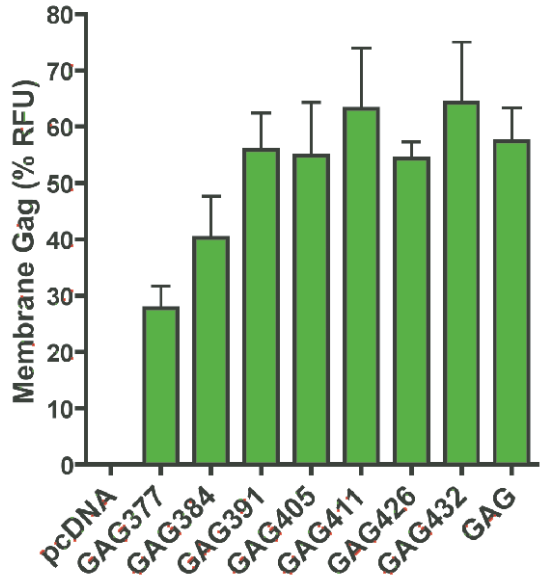
Membrane Gag (% RFU)
80
70
60
50
40
30
20
10
0
pcDNA
GAG377
GAG384
GAG391
GAG405
GAG411
GAG426
GAG432
GAG

association was maximal with the inclusion of the N-terminal domain of NC. Addition of the basic linker did not enhance Gag-membrane association in this context (Fig. 9B). The association of Gag constructs bearing only the N-terminal subdomain of NC with membranes is consistent with our previous description of the I domain (164), and indicates that the determinants mapped as the I domain are distinct from the packaging requirements for APOBEC3G. These data support a more specific role for the basic linker region in APOBEC3G interaction and recruitment to cellular membranes.

RNAse disrupts APOBEC3G binding to NC

Indirect evidence has indicated the importance of RNA in the recruitment of APOBEC3G into Gag VLPs. To directly assess the question of RNA involvement a GST sedimentation assay was employed. Cell lysates expressing APOBEC3G-HA were added to each Gag subunit, fused to GST, and conjugated to glutathione sepharose beads. After extensive washing, it was found that APOBEC3G-HA bound only to the NC region, and not to other Gag subunits (Fig. 10A). When cell lysates were treated with nucleases, this binding was abolished (Fig. 10B). These results are consistent with those already published by several groups, further supporting an important role for RNA in particle incorporation of APOBEC3G (169, 182, 202).

Discussion

APOBEC3G (A3G) is a very potent inhibitor of viral replication and therefore a complete understanding of its function is vital. A3G packaging into viral particles represents an essential step in A3G function and therefore the viral protein sequences

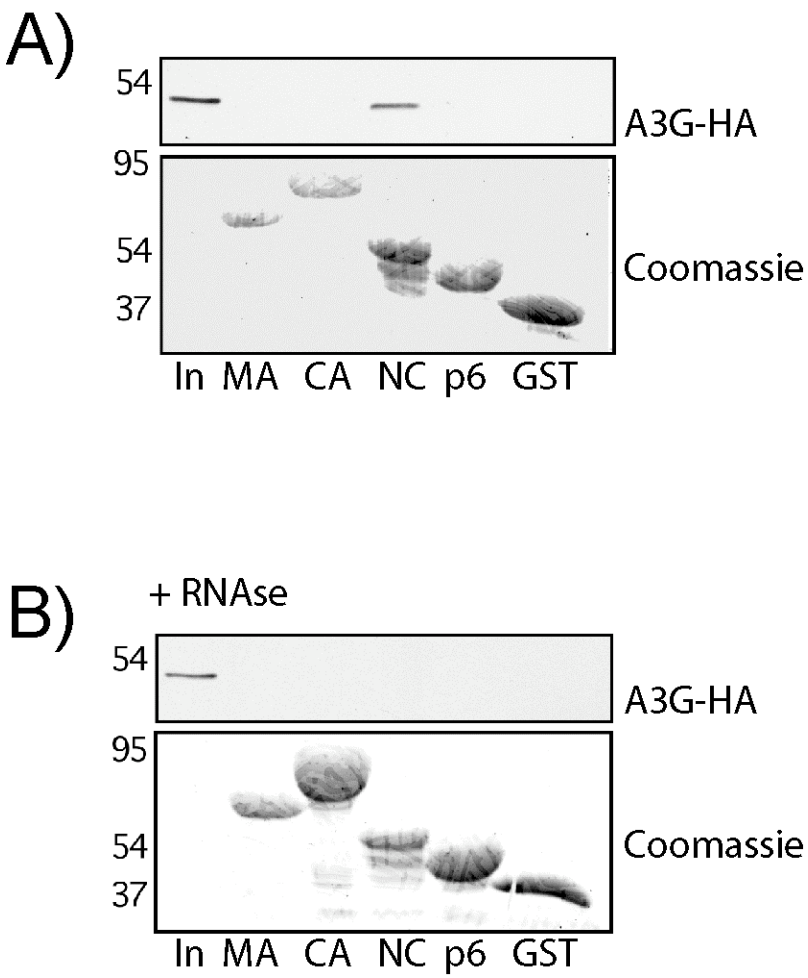

Figure 10. RNAse disrupts APOBEC3G binding to NC. (A) Cell lysates from 293T cells expressing APOBEC3G-HA were added to glutathione agarose beads containing the indicated bacterially purified Gag subunits. After extensive washing the glutathione beads were analyzed by SDS-PAGE followed by both coomassie blue staining and immunoblot analysis with αHA for APOBEC3G-HA. In = 5% of input (B) As described above following addition of RNAse and DNAse to the cell lysates prior to performing GST pulldown.

facilitating this process are of great interest within the field of A3G and the wider field of HIV research in general. The studies presented in this chapter provide three unique contributions to the field of A3G research. First, I have developed a novel method to quantitatively characterize the levels of A3G in the cytoplasm, on cellular membranes, and in particles using fluorescence spectroscopy. Secondly, I have mapped the Gag determinants of A3G packaging to a specific region of NC. Finally, I have demonstrated the requirement for RNA in A3G packaging using both correlative cell culture techniques and direct biochemical methods. These contributions advance the field in two main ways, by providing a new method that can be used to quantitatively study the steps in viral encapsidation of any fluorescent fusion protein, and in addition, my contributions have provided the field with new insights regarding the specific mechanisms driving A3G packaging into virus particles.

Previously, two methods were used to detect A3G content in particles involving either immunoblotting or a radiolabelled cytidine deamination assay (176, 181, 182). However, immunoblotting is only semi-quantitative and both procedures involve several hours of biochemistry before A3G concentration can actually be determined. Fluorescent analysis of GFP variant fusion-proteins within whole particles provides a linear and quantitative signal that can be obtained within minutes. Therefore, YFP fluorescence was used measures A3G-YFP levels, and CFP fluorescence was used to normalize A3G levels to the amount of Gag-CFP present. This assay provides a sensitive and reliable way to detect A3G that is also very quick to perform and easy to learn. This convenient assay can be adapted to measure viral incorporation of any fluorescent fusion protein, and can also be generalized to other viruses provided they have a structural protein that can

support GFP fusion. As a result this technique is of general utility and interest to the HIV field.

A number of published reports have established that the NC region of Gag is necessary for APOBEC3G packaging into virions or VLPs. The N-terminal subdomain of NC has been shown to be sufficient to allow the formation of particles of normal retroviral density. The "I" domain, which is located within this region, is widely believed to contribute to Gag-Gag multimerization, mediated by NC-RNA interactions. I was surprised in this study to find that the minimal "I" domain of Gag, an essential assembly determinant, did not correspond precisely with the packaging requirements for APOBEC3G. Rather, only those constructs that included the first zinc finger and basic linker packaged APOBEC3G. In contrast to my study is that of Luo et al. (124), who showed that one Gag protein truncated proximal to the first zinc finger packaged APOBEC3G. While the reason for this discrepancy is not certain, I propose that it reflects the fluorescent quantitation performed in my study versus the semi-quantitative Western blot analysis performed in the Luo et al. study. In agreement with their results, however, I observed a minor amount of APOBEC3G in all truncated constructs (Fig. 7D). Two additional lines of experimentation were used to verify the importance of the basic linker region of NC for A3G packaging into particles. First, these studies were repeated, with identical results, using untagged A3G and a quantitative western blotting technique (Fig. 7D). Second, using the same panel of C-terminal Gag truncation mutants and a membrane flotation assay, I demonstrated that the basic linker region of NC was also necessary for Gag to recruit A3G molecules to cellular membranes (Fig. 9A). This finding was particularly interesting because a logical timeline of assembly events would

suggest the necessity of localizing A3G to the plasma membrane prior to its incorporation into virus particles. Nevertheless, two possible explanations for how this might occur exist: 1) that Gag recruits A3G that is already on the plasma membrane into particles, or 2) that Gag recruits A3G from other cellular locations to the plasma membrane and then into particles. The membrane flotation evidence suggests the latter as the mechanistic explanation for A3G plasma membrane recruitment, but also confirms the importance of the basic linker region of NC for this process. Therefore, the quantitative packaging data, and the data indicating that membrane recruitment requires the same critical region, emphasizes the importance of the basic linker region of NC for APOBEC3G interaction and packaging. Furthermore, these studies provide the field with a deeper mechanistic understanding of how cellular A3G molecules make their way into virus particles.

The nature of RNA involvement in A3G packaging has been a controversial issue in the literature. The majority of reports support an essential role for RNA in mediating the APOBEC-NC interaction (169, 182, 202), although some investigators have found evidence for a direct protein-protein interaction (1, 24). Our findings support an RNA-dependent incorporation of APOBEC3G into particles using several lines of evidence. First, *in vitro* interactions of APOBEC3G and NC were shown to be RNAse sensitive as reported by others. Secondly, we found that the incorporation of APOBEC3G into particles generated from a series of truncated Gag protein constructs correlated well with the RNA-to-Gag ratio of the released particles. Essentially, particles generated from Gag constructs containing the basic linker region of NC that packaged wild-type levels of A3G also contained wild-type levels of RNA. The Gag426-CFP and Gag432-CFP constructs contain the basic linker region, additional C-terminal NC sequence with added

basic residues, but none of the p6 region. Particles produced from expression of these two constructs contained higher than wild type levels of A3G but also higher than wild type levels of RNA, supporting the hypothesis that A3G packaging depends upon RNA packaging. The exact explanation for why the particles generated from these two constructs contain higher than wild-type levels of both A3G and RNA remains unclear. Nevertheless, several possible hypothesis will be explored during my discussion of a model below. These studies are a significant contribution to the field because they help to resolve the conflict over the requirement for RNA in A3G packaging from the unexplored angle of using cell culture experiments in combination with biochemistry to make this point.

The studies presented in this chapter provide information that allows me to develop a mechanistic model of how A3G is recruited into virus particles. It is known that A3G molecules bind to single stranded RNA molecules within the cytoplasm that contain uridine and are longer than 16 base pairs in length (106). Therefore, during viral infection A3G molecules bind to viral genomic RNA as it traffics to the plasma membrane and into virus particles. This packaging of RNA is facilitated by the viral Gag protein which recruits viral RNA specifically, and cellular mRNA non-specifically, into virus particles through interactions with the NC region. Therefore, Gag is involved in causing viral packaging of A3G through its ability to package RNA into particles. It is of note to remark that whether the RNA binds first to A3G or Gag may have different implications. This model predicts that any virus whose RNA genome traffics through the cytoplasm of a cell expressing A3G would package A3G into viral particles unless specific mechanisms were employed by the virus to exclude A3G from particles. Of

course, other RNA viruses, that do not have a ssDNA replication intermediate, may package A3G but experience no resulting decrease in infectivity. Reports show that several other retroviruses, endogenous retroviruses, and the Hepatitis B Virus package A3G molecules (52, 60, 98, 126, 131, 167).

Several mechanisms are employed by HIV-1 to exclude A3G from virus particles. The first and most important method used by HIV-1 to exclude A3G from virus particles is by expression of the Vif protein which causes A3G degradation, reduction of its packaging into virus particles, and restoration of HIV-1 particle infectivity (176, 177) (Fig. 6). Secondly, one report has suggested that A3G may be removed from the cytoplasm by the production of non-infectious VLPs containing A3G (1). While the data presented in this chapter seems support this conclusion (Fig. 5A, 7D), the importance of this phenomenon during physiological virus replication is unknown. Thirdly, viral RNA can theoretically be protected from A3G binding through the action of a protein chaperone that forms a tight complex with the viral genomic RNA. This may be the reason why incoming HIV-1 RNA, tightly wrapped around NC subunits and further protected by a capsid shell, are not susceptible to mutation by A3G found in the target cell cytoplasm (76, 131). Lastly, structural studies suggest that A3G molecules may represent a large complex while bound to RNA (190). Therefore, unstructured C-Terminal regions of the Gag protein may sterically hinder the attachment of A3G molecules to the pre-existing Gag-RNA complex. Alternatively, C-terminal regions of Gag may be used to sterically hinder the attachment of A3G-RNA complexes to Gag molecules, preferentially selecting RNA that is not bound to A3G for packaging into virus particles. This certainly seems to be the case with HTLV-1, a retrovirus that

packages reduced levels of A3G and is therefore less susceptible to G-A hypermutation. HTLV-1 contains a long C-Terminal NC region with key acidic residues that inhibit A3G packaging, perhaps by the mechanisms outlined above (48). Therefore, although HTLV-1 lacks a Vif protein, A3G is unsuccessful at completely inhibiting the infectivity of HTLV-1 particles. Data from Figure 7C and 7D suggest that the p6 region of HIV-1 Gag may perform a similar function to the C-Terminal region of HTLV-1 Gag, but less effectively.

The model described above implies a structural relationship between A3G molecules, RNA, and Gag. It implies that there is no direct contact between Gag and A3G, this was shown above (Fig. 10). In addition, since RNA is known to induce the formation of A3G multimeric complexes, these may represent the functional form of A3G (190). As a result, the model further implies that A3G-RNA complexes are packaged into virus particles. This information would not only allow us to add greater depth to our model, but would also suggest a direction for experiments that would explore the earlier steps in trafficking of these complexes into particles. These questions are explored in Chapter III.

CHAPTER III

APOBEC3G MULTIMERIC COMPLEXES IN VIRUS-LIKE PARTICLES

Introduction

Studies presented in Chapter II showed that amino acid residues within the nucleocapsid (NC) region of Gag that are important for the efficient incorporation of RNA, are also important for both the recruitment of APOBEC3G (A3G) to cellular membranes, and the packaging of A3G into virus-like particles (VLPs). Essentially, A3G is packaged into VLPs, and by extension, packaged into virus particles in a manner suggesting RNA-dependent incorporation. In addition, molecules of A3G have been observed to multimerize when binding to RNA, according to studies from yeast two-hybrid experiments, immunoprecipitation assays, and 3D modeling of small angle x-ray scattering experiments (110, 190, 193). These results led me to hypothesize that A3G molecules interact closely with each other while binding to RNA strands within particles. I therefore set out to measure the presence of these A3G-RNA complexes within particles. Data from these experiments would enhance the model presented in Chapter II which suggested that Gag molecules bind to these RNA strands via the NC region of Gag, thereby causing the recruitment of A3G molecules into viral particles. This model was not universally accepted at the time these studies were initiated. In fact, intense controversy raged in the literature regarding whether A3G encapsidation into particles was driven by direct association with NC or by association with encapsidated RNA species as outlined in Chapter II. To address this issue, we used the technique of

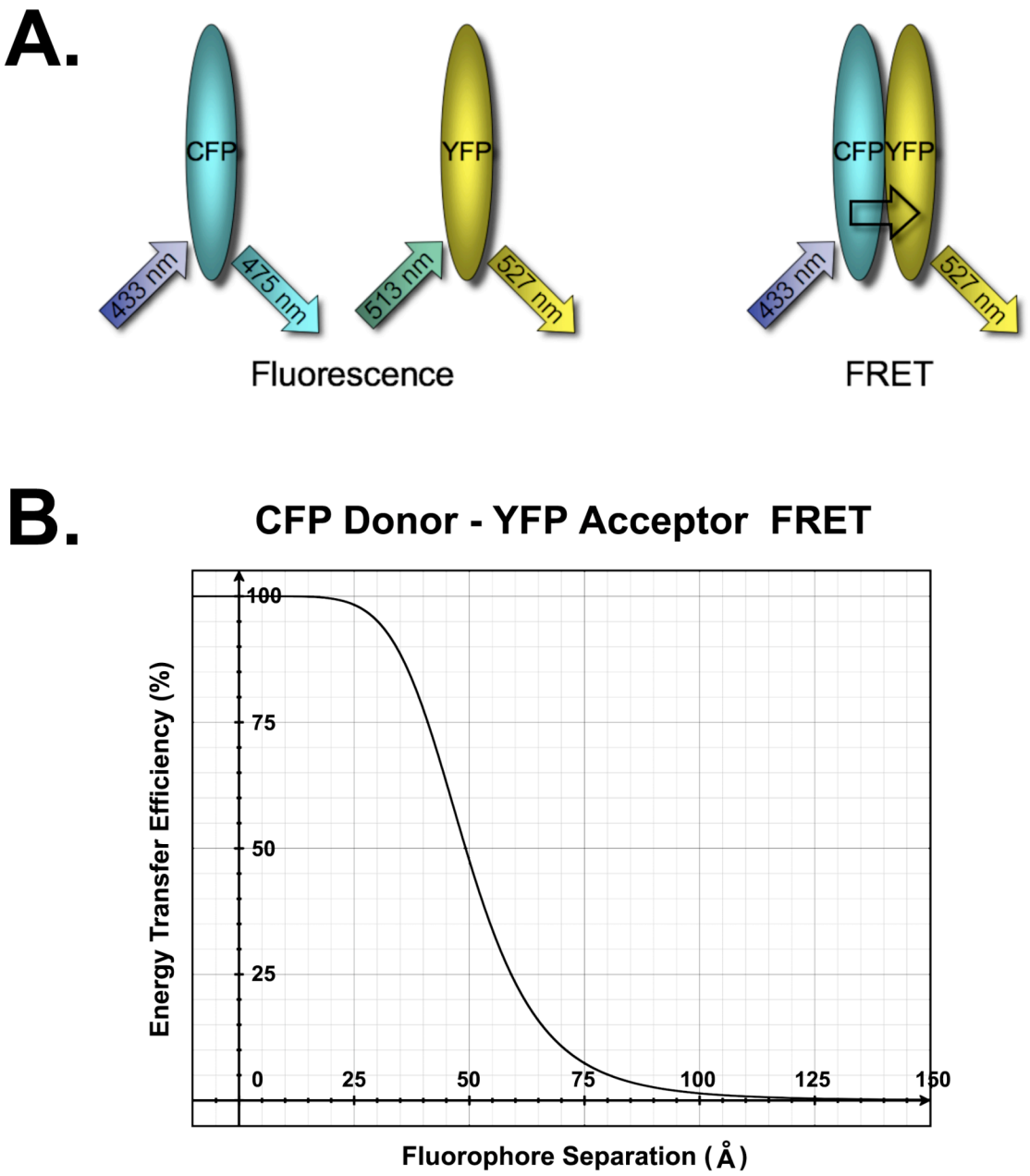

Figure 11. Fluorescent Resonance Energy Transfer (FRET). (A) Schematic diagram contrasting the process of fluorescence to the process of FRET. (B) Efficiency of energy transfer from CFP to YFP as a function of the distance separating the fluorophores.

CFP/YFP Fluorescent Resonance Energy Transfer (FRET) to determine whether direct interactions were occurring between A3G molecules forming multimers and between A3G and Gag molecules.

Förster or fluorescence resonance energy transfer (FRET) is a spectral technique used to measure nanometer distances between fluorescent molecules. First reported by Förster in 1948, this technique has experienced a rebirth in biological applications due to new fluorophores, optical methods, and instrumentation (69, 174). When a chromophore (dye or fluorophore) absorbs light it can dissipate this energy in one of three ways: 1) Dyes convert this energy to heat or vibrational energy, 2) fluorophores produce some heat but re-emit the remaining energy as light of a longer wavelength, or 3) either chromophore can transfer this energy to an acceptor molecule in close proximity, which may then emit the energy as light. By definition, FRET is a non-radiative transfer of quantum energy from excited electrons of the donor molecule to ground state electrons in the acceptor molecule. The energy gained by the acceptor electrons must equal the energy lost by the donor electrons, therefore, the emission spectrum of the donor must overlap the absorbance spectrum of the acceptor fluorophores. This process, which is essentially coupled simultaneous energy state transitions, requires the molecules to be in very close proximity because the efficiency of energy transfer drops off quickly as the distance increases. In general, FRET is used to measure protein-protein interactions for fluorophores approximately within 20-60 Angstroms (Å) of each other (174). Proteins can be conjugated to dyes such as Cy3 and Cy5, small molecule tags such as Europium and allophycocyanin, or fused to variants of the green fluorescent protein (GFP) (67, 114). The studies presented in this document focus on the latter strategy and utilize the

enhanced cyan fluorescent protein (CFP) as the donor fluorophore, and the enhanced yellow fluorescent protein (YFP) as the acceptor (shown in Figure 11A). The efficiency of energy transfer is described by the following equation, $E = [1 + (r/r_0)^6]^{-1}$ where r is the distance between fluorophores, and r_0 is the distance at which E = 50% or 49.2 Å (153). Therefore, the specific distance over which a FRET interaction greater than 5% can be detected for a CFP-YFP pair is theoretically less than 80 Å (Fig 11B). This is a relatively small distance considering the fact that a GFP molecule is 24 Å in diameter and 42 Å long (50, 151). Therefore, proteins that exhibit a FRET interaction are essentially touching.

Although to date FRET had not been used to measure A3G interactions, it was not a novel technique for the field of HIV-1. FRET assays have been used in the past to study the RNAse activity of reverse transcriptase, TAR-interacting proteins, nucleocapsid-amino acid interactions, Rev multimerization, HIV-1 virion fusion, HIV-1 Gag-Gag interactions, and RSV Gag-Gag interactions (23, 41, 47, 100, 119, 136, 141). Therefore, to assess A3G-A3G interactions using FRET, the following fusion proteins were used due to their feasibility for use in live cells: APOBEC3G-CFP, APOBEC3G-YFP, Gag-CFP, and Gag-YFP. FRET experiments in this thesis are performed in two different formats, FRET fluorometry and FRET microscopy, however, this chapter will focus on FRET fluorometry experiments. This particular technique was used to test the following predictions: 1) direct Gag-Gag interactions can be detected in cells and particles, 2) RNA-dependent APOBEC3G interactions can be found in cells and in particles, and 3) RNA mediated, but indirect, Gag-APOBEC3G interactions cannot be detected using FRET since the base-to-base distance of a nucleic acid is 70Å (83, 127, 142). The data

from these studies revealed that A3G complexes were packaged into Gag virus-like particles. However, despite the extensive biochemical evidence describing a Gag-APOBEC3G interaction, we did not detect a direct FRET interaction between these two molecules, suggesting that an RNA bridge may mediate this interaction at a distance. Although the absence of a FRET signal can, in rare cases, be explained by incorrect fluorophore orientation, taken together with previous results, these data suggest that APOBEC3G is packaged into virions as an RNA-dependent multimer that is recruited to the plasma membrane and into budding virions by an RNA-mediated association with the HIV Gag protein.

Materials and Methods

Plasmid construction

This study employed Gag and APOBEC3G expression constructs fused to variants of the codon-optimized version of CFP and YFP (Clonetech, Palo Alto, CA). The CFP and YFP expression vectors, the Gag expression constructs (47), and several of the APOBEC3G expression constructs were described in Chapter II. The APOBEC3G coding sequences for the YFP-A3G and A3G-CFP constructs were derived from the plasmid CEM15 that was obtained from Michael Malim (176). PCR cloning was used to amplify the APOBEC3G gene with an EcoRI site prior to the 5' ATG and an XmaI site at the 3' end. The amplified APOBEC3G gene was then ligated into pEYFP-C1 by digestion of the EcoRI and XmaI sites located within the multiple cloning region. This new construct was designated YFP-A3G. PCR cloning was used to amplify the CFP gene

from pECFP-N3 placing a SmaI site prior to the 5' ATG and a NotI site at the 3' end. The YFP gene in A3G-YFP was then removed by digestion with SmaI and NotI followed by gel purification. The amplified CFP gene was then ligated into the resulting plasmid to yield a new construct designated A3G-CFP.

The oligonucleotides used in PCR amplifications for YFP-A3G construct CGGAATTCGATGAAGCCTCACTTCAGA-(F), TCCCCCGGGTCAGTTTT CCTGATT-(R); for A3G-CFP construct GGCCCGGGATCCATCGCCACCATGGTGAGCAAG-(F), GAGTCGC GGCCGCTTTACTTGTACAGCTCGTCCATGCCG-(R).

Cell lines and transfections

The human kidney cell line 293T was maintained in Dulbecco's modified Eagle medium with 10% fetal bovine serum and antibiotics at 37°C in 5% CO_2, and grown in 100-cm^2 tissue culture dishes. Transfections were performed by either the calcium phosphate-BBS transfection method or with Lipofectamine 2000 (Invitrogen, Carlsbad, Calif.), with 10 μg of total plasmid DNA unless otherwise stated.

Production and purification of immature Gag virus-like particles (VLPs)

Cell culture supernatants from transfected 293T cells were harvested 48 to 72 hours post transfection, clarified by centrifugation, filtered through a 0.45-μm filter, and pelleted through a 20% sucrose cushion (100,000 × g for 2 h at 4°C). The pellets were resuspended in 1.0 mL of phosphate-buffered saline (PBS) and analyzed by scanning cuvette fluorometry using a tunable PTI cuvette fluorometer (Photon Tehnology

International, Lawrenceville, NJ).

FRET analysis by scanning cuvette fluorometry

Schematics of each of the experimental setups used in this chapter are depicted in Figure 12. Cells were harvested for analysis 24 hours following transfection. One 10 cm^2 dish of nearly confluent 293T cells was included for each experimental sample. Cells were washed in phosphate-buffered saline and whole cells or particles resuspended in PBS were analyzed. Each sample was kept at 4°C and analyzed by fluorometry in a PTI T-format scanning cuvette spectrofluorometer (Photon Tehnology international, Lawrenceville, N.J.). For analysis of CFP emission to compare the relative amount of CFP present, samples were excited at 433 nm, and performing an emission scan ranging from 460 to 550 nm. For analysis of YFP emission to compare the relative amount of YFP present, samples were exited at 513 nm, with an emission scan ranging from 524 to 534 nm. For FRET analysis, samples were excited at 433 nm, and an emission scan ranging from 460 to 550 nm was obtained. For nuclease-treated FRET experiments, the cells were allowed to swell in hypotonic buffer (10 mM Tris-Cl pH 8.0, plus protease inhibitors) for 20 min on ice, and broken by dounce homogenization. The lysis buffer was supplemented with 60 μg/ml of RNAse A (Qiagen Inc., Valencia, CA) and 10 units/ml of RQ1 DNAse with buffer (Promega Corp., Madison, WI) while the control lysis buffer was treated with 200 units/ml of RNAse Inhibitor (New England Biolabs Inc., Beverly, MA). The lysates were then adjusted to 0.1 M NaCl, and the nuclei and unbroken cells were removed by centrifugation at 1000 × g for 10 min. Note that a constant amount of untagged Gag expression plasmid was co-transfected in each arm of this experiment.

Figure 12. APOBEC3G FRET fluorometry. Schematic depiction of a model for the structural relationship between Gag and APOBEC3G (A3G) molecules at the plasma membrane when detecting (A) Gag-Gag FRET, (B) A3G-A3G FRET, and (C) Gag-A3G FRET.

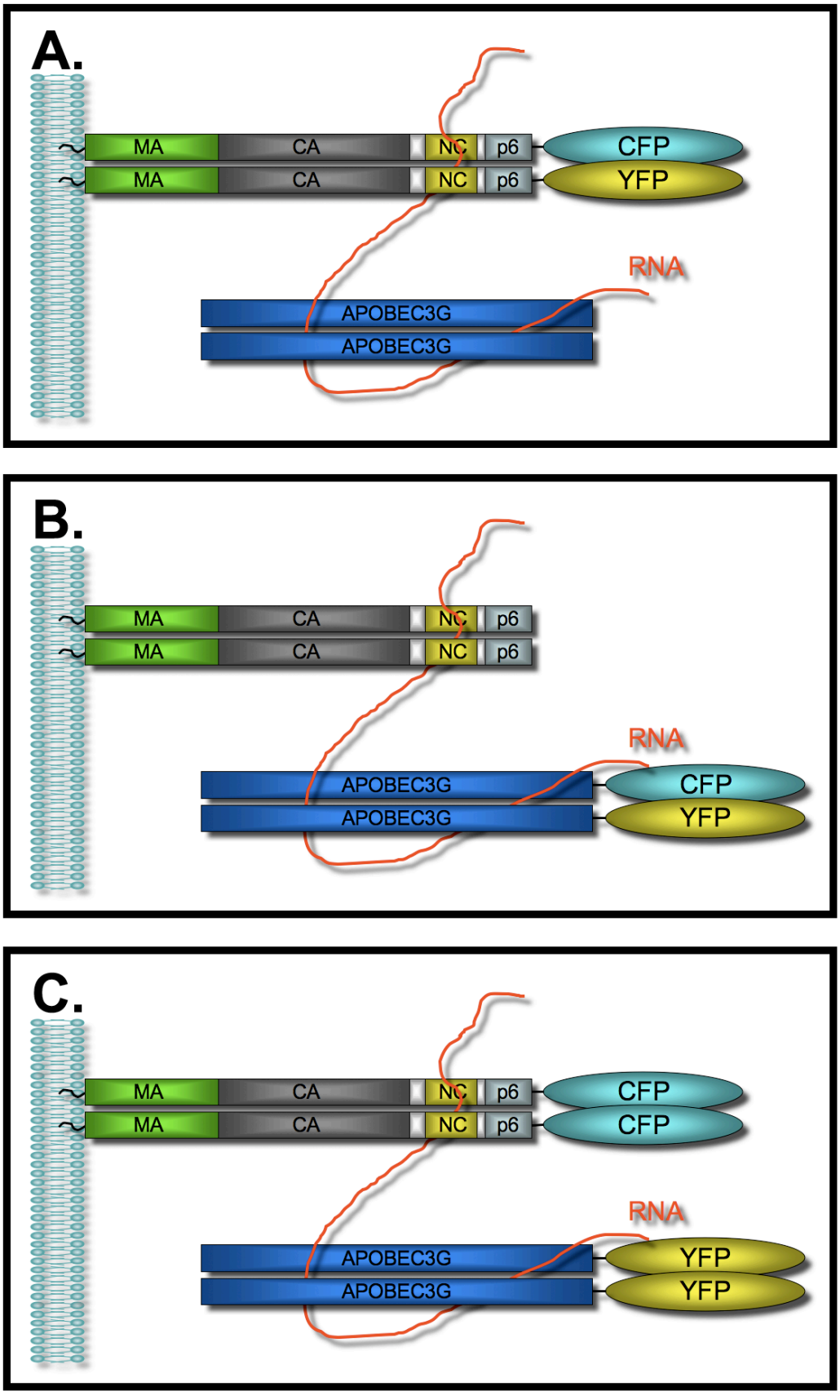
A.
MA
CA
NC
p6
MA
CA
NC
p6
CFP
YFP
RNA
APOBEC3G
APOBEC3G
B.
MA
CA
NC
p6
MA
CA
NC
p6
RNA
APOBEC3G
APOBEC3G
CFP
YFP
C.
MA
CA
NC
p6
MA
CA
NC
p6
CFP
CFP
RNA
APOBEC3G
APOBEC3G
YFP
YFP

Data were collected from at least three different independent experiments for each expression construct.

Results

APOBEC3G multimers bind to RNA in cells and particles

Fluorescence Resonance Energy Transfer (FRET) between CFP and YFP moieties have been used to detect interactions between Gag molecules in living cells. Briefly, stimulation of a CFP molecule at 433 nm normally leads to the emission of a strong peak at 475 nm, a shoulder from 490 – 510 nm, and a broad trail from 510 – 550 nm (Fig. 13A, A3G-CFP emission spectra). YFP molecules are maximally stimulated at 514 nm, therefore, if a YFP molecule is in contact (less than 100 angstrom) from an excited CFP molecule, the overlap in CFP emission and YFP excitation will allow energy transfer from the CFP to the YFP molecule. This will lead to the YFP molecule emitting at 527 nm. Therefore, to detect A3G-RNA-A3G complexes in live cells, A3G-YFP and A3G-CFP were coexpressed in 293T cells and the emission spectra of whole cells, resuspended in PBS, were obtained in a spectrofluorometer using an excitation wavelength of 433 nm. Cells expressing A3G-YFP and A3G-CFP exhibited a curve representative of efficient fluorescence energy transfer (Fig. 13A, blue squares), as did Gag-CFP and Gag-YFP (Fig. 13A, open squares), while cells expressing A3G-CFP and a control YFP resulted in a CFP emission peak with no YFP emission peak (Fig. 13A, open circles). Identical results were obtained with YFP-A3G (results not shown). Similar

levels of YFP emission were obtained upon YFP excitation for each experimental condition, indicating that the protein levels were similar (Fig. 13B).

To determine whether RNA is a necessary component of these APOBEC3G complexes, cell lysates from cells expressing A3G-YFP and A3G-CFP were prepared and treated with RNAse A and DNAse RQ1 while RNA in control lysates was preserved by the addition of RNAse inhibitor. Control lysates expressing A3G-YFP and A3G-CFP exhibited a curve representative of efficient fluorescence energy transfer (Fig. 13C, blue squares), while nuclease treated lysates resulted in a CFP emission peak with no YFP emission peak (Fig. 13C, open circles). The A3G-CFP emission curve remained unchanged by nuclease treatment (Fig. 13C, closed triangles, closed diamonds). The lack of FRET in the nuclease treated lysates was not a result of lower protein concentration or degradation since similar levels of YFP emission were obtained upon YFP excitation for each experimental condition (Fig. 13D). This establishes that FRET is an effective tool to measure the presence of APOBEC3G multimers bound to RNA, and that RNA is required for APOBEC3G multimerization.

We next employed A3G-CFP/A3G-YFP FRET to determine whether APOBEC3G is incorporated into particles as a multimeric complex bound to RNA. Gag VLPs were generated in cells expressing Gag, A3G-YFP, and A3G-CFP. The emission spectrum of these particles was obtained in a spectrofluorometer using an excitation wavelength of 433 nm. Particles containing A3G-CFP and A3G-YFP (Fig. 13E, open circles), or A3G-CFP and YFP-A3G (Fig. 13E, blue squares) exhibited a curve representative of efficient fluorescence energy transfer. However, particles containing A3G-CFP and a control YFP resulted in a CFP emission peak with no YFP emission

Figure 13. APOBEC3G is packaged as multimers that interact with RNA. (A) The indicated constructs were co-transfected into 293T cells. Cells were resuspended in PBS and read directly in a scanning quevette fluorometer. FRET was measured by stimulating the CFP fluorophore at 433 nm and the FRET peak was observed at 527 nm. FRET curve for A3G-YFP /A3G-CFP (blue squares), GagCFP / GagYFP (open squares). pEYFP coexpressed with A3G-CFP (open circles). Closed triangles, GagCFP VLPs. (B) Relative levels of cellular YFP expression are shown for the experiment depicted in panel A, as determined by peak YFP output following excitation of cell lysates at 514 nm. (C) Cell lysates prepared by treatment with hypotonic buffer and dounce homoginization. Half of cell lysates were treated with RNAse A and DNAse RQ1 prior to FRET analysis while RNA in the control lysates were preserved with RNAse inhibitor. FRET curve for A3G-YFP / A3G-CFP (blue squares), loss of FRET in nuclease treated A3G-YFP / A3G-CFP lysates (open cicles). A3G-CFP curve (closed triangles) and treated (closed diamonds). (D) Relative levels of cellular YFP expression are shown for the experiment depicted in panel A, as determined by peak YFP output following excitation of cell lysates at 514 nm. (E) Virus like particles (VLPs) created by coexpressing pVRC3900Gag with the indicated constructs in 293T cells. Supernatants were concentrated through a 20% sucrose cushion, resuspended in PBS and analyzed by scanning cuvette fluorometry. FRET curve for A3G-CFP / A3G-YFP (open circles) and A3G-CFP / YFP-A3G (blue boxes). A3G-CFP coexpressed with pEYFP (closed triangles). (F) Relative levels of virus like particle (VLP) YFP content are shown for the experiment depicted in panel C, as determined by peak YFP output following excitation of VLPs at 514 nm. Note that transfection of an untagged Gag expression construct was included in each of the transfections at a constant amount.

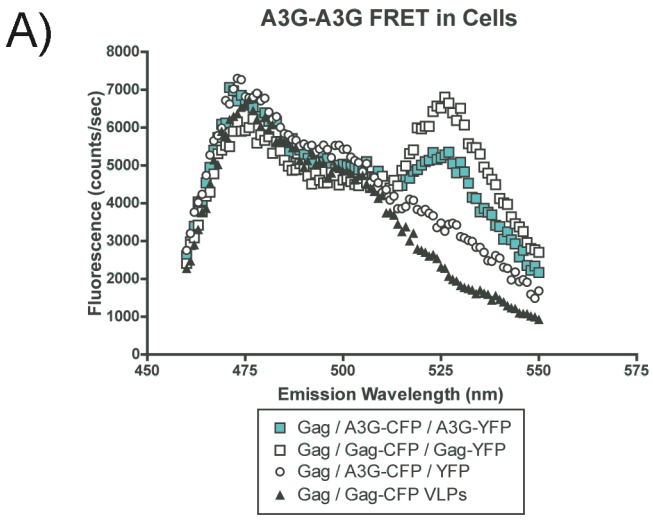
A)
A3G-A3G FRET in Cells
Fluorescence (counts/sec)
Emission Wavelength (nm)
Gag / A3G-CFP / A3G-YFP
Gag / Gag-CFP / Gag-YFP
Gag / A3G-CFP / YFP
Gag / Gag-CFP VLPs

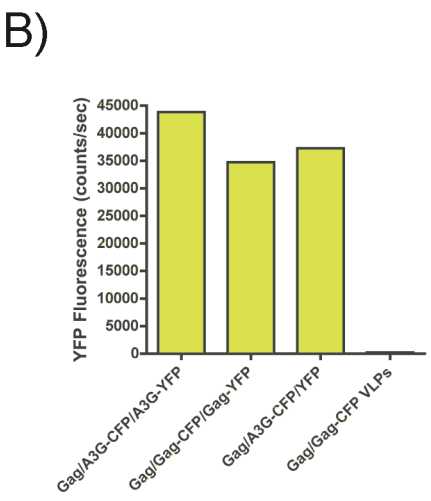
B)
YFP Fluorescence (counts/sec)
Gag/A3G-CFP/A3G-YFP
Gag/Gag-CFP/Gag-YFP
Gag/A3G-CFP/YFP
Gag/Gag-CFP VLPs

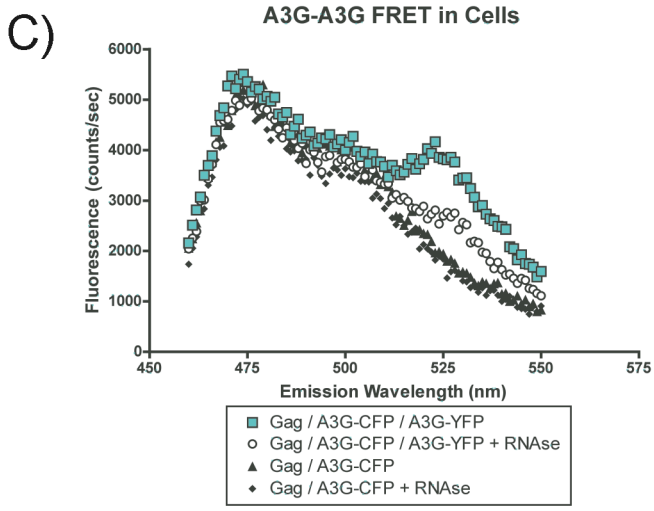
C)
A3G-A3G FRET in Cells
Fluorescence (counts/sec)
Emission Wavelength (nm)
Gag / A3G-CFP / A3G-YFP
Gag / A3G-CFP / A3G-YFP + RNAse
Gag / A3G-CFP
Gag / A3G-CFP + RNAse

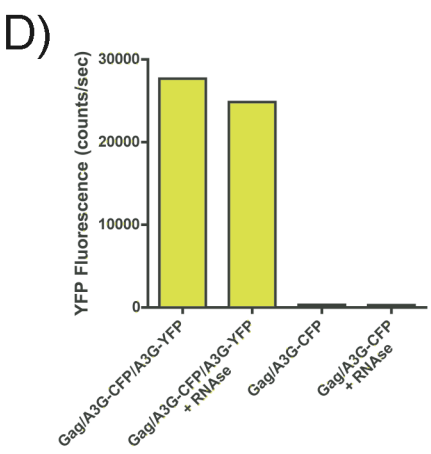
D)
YFP Fluorescence (counts/sec)
Gag/A3G-CFP/A3G-YFP
Gag/A3G-CFP/A3G-YFP + RNAse
Gag/A3G-CFP
Gag/A3G-CFP + RNAse

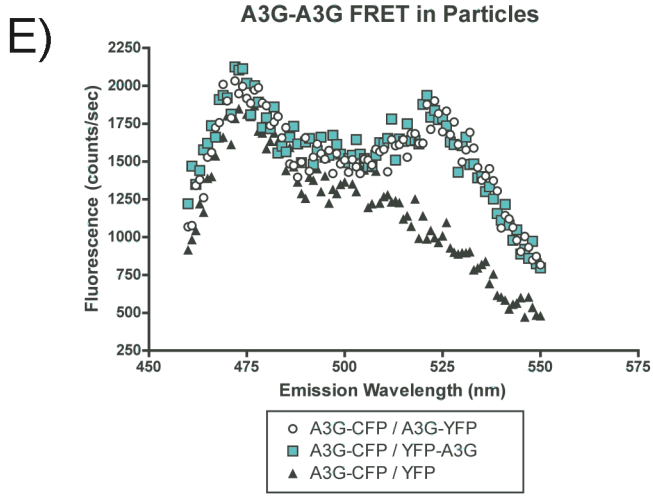
E)
A3G-A3G FRET in Particles
Fluorescence (counts/sec)
Emission Wavelength (nm)
A3G-CFP / A3G-YFP
A3G-CFP / YFP-A3G
A3G-CFP / YFP

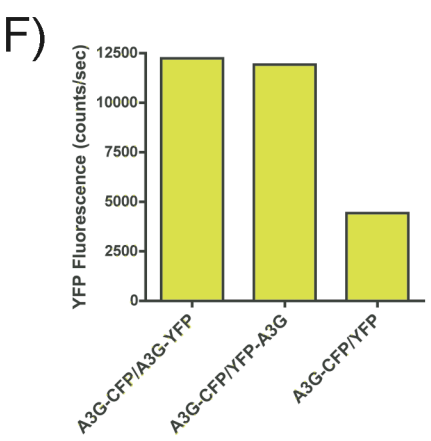
F)
YFP Fluorescence (counts/sec)
A3G-CFP/A3G-YFP
A3G-CFP/YFP-A3G
A3G-CFP/YFP

peak (Fig. 13E, closed triangles). Increased YFP over-expression was used in this experiment to increase the free YFP content of VLPs. We conclude that the FRET detected in Gag VLPs represents APOBEC3G multimers bound to RNA that have become incorporated in VLPs.

Lack of support for a direct Gag-APOBEC3G interaction by FRET

To further analyze the Gag-APOBEC3G interaction in living cells and particles, we asked whether we could detect a direct Gag-APOBEC3G interaction by FRET. Cells expressing Gag-YFP and Gag-CFP exhibited a curve representative of efficient fluorescence energy transfer (Fig. 14A, blue circles) as a positive control. In contrast, cells expressing Gag-YFP and A3G-CFP revealed a CFP emission peak with no YFP emission peak, indicating no FRET (Fig. 14A, open squares). Results with Gag-YFP and A3G-CFP were identical to the negative control of Gag-YFP co-expressed with CFP (Fig. 14A, closed triangles). Similar levels of YFP emission were obtained upon YFP excitation for each experimental condition, indicating that differential protein levels did not account for the differences in positive controls and the test molecules (Fig. 14B).

Gag VLPs were then generated in cells expressing Gag, Gag-CFP, and A3G-YFP. In the same system A3G-YFP was replaced by Gag-YFP as a FRET positive control and YFP-Mem (Clontech) as a FRET negative control. The emission spectrum of these particles was obtained in a spectrofluorometer using an excitation wavelength of 433 nm. Particles containing Gag-CFP and Gag-YFP exhibited a curve representative of efficient fluorescence energy transfer (Fig. 14C, blue circles), while particles containing Gag-CFP and A3G-YFP resulted in a CFP emission peak with no YFP FRET peak (Fig. 14C, open

Figure 14. Lack of FRET between APOBEC3G and Gag. (A) The indicated constructs were co-transfected into 293T cells. Cells were resuspended in PBS and read directly in a scanning quevette fluorometer. FRET was measured by stimulating the CFP fluorophore at 433 nm and the FRET peak was observed at 527 nm. FRET curve for Gag-YFP - Gag-CFP (blue circles). Gag-YFP coexpressed with A3G-CFP (open squares) and pECFP (closed triangles). (B) Relative levels of cellular YFP expression are shown for the experiment depicted in panel A, as determined by peak YFP output following excitation of cell lysates at 514 nm. (C) VLPs created by coexpressing the indicated constructs in 293T cells. Supernatants were concentrated through 20% sucrose cushion, resuspended in PBS and analyzed by scanning cuvette fluorometry. FRET curve for Gag-CFP / Gag-YFP (blue circles). Gag-CFP coexpressed with A3G-YFP (open squares) and pEYFP (closed triangles). (D) Relative levels of virus like particle (VLP) YFP content are shown for the experiment depicted in panel C, as determined by peak YFP output following excitation of VLPs at 514 nm.

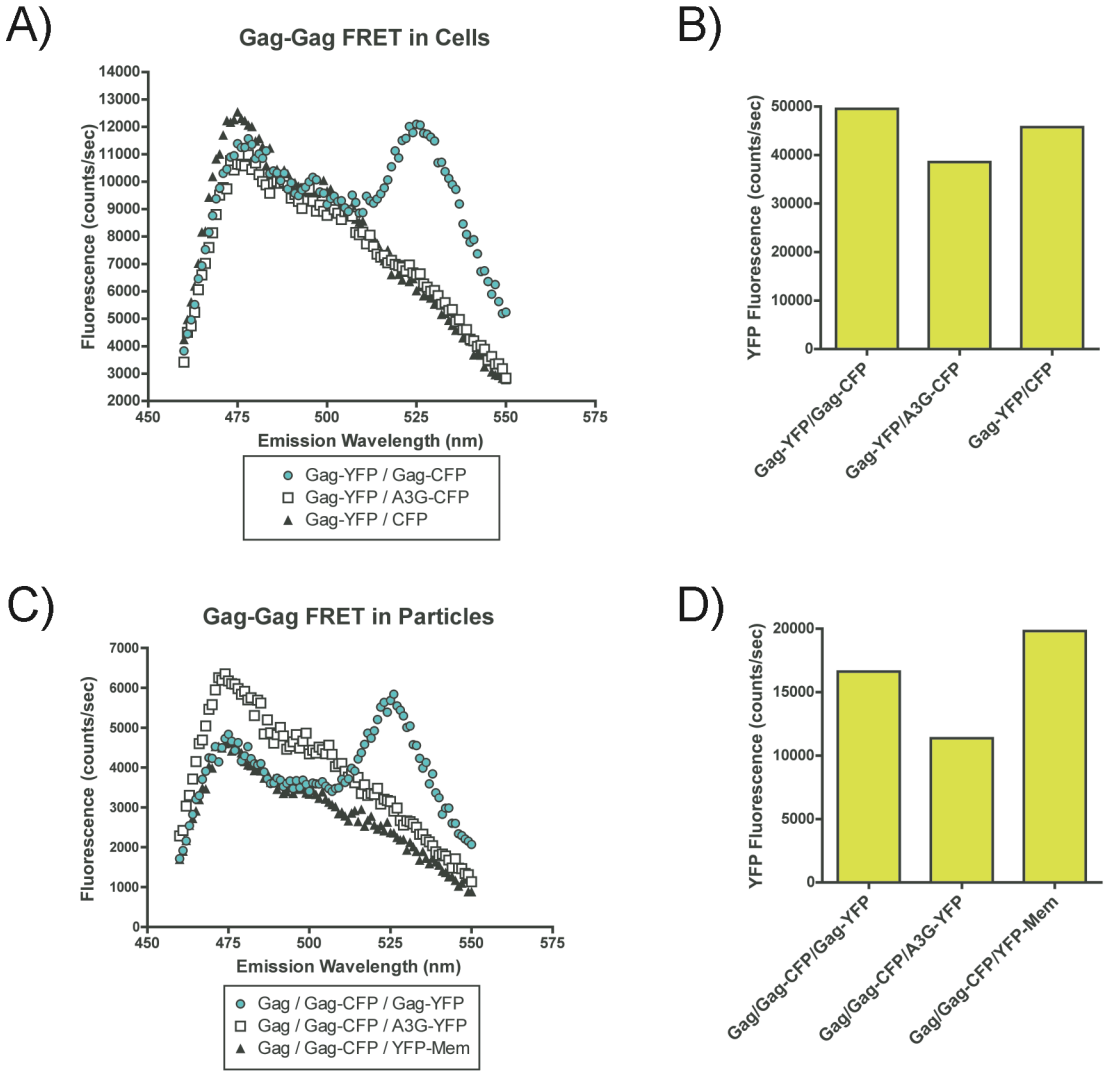
A)
Gag-Gag FRET in Cells
Fluorescence (counts/sec)
Emission Wavelength (nm)
Gag-YFP / Gag-CFP
Gag-YFP / A3G-CFP
Gag-YFP / CFP
B)
YFP Fluorescence (counts/sec)
Gag-YFP/Gag-CFP
Gag-YFP/A3G-CFP
Gag-YFP/CFP
C)
Gag-Gag FRET in Particles
Fluorescence (counts/sec)
Emission Wavelength (nm)
Gag / Gag-CFP / Gag-YFP
Gag / Gag-CFP / A3G-YFP
Gag / Gag-CFP / YFP-Mem
D)
YFP Fluorescence (counts/sec)
Gag/Gag-CFP/Gag-YFP
Gag/Gag-CFP/A3G-YFP
Gag/Gag-CFP/YFP-Mem

squares). The lack of FRET in particles containing Gag-CFP and A3G-YFP was not due to lower concentrations of A3G-YFP in this experiment, as similar levels of YFP emission were obtained for each experimental condition (Fig. 14D). These results indicate that we were unable to detect direct interactions between Gag and APOBEC3G in cells or VLPs using this technique. Interpretation of these results must include recognition that a negative result in a CFP-YFP FRET assay does not rule out a direct interaction, as FRET can be dependent on both the position and orientation of the CFP and YFP molecules (54, 153).

Discussion

Together with results from the previous Chapter, my findings support an RNA-dependent incorporation of multimeric APOBEC3G complexes into VLPs. First, *in vitro* interactions of APOBEC3G and the NC region of Gag were shown to be RNAse-sensitive as reported by our lab and others (Chapter II). Secondly, we found that the incorporation of APOBEC3G into a series of serially truncated Gag protein constructs quantitatively correlated with the RNA-to-Gag ratio of the released particles (Chapter II). Finally, data from FRET studies in this chapter provide indirect evidence for a requirement for RNA in A3G packaging by revealing both that RNA is required for APOBEC3G-APOBEC3G interactions, and that these APOBEC3G multimers are subsequently packaged into VLPs. Opi et al. reported a monomeric APOBEC3G mutant (C97A) that is packaged into VLPs and is catalytically active, indicating that it retains the ability to bind to RNA (150). This suggests that A3G-RNA binding does not require multimerization, but rather, that monomeric or dimeric forms of A3G initially bind to

RNA forming a transition state that subsequently recruits additional A3G molecules, leading to the formation of a multimeric A3G complex. Why does A3G bother to multimerize if the monomeric form contains antiviral activity? It is tempting to speculate that multimerization may play a role in an aspect of enzyme function not yet described in sufficient detail such as the efficiency or kinetics of deamination. Nevertheless, the majority of APOBEC3G in cells is present in an RNAse-sensitive multimeric form (150). In addition, several reports have suggested that APOBEC3G binds to itself in cells (110, 193) in an RNA-dependent manner (193) producing high molecular mass (HMM) complexes observed in activated T-cells and transfected 293T cells (27, 118). Therefore, in contrast to Opi et al. our FRET studies demonstrated that wild-type APOBEC3G multimers were incorporated into virions. In agreement, however, with previous reports, these oligomers were also detected in cell lysates and could be disrupted by RNAse treatment. These data demonstrate that APOBEC3G multimerizes on cellular or viral RNA, and that it is these APOBEC3G multimers, complexed with RNA, that are recruited into developing particles. It makes sense that these A3G complexes represent the enzymatically active enzyme during the reverse transcription process, as they are recruited directly into the viral core that becomes the location for reverse transcription following entry of the virus into a cell.

Under the same experimental conditions in which APOBEC3G-APOBEC3G FRET was detected, and in which Gag-Gag FRET is readily detected, we failed to detect Gag-APOBEC3G FRET. Together with data from Chapter II this indicates that there is not a direct protein-protein interaction between Gag and APOBEC3G in cells or virions. While the unlikely possibility that most of the CFP and YFP tags on Gag and

APOBEC3G are simply held rigidly in a sub-optimal orientation for FRET does exist, the presence of a flexible linker region between both proteins and the fluorescent moieties should have minimized these potential orientation effects (54, 153).

The data in this Chapter, in conjunction with current literature, can be used to refine the structural details of this model. The A3G monomer has recently been modeled after the APOBEC2 homodimer which forms a head-to-head tetramer 127 Å long (159, 205). In agreement with these results, the nanostructure of RNAse treated A3G from cells shows a 140 Å rod approximately 100 kDa in size, indicative of an A3G dimer (190). The fluorophores in these head-to-head dimers would be 180 Å apart, and therefore undetectable by FRET. In the same study the nanostructure of A3G, untreated by RNAse, resembled a cylinder with two rods of A3G dimers packed neatly inside (190). This would place the fluorophores in direct apposition to each other, making this structure visible by FRET. Therefore, the limited structural evidence is in agreement with my analysis that multimeric forms of A3G in complex with RNA are packaged into particles, implying that A3G is packaged as a functional unit no smaller than a tetramer (i.e. 4, 8, or 12 molecules). Supporting this notion was a recent analysis which indicated that the number of A3G molecules packaged into Δ*vif* virions produced from activated human peripheral blood mononuclear cells (PBMC) was between 3 and 11 molecules, suggesting that only one tetrameric A3G complex is actually required per virion for inhibition of replication (197). This enhanced view of my model for A3G packaging makes it clear that even small increases in A3G expression levels would provide significant antiviral properties in a patient. It is interesting that the large size of this A3G complex (~200Å × 100Å) compared to HIV-1 Gag (85Å × 34Å) reinforces the idea that steric forces may

play a big role in the inhibition of A3G packaging by the C-terminal portion of HIV-1 and HTLV-1 Gag molecules (148, 190). Nevertheless, and perhaps as a result of the relatively small number of A3G complexes packaged, their presence does not appear to disrupt particle assembly and seem to generate only subtle differences in virion morphology (11, 76, 149). Taken together, our findings support a model in which APOBEC3G multimers form on RNA species trafficking through the cytoplasm as they are recruited into the developing particle through interactions with NC.

In order to confirm the hypothesis that the plasma membrane is truly a step in the trafficking of A3G multimeric complexes into particles, I decided to microscopically image these A3G complexes as they traffic into particles. Therefore, in Chapter III I developed microscopic techniques to observe this activity.

CHAPTER IV

FLUORESCENT AND FRET IMAGING OF APOBEC3G COMPLEXES RECRUITED TO THE PLASMA MEMBRANE BY HIV-1 GAG

Introduction

The aim of Chapter III was to characterize APOBEC3G (A3G) complexes and A3G-Gag interactions using FRET analysis of whole cells and undisrupted particles. Although a direct A3G-Gag interaction was not detected, A3G-RNA complexes were found to exist in both cells and particles. Due to the fact that HIV-1 particle assembly occurs primarily at the plasma membrane, the next aim of my research was to analyze the recruitment of A3G complexes to the plasma membrane by Gag. Limited immunofluorescent studies were previously performed studying the native localization of A3G (131, 182) and its localization during co-expression of HIV-1 Gag (1, 55). Authors of these studies reported limited co-localization of A3G with Gag. However, recent and more detailed studies of native A3G localization in a variety of cell types suggested that these earlier studies were unable to show correct A3G subcellular localization (192, 193). Furthermore, studies describing the subcellular localization of A3G complexes in the absence and presence of Gag co-expression have been notably absent in the literature. To address this issue, I performed experiments employing a novel fluorescent resonance energy transfer (FRET) assay for the detection of A3G complexes in living cells. In these studies, a CFP donor-YFP acceptor approach to measure A3G-A3G interactions that are within 80 Å of each other (174). Microscopic visualization of FRET was accomplished by imaging the sample using YFP emission filters (527 nm) while stimulating the sample

with a CFP specific laser (405 nm) or filters (433 nm). The existence of FRET between two proteins in a sample was further verified in several cases by photobleaching the acceptor fluorophore (114). Photobleaching destroys the YFP in a FRET sample leading to a decrease in YFP emission, but also a corresponding increase in the CFP emission spectrum. Therefore, although previously FRET fluorometry was used to determine if FRET was occurring, in these experiments FRET microscopy was used to determine the location where a FRET interaction occurs. This approach showed that A3G-A3G multimers are detected in mRNA processing bodies (P-bodies), but additionally at the plasma membrane upon HIV-1 Gag expression.

Materials and Methods

Plasmids, cell lines, and transfections

Plasmids used were described in Chapter II and Chapter III. The human cervix epithelial cell line HeLa was maintained in Dulbecco's modified Eagle medium with 10% fetal bovine serum and antibiotics at 37°C in 5% CO^2, and grown in MatTek tissue culture dishes for live cell imaging or chamber slides for fixation. Transfections were performed with Lipofectamine 2000 (Invitrogen, Carlsbad, Calif.), with 2 μg of total plasmid DNA unless otherwise stated.

Fluorescence microscopic analysis of subcellular localization of A3G-YFP and Gag-CFP

Live HeLa cells expressing A3G-YFP alone or together with Gag-CFP were examined using a Nikon TE2000 equipped with automated filter wheels, stage, z-axis

motor and digital camera. All images were obtained using the 63X objective; serial sectioning was performed using MetaMorph software (Molecular Devices) and deconvolution was performed using constrained iterative algorithms with Autoquant software package. For the images shown in Fig. 8F-H, a digital mirror device (Digital Diaphragm, Photonic Instruments, St. Charles, IL) and 488nm laser was used to specifically photobleach the internal regions of the cell surrounding bright cytoplasmic bodies of A3G-YFP.

Fluorescence microscopic analysis of the subcellular localization of A3G-YFP and A3G-CFP FRET

Live HeLa cells expressing A3G-YFP alone or together with A3G-CFP were examined using the 63X objective on a Nikon TE2000. FRET images were obtained by the sensitized emission method followed by deconvolution with a constrained iterative algorithm (MetaMorph Autoquant software package, Molecular Devices). Briefly, donor and acceptor constants were first generated by the following method. A CFP image and a raw FRET image (CFPexcitation/YFPemission) were obtained from cells expressing Gag-CFP alone, and a YFP image and a raw FRET image were obtained from cells expressing Gag-YFP alone. The pixel intensity in the raw FRET image was divided by the pixel intensity in the corresponding CFP image to yield the donor constant A = 0.78. This was repeated for YFP to yield the acceptor constant B = 0.11. These constants were then used to generate true FRET images from raw FRET images in the following way. Each cell was serially sectioned using MetaMorph software (Molecular Devices) for all three wavelengths (CFP, YFP, raw FRET). A FRET image was then generated for each z-plane using the following formula applied to each pixel: FRET = raw FRET – A*CFP –

B*YFP. Finally, the same deconvoluted z plane was selected for the CFP, YFP, and FRET images and all were treated as follows. MetaMorph imaging software was used to set identical scaling for the YFP and CFP images; scaling of FRET images was set at 50% of the YFP image display value, so that the dimmer FRET images are represented in Fig. 10 with similar intensities as the YFP and CFP images. Each set of 3 images in this figure (CFP/YFP/FRET) was treated in the same manner. Images were colorized as cyan or yellow, exported as RGB TIF files, and converted to CMYK images using Adobe Illustrator.

FRET acceptor photobleaching and spectral analysis using laser confocal fluorescence microscopy

HeLa cells were grown and transfected in cell culture treated chamber slides and imaged following fixation in 4% paraformaldehyde for 10 min. Images were obtained with a Zeiss LSM 510 laser scanning confocal microscope (Carl Zeiss Inc., Thornwood, N.Y.) equipped with a Meta multichannel detector, making pixel intensity quantitation possible over a range of emission wavelengths. Emission scans were obtained by use of Zeiss LSM software following stimulation with a 405 nm laser. The 514 nm laser was used to provide high-intensity pulses of light for photobleaching of YFP to specified regions of interest in the cell. A standard YFP excitation-emission picture was taken before and after the photobleaching.

Results

APOBEC3G is recruited to the plasma membrane by Gag

APOBEC3G has been described as diffuse in the cytoplasm of the cell but has recently been shown to collect in dense cytoplasmic bodies identified as mRNA processing (P) bodies by Wichroski and colleagues (193). We assessed the subcellular localization of APOBEC-YFP using widefield deconvolution fluorescence microscopy. Very bright, punctate collections of A3G-YFP were noted in the cytoplasm of most transfected cells, consistent with the report of Wichroski (Fig. 15A). Under these conditions, diffusely cytoplasmic APOBEC3G could only be visualized under conditions allowing saturation of pixels in P-bodies (Fig. 15B). We observed little evidence of APOBEC3G on the plasma membrane even in these overexposed images. When Gag-CFP was co-expressed with A3G-YFP, a mixed pattern was observed. The most intense A3G-YFP signal was consistently present in P bodies, but a subset of cells demonstrated plasma membrane A3G-YFP signal (leftmost cell in panels 15D, 15E, and 15F). Note that as shown in the two rightmost cells in Fig. 15E, plasma membrane colocalization was not apparent in the majority of cells. When observed, however, the colocalization appeared in bright punctate patterns along the plasma membrane suggestive of sites of particle assembly, as indicated in Fig 15C (a higher magnification view of the cell in Fig. 15E). In many cells in which A3G-YFP was expressed, the extreme brightness of the P body did not allow assessment of potential colocalization with Gag at the plasma membrane. To better examine these cells, we performed laser photobleaching of the interior region surrounding the P bodies, followed by a longer exposure of the remaining

Figure 15. Subcellular localization of Gag and A3G-YFP. A3G-YFP and Gag-CFP were expressed in HeLa cells and visualized by optical sectioning on a Nikon TE2000 microscope equipped with an automated stage and z-axis motor, followed by deconvolution using constrained-iterative algorithms. (A) Bright cytoplasmic collections of A3G-YFP consistent with P body localization. (B) Longer exposure time allowing saturation of P body signal reveals diffuse cytoplasmic A3G-YFP signal. (C) Plasma membrane colocalization of Gag signal (red) and A3G-YFP (green); inset from leftmost cell in Fig. 8F. (D-F) Single channel images and image overlay indicating Gag signal (red), A3G-YFP signal (green). (G-I) Similar technique as in D-F above, but bright collections of A3G-YFP in interior of cell were bleached with 488nm laser to diminish brightness and facilitate visualization of plasma membrane fluorescence.

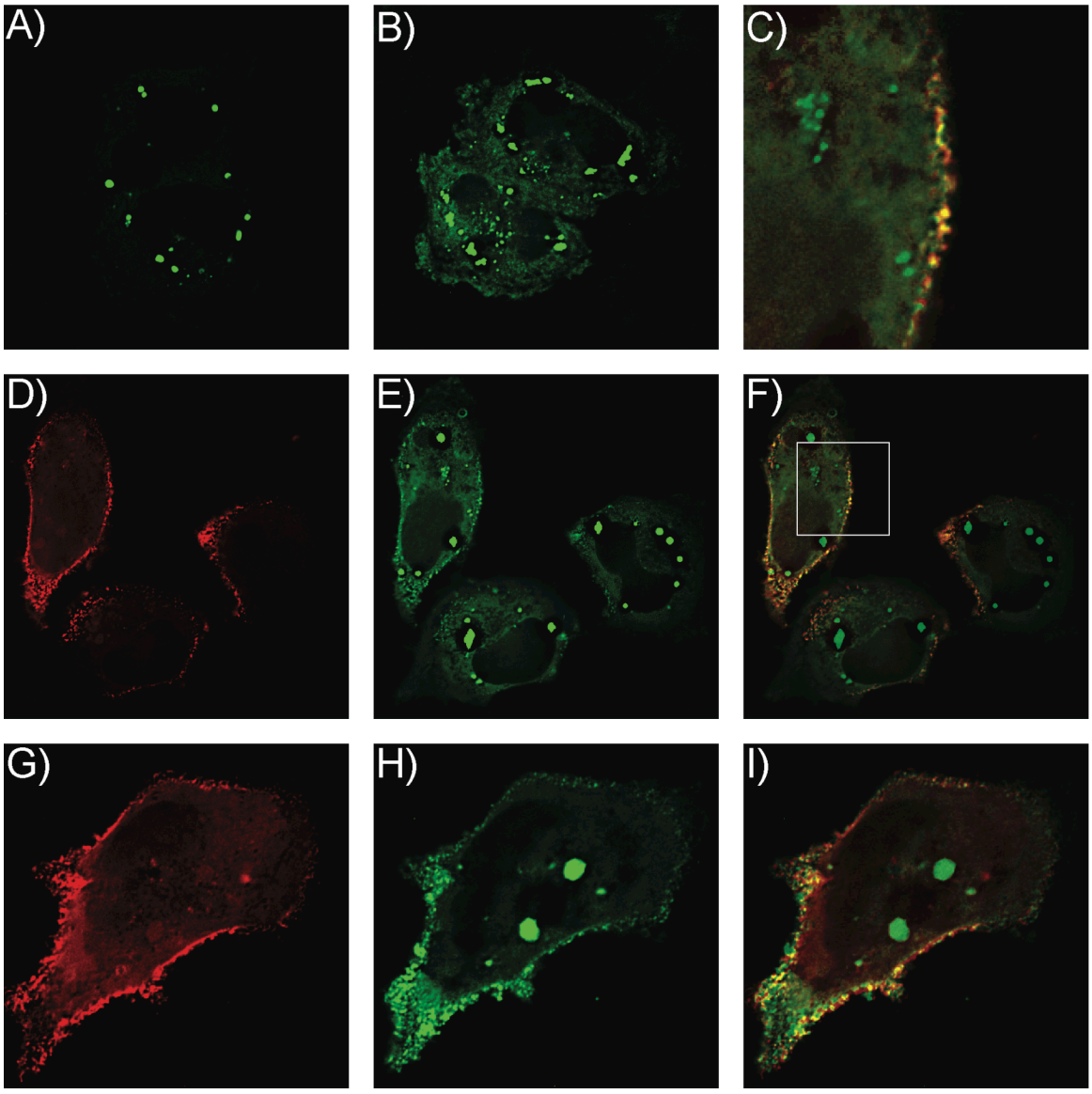
A)
B)
C)
D)
E)
F)
G)
H)
I)

fluorescent signal in the cell. Fig. 15G-I represents one such cell in which Gag-CFP is in red, A3G-YFP is shown in green, and plasma membrane colocalization is demonstrated as yellow pixels in 15H. Note that there is little apparent colocalization of Gag in the P bodies, but there appears to be recruitment of A3G-YFP from the cytoplasm to punctate spots on the plasma membrane. We conclude from these data that although overexpressed A3G-YFP appears most intensely in P bodies, a subset of A3G-YFP is recruited to the plasma membrane where it colocalizes with Gag in the developing particle.

APOBEC3G-APOBEC3G interactions were observed in structures consistent with P bodies by confocal spectral analysis

The laser confocal microscope allows the spectral separation of light emitted from selected pixels when equipped with a multichannel detector. To further establish the presence of A3G-A3G FRET and to determine the localization of this FRET we analyzed the emission spectrum from different regions of the cell before and after photobleaching the A3G-YFP acceptor molecule. If a transfer of energy were occurring between the CFP and YFP molecules, the destruction of YFP absorption by photobleaching would lead to retention of energy by the CFP molecules and an increase in CFP fluorescence. We had used spectral analysis on the Zeiss LSM510 Meta confocal microscope previously to demonstrate the interaction of Gag-CFP and Gag-YFP on the plasma membrane (47). We repeated this analysis, using Gag-CFP and Gag-YFP as positive controls in parallel with our APOBEC test constructs. Briefly, HeLa cells expressing Gag-CFP and Gag-YFP were imaged showing YFP localization before and after bleaching of the YFP at 514 nm (Fig. 16A-B). An emission scan of the cells in 16A-B was performed using excitation of CFP at 405 nm. The spectra from a bleached section of the plasma membrane (region of

Figure 16. Analysis of A3G-A3G interactions by confocal microscopy and fluorescence acceptor photobleaching. (A) Gag-CFP and Gag-YFP were cotransfected in HeLa cells, and images were obtained with a Zeiss LSM 510-Meta confocal microscope. The image represents YFP excitation-emission before photobleaching. The arrows indicate the selected plasma membrane region of interest to be bleached (ROI1) and the control region (ROI2). (B) The same cell as that shown in panel A is depicted following photobleaching at 514 nm in the indicated square. (C) Emission scans were obtained from region of interest 1, with excitation at 405 nm (CFP excitation), before (dashed line) and after (solid line) photobleaching of cells shown in panel A and B. (D) Emission scans were obtained from the control region of interest 2, with excitation at 405 nm, before (dashed line) and after (solid line) photobleaching of cells shown in panel A and B. (E) A3G-CFP and A3G-YFP were cotransfected in HeLa cells and the image shows the distribution of A3G-YFP prior to bleaching. The regions of interest selected are consistent with P body localization. (F) The same cell as that shown in panel E is depicted after photobleaching of the indicated square. (G) Spectra obtained from ROI1 before (dashed line) and after (solid line) photobleaching from cells shown in panel E and F. (H) Spectra obtained from ROI2 before (dashed line) and after (solid line) photobleaching from cells shown in panel E and F. Scale bar represents 10 micrometers.

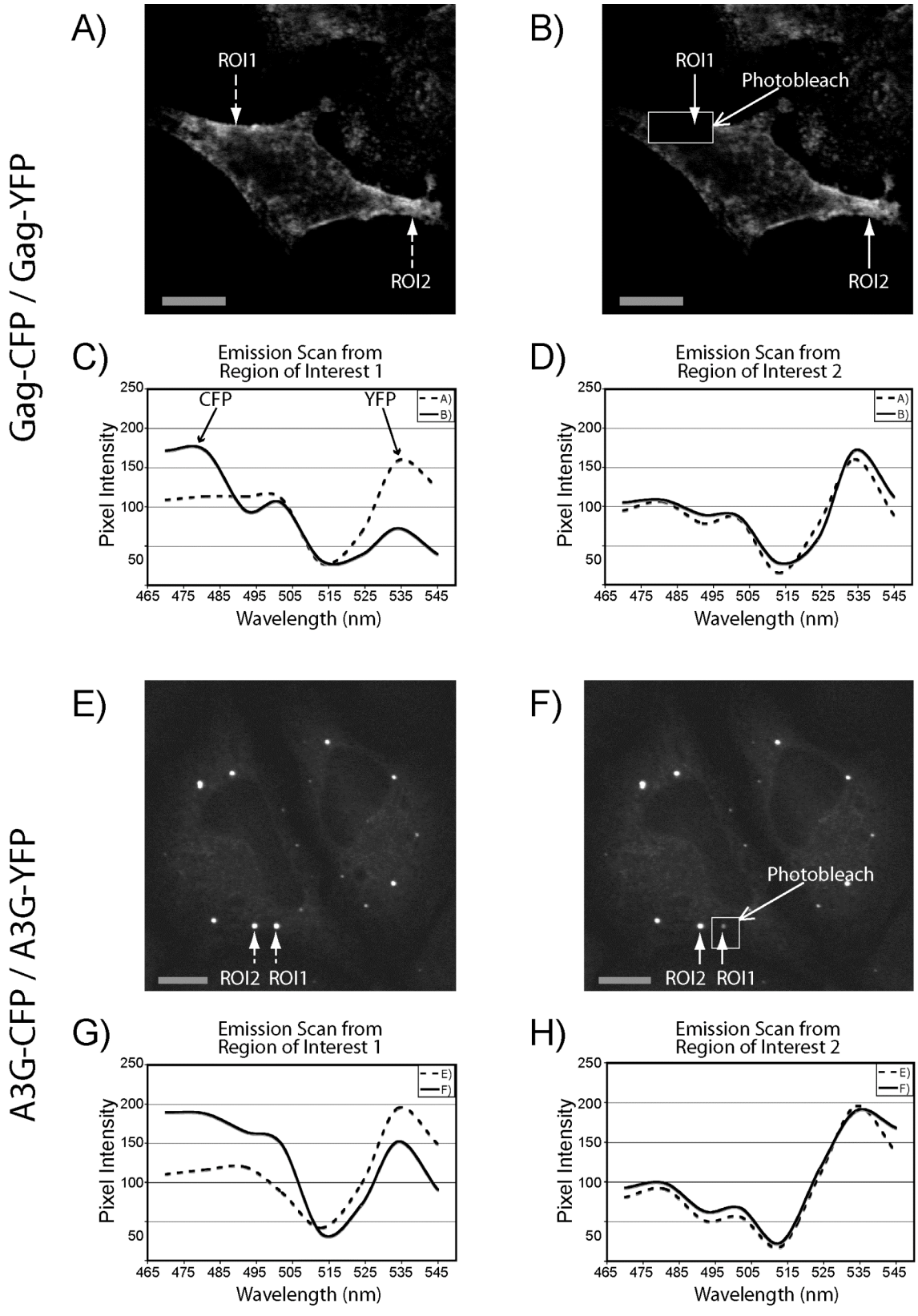
Gag-CFP / Gag-YFP
A3G-CFP / A3G-YFP
A)
ROI1
ROI2
B)
ROI1
Photobleach
ROI2
C)
Emission Scan from
Region of Interest 1
CFP
YFP
A)
B)
Pixel Intensity
250
200
150
100
50
465 475 485 495 505 515 525 535 545
Wavelength (nm)
D)
Emission Scan from
Region of Interest 2
A)
B)
Pixel Intensity
250
200
150
100
50
465 475 485 495 505 515 525 535 545
Wavelength (nm)
E)
ROI2 ROI1
F)
Photobleach
ROI2 ROI1
G)
Emission Scan from
Region of Interest 1
E)
F)
Pixel Intensity
250
200
150
100
50
465 475 485 495 505 515 525 535 545
Wavelength (nm)
H)
Emission Scan from
Region of Interest 2
E)
F)
Pixel Intensity
250
200
150
100
50
465 475 485 495 505 515 525 535 545
Wavelength (nm)

interest 1) revealed that after bleaching, the YFP peak at 530 nm was reduced while the CFP peak at 475 nm increased in fluorescence (Fig. 16C). The emission spectra from a control region of the plasma membrane (region of interest 2) remained unchanged (Fig. 16D). This confirms the existence of FRET between Gag-CFP and Gag-YFP molecules on the plasma membrane. Next, we employed this technique to determine the presence of a FRET interaction between A3G-CFP and A3G-YFP in structures consistent with P body subcellular localization. Figure 16E-F shows the localization of A3G-YFP in these cells before and after bleaching the region of interest 1 (ROI1). The emission spectra from pixels contained within the P body at ROI 1 reveal that the decrease in the YFP peak following bleaching is accompanied by a significant increase in the CFP peak (Fig. 16G). P body pixels in the nearby but unbleached region of interest 2 show unchanged spectra (Fig. H). Bleached cytoplasmic locations close to ROI1 exhibit neither a FRET peak nor an increase in CFP fluorescence following bleaching (data not shown). This confirms that A3G-A3G interactions can be observed by FRET, and occur primarily in P bodies.

APOBEC3G multimers are observed in P bodies and at the plasma membrane following Gag expression

In order to image the subcellular location of A3G-A3G interactions during Gag expression, we next employed FRET microscopy in living cells. Using distinct filter sets, we obtained individual CFP, YFP, and CFP-YFP (FRET) images, and corrected each FRET image for donor bleedthrough and acceptor cross-stimulation using an algorithm as described in Materials and Methods. Obtaining true FRET images using filter sets is complicated, even with the best filters and software algorithms, so we included known

positive controls that were treated identically to the APOBEC3G expression experiments. Controls included HeLa cells expressing Gag-CFP alone (Fig. 17A-C), and cells expressing Gag-YFP alone (Fig. 17D-F). These two negative controls were critical to establish that bleedthrough and cross-stimulation from CFP and YFP respectively can effectively be measured and subtracted from the final FRET image. We next employed this technique to examine the location of FRET in cells expressing Gag-CFP and Gag-YFP. Consistent with findings in Figure 16A-D and our previously published findings (47) Gag-Gag FRET was detected at the plasma membrane and at distinct intracellular puncta (Fig. 17I). Finally, we employed this assay to observe the locations of A3G-A3G FRET with and without Gag expression. Consistent with the results from Figure 16E-H, cells expressing A3G-CFP and A3G-YFP exhibit FRET only in the P bodies (Fig. 17J-L, arrows). However, the expression of Gag together with A3G-CFP and A3G-YFP resulted in detectable FRET signal at the plasma membrane in a subset of cells examined (Fig. 17M-O). This is consistent with a model in which Gag recruits A3G-RNA-A3G multimers to the plasma membrane.

Figure 17. Subcellular localization of A3G-CFP and A3G-YFP FRET. (A-C) CFP, YFP, and FRET images obtained from HeLa cells expressing Gag-CFP (negative control). (D-F) CFP, YFP, and FRET images from cells expressing Gag-YFP (negative control). (G-I) CFP, YFP, and FRET images from cells expressing both Gag-CFP and Gag-YFP. (J-L) CFP, YFP, and FRET images from cells expressing A3G-CFP and A3G-YFP (without Gag). Structures consistent with the subcellular localization of P bodies exhibit FRET. (M-O) CFP, YFP, and FRET images from a cell expressing Gag, A3G-CFP, and A3G-YFP. In addition to P body FRET, plasma membrane FRET and a low level of cytoplasmic FRET is shown. Scale bar represents 10 micrometers.

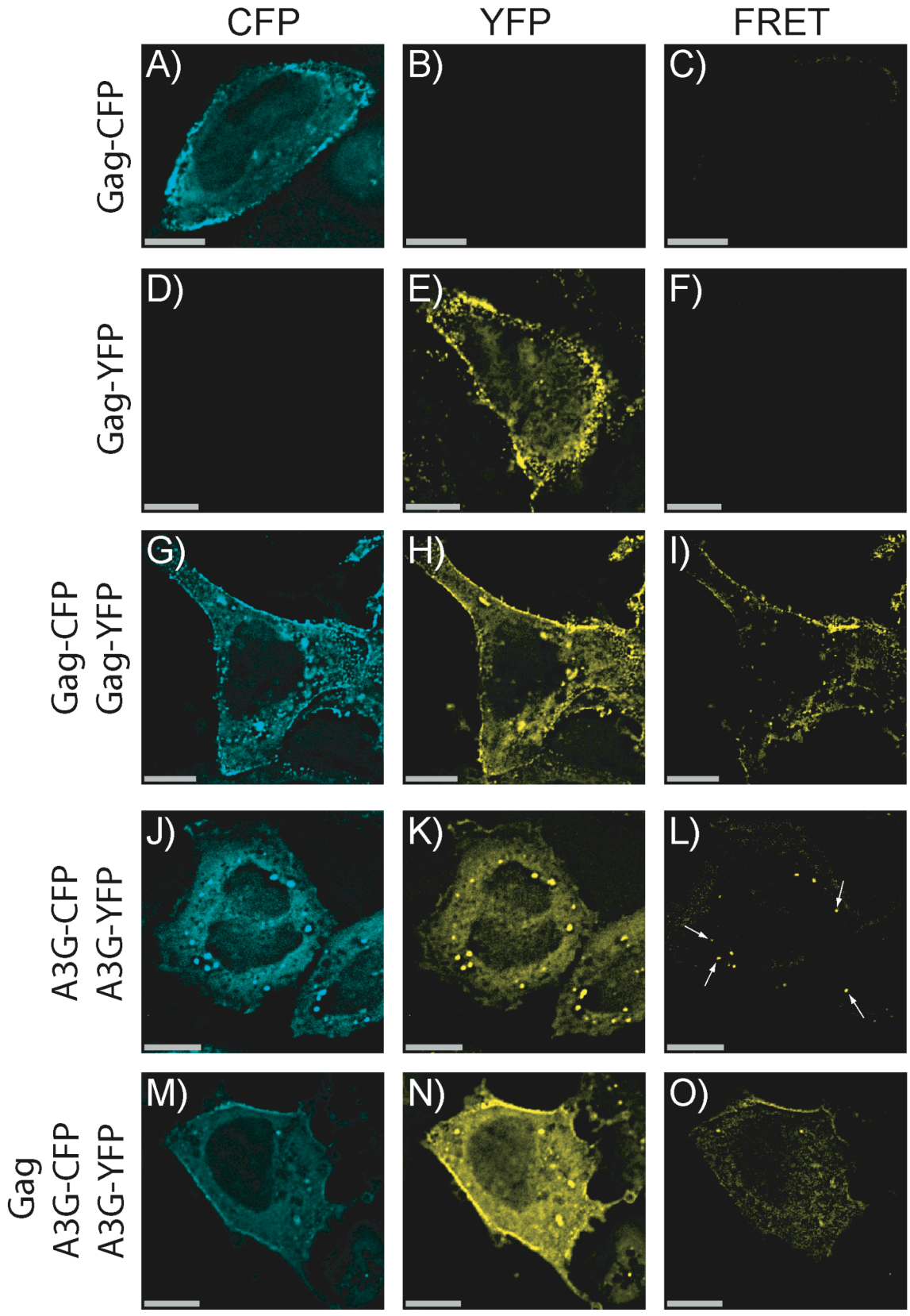
CFP
YFP
FRET
A)
B)
C)
Gag-CFP
D)
E)
F)
Gag-YFP
G)
H)
I)
Gag-CFP
Gag-YFP
J)
K)
L)
A3G-CFP
A3G-YFP
M)
N)
O)
Gag
A3G-CFP
A3G-YFP

Discussion

A unique aspect of this study was the finding that Gag recruits APOBEC3G to the plasma membrane. Three lines of evidence support this finding. First, membrane flotation data indicated a redistribution of APOBEC3G to cellular membranes following Gag expression (Chapter II). Second, APOBEC3G colocalized with Gag at the plasma membrane. Finally, APOBEC3G-RNA-APOBEC3G complexes, which were found predominantly in P bodies in the absence of Gag expression, were detected at the plasma membrane in cells cotransfected with Gag. Recruitment of APOBEC3G to the plasma membrane is somewhat intuitive, since Gag is responsible for the incorporation of RNA and APOBEC3G, and Gag must interact with membranes for intracellular trafficking and budding from the cell. It is tempting to speculate that Gag recruits APOBEC3G at early stages following translation on cytoplasmic ribosomes, in conjunction with viral genomic RNA. In this model, a Gag/RNA/APOBEC3G complex would then traffic along endosomal pathways to the plasma membrane for budding (or to the MVB in the infected macrophage). Despite the attractiveness of this model, we were not able to demonstrate significant colocalization of Gag and APOBEC3G within the cytoplasm of the cell, particularly in the punctate cytoplasmic collections reported by others to be P bodies (192, 193). However, we did note occasional faint colocalization at these sites (data not shown). Colocalization of Gag with APOBEC3G at the plasma membrane was detected, especially in cells in which the intensely bright signal from P bodies was reduced by photobleaching. It is possible that the population of APOBEC3G present in the dense P bodies is itself incorporated into particles, but perhaps more likely that Gag recruits APOBEC3G from the cytoplasmic pool that then multimerizes on the viral RNA. Kozak

et al. recently reported the binding of APOBEC3G to a pool of RNA that reversibly shuttles between polysomes and stress granules (117); it may be this pool that is packaged in the VLP in the absence of HIV genomic RNA. We acknowledge the caveat that the intensity of the signal observed in our microscopic studies result from overexpression of APOBEC3G fused to YFP rather than endogenous APOBEC3G. However, these results are consistent with others who have reported very intense cytoplasmic (P-body) collections of both endogenous and over-expressed APOBEC3G (192, 193).

One important caveat to this study was the difficulty we had observing plasma membrane localization of A3G in each and every cell. Perhaps one reason for this difficulty is the relatively low efficiency of A3G incorporation into particles. One study showed that as little as 3-11 A3G molecules are incorporated into each virion while, by comparison, each budding particle contains between 1500 to 5000 Gag molecules (16, 148, 197). Although it is known that this number can be increased by higher A3G concentrations (24), over-expression in my studies resulted in only 10% of all A3G synthesized by the cell being incorporated into particles (Figure 5B). Therefore, one might expect to find less than 10% of all cellular A3G to be found on the plasma membrane of a cell at any given time point. In fact, other authors have noted similar limitations in their studies (55). Nevertheless, further study is required to determine exactly why more prominent plasma membrane localization of A3G is not found on a higher proportion of cells.

The recruitment of A3G to the plasma membrane by Gag is a significant event because it is necessary for A3G to traffic through this location prior to getting into

particles. In Chapter II I demonstrated that the basic linker region of Gag was critical for causing the recruitment of A3G to all cellular membranes. The experiments in this chapter were necessary to show that this recruitment could be observed specifically at the plasma membrane. Although this effect was not demonstrated for the whole panel of Gag mutants, the biochemical data indicate that constructs lacking basic linker region of Gag would not recruit any more A3G to the plasma membrane than the negative control. The most important way in which these findings extend our understanding of A3G function is a determination of the location of A3G multimeric complexes during particle assembly. The discovery in Chapter III that this multimeric form of A3G represents the population packaged into particles indicates the importance of the intracellular trafficking of this form of A3G. My experiments showed that these complexes are observed at the plasma membrane along with Gag, demonstrating that A3G multimerize onto RNA at the plasma membrane or prior to trafficking to the plasma membrane. However, further studies need to be conducted to determine where in the cell multimerization takes place, whether it occurs on RNA species before or after they are bound to Gag, and the exact function that A3G multimerization plays in facilitating its antiviral properties.

CHAPTER V

CELLULAR TRAFFICKING OF HIV-1 GENOMIC RNA

Introduction

HIV genomic RNA molecules are synthesized in the nucleus but travel to sites of virus assembly following nuclear export through the Chromosome Region Maintenance 1 (Crm1) mediated pathway (9, 198). The nucleocapsid (NC) region of the HIV-1 Gag molecule specifically binds to the genomic RNA, facilitating its packaging into virus particles. However, the route taken by HIV RNA to the plasma membrane, and the specific role that Gag plays in its trafficking is not understood. Certain outstanding and important questions remain, for example: Does Gag bind to genomic RNA prior to its arrival at the plasma membrane? Where does this initial interaction between Gag and genomic HIV RNA take place? Which steps of RNA trafficking to the plasma membrane require Gag, and which steps are Gag-independent? In order to answer these questions, it is necessary to physically observe the microscopic subcellular localization of HIV genomic RNA as it moves from the nucleus to the plasma membrane, and compare it to the subcellular localization of Gag as assembly takes place. One way these experimental goals can be accomplished by using the MS2 RNA labeling system, which involves the fluorescent labeling of genomic viral RNA during HIV assembly (12).

MS2 is a bacteriophage with an RNA genome, which is packaged into phage particles through binding of the MS2 coat protein to an RNA stem-loop binding site (154). Therefore, the MS2 system which is used for the fluorescent labeling of RNA

contains two components: 1) a non-dimerizing MS2 coat protein fused to a fluorescent molecule (example: GFP) and a nuclear localization signal (NLS), 2) the RNA of interest (reporter RNA) fused to several repeats of the RNA-binding site for the MS2 coat protein (4, 7, 21, 58, 96, 162, 203). Expression of the MS2-GFP-NLS (component 1) produces an intense nuclear fluorescence. However, co-expression of both constructs should cause some of the MS2-GFP-NLS to be transported into the cytoplasm together with the reporter RNA. As a result, reporter RNA trafficking can be examined by following cytoplasmic fluorescence. The experiments described in this chapter focus on the development and characterization of such a system designed to observe the export, trafficking, and encapsidation of HIV genomic RNA into virus particles. The components of the system involves the MS2 coat protein fused to several different fluorescent proteins, and the MS2 RNA stem loops fused to both the LTR driven NL4-3 provirus and a CMV driven RNA species used as an over-expression positive control.

Materials and Methods

Plasmid Construction

The fluorescent tag fusion protein plasmids were created in three steps. The MS2 coat protein was first cloned into pcDNA3.1, each fluoroscent protein (FP) was then cloned into pcDNA3.1 with an adjoining NLS, and finally each FP-NLS sequence was transferred into the plasmid containing the MS2 coat protein. Specifically, PCR cloning was used to amplify the MS2 coat protein gene from the polII-MS2-YFP plasmid (received from the Singer lab via Richard Sutton) by placing a BamHI site prior to the 5'

ATG and an XhoI site at the 3' end. The amplified MS2 gene was then ligated into pcDNA3.1 to yield a new construct designated pMS2. The oligonucleotides used in the PCR amplifications were AGGATCCATGGCTTCTAAC-(F) and TCTCGAGGTAGATGCCGGA-(R). PCR cloning was then used to amplify the mCherry, mOrange, Venus, and Cerulean genes by placing an XhoI site prior to the 5' ATG and an XbaI-SV40 NLS sequence at the 3' end. The amplified fluorescent protein genes were then ligated into pcDNA3.1 to yield new constructs designated mCherry-NLS, mOrange-NLS, Venus-NLS, and Cerulean-NLS respectively. The oligonucleotides used in the PCR amplifications were ACTCGAGATGGTGAGCAAG-(F) and TTCTAGATTATACCTTTCTCTTCTTTTTTGGCATCTTGTACAGCTCGTC-(R). Finally, the fluorescent protein sequences were extracted from the Fluorescent Protein-NLS plasmids by restriction digestion of the XhoI and XbaI sites flanking these genes. The purified products were then ligated into the pMS2 vector creating the constructs termed MS2-Cherry-NLS, MS2-Orange-NLS, MS2-Venus-NLS, and MS2-Ceru-NLS. These constructs were verified by restriction digest of selected clones.

The MS2-PAGFP-NLS construct was created by a modification of the strategy described above. Briefly, PCR cloning was used to amplify the photoactivatable green fluorescent protein (PAGFP) gene by placing an XhoI site prior to the 5' ATG and an XbaI-SV40 NLS sequence at the 3' end as described above. The amplified fluorescent protein gene was then ligated directly into the pMS2 vector creating the construct termed MS2-PAGFP.

The mCherry(-) construct was created by using PCR cloning to amplify the mCherry gene by placing an XhoI site prior to the 5' ATG and a NotI site at the 3' end.

The amplified fluorescent protein gene was then ligated into pcDNA3.1(-) and verified by restriction digest of selected clones. The oligonucleotides used in PCR amplifications were ACTCGAGATGGTGAGCAAG-(F) and GAGTCGCGGCCGCTTTACTTGTACAGCTCGTCCATGCCG-(R).

The Cherry-6X and Cherry-6Xa constructs were created by the following strategy. First, the mCherry(-) plasmid was digested with BamHI and purified. Six MS2 stem loops were then extracted from the MS2-6X plasmid (obtained from the Singer lab through Gary Bassell) by digestion with BamHI and BglII, followed by a gel purification step. The stem loops were then ligated into mCherry(-) creating two possible orientations: The forward orientation termed Cherry-6X, and the reverse orientation termed Cherry-6Xa. Both constructs were digested with BamHI and purified. Six MS2 stem loops were again extracted from the MS2-6X plasmid by digestion with BamHI and BglII, followed by a gel purification step. The stem loops were then ligated into both the Cherry-6X and Cherry-6Xa plasmids, creating two possible orientations for each: The forward orientation of the six additional stem loops in Cherry-6X created the construct termed Cherry-12X, while the reverse orientation of the six additional stem loops in Cherry-6Xa created the construct termed Cherry-12Xa.

Creation of NL4-3ΔEnv-6X and NL4-3ΔEnv-12X occurred in four steps. First, the NotI and EcoRI sites flanking the 1020 XbaI site in pEYFP were digested, the overhangs were filled in using Klenow polymerase, and the blunt ends were then ligated to create the pEYFPΔXba transfer vector. Secondly, the mCherry sequence was eliminated from Cherry-6Xa and Cherry-12Xa by digestion with XhoI and EcoRI, the overhangs were filled in using Klenow polymerase, and the blunt ends were then ligated

to create pc6Xa and pc12Xa. Next, the pEYFPΔXba construct was digested with XbaI and BamHI and purified. Stem-loop sequences in pc6Xa and pc12Xa were extracted by digestion with NheI and BamHI. These stem-loops were then ligated into pEYFPΔXba creating p6Xa-EYFP and p12Xa-EYFP. Finally, NL4-3ΔEnv was digested with AgeI and SbfI and purified, eliminating a 640 bp region of RT. Stem loop sequences were then extracted from p6Xa-EYFP and p12Xa-EYFP by digestion with AgeI and SbfI, and then ligated into NL4-3ΔEnv creating the constructs NL4-3ΔEnv-6X and NL4-3ΔEnv-12X.

Cell lines, and transfections

The human cervix epithelial cell line HeLa was maintained in Dulbecco's modified Eagle medium with 10% fetal bovine serum and antibiotics at 37°C in 5% CO^2, and grown in MatTek tissue culture dishes for live cell imaging or chamber slides for fixation. Transfections were performed with Lipofectamine 2000 (Invitrogen, Carlsbad, Calif.), using 2 μg of total plasmid DNA unless otherwise stated.

Fluorescence microscopic analysis

Live HeLa cells were examined using a Nikon TE2000 equipped with automated filter wheels, stage, z-axis motor and digital camera. All images were obtained using the 63X objective.

Results

Experimental strategy and constructs

In order to track the movement of the reporter RNAs from the nucleus to the cytoplasm, I created five MS2-fluorescent tags to label the RNA, and we obtained one MS2-fluorescent tag protein, polII-MS2-YFP, from the Singer Lab. Figure 18A schematically depicts the structure of these fusion proteins, and they are listed in Table 1 as follows: 1) polII-MS2-YFP, 2) MS2- PAGFP-NLS, 3) MS2-Ceru-NLS, 4) MS2-Venus-NLS, 5) MS2-Cherry-NLS, and 6) MS2-Orange-NLS. The polII-MS2-YFP construct was obtained first and therefore used in the initial experiments. The photoactivatable GFP – MS2 fusion protein (MS2-PAGFP-NLS) was created to pulse label nuclear proteins and observe the egress of RNA that occurs only after the nuclear labeling event. The Venus and Cerulean - MS2 fusion proteins were created to look at FRET interactions between RNA and Gag, while the mCherry and mOrange - MS2 fusion proteins were created to provide a selection of alternative colors for visualizing RNA export. Data will be presented in the following section for polII-MS2-YFP, MS2-PAGFP-NLS, and MS2-Cherry-NLS.

The second part of the system consists of a series of two over-expression RNAs, and two modified retroviral RNAs engineered to contain the MS2 binding sites, termed Cherry-6X, Cherry-12X, NL4-3ΔEnv-6X, and NL4-3ΔEnv-12X respectively. Finally, one overexpression RNA lacking MS2 binding sites was created as a negative control, termed Cherry(-). Figure 18B schematically depicts Cherry-6X, while Figure 18C schematically depicts NL4-3ΔEnv-6X. Cherry-12X and NL4-3ΔEnv-12X contain 12 MS2 binding site

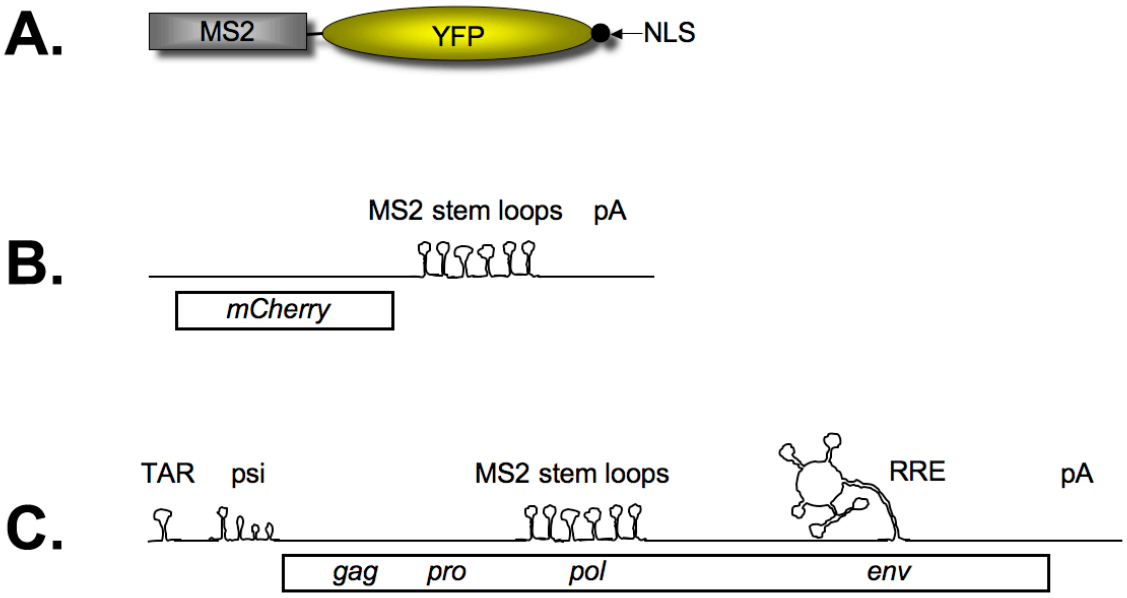

Figure 18. A system for real time RNA tracking using MS2-fluorescent protein labeling. (A) Schematic depiction of an MS2-YFP-NLS fusion protein. Several versions with different fluorescent moieties have been constructed and are listed in Table 1. (B) Schematic depiction of the positive control, Cherry-6X reporter RNA. RNA secondary structures are listed above, open reading frames are listed below. (C) Schematic depiction of the NL4-3ΔEnv-6X reporter RNA. RNA secondary structures are listed above, open reading frames are listed below.

Table 1. Reporter RNA and fluorescent tag constructs for live cell RNA imaging.

Name	Description
polII-MS2-YFP	Obtained from Singer lab via Dr. Sutton. Contains a polII promoter and an MS2-YFP-NLS fusion protein.
MS2-PAGFP-NLS (Photoactivatable GFP)	Identical to Fig. 18A except the fluorescent moiety is the photoactivatable green fluorescent protein. MS2-PAGFP-NLS is designed to be exported from the nucleus when attached to a reporter RNA to allow cytoplasmic visualization of subcellular RNA trafficking. Photoactivation allows pulse-chase experiments to eliminate potential widespread background fluorescence.
MS2-Ceru-NLS	Identical to Fig. 18A except the fluorescent moiety is the Cerulean version of the cyan fluorescent protein. MS2-Ceru-NLS is designed to be exported from the nucleus when attached to a reporter RNA to allow cytoplasmic visualization of subcellular RNA trafficking.
MS2-Venus-NLS	Identical to Fig. 18A except the fluorescent moiety is the Venus version of the yellow fluorescent protein. Designed to be used as above.
MS2-Cherry-NLS	Identical to Fig. 18A except the fluorescent moiety is the mCherry fluorescent protein. Designed to be used as above.
MS2-Orange-NLS	Identical to Fig. 18A except the fluorescent moiety is the mOrange fluorescent protein. Designed to be used as above.
Cherry-6X	Identical to Fig. 18B. Cherry-6X is designed to express soluble cytoplasmic mCherry as a marker for reporter RNA expression.
Cherry-12X	Identical to Fig. 18B except 12 stem loop repeats are used instead of 6. Designed to be used as above.
mCherry(-)	Contains the mCherry sequence cloned into pcDNA3.1(-). Used to create the Cherry-6X and Cherry-12X constructs.
NL4-3ΔEnv-6X	Identical to Fig. 18C. This construct contains a premature stop codon in *env* for safe handling. Designed to produce a retroviral HIV reporter RNA that can be tagged and followed as it traffics to sites of assembly.
NL4-3ΔEnv-12X	Identical to Fig. 18C except 12 stem loop repeats are used instead of 6. Designed to be used as described above.

stem loops but are otherwise identical to the depictions in Figure 18B and 18C respectively. These reporter RNAs are listed in Table 1. In the Cherry overexpression reporter RNA constructs the MS2 binding site stem loops were engineered between the mCherry stop codon and the polyadenylation sequence (Figure 18B). These constructs allow the selection of cells for microscopic analysis in which reporter RNA expression can be confirmed by observing mCherry fluorescence. The retroviral RNA reporter constructs actually contain several RNA secondary structures both naturally occurring and artificially engineered. TAR, psi, and the RRE occur naturally in all HIV-1 and their functions are reviewed in Chapter I. However, in these retroviral RNA reporter constructs, the MS2 binding sites replace a large section of the RT gene, which ensures that only full length genomic RNA will be fluorescently labeled. In the following section data will be presented on the Cherry-6X construct.

Characterization of the MS2 RNA tracking system involves verifying three main functions. First, the MS2-fluorescent tags should localize exclusively to the nucleus when expressed alone. Secondly, co-expression of the MS2-fluorescent tags with the positive control reporter RNA containing the MS2 binding sites should produce export of the MS2-fluorescent tags into the cytoplasm. Finally, co-expression of the MS2-fluorescent tags with the retroviral reporter RNA containing the MS2 binding sites should produce export of the MS2-fluorescent tags into the cytoplasm and ultimately to sites of retroviral assembly such as the plasma membrane. Therefore, the ability of this system to accurately track the movement of retroviral RNA from the nucleus and into particles will be assessed based on these parameters.

MS2-Fluorescent tags localize to the nucleus

The localization of the MS2-fluorescent tags to the nucleus was tested by the independent expression of each construct in a human osteosarcoma cell line (Hos). Expression of MS2-PAGFP-NLS yielded a very low signal (Figure 19A) that was significantly enhanced by photoactivation of the whole cell (Figure 19B). The activated GFP signal was localized predominantly to the nucleus. Expression of polII-MS2-YFP and MS2-Cherry-NLS in Hos cells also showed a predominantly nuclear localization (Figure 19C and D respectively).

MS2-Fluorescent tags localize to the cytoplasm upon reporter RNA expression

Subcellular localization of the MS2-fluorescent tags to the cytoplasm was tested by co- expression of polII-MS2-YFP with Cherry-12X. Expression of polII-MS2-YFP with the negative control mCherry(-) produces an exclusively nuclear localization identical to independent expression of polII-MS2-YFP (Figure 20A). However, expression of polII-MS2-YFP simultaneously with Cherry-6X produces an intense diffuse cytoplasmic localization of the fluorescent tag consistent with the expected localization of diffuse cellular RNA (Figure 20B). Similar results were obtained when using MS2-Venus-NLS (C – D) and MS2-Ceru-NLS (E – F). This data indicates that the MS2-fluorescent fusion proteins bind to the stem loop elements and thus get exported into the cytoplasm.

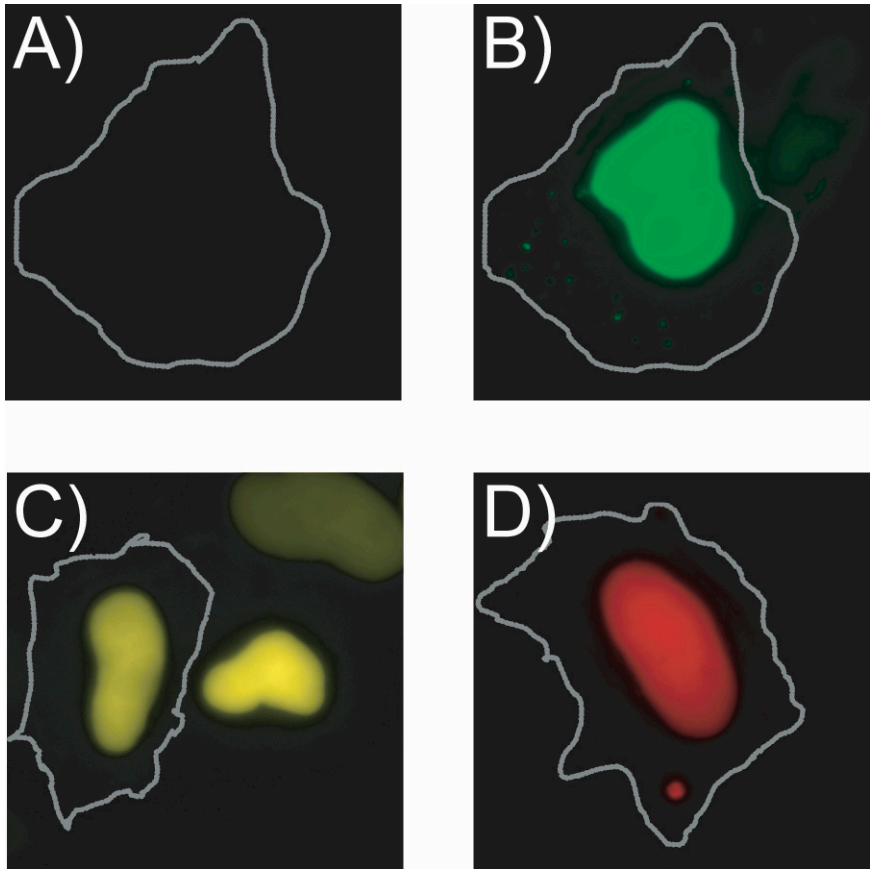

Figure 19. MS2-fluorescent molecules localize to the nucleus. (A) MS2-PAGFP-NLS expression prior to photoactivation. (B) MS2-PAGFP-NLS has a nuclear localization after photoactivation. (C) polII-MS2-YFP and (D) MS2-Cherry-NLS exhibit nuclear localization when expressed alone.

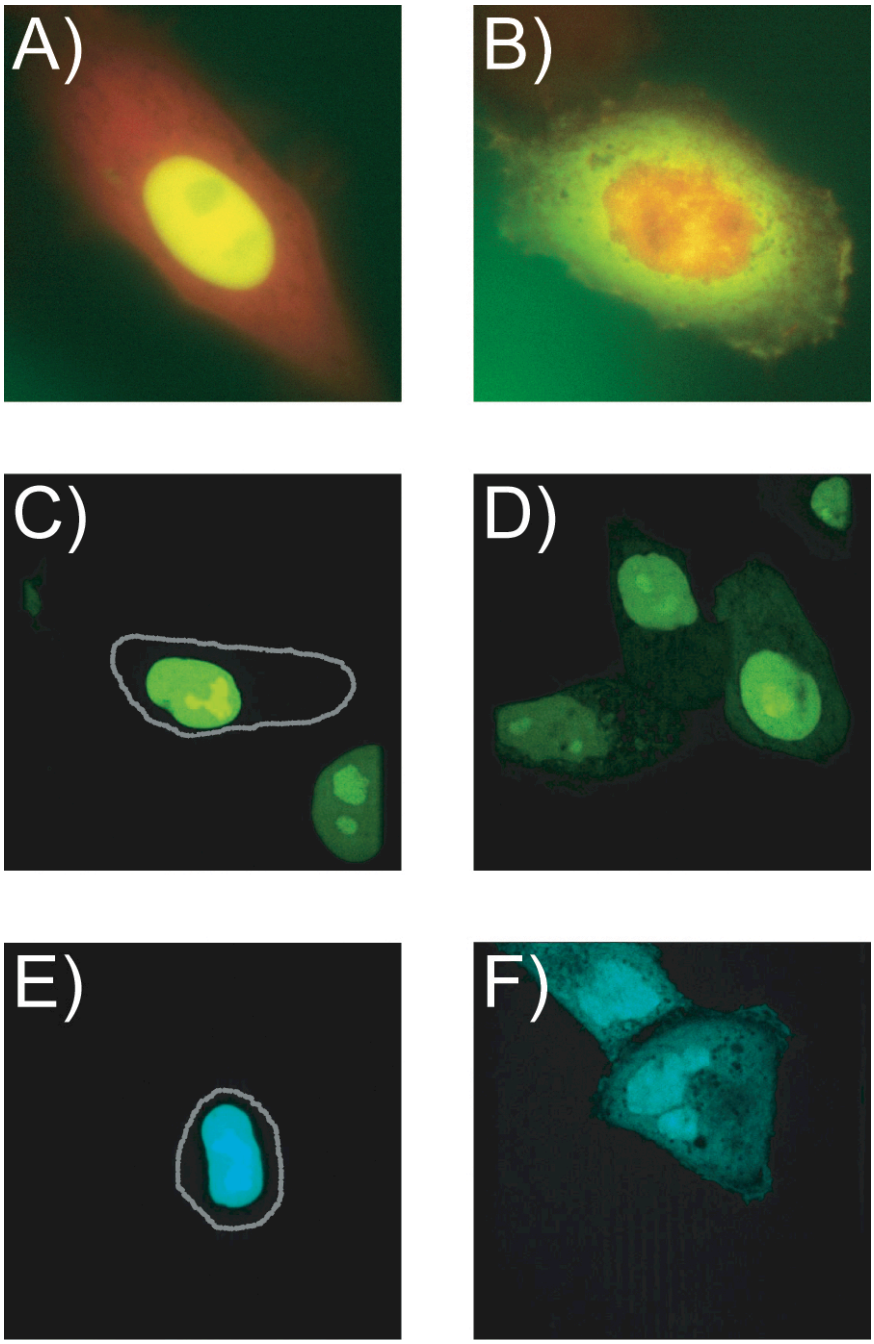

Figure 20. MS2-fluorescent molecules are exported from the nucleus by reporter RNA. (A) PolII-MS2-YFP, (C) MS2-Venus-NLS, and (E) MS2-Ceru-NLS are retained in the nucleus when co-expressed with Cherry(-). (B) PolII-MS2-YFP, (D) MS2-Venus-NLS, and (F) MS2-Ceru-NLS are exported into the cytoplasm when co-expressed with Cherry-6X.

Localization of MS2-Fluorescent tags to sites of assembly upon retroviral reporter RNA expression

NL4-3ΔEnv-6X and NL4-3ΔEnv-12X are in the final stage of cloning. This project is currently being continued by others in the Spearman lab.

Discussion

A major gap exists in the field of HIV relating to the events that take place after genomic RNA leaves the nucleus. In fact, without correct trafficking and incorporation of the virus' genetic material, viral particles would be completely incapable of infecting new cells. Therefore, understanding the fundamental nature of how viral genomic RNA travels to sites of assembly is critical to our understanding of how, ultimately, to disrupt this process.

Several obstacles present themselves traditionally when trying to determine the viral genomic egress pathway. First, biochemical studies that fractionate whole populations of cells lose the precise information gained from observing a single cell. Secondly, biochemical fractionation studies are also not precise enough to separate multiple and overlapping subcellular compartments while maintaining native protein-protein interactions. Thirdly, although the application of microscopic techniques to protein trafficking studies has been greatly facilitated by the use of fluorescent fusion proteins as illustrated in Chapters II - IV, a similar technique to label RNA in live cells has not been available as in-situ RNA hybridization techniques are primarily used to microscopically image cellular RNA in fixed samples. A technique that has emerged recently as another novel method of imaging RNA movement in live cells is the use of a molecular beacon conjugated to an oligonucleotide probe that allows the visualization of

only hybridized probes (15, 134, 135, 166). However, we chose to pursue the development of the two-part MS2-fluorescent labeling system for RNA visualization. This new and exciting technique provides several advantages that overcome many of the limitations noted above. First, this approach can be used in living cells and is easily adapted to DNA transfection techniques. Secondly, this technique can be used to observe a single RNA molecule moving in single cell, providing precise information about RNA localization at specific time points. Lastly, it lends itself to the imaging of RNA as it moves through overlapping subcellular compartments, provided the correct subcellular markers are employed. Therefore, the data presented here provide the framework for a tractable system that can be used to determine detailed steps in the trafficking and assembly of retroviral RNA.

The MS2-fluorescent protein RNA tracking system is not without its limitations however. Two of the most significant but contradictory limitations are nuclear leakiness to MS2 fusion proteins, and the artificial nuclear retention of labeled RNA due to the attachment of multiple NLS to its secondary structure. MS2 fusion proteins can leak into the cytoplasm during cell death and nuclear disintegration, therefore, keeping cells alive is an important consideration. However, the photoactivatable GFP fused MS2 construct was created to circumvent this potential problem. By activating in the nucleus only, background fluorescence is eliminated. The second issue, the retention of retroviral RNA in the nucleus is a more complicated problem. However, we have already established the efficient export of the over-expression reporter RNAs during robust polII-MS2-YFP expression. A final potential limitation is that the RNA stem loops must be artificially engineered into the RNA of interest which may cause unforeseen artifacts in RNA

behavior. Nevertheless, based on the data presented here, the use of this system to study HIV-1 genomic RNA trafficking will provide invaluable insights into this aspect of virus biology.

CHAPTER VI

SUMMARY AND FUTURE DIRECTIONS

Summary

HIV-1 genomic RNA performs diverse and important functions during the virus life cycle. Some of these benefit the virus, while others inadvertently benefit the host. Interestingly, unrelated cellular RNA can perform many functions performed by genomic viral RNA, because for many functions specific viral sequences are not required. As a result, the study of processes that require RNA (either viral or unrelated) have been hindered by the ubiquitous nature of cellular RNA during virus assembly. One potential viral RNA-independent function is the incorporation of a particular cellular RNA-binding protein into virus particles. This cellular protein, APOBEC3G, exhibits potent anti-viral properties that are dependent upon its ability to be packaged into virus particles. The specific mechanism of APOBEC3G packaging into virus particles was of great interest to us given the possible involvement of RNA in this phenomenon. Consequently, the overall goal of this project was the study of RNA involvement in HIV assembly, but specifically, to determine the extent of RNA involvement in the packaging of APOBEC3G into virus particles.

Our initial studies determined that A3G is packaged into Gag virus-like particles, proving that Gag is responsible for A3G packaging (Figure 5). Furthermore, using a GST co-sedimentation assay I showed that A3G from cell lysates interacted with NC but only in the presence of RNA (Figure 10). I was surprised to discover, however, that the NC

region responsible for causing A3G packaging was the basic linker region and not the N-terminal I domain (Figure 7). Therefore, to confirm these findings, we purified cell membranes and used fluorometry to quantitatively determine that the NC basic linker region was also responsible for causing a redistribution of A3G to cellular membranes (Figure 9). To explore the hypothesis that RNA binding was the underlying mechanism governing A3G packaging I examined the RNA content of these mutant Gag particles. My data confirmed that constructs containing the basic linker region also packaged significantly increased amounts of RNA (Figure 8A). The importance of the basic linker region of NC in causing the packaging of both RNA and A3G indicate that they may be packaged together as part of a multimeric complex.

The intermolecular relationship of A3G molecules bound to RNA was examined in particles using a FRET assay. I first established that both whole cells and cell lysates showed the presence of multimeric A3G complexes that could be disrupted with the application of RNAse. I next applied FRET to A3G molecules contained within virus-like particles, demonstrating that A3G is packaged into Gag VLPs as a multimeric A3G-RNA complex (Figure 13E-F). Finally, I attempted to use the FRET assay to detect direct Gag-A3G interactions by co-expressing Gag-CFP and A3G-YFP in 293T cells. However, the examination of both cells and particles yielded no detectable Gag-A3G interaction by FRET (Figure 14). Taken together, these studies demonstrate that multimeric A3G complexes, containing RNA, are associated indirectly with Gag through an RNA interaction.

I next wanted to observe the subcellular distribution of multimeric A3G complexes during the process of VLP production. Using fluorescent microscopic analysis

I first identified cells with prominent plasma membrane Gag-CFP patterns that had colocalization with A3G-YFP at the plasma membrane (Figure 15C-F). Next, using the FRET spectral analysis technique of acceptor photobleaching, I determined that A3G located in the cytoplasm was either monomeric or dimeric, while A3G located in P-Body structures was multimeric (Figure 16). In a complementary technique, FRET images of A3G were acquired using specific emission filters and digital image correction. Images of A3G expression without Gag using this assay also showed A3G FRET exclusively in P-Bodies, confirming our earlier results. However, co-expression of Gag in these cells caused a visible redistribution of A3G complexes to the plasma membrane in several cells that we observed (Figure 17). These data suggest that Gag causes the redistribution of A3G complexes to the plasma membrane and into particles during Gag expression as a result of an RNA mediated association of A3G complexes with the basic linker region NC.

Finally, to explore other roles that viral RNA may play during HIV infection, we have proposed the development of a method to observe genomic HIV RNA in cells. To this end, we developed and characterized several tools to accomplish this task. Essentially, viral and cellular reporter RNA were engineered to contain binding sites for the bacteriophage MS2 coat protein. The MS2 coat protein was then fused to fluorescent proteins and an NLS element. Co-transfection of this two-plasmid system allowed us to observe the export of reporter RNA molecules into the cytoplasm (Figure 20). This work lays the foundation for a system that can eventually become a powerful tool for the study of retroviral RNA functions during HIV assembly.

RNA Involvement In A3G Packaging

The ability to bind and edit RNA is a surprisingly ubiquitous ability present in many different species. In bacteria, cytidine to uridine deamination serves mainly a metabolic function; however, genera ranging from trypanosomes to plants use this technique in addition to other base changes, insertion of bases, and deletion of bases to extensively change the information content of their mRNAs (5, 8, 93, 111). In many plants, cytidine deaminations are sequence specific edits that are especially pronounced in the correction of mitochondria and chloroplast mRNA sequences (38, 90, 102, 128, 172). Interestingly, the use of this type of editing to create mRNA information appears to be much less prevalent in vertebrates. Nevertheless, Cytidine to Uridine editing is responsible for creating the transfer RNA for glycine in marsupials and the mRNA for apolipoprotein B in mammals (25, 109, 158, 183). In addition, a related type of editing, adenosine to inosine editing, has been found to occur in the pre-mRNA of ion channels, neurotransmitter receptors, and transfer RNA (20, 82, 139, 156). Recently, the discovery was made that a specific cytidine deaminase enzyme, activation-induced cytidine deaminase (AID), was responsible for causing widespread hypermuation of somatic B cell DNA during antibody maturation and class switching in vertebrates (145, 146, 161). This manifestation of permanent, non-sequence specific, and prolific changes to the genetic code is in contrast to previously described cytidine deaminase enzymes which conduct a limited number of sequences specific changes to relatively temporary RNA molecules. In a second drastic paradigm shift in our understanding of the roles that Cytidine to Uridine editing plays in biology, it was discovered that the APOBEC3 proteins lethally hypermutate the genetic cDNA of invading retroviruses (176). The

studies in this thesis help to demonstrate the unique and interesting role that RNA binding plays in the targeting of antiviral activity towards retroviral genomes.

APOBEC3G, and subsequently 3F, are the first proteins described that deliberately induce genetic mutation in a parasite as an effector mechanism of the innate immune system. These fascinating proteins are reminiscent of bacterial innate defense proteins called restriction modification systems (RM), which defend bacterial cells by targeting invading bacteriophage DNA for destruction by endonuclease activity. Two important characteristics of both of these innate immune systems are the method by which self and non-self nucleic acids are differentiated, and the effector mechanisms that mediate destruction of the pathogen. For RM systems self-DNA is methylated, therefore, restriction is only performed on non-methylated viral DNA. In contrast, the targeting system that enables APOBEC3 enzymes to differentiate between self-DNA and retroviral DNA was not known when these studies were initiated. In this thesis I show that A3G is targeted to cellular RNA molecules. However, several studies have shown that A3G only lethally mutates ssDNA that is produced using these RNA as a template. Since DNA is never produced from cellular RNA molecules A3G is harmless towards cellular nucleic acids. A3G is, however, uniquely targeted towards the retroviral genome whose RNA is converted to ssDNA soon after infection of a cell during reverse transcription. This process would require the A3G molecules to travel with viral RNA into the virus particles and eventually into the target cell cytoplasm where reverse transcription occurs. In fact, this provides an explanation for why A3G must become incorporated into virus particles to function, a major question in the field. Therefore, the studies presented in this thesis help to explain how the RNA binding properties of A3G help target its mutagenesis

specifically to retroviral DNA, and as a result explain how and why A3G must become incorporated into virus particles to function correctly. While the mechanisms of innate immunity described here for A3G represent a deviation from the traditional context of cytidine deaminase enzymes as creators of temporary mRNA information, this deviation has opened up a fascinating and unexpected field of research in the role of these hypermutation enzymes as a type of mammalian innate immunity against retroviruses.

The retroviral RNA genome is believed to also function as a catalyst for the assembly of retroviral particles. Several assembly functions, believed to be mediated by RNA, have been mapped to two interaction (or "I") domains located within the NC region of Gag (14). Basic residues within the N-terminal I domain are sufficient for causing Gag-Gag multimerization, Gag-membrane binding, and the formation of particles of proper retroviral density (164, 165). In light of these preceding studies I was surprised to discover that the NC region that was critical for causing A3G packaging required the inclusion of the basic linker region but not the N-terminal I domain acting alone. This was also true for the RNA content of particles. In addition, molecules packaged into VLPs must first travel to the plasma membrane, therefore, I confirmed that the NC basic linker region was also responsible for causing a redistribution of A3G to cellular membrane. Although the basic linker region does not overlap with the N-terminal I domain, it is part of the second I domain and contains 4 basic residues that are critical for RNA binding (14, 29, 43, 157, 170). Further studies, however, will have to be conducted to determine if the basic linker region can recruit A3G in isolation, without the presence of the N-terminal sequences.

Many authors now agree that mounting evidence affirms that the presence of RNA is critical for A3G recruitment into particles by Gag. This mechanism makes sense in light of the fact that both A3G and NC are RNA binding proteins. The studies presented in this thesis have emphasized this point by showing that the level of RNA recruited into virus-like particles correlates closely with the amount of A3G found in those particles. This novel finding has advanced the field not only by determining the region of Gag needed for maximal RNA binding but also the region of Gag necessary for efficient A3G packaging into particles. This approach was necessary because the reliable separation of the specific roles played by NC in comparison to RNA during A3G recruitment was proving to be challenging to dissect by biochemical methods. Any production of Gag or A3G contained ubiquitous amounts of RNA, confounding the results. Furthermore, the treatment of these preparations with RNAse produced conflicting reports by different authors. Therefore, this experimental approach provided a way to determine the relative contribution of RNA to A3G recruitment without having to physically separate RNA from NC. This approach proved to be successful method to evaluate RNA contribution and complemented the data produced from biochemical experiments. Ultimately, however, fine structural determinations may be required to determine for certain whether some A3G atoms do in fact interact directly with NC atoms. However, overall these data suggest that the NC basic linker region binds to large amounts of RNA, which then function to recruit A3G into particles.

The Structure of APOBEC3G Complexes

The structure of a protein complex often plays a critical role in its function. For example, the HIV Rev protein must form a homo-multimeric complex in order to cause the efficient export of HIV genomic RNA from the nucleus, presumably through the action of multiple cooperative nuclear export signals (129, 130). Studies have shown that an initial binding event between a Rev monomer and the high affinity RRE RNA binding site occurs in low Rev concentrations. As the late phase of virus replication approaches and Rev accumulates in the nucleus, additional Rev molecules are able bind to low affinity non-specific sites on the RNA by multimerizing with the initial Rev monomer. In this manner, genomic HIV export is regulated by Rev multimerization which is in turn regulated by Rev concentration (41, 108). Rev and A3G proteins share similarities in that they both bind to RNA and they both form homo-multimers. The exact function that multimerization serves in the antiviral activities of A3G is unclear. Perhaps A3G multimerization enhances the RNA binding avidity of the complex compared with A3G monomers, and as a result, increasing its packaging efficiency. Although the studies presented here did not address this question of the nature in which multimerization facilitates A3G function, future studies will certainly explore this question. Nevertheless, due to the significance that A3G structure may play in its function I undertook the first step, a careful study to determine if A3G is packaged into virus particles as a multimeric complex.

A major question that the studies in this thesis have attempted to answer is: What structure do A3G molecules assume during the course of their antiviral activities? Several lines of evidence have indicated that nuclease treated A3G molecules extracted from cells

lysates results in either monomeric forms or head-to-head dimers that are undetectable by FRET. This suggests the possibility that A3G dimers may be the result of an initial RNA-independent A3G-A3G interaction. These dimers then appear to form higher order tetrameric or possibly hexameric structures on RNA substrates, visible by FRET (27, 190). Some authors have proposed that there is sequence specificity to A3G binding, however, no conclusive evidence beyond the clear preference for poly U and T sequences has been demonstrated (106). Structurally, Gag appears to associate loosely with A3G complexes through a common RNA strand like beads on a string. Thus, allowing its separation from A3G complexes by nuclease treatment, and the absence of a detectable FRET interaction between Gag and A3G. Therefore, so-called low molecular weight (LMW) A3G probably consists of A3G dimers that are "active" due to their availability to bind viral RNA, whereas the so-called high molecular weight (HMW) A3G consists of multimeric A3G that is already in complex with RNA and thus unavailable to engage viral RNA. This explains why *in vitro* studies indicate that HMW A3G can be activated by nuclease treatment (27, 118). However, it is clear that in the process of viral restriction by A3G, LMW forms must first condense onto virally packaged RNA to create HMW forms which become packaged into particles. Therefore, it seems evident that it is the HMW forms which are active against HIV when they are bound to HIV RNA within particles. The timing and location of A3G complex formation and dissolution during the HIV life cycle is a fascinating area for future studies. It is important to note that the presence and possible functions of dimeric (LMW) A3G in viral particles has not been determined. This can be investigated using HPLC separation of viral components similar to the methods used by Chiu et al. on cell lysates (27).

The Intracellular Trafficking of APOBEC3G

The intracellular trafficking of a protein is integral to its function in many ways. Trafficking can determine such properties as which substrates an enzymatic protein works on, the timing of when a protein is activated depending on its subcellular location, or how a protein's function is influenced by changes in the cellular trafficking patterns. The basic biology of several cytidine deaminases have been illuminated by an understanding of their subcellular localization and trafficking. For instance, the AID protein which functions as a mutator of somatic B cell DNA can cause a general mutator phenotype leading to the development of lymphoma when its activity is unregulated. Therefore, AID contains both a strong C-terminal nuclear export signal (NES) and a weak N-terminal nuclear localization signal (NLS). This leads to a predominantly cytoplasmic localization, thereby protecting cellular DNA from mutation. However, upon the initiation of somatic hypermutation AID relocalizes to the nucleus, possibly by disabling the NES or activating the NLS, and leading to mutation of only the correct segment of DNA. In this fashion, AID trafficking events are critical to the biology of protein function. The experiments described in this thesis indicate that the trafficking of A3G is also just as critical to its function.

In the absence of Gag expression A3G proteins are found predominantly in two locations, diffuse cytoplasmic populations and collections of A3G in mRNA processing body (p-body) structures. A third compartment, called stress granules, has been identified in which A3G shuttles to during cellular stress, however, it's significance during HIV infection has not been conclusively established. If A3G found in P-bodies is multimeric while A3G found diffusely in the cytoplasm is monomeric or dimeric, from which pool

of A3G is virally encapsidated forms recruited? Although this question is not directly answered by experiments presented here, it is tempting to speculate on this question based on what is known about the relationship between A3G structure and function. Cytoplasmic A3G found in the monomeric or dimeric form is not in complex with RNA and therefore is an "active" form that can attach itself to Gag-RNA complexes trafficking to the plasma membrane. This hypothesis fits with the observation an abundance of LMW A3G expression in a cell causes an inhibition of HIV replication. Nevertheless, this question represents another fascinating area for further research. This line of research will certainly benefit from microscopic techniques designed to activate and track specific subpopulations of tagged molecules such as the photoactivatable GFP system.

The existence of A3G subpopulations in the cell suggests that cellular trafficking may be a method of A3G regulation by the cell. In fact, future research may illuminate currently unknown aspects of A3G biology by studying the cellular mechanisms that govern movement of A3G between different cellular compartments. However, until such definite data is available, it is tempting to speculate on this subject based on what is known. Greene and colleagues have made the observation that HMW A3G (consistent with RNA bound multimeric A3G found in P-bodies) does not readily inhibit HIV replication suggesting that its ability to release one strand of (cellular) RNA and engage another (viral) is limited (27, 118). However, Kozak and colleagues suggest that A3G-mRNA complexes can shuttle between protein synthesis polysomes and stress granules (117). Nevertheless, it seems plausible that the cell can direct A3G-RNA complexes to different cellular locations. It is also a reasonable hypothesis that the cellular proteins and mechanisms involved in these processes may also be involved in the trafficking of A3G

into retroviral particles. Among the questions to be answered by this active area of investigation are whether or not there is equilibrium of A3G between various cellular compartments that is perturbed by HIV infection of a cell. What structure do A3G complexes take within the various cellular compartments and how is this important to A3G function? More specifically, can the multimeric forms of A3G return to their dimeric/monomeric forms or subcellular locations? The experiments in this thesis have framed these questions by outlining the structure in which A3G exists in several subcellular locations.

Model of APOBEC3G Packaging

My research has addressed many gaps in our understanding of the functions for retroviral RNA. We have developed a robust model for RNA functions in A3G packaging into particles, summarized in Figure 21. In our model, A3G normally exists in two main cellular compartments, a diffusely cytoplasmic dimer or monomer undetectable by FRET, and a multimer detectable by FRET in structures consistent with mRNA processing bodies (P-bodies). Gag forms multimers on cellular membranes using RNA as a catalyst and traffics to the plasma membrane. Dimeric A3G from the diffuse cytoplasmic pool multimerizes onto the RNA that is traveling with Gag. Finally, Gag arrives at the plasma membrane bringing both RNA and A3G with it into virus particles. In summary, our results provide strong support for the importance of RNA in mediating the incorporation of multimeric forms of APOBEC3G into virions or VLPs. This incorporation is dependent upon regions of Gag within NC that allow efficient RNA incorporation, especially the basic linker region.

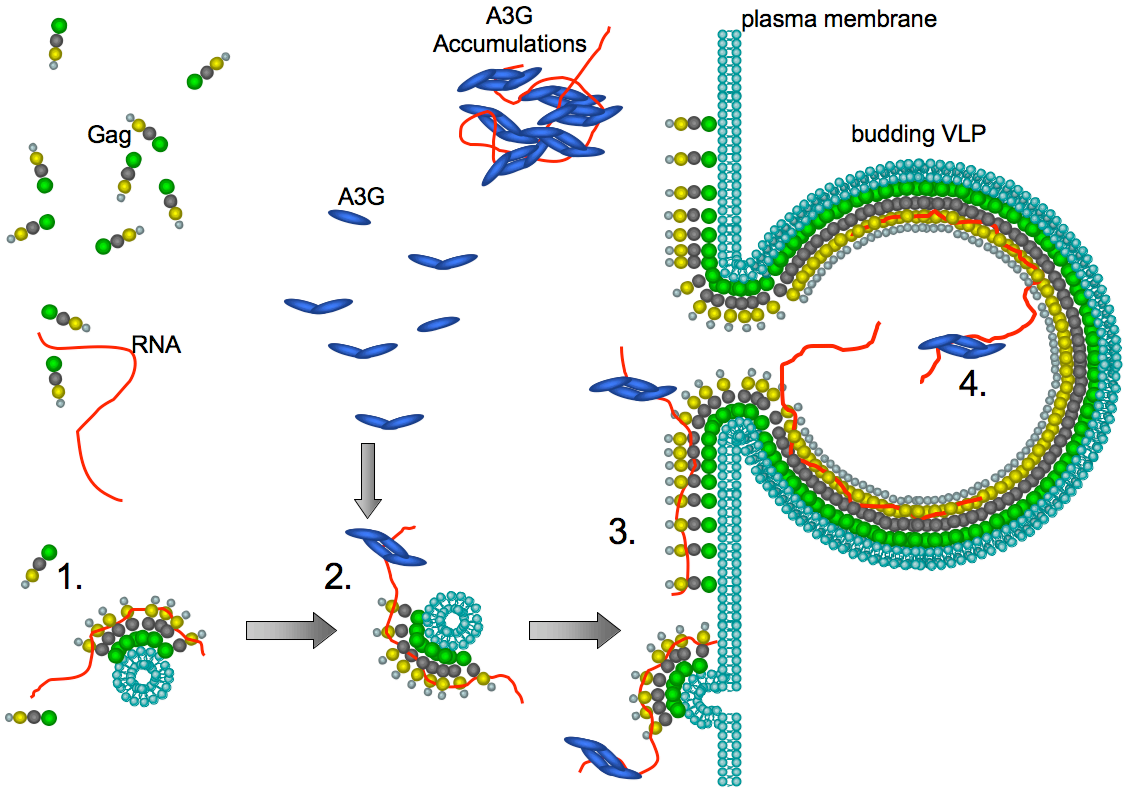

Figure 21. Model of APOBEC3G recruitment into virus particles. APOBEC3G (A3G) exists as diffuse cytoplasmic dimers and also as multimers in cytoplasmic accumulations. Step 1: Gag multimerizes on cellular membranes using RNA as a catalyst, Step 2: A3G multimerizes on RNA that is bound to Gag multimers. Step 3: Gag traffics to the plasma membrane taking the RNA and A3G with it. Step 4: Particles form containing A3G multimers.

Future Directions in Therapeutics

The experiments in this thesis provide basic information about mechanisms governing A3G packaging that can be used to design novel anti-retroviral therapies. I have learned that the same mechanisms responsible for recruiting viral genome into the particle are also responsible for recruiting A3G. As a result, any attempt by the virus to disrupt A3G packaging by interfering with these mechanisms would also result in a disruption of viral genomic packaging. This helps to explain why the virus would need to evolve a defense mechanism centered around the reduction of A3G expression levels. The theoretical interventions described in this section fall into two categories: 1) increasing A3G expression levels, 2) developing ways to concentrate any remaining A3G onto HIV genomic RNA, the latter being most specific to the studies presented in this thesis.

Any intervention that overexpresses or restores the expression levels of the circulating pool of diffuse cytoplasmic A3G may promote uptake of A3G into virus particles and achieve a therapeutic effect. It is tempting to speculate on how this could be accomplished. The simplest way to do this would be to induce increased expression of A3G. The experiments in Figure 6 demonstrate that the effect of the Vif protein can be saturated by overexpression of A3G. Therefore, a pharmaceutical compound that increases expression of A3G without increasing CD4+ cell activation could help to limit virus replication. Another way to approach this strategy would be to disrupt the interaction between A3G and Vif. Essentially, a small molecule that binds to either A3G or Vif could inhibit this interaction and prevent A3G polyubiquitination and degradation.

This is approach provides the most direct route to a pharmaceutical solution and is being pursued actively by several investigators (138).

Several key studies in this thesis have shown that A3G exists in at least two forms in at least two different cellular compartments. The dimeric/monomeric state appears to be the state able to engage retroviral RNA. Therefore, one way to increase the functional A3G in the cell would be to develop therapies designed to convert multimeric A3G found in accumulations of A3G into to cytoplasmic dimeric/monomeric A3G. Although RNAse treatment has been shown to liberate and activate multimeric A3G into the dimeric/monomeric form, it is likely that the potential toxicity from over-expression of a cytoplasmic RNAse would be quite toxic all protein synthesis. Nevertheless, future studies of A3G trafficking and multimerization should reveal additional molecules both cellular and viral that are involved in the regulation of these states and can therefore be used as targets for therapeutic modalities. For instance, these modalities could be targeted to inhibit A3G trafficking to P-bodies or encouraging the liberation of A3G from P-bodies. This could potentially initiate a redistribute of large amounts of A3G stored in p-bodies as multimers back into the cytoplasm as monomers or dimers, causing a large infusion of A3G into all virus particles produced in a patient and terminating viral replication.

The second general category of therapeutics relates to designing strategies to enhance the targeting of A3G molecules specifically to viral RNA. This category represents a greater challenge since most small molecule pharmaceuticals are designed to inhibit or mimic biological molecules rather than promote the interaction of two specific proteins. Nevertheless, technical difficulties notwithstanding, one way to do this would

be by making a Tat-A3G fusion protein. This protein could be administered intravenously, and would enter CD4+ cells due to the membrane penetrating properties of the Tat domain. It could then preferentially bind to retroviral RNA containing the 5' Tar stem loop structure. In fact, the retroviral genome has several RNA stem-loop structures that could be used as targeting locations. These include the Psi packaging signal, the TAR element that promotes mRNA elongation, and the Rev Response Element (RRE) that promotes the export of genomic retroviral RNA from the nucleus. Fusion proteins of A3G with NC (which binds to Psi), Tat (mentioned above), or Rev (which binds to the RRE) could all be used to target any remaining A3G molecules to HIV genomic RNA. The delivery of a therapy based on a protein to human tissue is a very serious technical problem that has not been solved yet to a high degree of satisfaction yet. However, solutions that have been proposed and remain feasible possibilities include attaching cell-penetrating peptides to the A3G-fusion proteins (such as Tat-A3G, Tat-A3G-NC, Tat-A3G-Rev), conducting gene therapy with adenovirus or another retrovirus, or delivery using a fusion capable virus-like particle or nano-container that is filled with the protein of interest. It is of note that the target tissue, CD4+ T cells, conveniently circulates in the blood, which enhances their accessibility to such therapies.

As a final idea, current anti-retrovirals such as protease inhibitors could be conjugated to RNA binding molecules. This might help target these therapies into virus particles in a powerful and effective manner. Although each of these strategies would require extensive research and development, the basic biology of A3G packaging described in this thesis provides the framework for these future studies.

In conclusion, this thesis has provided insights into the role that RNA plays in mediating the packaging of APOBEC3G into HIV particles via the NC region of Gag. This demonstrates that therapeutics targeted into virus particles through RNA binding could be extremely effective at limiting virus replication. In this way, our data paves the way for the future development of novel anti-retroviral therapies that target viral RNA.

APPENDIX A

MA-DELETED HIV-1 GAG EXPRESSION CONSTRUCTS

MA-Deleted HIV-1 Gag Expression Constructs

Introduction

One of the first projects I worked on in the Spearman lab involved determining the role of the Adapter Protein 3 complex (AP-3) complex in Gag trafficking. Specifically we asked the following questions: 1) What subdomain of Gag does AP-3 bind to, 2) Where in the cell does the AP-3 complex traffic Gag to, 3) Does AP-3 complex trafficking of Gag have functional implications for particle assembly? Initial yeast two-hybrid experiments, GST co-sedimentation studies, and co-immunoprecipitation studies showed that the Matrix (MA) sub-domain of the HIV-1 Gag protein was responsible for binding to the AP-3. Confocal fluorescence microscopy and immuno-labeled electron microscopy was used to show that the AP-3 complex facilitated Gag trafficking to the multi-vesicular body (MVB), type of late endosome used for sorting. We then determined that this interaction and subsequent trafficking to the MVB was functional step in particle assembly by showing that Gag-Pol expression constructs experienced significant impairment of particle output in cells expressing a dominant negative fragment of the AP-3 complex termed AP3D-5'. It became clear that a Gag molecule able to bypass AP-3 trafficking and go directly to the plasma membrane would serve as an excellent negative control for functional studies of particle release involving siRNA depletion of the AP-3 complex. The SrcΔMAGag construct was made as just such a control given that the V-Src myristylation sequence is able to target proteins to the plasma membrane (6, 196). Therefore, SrcΔMAGag was used to show that siRNA

depletion of the AP-3 complex severely impaired release of pNL4-3 but not SrcΔMAGag particles in HeLa cells.

Materials and Methods

Plasmid Construction

The Gag coding sequences for all constructs were derived from the codon-optimized version of HXB2 Gag in expression plasmid pVRC3900 (104). PCR cloning was used to amplify the CA-p6 region of the *gag* gene from the pVRC3900 vector with the first 9 amino acids of the V-Src oncogene, including the myristylation sequence, added prior to the start of CA. A HindIII site was added prior to the 5' ATG and a BamHI site was added at the 3' end and for C-Terminal fluorescent fusion constructs the *gag* stop codon was omitted. The amplified *gag* gene was then ligated into pcDNA3.1(+), pEGFP-N3 and pEYFP-N3 by digestion of the BamHI and HindIII sites located within the multiple cloning regions. The forward oligonucleotide used in PCR amplifications for all constructs was AACAAGCTTGCCACCATGGGCTCCTCCAAGT CCAAGCCCAAGCCCATCGTGCAGAACATC-(F). Reverse oligonucleotides used in PCR amplifications were CGGGATCCTTATTGTGACGAGGGGTC-(R) (SrcΔMAGag), GGGGATCCTTGTGACGAGGGGTCGCTG-(R) (SrcΔMAGag-GFP and SrcΔMAGag-YFP). A schematic diagram of the Gag expression constructs employed in this study is shown in Fig. 22.

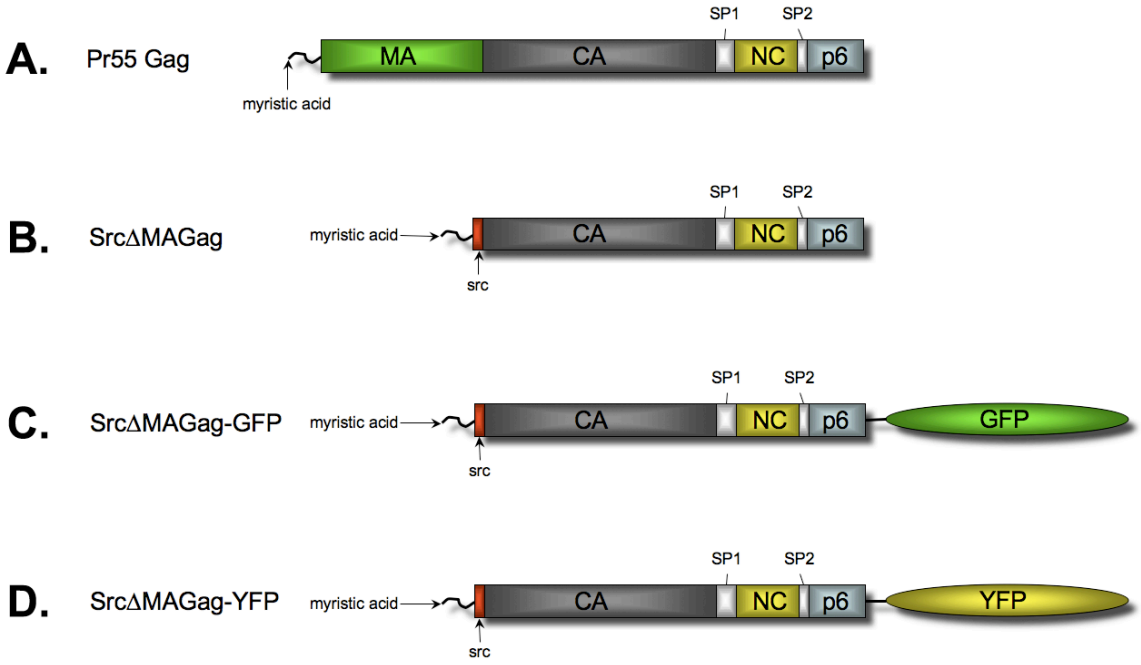

Figure 22. Gag constructs lacking the MA region. Schematic representation of (A) Pr55Gag, (B) SrcΔMAGag, (C) SrcΔMAGag-GFP, (D) SrcΔMAGag-YFP.

Cell lines and transfections

The human kidney cell line 293T was maintained in Dulbecco's modified Eagle medium with 10% fetal bovine serum and antibiotics at 37°C in 5% CO^2, and grown in 100-cm^2 tissue culture dishes. Transfections were performed by either the calcium phosphate-BBS transfection method or with Lipofectamine 2000 (Invitrogen, Carlsbad, Calif.), with 10 μg of total plasmid DNA unless otherwise stated.

Antibodies and Immunoblotting

Lysate preparations were analyzed by SDS-polyacrylamide gel electrophoresis followed by transfer to nitrocellulose membrane and immunoblotting. Gag was blotted with the monoclonal antibody CA-183, and GFP antisera was obtained from Santa Cruz (Santa Cruz, California). Secondary fluorescent conjugated antibodies for detection on the LiCor Odyssey were obtained from LI-COR, Inc. (Lincoln, Nebraska).

Results

293T cells were transfected with each expression construct and cell lysates were made by detergent lysis. To verify that each matrix deleted Gag expression construct was correct, immunoblots were performed on the cell lysates and the approximate size of each protein was compared to the predicted size. In the case of the GFP and YFP fusion proteins, immunobloting simultaneously with both the Gag and GFP antibodies indicated the size of the full-length protein by the band that showed up in the same location on both blots. Gag (55 kDa) and SrcΔMAGag (38 kDa) were detected at the correct sizes upon immunoblotting with a capsid (CA) specific antibody (Fig. 23A). GFP (28 kDa) was

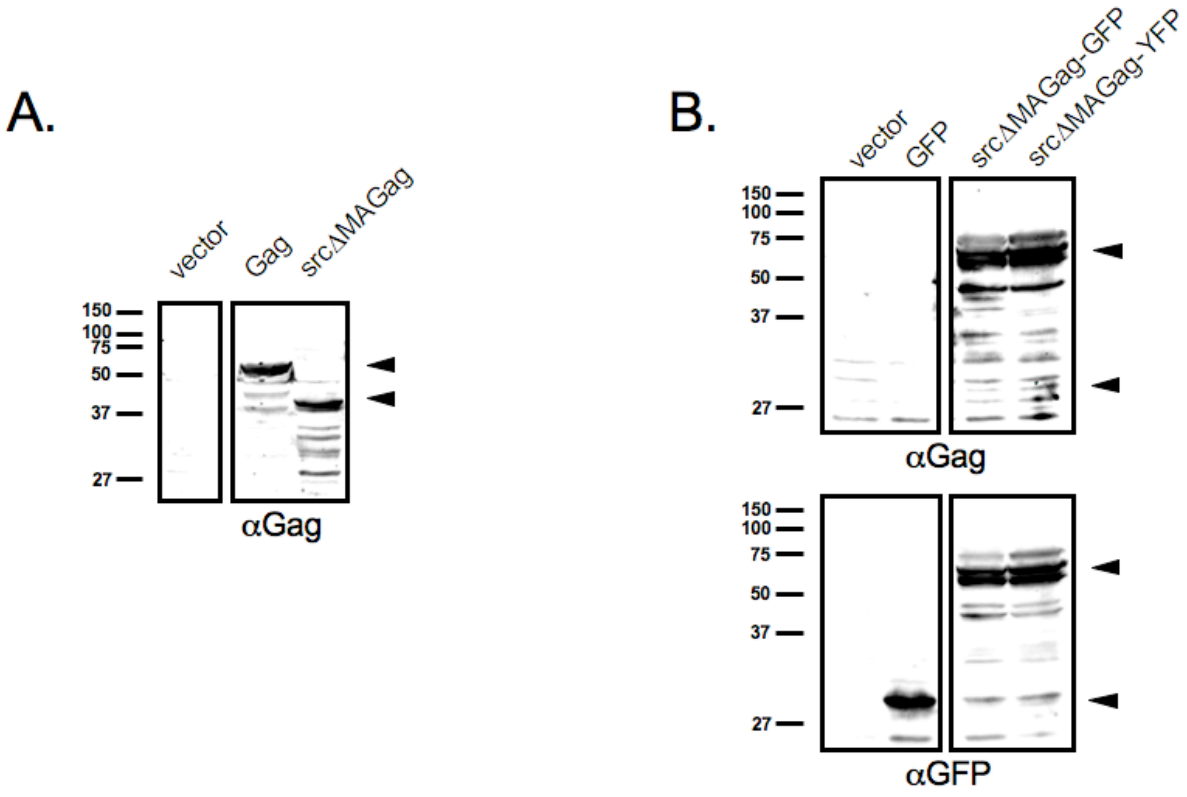

Figure 23. Expression of Gag constructs lacking the MA region. 293T cells were transfected with the indicated constructs. Following lysis, proteins were separated using SDS PAGE and blotted using (A) a Gag specific antibody (arrows indicate 55 kDa, 38 kDa) and (B) both GFP and Gag specific antibodies (arrows indicate 66 kDa, 28 kDa).

detected at the correct size upon immunoblot with a GFP specific antibody, while SrcΔMAGag-GFP (66 kDa) and SrcΔMAGag-YFP (66 kDa) were also detected at the corrected size but in both the Gag specific and GFP specific immunoblots (Fig 23B). This confirms the correct expression of these Gag constructs.

APPENDIX B

APOBEC3G EXPRESSION CONSTRUCTS

APOBEC3G Expression Constructs

Introduction

Chapters II through IV focus on APOBEC3G packaging determinants and the multimeric nature of packaged APOBEC3G. During the course of these studies, several APOBEC3G expression constructs were created but were not used in publication. These include recombinant bacterial and baculoviral APOBEC3G expression vectors whose creation and characterization is presented here.

Materials and Methods

Plasmids Construction

PCR cloning was used to amplify the APOBEC3G gene from the CEM15 plasmid (obtained from Michael Malim) by placing an EcoRI site prior to the 5' ATG and an XhoI site at the 3' end. The amplified APOBEC3G gene was then ligated into pCMV-HA to yield a new construct designated HA-A3G. The oligonucleotides used in the PCR amplifications were GGAATTCGGATGAAGCCTCACTTCAGA-(F) and CCGCTCGAGTCAGTTTTCCTGATTCTG-(R).

PCR cloning was used to amplify the HA-APOBEC3G sequence from the HA-A3G plasmid by placing an SmaI site prior to the 5' ATG and an XhoI site at the 3' end. The amplified APOBEC3G gene was then ligated into the bacterial expression vector pGEX-6P-1 to yield a new construct designated GST-HA-A3G. The oligonucleotides

used in the PCR amplifications were TACCCCCGGGGATGTACCCATACGAT-(F) and CCGCTCGAGTCAGTTTTCCTGATTCTG-(R).

PCR was used to amplify the APOBEC3G sequence from the CEM15 plasmid by placing an EcoRI site at the 3' end using the following oligonucleotides CTGGAAGTTCTGTTCCAGGGGCCCATGAAGCCTCAC-(F) and GGAATTCTCAGTTTTCCTGATTCTG-(R). PCR was then used to amplify the GST sequence from the pGEX-6P-1 plasmid by placing an EcoRI site prior to the 5' ATG using the following oligonucleotides CGAATTCATGTCCCCTATACTA-(F) and GAACAGAACTTCCAGATCCGATTTTGG-(R). These products were joined to create GST-A3G by overlap extension PCR, and ligated into the baculovirus transfer vector pVL1392 to create the construct GST-A3G1392.

Expression and purification

GST-HA-A3G was expressed in E. Coli and purified from bacterial cell lysates using glutathione agarose beads. HA-A3G was cleaved off the beads using PrescissionProtease and serial dilutions were analyzed by SDS polyacrylamide gel electrophoresis (PAGE) followed by immunoblotting with an APOBEC3G specific antibody Warner C. Greene through the NIH AIDS Research and Reference Reagent Program (181). A GST-A3G expressing baculovirus was made by genetic recombination after cotransfection of insect SF9 cells with GST-A3G1392 and BaculoGold Bright linearized baculovirus DNA. Virus was amplified and titerred using GFP fluorescence. This virus was then used to infect SF9 insect cells, and GST-A3G was purified and analyzed from insect cell lysates as described above.

Results

HA-A3G was purified from bacterial cell lysates and separated by SDS PAGE and immunoblotted using A3G antisera. Correct expression was verified by the correct size (50 kDa) of serial dilutions shown in Figure 24A. A3G was purified from bacterial cell lysates and separated by SDS PAGE and immunoblotted using A3G antisera. Correct expression was verified by the correct size (50 kDa) of serial dilutions shown in Figure 24B.

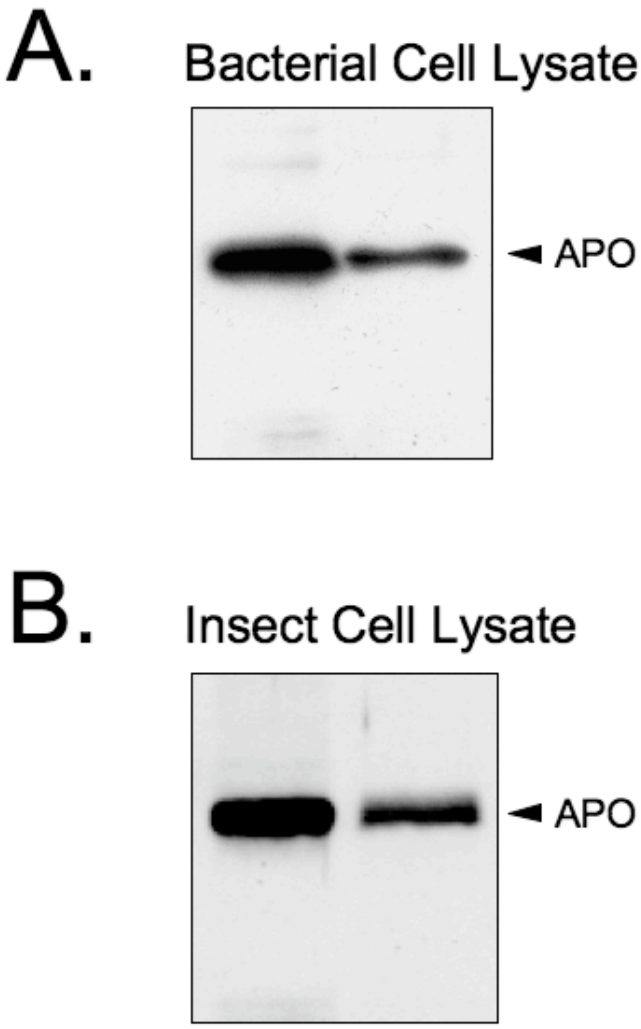

Figure 24. APOBEC3G expression constructs. (A) E. Coli bacteria were induced to express GST-HA-APOBEC3G. Following lysis, GST purification, and preatease cleavage, immunoblot with an APOBEC3G (A3G) specific antibody revealed correct expression of A3G. (B) Insect cells were infected with a GST-APOBEC3G expressing baculovirus. Following lysis, GST purification, and protease clavage, immunoblot with an A3G specific antibody revealed correct expression of A3G.

APPENDIX C

THE HUMAN METAPNEUMOVIRUS NUCLEOPROTEIN AND PHOSPHOPROTEIN INTERACT BY FRET ANALYSIS

The Human Metapneumovirus Nucleoprotein and Phosphoprotein Interact by FRET Analysis

Introduction

Human metapneumovirus (hMPV) is a recently discovered paramyxovirus of the Pneumovirinae subfamily, which also includes avian pneumovirus and respiratory syncytial virus (RSV). hMPV is an important cause of respiratory disease worldwide. To understand early events in hMPV replication, the cDNA encoding the hMPV nucleoprotein (N), phosphoprotein (P), was cloned from cells infected with the genotype A1 hMPV wild-type strain TN/96/12. We used the Förster resonance energy transfer (FRET) technique to show that hMPV N interacts with hMPV P.

Materials and Methods

FRET analysis by scanning cuvette fluorometry. One 10-cm2 dish of nearly confluent 293T cells were transfected for each experimental condition using Lipofectamine 2000 (Invitrogen, Carlsbad, Calif.). Cells were harvested for analysis 24 h following transfection and washed in phosphate-buffered saline and kept at 4°C. Whole cells were then analyzed by fluorometry in a PTI T-format scanning cuvette spectrofluorometer (Photon Tehnology international, Lawrenceville, N.J.). Samples were excited at 433 nm, and a resulting emission scan ranging from 450 to 550 nm was obtained. Samples were exited at 514 nm, with a resulting emission scan of 526 to 600 nm, for analysis of YFP emission to compare the relative amount of YFP present.

Results

The Venus-P and Cerulean-N fusion proteins were co-expressed in HEK 293T cells. As a negative control, each was also co-expressed with either CFP or YFP, respectively. The emission spectrum of whole cells was then obtained in a spectrofluorometer using an excitation wavelength of 433 nm. Cells expressing Venus-P and Cerulean-N (Fig. 25A, red squares), exhibited a curve representative of efficient fluorescence energy transfer. However, analysis of cells co-expressing Venus-P with CFP, or Cerulean-N with YFP resulted in CFP emission peaks with no FRET emission peak (Fig. 25A, closed circles and closed triangles, respectively). Similar levels of YFP emission were obtained upon YFP excitation for each experimental condition, indicating that differential protein levels did not account for the differences between negative controls and the test molecules (Fig. 25B). We conclude that the N and P proteins interact by FRET analysis. The studies presented in this appendix were performed in collaboration with Aaron Derdowski in Timothy Peters' lab. The results are in the process of being submitted as a manuscript for publication along with other supporting data.

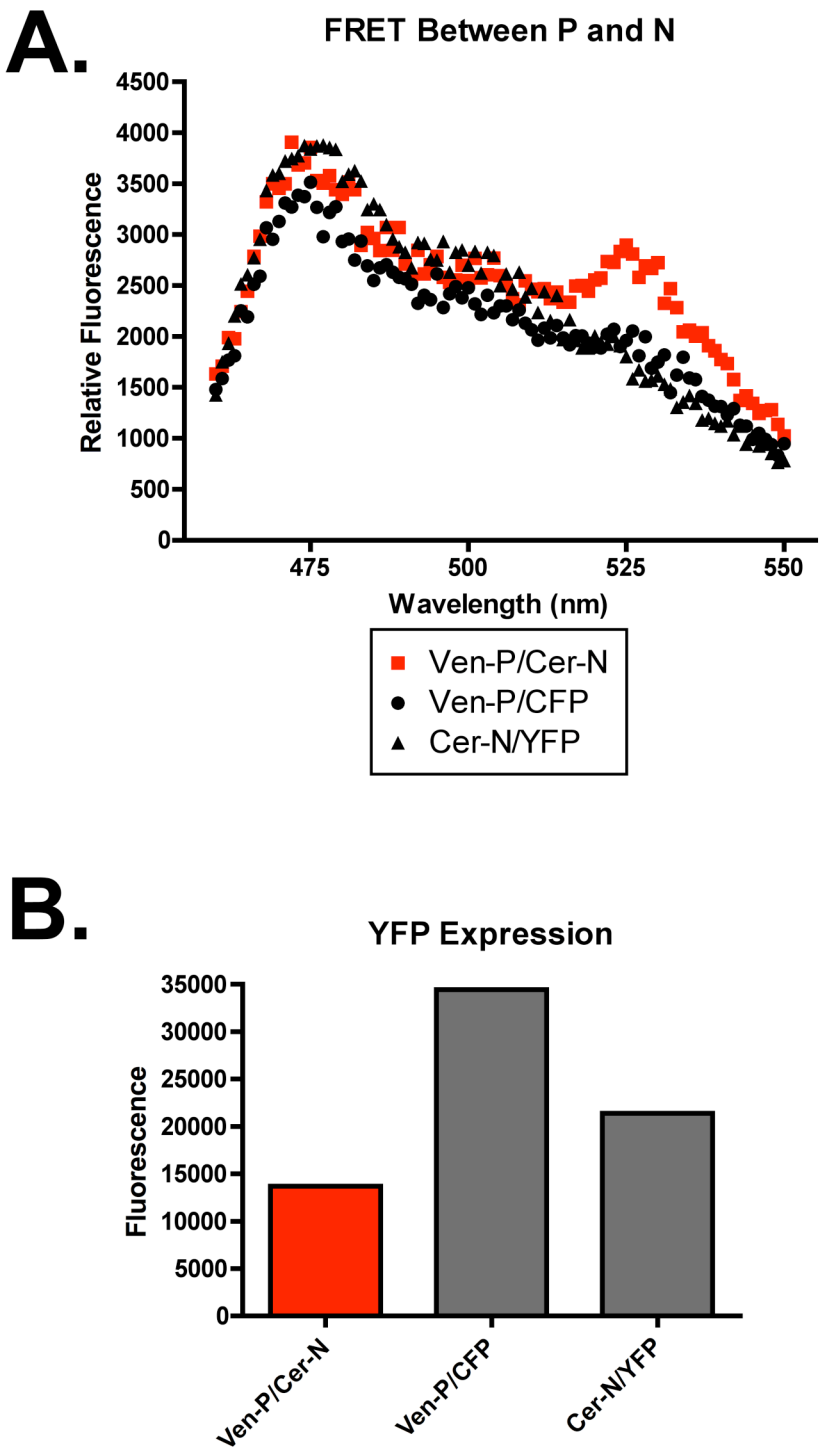

Figure 25. Analysis of P and N protein interactions by FRET fluorometry. Whole 293T cells were analyzed in a scanning cuvette fluorometer as described in Materials and Methods. Venus hMPV P-Cerulean hMPV N FRET curve (red diamonds) shows a Venus emission peak at 527 nm in cells expressing both proteins. Closed circles: Venus hMPV P expressed with CFP control protein. Closed triangles: Cerulean hMPV N expressed with YFP control protein.

APPENDIX D

AP-3 DIRECTS THE INTRACELLULAR TRAFFICKING OF HIV-1 GAG AND PLAYS A KEY ROLE IN PARTICLE ASSEMBLY

DONG X, LI H, DERDOWSKI A, DING L, **BURNETT A,** CHEN X, PETERS TR, DERMODY TS, WOODRUFF E, WANG JJ, AND P SPEARMAN

Cell. 120(5):663-674, 2005

Cell, Vol. 120, 663–674, March 11, 2005, Copyright ©2005 by Elsevier Inc. DOI 10.1016/j.cell.2004.12.023

AP-3 Directs the Intracellular Trafficking of HIV-1 Gag and Plays a Key Role in Particle Assembly

Xinhong Dong,[1] Hua Li,[1] Aaron Derdowski,[1] Lingmei Ding,[1] Atuhani Burnett,[1] Xuemin Chen,[1] Timothy R. Peters,[1] Terence S. Dermody,[1] Elvin Woodruff,[2] Jaang-Jiun Wang,[3] and Paul Spearman[1,*]

[1]Department of Pediatrics and Microbiology and Immunology
[2]Department of Biological Sciences
Vanderbilt University
Nashville, Tennessee 37232
[3]Department of Cell Biology
Fu-Jen Catholic University
Taipei, Taiwan

Summary

Gag proteins direct the process of retroviral particle assembly and form the major protein constituents of the viral core. The matrix region of the HIV-1 Gag polyprotein plays a critical role in the transport of Gag to the plasma membrane assembly site. Recent evidence indicates that Gag trafficking to late endosomal compartments, including multivesicular bodies, occurs prior to viral particle budding from the plasma membrane. Here we demonstrate that the matrix region of HIV-1 Gag interacts directly with the δ subunit of the AP-3 complex, and that this interaction plays an important functional role in particle assembly. Disruption of this interaction eliminated Gag trafficking to multivesicular bodies and diminished HIV particle formation. These studies illuminate an early step in retroviral particle assembly and provide evidence that the trafficking of Gag to late endosomes is part of a productive particle assembly pathway.

Introduction

The process of retroviral particle assembly is directed by the Gag polyprotein (Freed, 1998; Wills and Craven, 1991). Gag proteins expressed in the absence of any other viral components are capable of eliciting the formation of virus-like particles (pseudovirions) of the authentic size, density, and morphology of the infectious virion. HIV Gag proteins are cleaved by the viral protease during the budding process into four structural proteins that perform unique functions in the mature virion (MA, CA, NC, and p6, listed from amino to carboxyl terminus). During assembly, the uncleaved Gag polyprotein interacts with the viral RNA and the envelope glycoprotein complex (Env) to coordinate the production of infectious virions. Gag interacts with a number of cellular factors that play an essential role in particle budding as Gag makes its way to the plasma membrane assembly site (Luban, 2001; Martin-Serrano et al., 2003; Strack et al., 2003; von Schwedler et al., 2003).

*Correspondence: paul.spearman@vanderbilt.edu

HIV budding occurs predominantly at the plasma membrane in T lymphocytes and most transformed epithelial cell lines (Freed, 1998; Ono and Freed, 2004; Spearman et al., 1994). $Pr55^{Gag}$ is synthesized on free cytosolic ribosomes and traffics to the plasma membrane assembly site by pathways that are not yet completely defined. The discovery that Gag interacts with TSG101 and other components of the *v*acuolar *p*rotein *s*orting (Vps) pathway has led to new insights into the route taken by Gag in the cell (Garrus et al., 2001; VerPlank et al., 2001). TSG101 is a component of the ESCRT-I complex and plays a key role in the biogenesis of multivesicular bodies (MVBs) (Babst et al., 2000; Katzmann et al., 2001). Gag binds directly to the UEV domain of TSG101 through a tetrapeptide (PTAP) domain located in the carboxyl-terminal p6 domain. In this manner, Gag acts as an Hrs homolog and diverts TSG101 and other ESCRT components from their role in MVB formation to assist in the late steps of particle assembly (Pornillos et al., 2003).

In some cells, HIV particle budding occurs directly into the MVB rather than from the plasma membrane. This phenomenon is prominent in primary macrophages, where it appears to be the major productive pathway involved in particle formation and release (Nguyen et al., 2003; Ono and Freed, 2004; Raposo et al., 2002). Some investigators have postulated that budding into late endosomes is important in most cell types and have suggested that Gag acts as a cargo molecule for normal cellular exocytic machinery (the "Trojan exosome" hypothesis) (Gould et al., 2003; Nguyen et al., 2003). While the role of HIV budding into endosomes in most relevant cell types such as primary T cells is debated, it is clear that Gag and MVB markers colocalize in a wide variety of cells (Nydegger et al., 2003; Sherer et al., 2003). It is likely that specific cellular trafficking machinery is responsible for bringing Gag to the MVB.

In order to better understand the process of HIV particle assembly, it is necessary to identify the specific cellular factors responsible for the trafficking of Gag within the cell. Here we report that Gag interacts directly with the δ subunit of the AP-3 complex, in an interaction mediated by the amino-terminal α-helical segment of matrix (MA). Disruption of this interaction prevents Gag from reaching the MVB compartment and inhibits particle formation. Our observations highlight an early step in the HIV assembly pathway that takes Gag to the late endosome/MVB compartment and suggest that the trafficking of Gag to this compartment is part of the normal productive pathway of HIV-1 assembly.

Results

HIV-1 Gag Binds Specifically to the δ Subunit of the AP-3 Complex

We performed a yeast two-hybrid screen of a HeLa cDNA library using full-length HIV-1 Gag as bait to iden-

tify Gag binding partners. Our screen identified TSG101 and cyclophilin B, two previously identified Gag-interacting proteins (Franke et al., 1994; Garrus et al., 2001; VerPlank et al., 2001), as well as new candidate Gag binding partners. One candidate chosen for further evaluation was the δ subunit of AP-3. Our screen identified a fragment representing amino acids 554–844 of the δ subunit, which overlaps the hinge region and the C-terminal portion of the head of AP-3 δ. The interaction was confirmed in yeast by measuring β-galactosidase levels in liquid culture assays (Figure 1B). Additional truncation constructs narrowed the Gag binding region on AP-3 δ to amino acids 641–742, located entirely within the hinge region (data not shown).

Directed yeast two-hybrid experiments were used to map the AP-3 δ subunit binding site within Gag. Deletion of MA from Gag eliminated specific binding, while C-terminal truncations of Gag that retained an intact MA region maintained the binding characteristics of the full-length molecule (Figure 1B). We next examined individual fragments representing each major cleavage product of Gag (MA, CA, NC, p6); only the MA fragment bound at levels significantly above background (Figure 1B). A set of nested deletions within MA were then evaluated (Yu et al., 1992) and revealed loss of interaction with deletions surrounding the N-terminal α helix of MA (MAD-1 and MAD-2, Figure 1C). To confirm the importance of the N-terminal α helix (H1), a fragment expressing the N terminus of MA up to residue 19 demonstrated interaction in yeast (pGBKT7-H1), while a specific deletion of this same fragment failed to bind to the AP-3 δ subunit (Figure 1D). An N-terminal fragment of MA truncated after residue 12 failed to interact (data not shown). We conclude that the N-terminal α helix of MA, a region previously implicated in Gag trafficking (Ono et al., 2000), is the binding site for the AP-3 δ subunit.

We next sought to verify the Gag-AP-3 δ interaction using recombinant Gag protein produced in *E. coli*. Gag-GST fusion constructs were prepared and evaluated for binding to the AP-3 δ subunit from 293T cell lysates. No interaction was seen with GST alone or with GST fusions with CA, NC, or p6 (Figure 2A). Cellular AP-3 δ bound to full-length GST-Gag, Gag lacking p6 (GST-MACANC), Gag lacking NC and p6 (GST-MACA), and with GST-MA alone (Figure 2A). A purified protein fragment representing the interacting domain of the AP-3 δ subunit (amino acids 554–844) bound directly to GST-MA and not to fusion proteins representing other major regions of Gag (Figure 2C, asterisk). These results indicate that there is a direct and specific protein-protein interaction between the MA region of Gag and the AP-3 δ subunit.

Gag Interacts with the AP-3 δ Subunit in Mammalian Cells

An N-terminal fragment of the AP-3 δ subunit bearing an HA epitope tag (HA-AP-3D-5′) was expressed together with a full-length Gag molecule bearing a C-terminal myc epitope tag (Gag-myc) in 293T cells. Immunoprecipitation of Gag demonstrated interaction with HA-AP-3D-5′ as detected by anti-HA immunoblotting (Figure 3A). HA-tagged TSG-5′, an N-terminal fragment

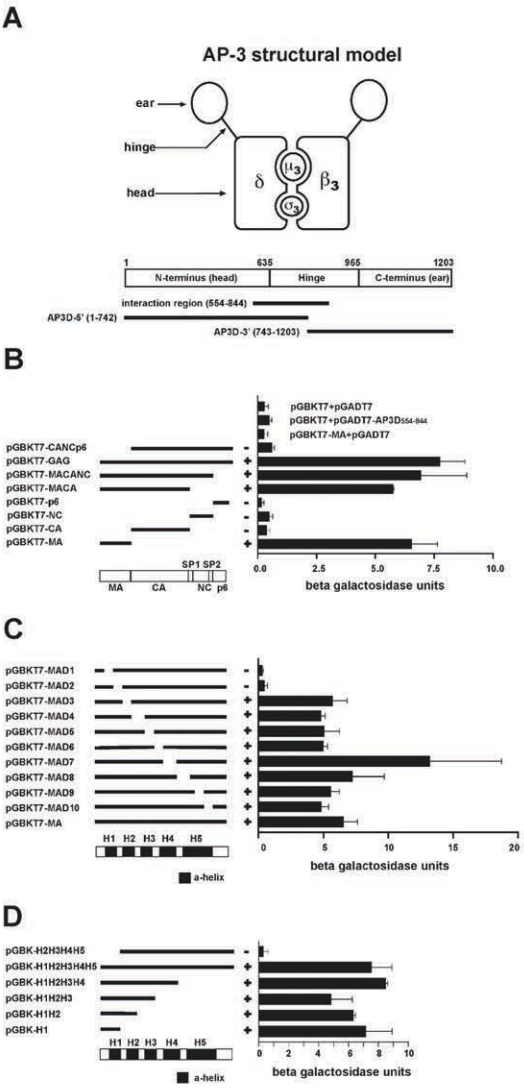

Figure 1. Yeast Two-Hybrid Analysis of the Gag-AP-3 δ Subunit Interaction

(A) Schematic illustration of AP-3 adaptor complex and position of relevant fragments. The original interacting fragment (554–844) isolated from a HeLa cDNA library is shown, together with the position of the AP-3D-5′ and AP-3D-3′ fragments.

(B) Mapping studies of the AP-3 δ subunit binding domain within Gag. The interactions between different Gal4 DNA-BD fusion proteins (left graph) and Gal4 AD fusion protein bearing the interacting region of AP-3 δ were tested for growth and α-galactosidase activity on solid media (indicated by +) and by liquid β-galactosidase assays (right) in replicate experiments. Liquid β-galactosidase data represent the mean ± SD from triplicate experiments. The top three assays are negative controls.

(C) Mapping of the AP-3 δ subunit binding domain within MA. MA deletion constructs expressed in yeast were assayed for interaction with the AP-3 δ 554–844 fragment as in (B).

(D) Fine mapping of the AP-3 δ subunit binding domain within MA.

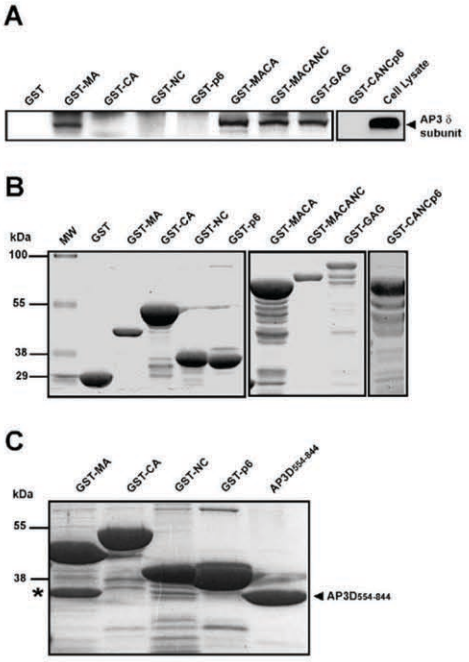

Figure 2. GST Pulldown Analysis of the Gag-AP-3 δ Subunit Interaction

(A) HIV-1 MA binds to endogenous AP-3 δ subunit. GST fusion proteins representing the indicated regions of Gag bound to glutathione beads were incubated with cell lysates of 293T cells, followed by immunoblotting for adaptin δ. The input adaptin δ protein from the 293T cell lysate is shown on the right.

(B) Coomassie blue staining of fusion proteins used in (A).

(C) The purified interacting fragment (AP-3 δ 554–844) was incubated with bead bound GST-Gag fusion proteins, followed by elution and analysis by Coomassie blue staining. Purified interacting fragment is shown in the rightmost lane and is indicated in the GST-MA lane by an asterisk.

of TSG101 that includes the p6 binding region, was coprecipitated with Gag-myc in this assay as a positive control. The reciprocal immunoprecipitation was then performed and again demonstrated the coimmunoprecipitation of Gag-myc with HA-AP-3D-5′ (Figure 3B).

In order to detect the interaction of Gag with endogenous AP-3 in mammalian cells, immunoprecipitation of Gag-myc was performed using an anti-myc monoclonal antibody followed by immunoblotting for the AP-3 δ subunit. Gag-myc precipitated the full-length endogenous AP-3 δ subunit (Figure 3C). In contrast, a particle-competent Gag-myc construct bearing the v-src myristylation signal and lacking MA failed to precipitate the AP-3 δ subunit (SrcΔMAGag-myc, lane 3 of Figure 3C). To further examine this interaction, full-length proviral DNA (pNL4-3) was transfected into HeLa cells, then Gag was immunoprecipitated using an anti-CA monoclonal antibody. The endogenous AP-3 δ subunit coprecipitated with Gag (Figure 3D). These results demonstrate that Gag interacts with the AP-3 δ subunit in mammalian cells when Gag alone is expressed and in the context of expression of an infectious provirus.

An N-Terminal Fragment of the AP-3 δ Subunit Acts as a Dominant-Negative Inhibitor of Particle Assembly

We next performed experiments designed to investigate the biological significance of the Gag-AP-3 interaction. We reasoned that expression of a fragment of AP-3 δ overlapping the Gag binding domain (AP-3D-5′) could block the interaction of Gag with the endogenous AP-3 complex. To study the effects of this molecule on particle formation, we expressed AP-3D-5′ together with pNL4-3 in 293T cells and measured particle release by p24 antigen ELISA. AP-3D-5′ expression inhibited particle assembly/release from 293T cells in a manner similar to that of a dominant-negative TSG101 construct (Figure 4A). AP-3D-5′ demonstrated a significant inhibition of particle release by a Gag/protease expression construct (Figure 4B), eliminating the possibility that Env or additional viral gene products are required for AP-3D-5′-mediated inhibition of assembly. The inhibitory effect of AP-3D-5′ was dose dependent (Figure 4C). Western blotting of cell lysates and of pelleted virion particles revealed an AP-3D-5′ dose-dependent decrease in released p24 antigen corresponding to the ELISA results (Figure 4D). We considered the possibility that the inhibition of particle release seen upon overexpression of AP-3D-5′ was due to cellular toxicity or enhanced degradation of $Pr55^{Gag}$. However, intracellular levels of $Pr55^{Gag}$ and of endogenous AP-3 δ subunit did not decrease substantially at ratios of pNL4-3 DNA/AP-3D-5′ DNA ranging from 1:1 to 1:3 (Figure 4D). The half-life of $Pr55^{Gag}$ in cells expressing AP-3D-5′ was prolonged compared to that observed in cells lacking AP-3D-5′, reflecting the fact that $Pr55^{Gag}$ was retained within cells in which the dominant-negative construct was expressed and indicating that the effects of AP-3D-5′ on particle release were not due to enhanced degradation of Gag (Figures S1A and S1B available with this article online). The inhibitory effects of AP-3D-5′ on particle release were not seen upon expression of a C-terminal fragment of AP-3 δ subunit that lacked the Gag interaction domain (AP-3D-3′, Figure 4E). Taken together, these data demonstrate that AP-3D-5′ acts as a dominant-negative inhibitor of assembly.

Depletion of the AP-3 Complex Inhibits HIV Particle Assembly

To further define the role of the AP-3 complex in HIV particle assembly, we depleted the cellular AP-3 complex from 293T or HeLa cells using siRNA techniques. To achieve a significant depletion of the AP-3 complex in 293T cells, we expressed siRNA for both the δ and μ subunits of the complex and transfected 293T cells with the combined siRNA at two time points. In cells cotransfected with pNL4-3 following a single treatment with siRNA, particle release was inhibited by more than 50% as compared with cells receiving control siRNA (Figure 5A, T1). A second treatment with siRNA resulted in enhanced depletion of the μ and δ subunits, and particle release was inhibited by more than 80% as compared with transfection of control siRNA (Figure 5A, T2). The progressive depletion of particle release corresponded to enhanced depletion of endogenous AP-3

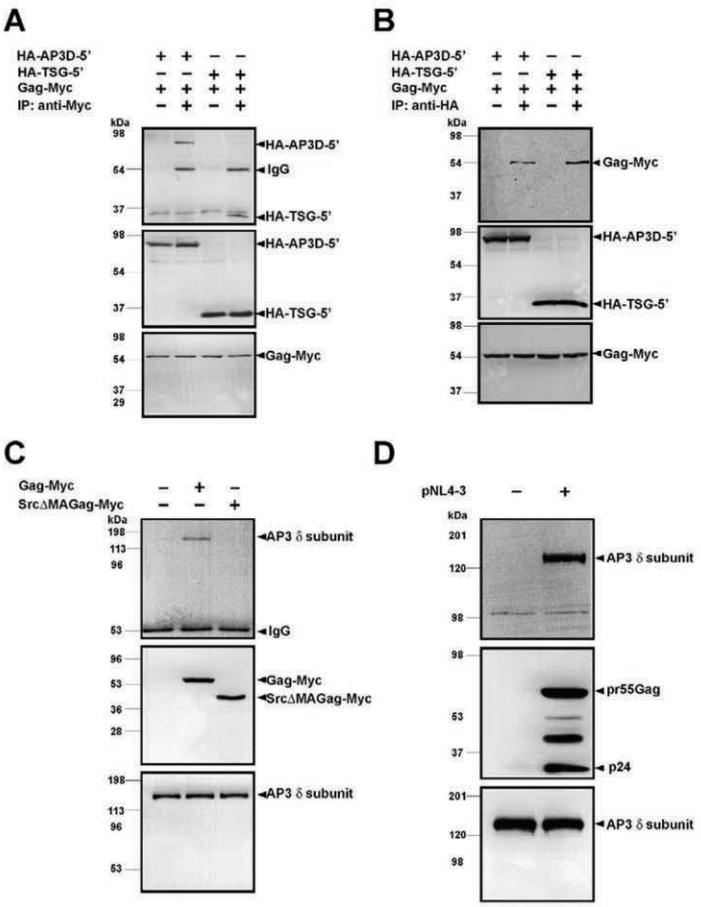

Figure 3. Coimmunoprecipitation of Gag and the AP-3 δ Subunit

(A) Coimmunoprecipitation of AP-3D-5′ and HIV-1 Gag. 293T cells were cotransfected with Gag-myc and either HA-AP-3D-5′ or HA-TSG-5′ as a positive control. Proteins were immunoprecipitated using anti-myc antibodies (second and fourth lanes) or using only protein G sepharose beads (first and third lanes). Coprecipitated HA-AP-3D-5′ was detected by immunoblotting with an anti-HA monoclonal antibody (top panel). Cell lysates are shown prior to immunoprecipitation as probed by the anti-HA antibody (middle panel) or anti-myc antibody (bottom panel).

(B) Reciprocal coimmunoprecipitation of HIV-1 Gag and AP-3D-5′. Cell lysates were prepared as in (A), with immunoprecipitation using anti-HA antibody and detection using anti-myc monoclonal antibody.

(C) Immunoprecipitation of HIV-1 Gag and endogenous AP-3 δ subunit. Proteins were immunoprecipitated from the untransfected 293T cell lysates (input) or transfected lysates using anti-myc polyclonal antisera and detected by Western blot with anti-adaptin δ (top panel). Anti-myc Western blot (middle panel) and anti-adaptin δ Western blot (bottom panel) of the whole-cell lysates are shown.

(D) Immunoprecipitation of NL4-3 and endogenous AP-3 δ subunit. Gag proteins were immunoprecipitated from the mock-transfected HeLa cell lysates (lane 1) or pNL4-3 transfected cell lysates (lane 2) using an anti-capsid monoclonal antibody and immunoblotted with anti-adaptin δ (top panel) and anti-capsid antibodies (middle panel). Western blot with anti-adaptin δ of samples prior to immunoprecipitation is shown in the bottom panel.

components seen in cell lysates, while the AP-1 γ subunit was unaffected (Figure 5B). In HeLa cells, a marked and reproducible inhibition of particle release was demonstrated following siRNA transfection targeting only the δ subunit (Figure 5C). As an additional control for the specificity of this effect, we expressed a myristylated Gag molecule in which MA has been deleted (SrcΔMAGag). The release of SrcΔMAGag was not significantly diminished following siRNA-mediated depletion of the AP-3 δ subunit in HeLa cells (Figure 5D). These results indicate that the Gag-AP-3 δ subunit interaction mediates a productive pathway in particle assembly and suggest that the v-src myristylation signal in the context of MA-deleted Gag allows Gag to bypass the AP-3 trafficking pathway.

The Gag-AP-3 Interaction Is Required for Gag Trafficking to MVBs

The AP-3 adaptor complex is known to direct the intracellular trafficking of protein components, such as CD63, of the MVB (Dell'Angelica et al., 1999; Pelchen-Matthews et al., 2003; Rous et al., 2002). We hypothesized that the trafficking of Gag to MVBs may similarly be under the control of AP-3. To test this hypothesis, we analyzed by confocal microscopy the subcellular distribution of Gag-CFP and endogenous CD63 in the presence or absence of the dominant-negative YFP-tagged AP-3D-5′ fragment. When analyzed at early time points in HeLa cells (12–14 hr posttransfection), a significant fraction of Gag-CFP expressed alone was found in intracellular, punctate sites (Figure 6A). There was significant colocalization seen with Gag-CFP and endogenous CD63 (Figures 6A, 6E, and 6I). In the majority of cells in which Gag-CFP was coexpressed with YFP-AP-3D-5′, Gag was found in a more diffuse cytoplasmic distribution (Figures 6P, 6R, and 6U). However, even in those cells, expressing YFP-AP-3D-5′, that retained a punctate pattern of Gag (Figure 6B), colocalization with CD63 was not observed (Figure 6J). This effect was not unique to the Gag-CFP molecule, as wild-type Gag colocalization with CD63 analyzed by immunostaining was similar to that seen with Gag-CFP (Figures 6C, 6G, and 6K). YFP-AP-3D-5′ similarly resulted in a significant decrease in Gag-CD63 colocalization (Figure 6L). The pattern of endogenous CD63 remained predominantly intracellular and punctate in all cells expressing YFP-AP-3D-5′ (represented by Figures 6F and 6H). The percentage of colocalization of Gag-CFP to CD63 over

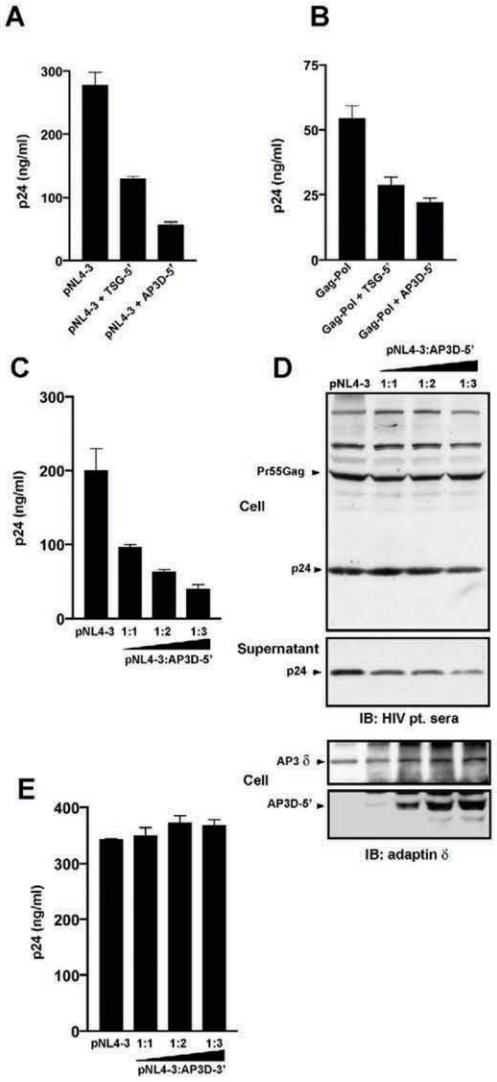

Figure 4. Dominant-Negative Inhibition of Particle Assembly/Release by AP-3D-5′

(A) AP-3D-5′ effects on NL4-3 particle assembly. 293T cells were cotransfected with pNL4-3 in a 1:1 mixture with control pcDNA3.1, TSG-5′, or AP-3D-5′ expression vectors. p24 antigen release into supernatants was measured at 72 hr by antigen-capture ELISA. Data shown represent mean ± SD from triplicate wells.

(B) AP-3D-5′ effects on Gag/pro-mediated particle assembly. 293T cells were transfected with Gag/pro expression vector in a 1:1 mixture with control pCDNA 3.1, TSG-5′, or AP-3D-5′ expression vectors. p24 antigen release into supernatants was measured at 72 hr by antigen-capture ELISA.

(C) Dose-dependent inhibition of assembly by AP-3D-5′. 293T cells were cotransfected with NL4-3 expression vector and AP-3D-5′ expression vector at the indicated ratios (pNL4-3/AP-3D-5′). Supernatant p24 was quantified at 72 hr posttransfection by ELISA.

(D) Western blot analysis of dose-dependent inhibition. Cytoplasmic extracts (top panel) and pelleted virus (middle panel) of samples obtained 72 hr after transfection from the experiment outlined in (C) were harvested and analyzed by Western blot using pooled sera from HIV+ patients. The levels of expressed endogenous AP-3 δ subunit (AP-3D) and overexpressed AP-3D-5′ as detected by anti-adaptin δ Western blot are shown below.

(E) Lack of inhibition on particle assembly by AP-3D-3′. 293T cells were cotransfected with NL4-3 expression vector and AP-3D-3′ expression vector at the indicated ratios, and p24 output in the supernatant was analyzed as in (C).

time was then calculated using the Metamorph software package in cells that did or did not express YFP-AP-3D-5′. Figure 6M demonstrates that Gag-CFP-CD63 colocalization increased over time, but that colocalization was significantly disrupted by the expression of AP-3D-5′. Similarly, Gag (without CFP) colocalization with CD63 was quantitatively diminished by expression of YFP-AP-3D-5′ (Figure 6N). The expression of a YFP-tagged dominant-negative AP-3 fragment allowed us to sometimes identify cells that differed dramatically in expression of this inhibitory molecule within the same microscopic field. Figures 6O and 6P demonstrate a pair of cells expressing Gag-CFP, of which only the bottom cell expresses the inhibitor. Colocalization of endogenous CD63 and Gag-CFP is observed in the upper cell (Figure 6P, an overlay of Gag-CFP and CD63 images), while no colocalization is apparent in the cell expressing the inhibitor (Figure 6P, lower cell).

We next asked if Gag was prevented from trafficking to the plasma membrane in cells expressing AP-3D-5′. To address this, cells were transfected with Gag-CFP and YFP-AP-3D-5′ and examined for Gag-CFP distribution at a later time point (20 hr posttransfection). Figures 6Q and 6R present a pair of cells with differential expression of YFP-AP-3D-5′ examined at 20 hr posttransfection. Note that the cell expressing the dominant-negative inhibitor (the lower cell) exhibits a more diffuse, cytoplasmic pattern of Gag than the upper cell, which retains a punctate pattern. This is representative of the predominant pattern seen by confocal microscopy at this time point. In order to apply quantitative methods to this observation, we first identified three patterns of Gag-CFP seen within the population of cells. Figure 6S represents the plasma membrane distribution pattern, Figure 6T represents the intracellular punctate distribution pattern, and Figure 6U represents the intracellular diffuse pattern. We then enumerated each pattern from images taken of cells expressing Gag-CFP alone or in the presence of YFP-AP-3D-5′. Figure 6V demonstrates that the punctate and plasma membrane patterns of Gag were prominent in cells expressing Gag-CFP alone, while the diffuse pattern was the dominant phenotype in cells expressing the dominant-negative inhibitor. We noted that a subset of cells exhibited a plasma membrane distribution of Gag even in the presence of the inhibitor, suggesting either incomplete inhibition of the AP-3 interaction in these cells or that alternative pathways exist that can lead to Gag-plasma membrane association. Overall, the major conclusions from our imaging data were (1) disruption of the Gag-AP-3 interaction eliminates Gag-CD63 colocalization and (2) AP-3D-5′ disrupts both punctate intracellular and plasma membrane patterns of Gag and elicits a diffuse cytoplasmic distribution pattern of Gag.

We considered the possibility that some of our re-

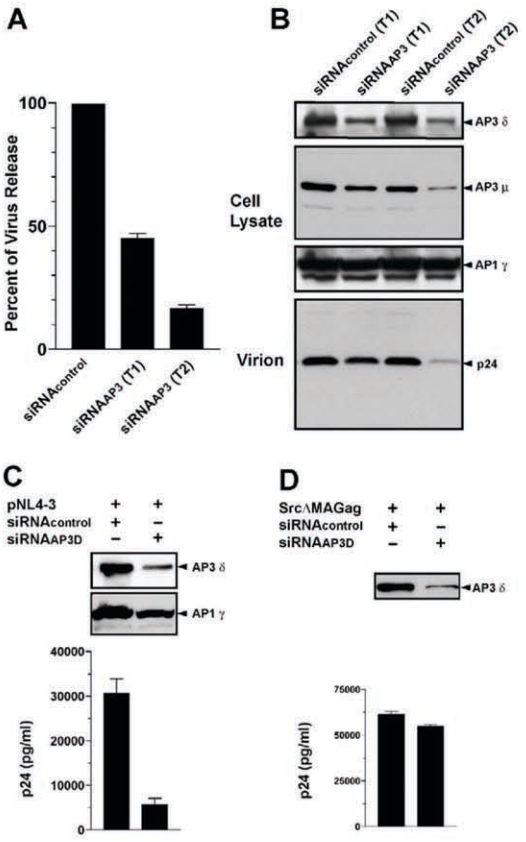

Figure 5. Inhibition of HIV-1 Particle Assembly by siRNA-Mediated Depletion of the AP-3 Complex

(A) 293T cells were transfected with a pool of anti-AP-3 δ and anti-AP-3 μ siRNA duplexes or with control RNA duplexes. A second transfection with siRNA and pNL4-3 was performed 24 hr later, and supernatants were harvested 24 hr following the second transfection (T1). In a parallel experiment, two siRNA transfections were performed 24 hr apart, followed 24 hr later by the siRNA/pNL4-3 cotransfection, and harvesting after an additional 24 hr (T2). Control siRNA transfections were performed separately for each of these experimental arms, and the results are presented as percent of the p24 antigen release as compared with the corresponding control arm. Data shown represent mean ± SD from triplicate experiments.

(B) Western blot demonstrating enhanced depletion of AP-3 δ and μ subunits at T2 of the same experiment depicted in (A), and the corresponding decrease in released viral particles as indicated by p24. Control Western blot of cell lysates demonstrating AP-1 γ subunit is shown.

(C) Depletion of AP-3 δ in HeLa cells inhibits particle assembly. Cells were transfected with a pool of siRNA directed against AP-3 δ or control RNA duplexes and 24 hr later were cotransfected with the same RNA pool and pNL4-3. Top panel demonstrates depletion of AP-3 δ subunit. Bottom graph indicates p24 antigen release following control (left) or following specific depletion of the AP-3 δ subunit.

(D) Resistance of SrcΔMAGag to inhibition by depletion of AP-3. HeLa cells were treated with inhibitory RNA or control RNA exactly as in (C) except that SrcΔMAGag was cotransfected instead of pNL4-3. Top panel indicates δ subunit depletion, bottom graph depicts particle release.

sults could reflect an effect of AP-3D-5′ on late endosomal trafficking in general. However, AP-3D-5′ expression did not alter the plasma membrane expression of CD63 as quantified by flow cytometry, and the lysosomal enzyme cathepsin D was processed in the lysosome at normal levels (Figure S2), indicating that late endosomal trafficking remained intact in the presence of the dominant-negative inhibitor.

Dominant-Negative Inhibition of the Gag-AP-3 Interaction Creates an Assembly Block Distinct from that of TSG-5′

We used transmission electron microscopy to define the stage of the block to assembly introduced by AP-3D-5′ and compared it with TSG-5′. Normal particle budding was readily observed in 293T cells expressing the NL4-3 provirus in control experiments (Figures 7A and 7B). Cells transfected with pNL4-3 and TSG-5′ demonstrated prominent particle buds that were arrested at the plasma membrane, as previously reported for a late budding defect (Figure 7C). In cells transfected with pNL4-3 and AP-3D-5′ at a 1:1 ratio, in contrast, very few budding particles were observed (illustrated by the cell shown in Figure 7D). To provide some quantitation of this observation, we examined 100 consecutive cells prepared for thin-section electron microscopy expressing NL4-3 alone, NL4-3 with TSG-5′, or NL4-3 with AP-3D-5′. Of 100 consecutive cells counted, we observed 10 cells with obvious particle budding in pNL4-3-transfected preparations, 12 in cells expressing NL4-3 and TSG-5′ at a 1:1 ratio, and 0 cells demonstrating particle budding from preparations expressing NL4-3 and AP-3D-5′. We were able to find rare cells demonstrating particle budding in cells expressing NL4-3 and AP-3D-5′ only after examining several hundred additional fields of cells. Particle budding was similarly extremely rare in cells in which the AP-3 complex was depleted using siRNA (data not shown). We interpret the paucity of observed particle budding events to mean that the block to particle assembly introduced by AP-3D-5′ occurs predominantly at a step preceding particle budding. This would be consistent with the predominance of the diffuse cytoplasmic distribution of Gag seen by fluorescence microscopy.

We next utilized a 293 cell clone in which Gag is inducibly expressed to examine particle assembly in MVBs. We transfected these cells with YFP-tagged AP-3D-5′ then sorted cells for YFP expression prior to induction of Gag expression. At 24 hr postinduction, particles were readily observed at both the plasma membrane and at intracellular sites in the control cells (Figures 7E and 7F), while the great majority of cells expressing YFP-AP-3D-5′ demonstrated no particle formation at either location (Figure 7I). The intracellular sites of budding detected in the absence of AP-3D-5′ were MVBs, as revealed by immunogold labeling electron microscopy for CD63 (15 nm beads, Figure 7G). Double labeling for CD63 and Gag revealed that particles were present in the CD63-positive endosomes (inset, Figure 7G and 6 nm beads, Figure 7H). We next evaluated the 293 cells in which AP-3D-5′ was expressed to determine if MVBs were present in these cells in equal numbers. Morphologically, MVBs were easily identified in

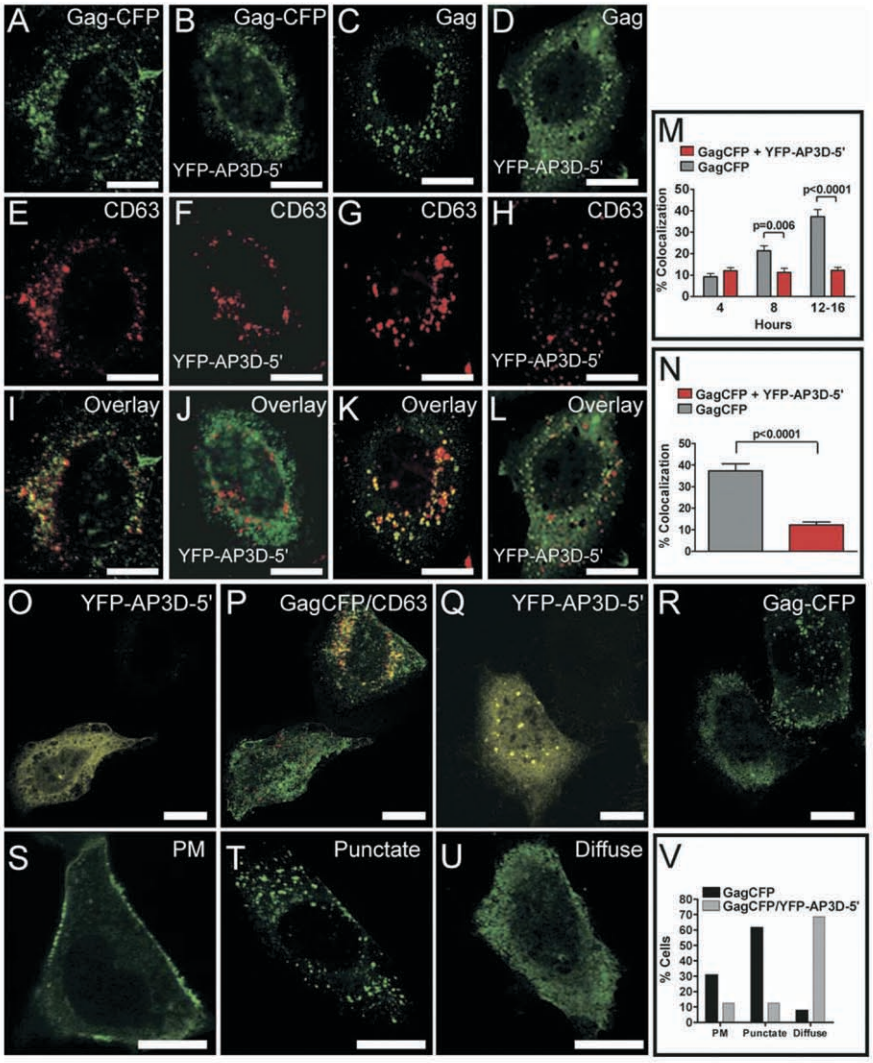

Figure 6. AP-3D-5′ Alters Intracellular Gag Trafficking

HeLa cells were transfected with Gag-CFP and empty control plasmid, Gag-CFP and YFP-AP-3-5′, or with Gag (no CFP tag) with and without YFP-AP-3-5′. Cells were fixed at early (12–14 hr) or late (20 hr, panels Q–V) time points posttransfection and immunostained for Gag and CD63. Gag-CFP and Gag are shown in green, CD63 in red, and colocalized pixels in yellow. Size bars represent 10 microns.

(A–L) AP-3D-5′ inhibits Gag-CD63 colocalization. At early time points, Gag is seen predominantly at intracellular sites (A) and colocalizes with CD63 (E and overlay, I). In the presence of YFP-AP-3D-5′, even those cells demonstrating punctate Gag-CFP (B) do not demonstrate colocalization with CD63 (F and overlay, J). Similarly, Gag was detected by immunostaining in a pattern that colocalized extensively with CD63 (C, G, and overlay, K). YFP-AP-3D-5′ expression inhibited colocalization (D, H, and overlay, L).

(M) Quantitation of Gag-CFP/CD63 colocalization over time. The percentage of Gag-CFP colocalizing with CD63 was quantified using the MetaMorph software application for 25 evaluable cells in the Gag-CFP alone arm and 25 cells in the Gag-CFP + YFP-AP-3D-5′ arm for each time point. Error bars = SEM; p values were derived by paired t test.

(N) Quantitation of Gag/CD63 colocalization. Data were collected as in (M), from cells immunostained for Gag and CD63.

(O) YFP image of a pair of cells expressing Gag-CFP and YFP-AP-3D-5′.

(P) Gag-CFP (green) + CD63 (red) image of same pair of cells depicted in (O).

(Q) YFP image of a pair of cells expressing Gag-CFP and YFP-AP-3D-5′.

(R) CFP image of the same pair of cells as (Q).

(S) Plasma membrane pattern of Gag-CFP.

(T) Intracellular punctate distribution pattern of Gag-CFP.

(U) Intracellular diffuse distribution pattern of Gag-CFP.

(V) Quantitation of the three patterns of Gag-CFP distribution at 20 hr posttransfection for Gag-CFP or Gag-CFP + YFP-AP-3D-5′ arms. PM = plasma membrane pattern. Twenty-six cells were counted in the Gag-CFP alone arm, and thiry-two expressing Gag-CFP with YFP-AP-3D-5′.

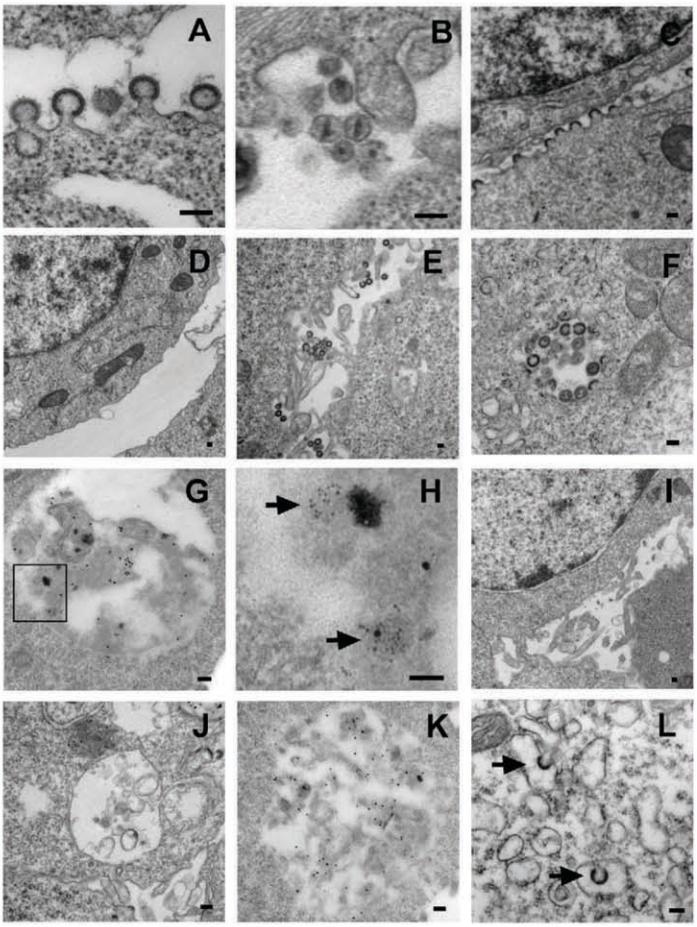

Figure 7. Electron Microscopic Analysis of Particle Assembly Inhibition by AP-3D-5′

(A and B) 293T cells transfected with NL4-3 DNA alone.

(C) 293T cells expressing NL4-3 and TSG-5′.

(D) Lack of particles seen in 293T cells expressing NL4-3 and AP-3D-5′.

(E and F) Plasma membrane and intracellular particle formation from 293 cell clone expressing inducible Gag and Env.

(G) MVB from 293 cell clone demonstrating staining with 15 nm gold beads representing CD63 immunostaining. Six nanomolar beads used for Gag immunolabeling are difficult to appreciate at this magnification.

(H) Magnified view from region indicated in (G) by square. Six nanomolar beads indicate anti-p17 immunogold staining of particles in MVB (arrows); two larger (15 nm) beads are also apparent in this field.

(I) Lack of particle formation in 293 cell clone expressing Gag and Env following expression of YFP-AP-3D-5′.

(J) Transmission electron micrograph of MVB in 293 cell expressing Gag, Env, and YFP-AP-3D-5′.

(K) Immunolabeling of MVB in 293 cell expressing Gag, Env, and YFP-AP-3D-5′. Fifteen nanomolar gold beads represent anti-CD63 immunolabeling.

(L) Intracellular particle formation upon coexpression of NL4-3 bearing a large deletion in MA and YFP-AP-3D-5′ in Cos-7 cells. Double-label immunogold analysis in (G), (H), and (K) was performed using a monoclonal anti-CD63 antibody together with anti-mouse IgG conjugated to 15 nm gold beads and by rabbit anti-p17 polyclonal sera marked by anti-rabbit IgG conjugated to 6 nm gold beads. Magnification is 61,600× (A and B), 17,500 (C), 8800 (D), 13,500 (E), 30,000 (F and G), 116,000 (H), 10,800 (I), 20,000 (J), 24,800 (K), and 34,000 (L). Scale bars represent 100 nm.

these cells (Figure 7J), and CD63 immunostaining proved that these structures were indeed MVBs (Figure 7K, 15 nm beads). The number of CD63-positive endosomes present in serial sections from cells expressing YFP-AP-3D-5′ or control YFP was not significantly different (30 cell sections counted for each, average of 2.4 MVBs for YFP and 2.2 MVBs for YFP-AP-3D-5′-treated cells). Thus, in this cell type, AP-3D-5′ blocked particle formation at the plasma membrane and at intracellular sites but did not disrupt the formation of MVBs. We noted that at late time points postinduction, the high level of Gag expression was able to overcome the effect of AP-3D-5′, and both intracellular and plasma membrane particle assembly could be restored in these cells (data not shown). We conclude that AP-3D-5′ blocked trafficking of Gag to MVBs, as revealed by immunofluorescence, and that particle formation at both intracellular and plasma membrane sites was inhibited by blocking this pathway. Finally, we examined the effect of AP-3D-5′ on the behavior of NL4-3 bearing a large deletion in MA, a construct previously shown to bud predominantly into the endoplasmic reticulum in Cos-7 cells (Facke et al., 1993). Expression of AP-3D-5′ did not block the intracellular budding of the MA-deleted virus (Figure 7L), suggesting that this MA deletion targets Gag to alternative intracellular membranes by a pathway that does not involve the AP-3 complex.

Discussion

Our experiments demonstrate that HIV-1 Gag binds to the δ subunit of the AP-3 complex. The extreme N terminus of the MA region bound specifically to the hinge region of the δ subunit, and Gag constructs lacking MA failed to interact with AP-3. Particle formation by wild-type Gag was substantially diminished by a dominant-negative AP-3δ fragment and by siRNA depletion of AP-3, indicating that the Gag-AP-3 interaction is part of the normal productive trafficking pathway of Gag in the cell. The trafficking of Gag to CD63-positive intracellular compartments was effectively eliminated by the disruption of the Gag-AP-3 interaction. Substitution of the myristyl anchor from v-src for MA allowed efficient particle formation in the presence of the dominant-negative inhibitor of the Gag-AP-3 interaction, suggesting that this modification takes Gag to the plasma

membrane via a distinct pathway. These findings illuminate a previously undescribed early step in the HIV assembly pathway.

Adaptor Complexes and Intracellular Trafficking

Adaptor protein complexes are heterotetramers that mediate the sorting of cargo proteins to specific membrane compartments within the cell (Boehm and Bonifacino, 2002; Nakatsu and Ohno, 2003; Robinson and Bonifacino, 2001). Four adaptor protein complexes have been described in mammalian cells, designated AP-1 through AP-4. AP-3 was first identified through a homology search of cDNA libraries together with database searches (Dell'Angelica et al., 1997; Pevsner et al., 1994; Simpson et al., 1996). Initial immunofluorescence experiments localized AP-3 to the *trans*-Golgi network and to more peripheral endosomal compartments (Dell'Angelica et al., 1997; Simpson et al., 1997). Cells that are deficient in AP-3 demonstrate missorting of lysosomal membrane proteins, including lamp-1, lamp-2, and CD63 (Dell'Angelica et al., 2000; Dell'Angelica et al., 1999; Le Borgne et al., 1998; Rous et al., 2002). Genetic deficiency of the AP-3 β3a subunit in humans leads to a disorder termed Hermansky-Pudlak syndrome, in which defects in lysosome-related organelles such as melanosomes and platelet dense granules are apparent (Dell'Angelica et al., 2000; Starcevic et al., 2002). AP-3 has been implicated in the movement of lytic granules to the immunologic synapse (Clark et al., 2003). A recent immuno-electron microscopy study demonstrated that AP-3 localizes to a tubular sorting endosome compartment (Peden et al., 2004).

We found that the N terminus of the MA region of Gag interacts directly with the AP-3 δ subunit. A number of previous findings make arguments for the biological relevance of this Gag-AP-3 interaction compelling. The MA region has been strongly implicated in the intracellular trafficking of Gag (Facke et al., 1993; Ono and Freed, 1999; Ono et al., 1997; Ono et al., 2000; Spearman et al., 1994). Recent observations by multiple groups indicate that Gag traffics to late endosomes, where Gag and CD63 are found to strongly colocalize (Nguyen et al., 2003; Nydegger et al., 2003; Ono and Freed, 2004; Sherer et al., 2003; von Schwedler et al., 2003). AP-3 is involved in the trafficking of CD63 itself through an interaction between the μ subunit and the lysosomal targeting motif GYEVM on the cytoplasmic tail of CD63 (Dell'Angelica et al., 1999; Rous et al., 2002). Thus Gag may traffic together with CD63 to late endosomal compartments, explaining the previously recognized high degree of colocalization of these two molecules. Interaction with AP-3 thereby provides a specific means by which Gag can reach the late endosome/MVB, where it may acquire components of the ESCRT pathway that are essential to the normal HIV budding process. In most cell types, Gag may then move by other mechanisms from the MVB to the plasma membrane. This model of Gag trafficking and particle assembly predicts that essential components of the particle budding machinery must be acquired in the MVB, and this machinery is redirected to the plasma membrane by Gag. In some cells, such as macrophages, AP-3-mediated trafficking of Gag to the MVB is followed by viral budding into the lumen of the MVB. The intact viral particles within the MVB or "viral exosome" may be transported subsequently to the cell surface for release.

It is important to recognize that alternative trafficking models can be proposed to explain our data. One intriguing model states that Gag first reaches the tubular recycling endosome in an AP-3-dependent manner. From there, Gag may follow either a "default" recycling pathway to reach the plasma membrane or continue on an AP-3-dependent path to the MVB in a manner similar to the trafficking of lysosomal membrane proteins (Peden et al., 2004). Factors that regulate the choice of one of these pathways may differ by cell type and may be invoked to explain plasma membrane budding seen in lymphocytes versus MVB budding in macrophages. These models require direct testing in future experiments. Recently a dileucine motif in the capsid region of Gag has been identified as an interaction site for the AP-2 μ subunit (Lindwasser and Resh, 2004). This motif was functionally active in the context of a Gag-CD4 chimeric molecule, suggesting that it may act to bring plasma membrane Gag into endocytic trafficking pathways. The potential involvement of multiple adaptor family members in Gag trafficking thus may contribute to the overall complexity of Gag trafficking in the cell.

Implications for Adaptor Protein Involvement in Additional Steps in Virus Assembly

Our data demonstrating that productive HIV particle formation utilizes the AP-3 trafficking pathway have several potential implications for HIV particle assembly. It is not yet known where Gag and Env meet within the cell. The cytoplasmic tail of gp41 contains a tyrosine-based signal that is active in promoting clathrin-mediated endocytosis through an interaction with the μ subunit of AP-2 (Berlioz-Torrent et al., 1999; Boge et al., 1998). It is possible that cell-surface Env complexes are internalized to a sorting/recycling endosome compartment, where they may become associated with Gag. Notably, the μ3A subunit is also capable of interacting with the endocytosis motif in the gp41 cytoplasmic tail (Ohno et al., 1997), raising the possibility that Gag and Env may interact on the same adaptor protein complex. Trafficking of both Gag and Env to the MVB through AP-3 interactions would be consistent with the observation that Gag and Env both traffic to the MVB and that infectious particles form within the MVB lumen of macrophages (Pelchen-Matthews et al., 2003).

The identification of the δ subunit of AP-3 as a Gag binding partner may also help to elucidate unique functions of this subunit. To our knowledge, there are no known cellular binding partners for the hinge region of this subunit. In yeast, a component of the Vps pathway, Vps41, binds to the carboxyl terminus of the δ subunit homolog Apl5p and contributes to the transport of alkaline phosphatase to the vacuole (Darsow et al., 2001; Rehling et al., 1999). It will be important to identify δ subunit binding partners in mammalian cells in order to better understand the role played by this subunit in vesicular trafficking. It is possible that Gag binds to a site on the δ subunit that is also utilized by cellular cargo proteins, in a manner analogous to that in which

Gag competes with the Hrs protein for binding to cellular pools of TSG101.

In summary, Gag binds to the AP-3 complex and uses this route to reach the MVB. This appears to be a productive pathway for HIV particle assembly, even in cell types in which particle assembly takes place predominantly on the plasma membrane. The identification of the Gag-AP-3 interaction elucidates one piece of an increasingly complex pathway by which viral and cellular components interact to generate HIV particles.

Experimental Procedures

Plasmid Constructs

pNL4-3 was obtained from Dr. Malcolm Martin through the NIH AIDS Reference and Reagent Program. Expression constructs for the AP-3 δ subunit (AP-3D) were derived from full-length cDNA kindly provided by Margaret Robinson (University of Cambridge, United Kingdom); AP-3 δ constructs including residues 1–742 (AP-3D-5′) with or without an HA tag and 743–1203 (AP-3D-3′) were generated by PCR cloning into pcDNA3.1. DNA encoding AP-3 δ subunit residues 1–742 was also amplified and inserted into pEYFP-C1 (Clontech) to generate YFP-AP-3D-5′. Full-length TSG101 was cloned from a HeLa cDNA library, and a 5′ fragment (residues 10–240) was amplified and cloned into pCMV-HA (Clontech) to generate HA-TSG-5′. Codon-optimized Gag constructs were derived from pVRC3900 provided by Gary Nabel (VRC, NIH) (Huang et al., 2001). Gag constructs with or without a carboxy-terminal myc epitope tag and with a deletion of the MA region (codons 1–132) fused to the N-terminal 9 residues of v-src were generated by PCR cloning into pCDNA3.1. Matrix deletion constructs (pMAD1-10) were provided by Max Essex (Harvard University, Boston, Massachusetts) (Yu et al., 1992) and were cloned into yeast 2-hybrid vector pGBKT7 for yeast expression (Clontech) using the Nde1 and BamH1 sites. A series of Gag protein truncation products were also cloned into pGBKT7 for directed yeast 2-hybrid assays. GST fusion constructs with specific regions derived from the codon-optimized *gag* gene were created (MA, CA, NC, p6, MACA, MACANC, CANCp6, full-length Gag) by PCR cloning into pGEX-2T (Amersham Pharmacia), as was a GST fusion with the AP-3 binding domain (residues 554–844). All expression constructs were verified by sequencing throughout the amplified regions. Expression vector Gag-CFP has been previously described (Derdowski et al., 2004), and the construct 3-CCCC for Gag-Pol expression was a gift from Hans-Georg Krausslich (University of Hamburg, Germany) (Wodrich et al., 2000). pNL4-3 bearing a large deletion in the MA coding region (lacking codons 16 to 99) identical to a construct previously described (Facke et al., 1993) was created by PCR mutagenesis. A stably transduced 293 cell line expressing Gag and Env from a tetracycline-inducible promoter was created using the RevTet vector system (Clontech). This cell line (293/Gag-Env) incorporates codon-optimized *gag* and *env* genes separated by an internal ribosome entry site under the control of the tetracycline-responsive promoter for coordinated, inducible expression of Gag and Env.

Yeast Two-Hybrid Assays

Two-hybrid library screening was performed using full-length codon-optimized Gag (codons 1–1503) as bait fused to codons 1–147 of the Gal4 DNA binding domain (BD) in vector pGBKT7 (Clontech). Prey constructs were derived from a human HeLa cDNA library fused to the C terminus of codons 768–881 from the Gal4 activation domain in vector pACT2, and yeast 2-hybrid screening performed according to the manufacturer's instructions (Clontech). For liquid culture assays, cells in mid-log phase were processed as described (Schneider et al., 1996) and β-galactosidase units were quantitated in a spectrophotometer.

Protein Expression and GST Pulldown

GST fusion proteins were expressed in *E. coli* BL21 (DE3) cells (Novagen) and purified using glutathione-sepharose beads. The immobilized GST fusion proteins were incubated for 2–4 hr at 4°C with 293T cell lysates, washed extensively, and eluted, followed by detection by Western blotting using the monoclonal antibodies indicated below. The interaction region fragment was produced similarly as a GST fusion and then exposed to ρ-amino-benzamidine-agarose beads for removal of thrombin. The interaction domain protein was then dialyzed against PBS in a Slide-A-Lyzer Dialysis Cassette (Pierce). For interaction experiments, 30 μl of a concentrated preparation was added to each of the Gag-GST fusion proteins, and an equal amount analyzed on the gel used to detect the eluted proteins by Coomassie staining.

Antibodies and Coimmunoprecipitation

293T cells were maintained in Dulbecco's modified Eagle medium with 10% fetal bovine serum and antibiotics at 37°C in 5% CO_2 and grown in 10 cm^2 culture dishes. Transfections were performed by the calcium phosphate method. Cells were harvested 36–48 hr posttransfection, washed, and broken by dounce homogenization in hypotonic buffer. The cell lysates were centrifuged at 1500 × g for 10 min, and the supernatants were immunoprecipitated with anti-HA, anti-Myc, or anti-p24 monoclonal antibody 183-H12-5C (provided by Bruce Chesebro and Kathy Wehrly through the NIH AIDS Research and Reference Reagent Program) then detected by Western blotting. Antibodies used for detection of AP subunits were from BD Biosciences 611328 for AP-3 δ subunit, 610900 for AP-3 μ subunit, and 610385 for AP-1 γ subunit; antibody for cathepsin D was sc-6486 (Santa Cruz).

RNA Interference (RNAi)

Twenty-one nucleotide siRNA duplexes with symmetric two nucleotide 3′-UU overhangs were obtained from Dharmacon and correspond to the following AP-3 δ subunit targets: nucleotides 176–194 (TCTGCAAGCTGACGTATTT), 489–507 (GAAGAAGGCTGTGCT GATC), 2438–2456 (GCGAGAAACTGCCTATTCA), and 2493–2511 (GAAGGACGTTCCCATGGTA). An additional siRNA reagent was generated in our laboratory using the Silencer siRNA construction kit (Ambion) following the manufacturer's instructions and targeting the AP-3 μ subunit nucleotides 237–255 (TTGAGTTCCTACATCG AGT). Control siRNA duplexes were duplex I sense strand (GCUGA GUAUACGCGGAUGUUU) with 53% GC content and control duplex II (ACCACCAACAUAUCUACGCUU) with 47% GC content. siRNA transfection was performed with Lipofectamine 2000 (Invitrogen). For each siRNA knockdown experiment, 100 nM siRNA was used in experimental and control arms, and the control siRNA used was matched for GC content to the active arm.

Immunofluorescence Microscopy

HeLa cells were grown on glass cover slips in 6-well plates and were transfected using with Lipofectamine 2000 (Invitrogen). Transfected cells were fixed with 3.8% formaldehyde in sodium phosphate buffer, stabilized in cytoskeletal stabilization buffer (100 mM PIPES, 1 mM EDTA, 3% PEG6000, pH 6.9), permeabilized with 0.1% Triton X-100, and blocked with 5% bovine serum albumin. Cells were incubated with mouse anti-Lamp-3 (1:100, Santa Cruz), washed, and incubated with goat anti-mouse Alexa 546-conjugated antibodies (1:3000, Molecular Probes). In some experiments, Gag staining was performed with polyclonal anti-p17 antisera (Varthakavi et al., 2002) detected via goat anti-rabbit Alexa 546-conjugated antibodies, and CD63 was revealed by mouse anti-Lamp-3 followed by anti-mouse Alexa 633-conjugated antibodies. Confocal images were acquired using a Zeiss LSM510 laser-scanning confocal microscope (Carl Zeiss Inc.), and data analysis performed with MetaMorph software (Universal Imaging Corporation).

Electron Microscopy

Transfected 293T cells or doxycycline-induced 293/Gag-Env cells were fixed, sectioned, and stained in preparation for transmission electron microscopy as previously described (Sandefur et al., 2000). Post-embedding immunogold labeling of samples for CD63 and Gag was performed using LR white-embedded 100 nm sections essentially as previously described (Wang et al., 2001). Antibodies for these studies included polyclonal anti-p17 antisera (Varthakavi et al., 2002) and anti-LAMP3 murine monoclonal antibody (sc-5275, Santa Cruz Biotechnology). Fifteen nanomolar gold beads conjugated to goat anti-mouse IgG antibody and 6 nm gold beads

conjugated to goat anti-rabbit IgG were purchased from EM Sciences. Images were obtained on a Philips CM-12 electron microscope equipped with a high-resolution CCD camera.

Supplemental Data

Supplemental Data include two figures and can be found with this article online at http://www.cell.com/cgi/content/full/120/5/663/DC1/.

Acknowledgments

We thank the Vanderbilt Cell Imaging Shared Resource for assistance with confocal microscopy and its Electron Microscopy Core for help with EM studies (supported by NIH grants CA68485, DK20593, DK58404, and HD15052). We thank Margaret Robinson for the gift of the AP-3 δ subunit cDNA. The Vanderbilt-Meharry CFAR (P30 AI054999) was instrumental in providing key reagents and stimulating collaborations. This work was supported primarily by NIH R01 AI40338 and NIH R21 AI055441. Additional support was from the Howard Hughes Medical Institute (T.R.P.), RO1 AI32539 (T.S.D.), and the Elizabeth B. Lamb Center for Pediatric Research (T.R.P. and T.S.D.).

Received: July 2, 2004
Revised: December 21, 2004
Accepted: December 23, 2004
Published: March 10, 2005

References

Babst, M., Odorizzi, G., Estepa, E.J., and Emr, S.D. (2000). Mammalian tumor susceptibility gene 101 (TSG101) and the yeast homologue, Vps23p, both function in late endosomal trafficking. Traffic *1*, 248–258.

Berlioz-Torrent, C., Shacklett, B.L., Erdtmann, L., Delamarre, L., Bouchaert, I., Sonigo, P., Dokhelar, M.C., and Benarous, R. (1999). Interactions of the cytoplasmic domains of human and simian retroviral transmembrane proteins with components of the clathrin adaptor complexes modulate intracellular and cell surface expression of envelope glycoproteins. J. Virol. *73*, 1350–1361.

Boehm, M., and Bonifacino, J.S. (2002). Genetic analyses of adaptin function from yeast to mammals. Gene *286*, 175–186.

Boge, M., Wyss, S., Bonifacino, J.S., and Thali, M. (1998). A membrane-proximal tyrosine-based signal mediates internalization of the HIV-1 envelope glycoprotein via interaction with the AP-2 clathrin adaptor. J. Biol. Chem. *273*, 15773–15778.

Clark, R.H., Stinchcombe, J.C., Day, A., Blott, E., Booth, S., Bossi, G., Hamblin, T., Davies, E.G., and Griffiths, G.M. (2003). Adaptor protein 3-dependent microtubule-mediated movement of lytic granules to the immunological synapse. Nat. Immunol. *4*, 1111–1120.

Darsow, T., Katzmann, D.J., Cowles, C.R., and Emr, S.D. (2001). Vps41p function in the alkaline phosphatase pathway requires homo-oligomerization and interaction with AP-3 through two distinct domains. Mol. Biol. Cell *12*, 37–51.

Dell'Angelica, E.C., Ohno, H., Ooi, C.E., Rabinovich, E., Roche, K.W., and Bonifacino, J.S. (1997). AP-3: an adaptor-like protein complex with ubiquitous expression. EMBO J. *16*, 917–928.

Dell'Angelica, E.C., Shotelersuk, V., Aguilar, R.C., Gahl, W.A., and Bonifacino, J.S. (1999). Altered trafficking of lysosomal proteins in Hermansky-Pudlak syndrome due to mutations in the beta 3A subunit of the AP-3 adaptor. Mol. Cell *3*, 11–21.

Dell'Angelica, E.C., Aguilar, R.C., Wolins, N., Hazelwood, S., Gahl, W.A., and Bonifacino, J.S. (2000). Molecular characterization of the protein encoded by the Hermansky-Pudlak syndrome type 1 gene. J. Biol. Chem. *275*, 1300–1306.

Derdowski, A., Ding, L., and Spearman, P. (2004). A novel fluorescence resonance energy transfer assay demonstrates that the human immunodeficiency virus type 1 Pr55Gag I domain mediates Gag-Gag interactions. J. Virol. *78*, 1230–1242.

Facke, M., Janetzko, A., Shoeman, R.L., and Krausslich, H.G. (1993). A large deletion in the matrix domain of the human immunodeficiency virus gag gene redirects virus particle assembly from the plasma membrane to the endoplasmic reticulum. J. Virol. *67*, 4972–4980.

Franke, E.K., Yuan, H.E., and Luban, J. (1994). Specific incorporation of cyclophilin A into HIV-1 virions. Nature *372*, 359–362.

Freed, E.O. (1998). HIV-1 gag proteins: diverse functions in the virus life cycle. Virology *251*, 1–15.

Garrus, J.E., von Schwedler, U.K., Pornillos, O.W., Morham, S.G., Zavitz, K.H., Wang, H.E., Wettstein, D.A., Stray, K.M., Cote, M., Rich, R.L., et al. (2001). Tsg101 and the vacuolar protein sorting pathway are essential for HIV-1 budding. Cell *107*, 55–65.

Gould, S.J., Booth, A.M., and Hildreth, J.E. (2003). The Trojan exosome hypothesis. Proc. Natl. Acad. Sci. USA *100*, 10592–10597.

Huang, Y., Kong, W.P., and Nabel, G.J. (2001). Human immunodeficiency virus type 1-specific immunity after genetic immunization is enhanced by modification of Gag and Pol expression. J. Virol. *75*, 4947–4951.

Katzmann, D.J., Babst, M., and Emr, S.D. (2001). Ubiquitin-dependent sorting into the multivesicular body pathway requires the function of a conserved endosomal protein sorting complex, ESCRT-I. Cell *106*, 145–155.

Le Borgne, R., Alconada, A., Bauer, U., and Hoflack, B. (1998). The mammalian AP-3 adaptor-like complex mediates the intracellular transport of lysosomal membrane glycoproteins. J. Biol. Chem. *273*, 29451–29461.

Lindwasser, O.W., and Resh, M.D. (2004). Human immunodeficiency virus type 1 Gag contains a dileucine-like motif that regulates association with multivesicular bodies. J. Virol. *78*, 6013–6023.

Luban, J. (2001). HIV-1 and Ebola virus: the getaway driver nabbed. Nat. Med. *7*, 1278–1280.

Martin-Serrano, J., Zang, T., and Bieniasz, P.D. (2003). Role of ESCRT-I in retroviral budding. J. Virol. *77*, 4794–4804.

Nakatsu, F., and Ohno, H. (2003). Adaptor protein complexes as the key regulators of protein sorting in the post-Golgi network. Cell Struct. Funct. *28*, 419–429.

Nguyen, D.G., Booth, A., Gould, S.J., and Hildreth, J.E. (2003). Evidence that HIV budding in primary macrophages occurs through the exosome release pathway. J. Biol. Chem. *278*, 52347–52354.

Nydegger, S., Foti, M., Derdowski, A., Spearman, P., and Thali, M. (2003). HIV-1 egress is gated through late endosomal membranes. Traffic *4*, 902–910.

Ohno, H., Aguilar, R.C., Fournier, M.C., Hennecke, S., Cosson, P., and Bonifacino, J.S. (1997). Interaction of endocytic signals from the HIV-1 envelope glycoprotein complex with members of the adaptor medium chain family. Virology *238*, 305–315.

Ono, A., and Freed, E.O. (1999). Binding of human immunodeficiency virus type 1 Gag to membrane: role of the matrix amino terminus. J. Virol. *73*, 4136–4144.

Ono, A., and Freed, E.O. (2004). Cell-type-dependent targeting of human immunodeficiency virus type 1 assembly to the plasma membrane and the multivesicular body. J. Virol. *78*, 1552–1563.

Ono, A., Huang, M., and Freed, E.O. (1997). Characterization of human immunodeficiency virus type 1 matrix revertants: effects on virus assembly, Gag processing, and Env incorporation into virions. J. Virol. *71*, 4409–4418.

Ono, A., Orenstein, J.M., and Freed, E.O. (2000). Role of the Gag matrix domain in targeting human immunodeficiency virus type 1 assembly. J. Virol. *74*, 2855–2866.

Peden, A.A., Oorschot, V., Hesser, B.A., Austin, C.D., Scheller, R.H., and Klumperman, J. (2004). Localization of the AP-3 adaptor complex defines a novel endosomal exit site for lysosomal membrane proteins. J. Cell Biol. *164*, 1065–1076.

Pelchen-Matthews, A., Kramer, B., and Marsh, M. (2003). Infectious

HIV-1 assembles in late endosomes in primary macrophages. J. Cell Biol. *162*, 443–455.

Pevsner, J., Volknandt, W., Wong, B.R., and Scheller, R.H. (1994). Two rat homologs of clathrin-associated adaptor proteins. Gene *146*, 279–283.

Pornillos, O., Higginson, D.S., Stray, K.M., Fisher, R.D., Garrus, J.E., Payne, M., He, G.P., Wang, H.E., Morham, S.G., and Sundquist, W.I. (2003). HIV Gag mimics the Tsg101-recruiting activity of the human Hrs protein. J. Cell Biol. *162*, 425–434.

Raposo, G., Moore, M., Innes, D., Leijendekker, R., Leigh-Brown, A., Benaroch, P., and Geuze, H. (2002). Human macrophages accumulate HIV-1 particles in MHC II compartments. Traffic *3*, 718–729.

Rehling, P., Darsow, T., Katzmann, D.J., and Emr, S.D. (1999). Formation of AP-3 transport intermediates requires Vps41 function. Nat. Cell Biol. *1*, 346–353.

Robinson, M.S., and Bonifacino, J.S. (2001). Adaptor-related proteins. Curr. Opin. Cell Biol. *13*, 444–453.

Rous, B.A., Reaves, B.J., Ihrke, G., Briggs, J.A., Gray, S.R., Stephens, D.J., Banting, G., and Luzio, J.P. (2002). Role of adaptor complex AP-3 in targeting wild-type and mutated CD63 to lysosomes. Mol. Biol. Cell *13*, 1071–1082.

Sandefur, S., Smith, R.M., Varthakavi, V., and Spearman, P. (2000). Mapping and characterization of the N-terminal I domain of human immunodeficiency virus type 1 Pr55(Gag). J. Virol. *74*, 7238–7249.

Schneider, S., Buchert, M., and Hovens, C.M. (1996). An in vitro assay of beta-galactosidase from yeast. Biotechniques *20*, 960–962.

Sherer, N.M., Lehmann, M.J., Jimenez-Soto, L.F., Ingmundson, A., Horner, S.M., Cicchetti, G., Allen, P.G., Pypaert, M., Cunningham, J.M., and Mothes, W. (2003). Visualization of retroviral replication in living cells reveals budding into multivesicular bodies. Traffic *4*, 785–801.

Simpson, F., Bright, N.A., West, M.A., Newman, L.S., Darnell, R.B., and Robinson, M.S. (1996). A novel adaptor-related protein complex. J. Cell Biol. *133*, 749–760.

Simpson, F., Peden, A.A., Christopoulou, L., and Robinson, M.S. (1997). Characterization of the adaptor-related protein complex, AP-3. J. Cell Biol. *137*, 835–845.

Spearman, P., Wang, J.J., Vander Heyden, N., and Ratner, L. (1994). Identification of human immunodeficiency virus type 1 Gag protein domains essential to membrane binding and particle assembly. J. Virol. *68*, 3232–3242.

Starcevic, M., Nazarian, R., and Dell'Angelica, E.C. (2002). The molecular machinery for the biogenesis of lysosome-related organelles: lessons from Hermansky-Pudlak syndrome. Semin. Cell Dev. Biol. *13*, 271–278.

Strack, B., Calistri, A., Craig, S., Popova, E., and Gottlinger, H.G. (2003). AIP1/ALIX is a binding partner for HIV-1 p6 and EIAV p9 functioning in virus budding. Cell *114*, 689–699.

Varthakavi, V., Smith, R.M., Deng, H., Sun, R., and Spearman, P. (2002). Human immunodeficiency virus type-1 activates lytic cycle replication of Kaposi's sarcoma-associated herpesvirus through induction of KSHV Rta. Virology *297*, 270–280.

VerPlank, L., Bouamr, F., LaGrassa, T.J., Agresta, B., Kikonyogo, A., Leis, J., and Carter, C.A. (2001). Tsg101, a homologue of ubiquitin-conjugating (E2) enzymes, binds the L domain in HIV type 1 Pr55(Gag). Proc. Natl. Acad. Sci. USA *98*, 7724–7729.

von Schwedler, U.K., Stuchell, M., Muller, B., Ward, D.M., Chung, H.Y., Morita, E., Wang, H.E., Davis, T., He, G.P., Cimbora, D.M., et al. (2003). The protein network of HIV budding. Cell *114*, 701–713.

Wang, J.J., Sandefur, S., Spearman, P., Chiou, C.T., Chiang, P.H., and Ratner, L. (2001). Tracking the assembly pathway of human immunodeficiency virus type 1 Gag deletion mutants by immunogold labeling. Appl. Immunohistochem. Mol. Morphol. *9*, 371–379.

Wills, J.W., and Craven, R.C. (1991). Form, function, and use of retroviral gag proteins. AIDS *5*, 639–654.

Wodrich, H., Schambach, A., and Krausslich, H.G. (2000). Multiple copies of the Mason-Pfizer monkey virus constitutive RNA transport element lead to enhanced HIV-1 Gag expression in a context-dependent manner. Nucleic Acids Res. *28*, 901–910.

Yu, X., Yuan, X., Matsuda, Z., Lee, T.H., and Essex, M. (1992). The matrix protein of human immunodeficiency virus type 1 is required for incorporation of viral envelope protein into mature virions. J. Virol. *66*, 4966–4971.

APPENDIX E

APOBEC3G MULTIMERS ARE RECRUITED TO THE PLASMA MEMBRANE FOR PACKAGING INTO HUMAN IMMUNODEFICIENCY VIRUS TYPE 1 VIRUS-LIKE PARTICLES IN AN RNA-DEPENDENT PROCESS REQUIRING THE NC BASIC LINKER

BURNETT A, AND P SPEARMAN

Journal of Virology. 81(10):5000-5013, 2007

JOURNAL OF VIROLOGY, May 2007, p. 5000–5013 Vol. 81, No. 10
0022-538X/07/$08.00+0 doi:10.1128/JVI.02237-06
Copyright © 2007, American Society for Microbiology. All Rights Reserved.

APOBEC3G Multimers Are Recruited to the Plasma Membrane for Packaging into Human Immunodeficiency Virus Type 1 Virus-Like Particles in an RNA-Dependent Process Requiring the NC Basic Linker▽

Atuhani Burnett[1,2] and Paul Spearman[2]*

Department of Microbiology and Immunology, Vanderbilt University School of Medicine, Nashville, Tennessee,[1] and Departments of Pediatrics and Microbiology and Immunology, Emory University School of Medicine, Atlanta, Georgia[2]

Received 11 October 2006/Accepted 27 February 2007

APOBEC3G is an endogenous host restriction factor that inhibits human immunodeficiency virus (HIV) replication. The antiviral activity of APOBEC3G is dependent upon its incorporation into the virus particle. The mechanisms governing incorporation of APOBEC3G into virus particles are not completely understood. In particular, some investigators have reported that APOBEC3G interacts directly with the nucleocapsid (NC) subunit of Gag, while others have found that an RNA intermediate is required for Gag-APOBEC3G interactions. In this study, we confirmed the RNA dependence of APOBEC3G packaging and performed detailed mapping of the determinants within NC that are required for virion incorporation. Surprisingly, APOBEC3G packaging did not correlate well with the presence of the N-terminal "I," or interaction, domain within NC. Specifically, Gag constructs containing only the N-terminal region of NC packaged minimal amounts of APOBEC3G, while significant levels of APOBEC3G packaging were achieved with Gag constructs containing the basic linker region of NC. Furthermore, membrane-binding experiments revealed that the basic linker region was essential for the membrane association of APOBEC3G in a Gag-APOBEC3G complex. Fluorescence resonance energy transfer was detected between labeled APOBEC3G in cells and in particles, indicating that APOBEC3G is packaged as a multimer that is bound to packaged RNA. Regions of APOBEC3G-Gag colocalization at the plasma membrane were detected that were distinct from the punctate cytoplasmic bodies where APOBEC3G accumulates within the cell. Together, our results indicate that APOBEC3G multimerizes in an RNA-dependent fashion and that RNA-APOBEC3G multimers are recruited to the plasma membrane and subsequently into virion particles by Gag.

Human immunodeficiency virus type 1 (HIV-1) infection is a major cause of morbidity and mortality worldwide. The ability of HIV to subvert natural human immune defenses has contributed highly to its success in infecting more than 40 million people worldwide. The cytidine deaminase APOBEC3G restricts the replication of retroviruses, including HIV, macaque simian immunodeficiency virus, murine leukemia virus (12, 20, 27, 36), retrotransposons (29), and other viruses containing a reverse transcription step, such as hepatitis B virus (32). APOBEC3G is incorporated into virions exiting the infected cell. Upon infection of the target cell, APOBEC3G causes deamination of cytidines on single-stranded DNA intermediates created during the reverse transcription process. This results in extensive G-to-A nucleotide substitutions in the proviral DNA (12, 18, 20, 39). HIV-1 counteracts the action of APOBEC3G through the action of the viral infectivity factor (Vif), which binds to APOBEC3G and links it to an E3 ligase for polyubiquitination and subsequent degradation by the ubiquitin proteasome pathway (6, 11, 37). A critical aspect of the antiviral function of APOBEC3G is, thus, its ability to be packaged into assembling virions (15, 21, 28).

* Corresponding author. Mailing address: Pediatric Infectious Diseases, Emory University School of Medicine, 2015 Uppergate Dr., Atlanta, GA 30322. Phone: (404) 727-5642. Fax: (404) 727-8249. E-mail: paul_spearman@oz.ped.emory.edu.

▽ Published ahead of print on 7 March 2007.

The HIV-1 Gag protein is responsible for facilitating APOBEC3G incorporation into virions as evidenced by the fact that Gag virus-like particles (VLPs) efficiently incorporate APOBEC3G (10, 31, 38). Furthermore, in vitro binding experiments have shown that APOBEC3G binds efficiently to the nucleocapsid (NC) region of the Gag polyprotein (1, 4, 19, 26, 31, 38). In fact, Gag constructs in which a leucine zipper protein-protein interaction domain replaced the nucleocapsid region produced particles devoid of APOBEC3G (19, 38). The mechanisms by which NC recruits APOBEC3G are not entirely clear. In particular, the role played by RNA and distinct RNA binding regions within NC has been controversial. In vitro binding experiments between NC and APOBEC3G that utilize RNA depletion by RNase A treatment have been reported which support (19, 26, 31, 38) or refute (1, 4) the role that an RNA bridge may play in this interaction.

An essential retroviral assembly function is contained within the N-terminal region of nucleocapsid (2, 3, 33). This assembly function, termed the interaction ("I") domain, is necessary for Gag-Gag multimerization, formation of detergent-resistant Gag complexes, plasma membrane localization of Gag, and formation of normal density retroviral particles (7, 24, 25). The "I" domain has been implicated in mediating RNA binding to NC through electrostatic interactions of basic residues with cellular or viral RNA. Furthermore, in experiments using a C-terminal NC truncation model in a Gag context, the "I"

domain phenotype correlated with the number of basic residues expressed (24). Therefore, it seemed reasonable to hypothesize that the underlying mechanisms governing APOBEC3G incorporation might be linked to the underlying mechanisms governing the "I" domain assembly functions.

In this report, we examine the requirements for APOBEC3G incorporation into HIV VLPs. Surprisingly, we found that APOBEC3G incorporation did not correlate closely with the presence of the I domain. Rather, mapping of APOBEC3G incorporation and RNA revealed a key role for the basic linker region between the two zinc finger domains of NC. The amount of RNA incorporated into particles did correlate with APOBEC3G recruitment to the plasma membrane and packaging into particles. Finally, we developed a fluorescence resonance energy transfer (FRET) assay to detect APOBEC3G-RNA-APOBEC3G complexes and showed that these complexes were packaged into Gag virus-like particles. Together, these data suggest that APOBEC3G is packaged into virions as an RNA-dependent multimer that is recruited to the plasma membrane and into budding virions by the HIV Gag protein.

MATERIALS AND METHODS

Plasmid construction. This study employed Gag and APOBEC3G expression constructs fused to variants of the codon-optimized version of cyan fluorescent protein (CFP) and yellow fluorescent protein (YFP) (Clontech, Palo Alto, CA). Some of the CFP and YFP expression vectors and several of the Gag expression constructs were previously described (7). Briefly, the C-terminal CFP and YFP expression constructs were created by first replacing the enhanced green fluorescent protein (EGFP) gene in pEGFP-N3 (Clontech) with either the CFP gene from pECFP-N1 or the YFP gene from pEYFP-N1. These new constructs were designated pECFP-N3 and pEYFP-N3, respectively (7). The N-terminal YFP expression construct was produced by replacing the EGFP gene in pEGFP-C1 (Clontech) with the YFP gene from pEYFP, using an AgeI site located 5′ to the ATG start site in both plasmids and a BsrGI site located in the 3′ end of both genes prior to the stop codon. This new construct was designated pEYFP-C1. The Gag coding sequences for all constructs were derived from the codon-optimized version of HIV-1 strain HXB2 Gag in expression plasmid pVRC3900 (13). PCR cloning was then used to amplify the *gag* gene from the pVRC3900 vector, with a HindIII site at the 5′ ATG and a BamHI site at the 3′ end. The amplified *gag* gene was then ligated into both pEYFP-N3 and pECFP-N3 by digestion of the BamHI and HindIII sites located within the multiple cloning regions. A schematic diagram of the Gag expression constructs employed in this study is shown in Fig. 2B. The APOBEC3G coding sequences for all constructs were derived from plasmid CEM15, which was obtained from Michael Malim, along with a C-terminal hemagglutinin (HA)-tagged version; both have been described previously (27). These constructs are referred to hereafter as APOBEC3G and APOBEC3G-HA. PCR cloning was used to amplify the APOBEC3G gene with an EcoRI site prior to the 5′ ATG codon and an SmaI site at the 3′ end. The amplified APOBEC3G gene was then ligated into pEYFP-N3 by digestion of the EcoRI and SmaI sites located within the multiple cloning region. This new construct was designated A3G-YFP. PCR cloning was used to amplify the APOBEC3G gene with an EcoRI site prior to the 5′ ATG codon and an XmaI site at the 3′ end. The amplified APOBEC3G gene was then ligated into pEYFP-C1 by digestion of the EcoRI and XmaI sites located within the multiple cloning region. This new construct was designated YFP-A3G. PCR cloning was used to amplify the CFP gene from pECFP-N3, placing a SmaI site prior to the 5′ ATG codon and a NotI site at the 3′ end. The YFP gene in A3G-YFP was then removed by digestion with SmaI and NotI, followed by gel purification. The amplified CFP gene was then ligated into the resulting plasmid to yield a new construct designated A3G-CFP.

The following oligonucleotides were used for PCR amplifications of Gag-CFP constructs. Forward oligonucleotides for all Gag-CFP constructs were GTCAAGCTTGTCGACATGG GCGCCCGCGCCAGC-(F); oligonucleotides used for Gag391-CFP were CGGGATCCCTTCACGATCTT GCGCT G-(R); for Gag405-CFP were CGGGATCCGCAGTTGCGGGCGGTGTG-(R); for Gag411-CFP were CGGGATCCCTTC TTGCGGGGGGCGCG-(R); for Gag426-CFP were CGGGATCCGCAGTCCTTCATCTGGTG-(R); and for Gag432-CFP were CGG GATCCATTAGCCTGTCGCTCGGTG-(R). Oligonucleotides used for PCR amplifications of the A3G-YFP construct were GGAATTCGCCACCATGAAGCCTCACTTCAGAAAC-(F) and TCG CCCGGGTTTTCCTGATTCTG GAG-(R); for the YFP-A3G construct were CGGAATTCGATGAAGCCTCACTTCAGA-(F) and TCCCCCGGGT CAGTTTT CCTGATT-(R); and for the A3G-CFP construct were GGCCC GGGATCCATCGCCACCATGGTGAGCAAG-(F) and GAGTCGC GGCC GCTTTACTTGTACAGCTCGTCCATGCCG-(R).

Cells and transfections. 293T cells were used for all studies, maintained in Dulbecco's modified Eagle medium with 10% fetal bovine serum and antibiotics at 37°C in 5% CO_2, and grown in 100-cm^2 tissue culture dishes. Transfections were performed either with the calcium phosphate-bis-buffered saline transfection method or with Lipofectamine 2000 (Invitrogen, Carlsbad, CA), with 10 μg of total plasmid DNA, unless otherwise stated.

Production and purification of immature Gag VLPs. Cell culture supernatants from transfected 293T cells were harvested 48 to 72 h posttransfection, clarified by centrifugation, filtered through a 0.45-μm-pore-sized filter, and pelleted through a 20% sucrose cushion (100,000 × *g* for 2 h at 4°C). The pellets were resuspended in 1.0 ml of phosphate-buffered saline (PBS) and analyzed by scanning cuvette fluorometry using a tunable PTI cuvette fluorometer (Photon Technology International, Lawrenceville, NJ).

Antibodies and immunoblotting. Particle and lysate preparations were analyzed by sodium dodecyl sulfate (SDS)-polyacrylamide gel electrophoresis (PAGE), followed by transfer to nitrocellulose membranes and immunoblotting. Gag was blotted with sera pooled from HIV-seropositive patients. APOBEC3G antisera was provided by Warner C. Greene through the NIH AIDS Research and Reference Reagent Program (30). Secondary horseradish peroxidase-conjugated antibodies for enhanced chemiluminescence film analysis were obtained from Promega (Madison, WI). Secondary fluorescence-conjugated antibodies for detection with a LI-COR Odyssey imaging system were obtained from LI-COR, Inc. (Lincoln, NE).

Gradient analysis of Gag VLPs. Gag VLPs, purified as described above, were analyzed by centrifugation on linear 20 to 60% sucrose gradients. Particles resuspended in PBS were overlaid on linear 20 to 60% sucrose gradients. Ultracentrifugation was performed at 100,000 × *g* overnight at 4°C in a Beckman SW41 rotor. Equal fractions were collected, and the density of each fraction was determined with a refractometer. Samples were subsequently diluted in PBS and pelleted at 100,000 × *g* for 2 h at 4°C in a Sorvall S45A rotor. Samples were resuspended in 100 μl of PBS. Protein content was analyzed by scanning cuvette fluorometry, and RNA content was analyzed by RiboGreen dye incorporation after treatment with RQ1 DNase according to the manufacturer's instructions. Briefly, 10 μl of each fraction was incubated with 0.1 unit/μl of RQ1 DNase and half of the supplied reaction buffer (5 mM $MgSO_4$, 20 mM Tris-HCl, 0.5 mM $CaCl_2$) in PBS for 2 h at 37°C. Samples were then incubated with 0.1% SDS at 65°C for 20 min to lyse particles. An equivalent volume of RiboGreen (Invitrogen, Carlsbad, CA), diluted 200 times in Tris-EDTA buffer, was then added and allowed to sit in the dark for 10 min. Samples were read on a VersaFluor (Bio-Rad Laboratories, Hercules, CA) cuvette fluorometer along with RNA standards. The original concentration of RNA was then calculated.

Isolation of membrane fractions and analysis by scanning cuvette fluorometry. Cells were harvested for analysis 48 h following transfection. Three 10-cm^2 dishes of nearly confluent 293T cells were included for each experimental sample. Cells were washed in phosphate-buffered saline, allowed to swell in hypotonic buffer (10 mM Tris-Cl [pH 8.0], plus protease inhibitors) for 20 min on ice, and broken by Dounce homogenization. For nuclease-treated FRET experiments, the lysis buffer was supplemented with 60 μg/ml of RNase A (QIAGEN Inc., Valencia, CA) and 10 units/ml of RQ1 DNase with buffer (Promega Corp., Madison, WI), while the control lysis buffer was treated with 200 units/ml of RNase inhibitor (New England Biolabs Inc., Beverly, MA). The lysates were then adjusted to 0.1 M NaCl, and the nuclei and unbroken cells were removed by centrifugation at 1,000 × *g* for 10 min. Postnuclear supernatants containing cytosolic and membrane components were then adjusted to 50% iodixanol from a stock solution of 60% iodixanol (Nycomed Pharma, Oslo, Norway). Forty percent and 10% solutions of iodixanol were layered on top of the 50% iodixanol layer. The preparation was centrifuged in a Beckman SW41 rotor at 41,000 rpm for 2 h at 4°C. The membrane fraction was taken from the 10% to 40% iodixanol interface as a 1-ml sample. Each sample was kept at 4°C and analyzed by fluorometry in a PTI T-format scanning cuvette spectrofluorometer (Photon Technology international, Lawrenceville, NJ). For analysis of CFP emission, to compare the relative amounts of CFP present, samples were excited at 433 nm, and an emission scan ranging from 460 to 550 nm was performed. For analysis of YFP emission, to compare the relative amounts of YFP present, samples were excited at 513 nm, with an emission scan ranging from 524 to 534 nm. For FRET analysis, whole cells or particles resuspended in PBS were excited at 433 nm, and

an emission scan ranging from 460 to 550 nm was obtained. It should be noted that a constant amount of untagged Gag expression plasmid was cotransfected in each arm of this experiment. Data were collected from at least three different independent experiments for each expression construct.

Fluorescence microscopy analysis of subcellular localization of A3G-YFP and Gag-CFP. Live HeLa cells expressing A3G-YFP alone or together with Gag-CFP were examined using a Nikon TE2000 microscope equipped with automated filter wheels, a stage, a *z*-axis motor, and a digital camera. All images were obtained using the 63× objective; serial sectioning was performed using MetaMorph software (Molecular Devices), and deconvolution was performed using constrained iterative algorithms with Autoquant software. For the images shown in Fig. 8F to H, a digital mirror device (Mosaic Digital Diaphragm, Photonic Instruments, St. Charles, IL) and a 488-nm laser were used to specifically photobleach the internal regions of the cell surrounding bright cytoplasmic bodies of A3G-YFP.

Fluorescence microscopy analysis of the subcellular localization of A3G-YFP and A3G-CFP FRET. Live HeLa cells expressing A3G-YFP alone or together with A3G-CFP were examined using the 63× objective on a Nikon TE2000 microscope. FRET images were obtained by the sensitized emission method, followed by deconvolution with a constrained iterative algorithm (MetaMorph Autoquant software package; Molecular Devices). Briefly, donor and acceptor constants were first generated by the following method. A CFP image and a raw FRET image (CFP excitation/YFP emission) were obtained from cells expressing Gag-CFP alone, and a YFP image and a raw FRET image were obtained from cells expressing Gag-YFP alone. The pixel intensity of the raw FRET image was divided by the pixel intensity of the corresponding CFP image to yield the donor constant, *A*, of 0.78. This was repeated for YFP to yield the acceptor constant, *B*, of 0.11. These constants were then used to generate true FRET images from raw FRET images in the following way. Each cell was serially sectioned using MetaMorph software (Molecular Devices) for all three wavelengths (CFP, YFP, and raw FRET). A FRET image was then generated for each *z* plane using the following formula applied to each pixel: FRET = raw FRET − $A \times$ CFP − $B \times$ YFP. Finally, the same deconvoluted *z* plane was selected for the CFP, YFP, and FRET images, and all were treated as follows. MetaMorph imaging software was used to set identical scaling for the YFP and CFP images; scaling of FRET images was set at 50% of the YFP image display value, so that the dimmer FRET images are represented in Fig. 10 with intensities similar to those of the YFP and CFP images. Each set of three images in this figure (CFP/YFP/FRET) was treated in the same manner. Images were colorized as cyan or yellow, exported as red-green-blue tagged image files (TIF), and converted to cyan-magenta-yellow-black (CMYK) images using Adobe Illustrator.

FRET acceptor photobleaching and spectral analysis using laser confocal fluorescence microscopy. HeLa cells were grown and transfected in cell culture-treated chamber slides and imaged following fixation in 4% paraformaldehyde for 10 min. Images were obtained with a Zeiss LSM 510 laser scanning confocal microscope (Carl Zeiss Inc., Thornwood, NY) equipped with a Meta multichannel detector, making pixel intensity quantitation possible over a range of emission wavelengths. Emission scans were obtained by using Zeiss LSM software following stimulation with a 405-nm laser. A 514-nm laser was used to provide high-intensity pulses of light for photobleaching of YFP to specified regions of interest in the cell. A standard YFP excitation-emission picture was taken before and after the photobleaching.

RESULTS

Specificity of APOBEC3G packaging into Gag VLPs. We first confirmed the findings of other groups that Gag alone was sufficient to package APOBEC3G. Gag VLPs were produced with 293T cells in the presence and absence of APOBEC3G-HA overexpression. When APOBEC3G-HA was expressed alone, it was not released into the cell culture medium. However, Gag expression and VLP production were sufficient and necessary to release APOBEC3G into the cell culture medium (Fig. 1A). In order to facilitate quantitative studies of the specificity of APOBEC3G packaging into Gag VLPs, a fluorescence system for tracking the relative amounts of APOBEC3G and Gag was developed using an APOBEC3G-YFP fusion protein (hereafter referred to as A3G-YFP). Packaging of A3G-YFP into Gag VLPs was readily demonstrated (Fig. 1B), indicating that

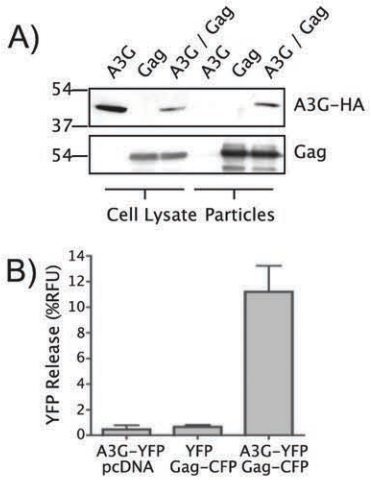

FIG. 1. APOBEC3G incorporation into Gag VLPs. (A) APOBEC3G bearing an HA tag was expressed in 293T cells in the presence or absence of Gag. Shown are immunoblots probed with anti-HA antibody (top) and pooled HIV patients' sera (bottom). (B) A3G-YFP or YFP alone was coexpressed with Gag-CFP, and the amounts of YFP incorporated into Gag-CFP particles and corresponding cell lysates were quantified using a scanning cuvette fluorometer. Results are shown as a percentage of total relative fluorescence units (%RFU) released (supernatant/supernatant + cell).

APOBEC3G-fluorescent protein fusions could be useful tools to further characterize the determinants of APOBEC3G packaging.

Efficient APOBEC3G incorporation requires the NC basic linker region. The packaging of APOBEC3G into virions or VLPs has been shown by a number of groups to be dependent on NC (1, 4, 19, 26, 31, 38). We sought to better define the region of NC required for APOBEC3G packaging and to determine if APOBEC3G packaging sequences correlate directly with the "I" domain that localizes to NC (7, 24, 25). In order to do this, we utilized a panel of Gag protein constructs fused to CFP that spans the NC region (Fig. 2B). These constructs have been extensively characterized for the production of particles of normal density, for membrane-binding properties, and for their ability to interact with detergent-resistant membrane fractions (8, 24, 25). We reasoned, therefore, that we could correlate these properties with APOBEC3G packaging.

VLPs were collected and purified from 293T cells cotransfected with A3G-YFP and each of the Gag-CFP fusion constructs. Relative levels of Gag were determined by CFP fluorescence, and relative APOBEC3G levels were determined by YFP fluorescence. Approximately equivalent expression levels of APOBEC3G in each of the cell lysates examined were verified by YFP fluorescence (data not shown). Very small amounts of APOBEC3G were released in the absence of Gag (Fig. 1B), presumably in microvesicles that copurify with the VLPs. The small amount of A3G-YFP released in the absence of Gag (always less than 5% of values in the presence of Gag) was subtracted from the fluorescence values in the presence of each of the Gag-CFP constructs, and the Gag-dependent packaging of A3G-YFP was plotted (Fig. 2C). Values were ex-

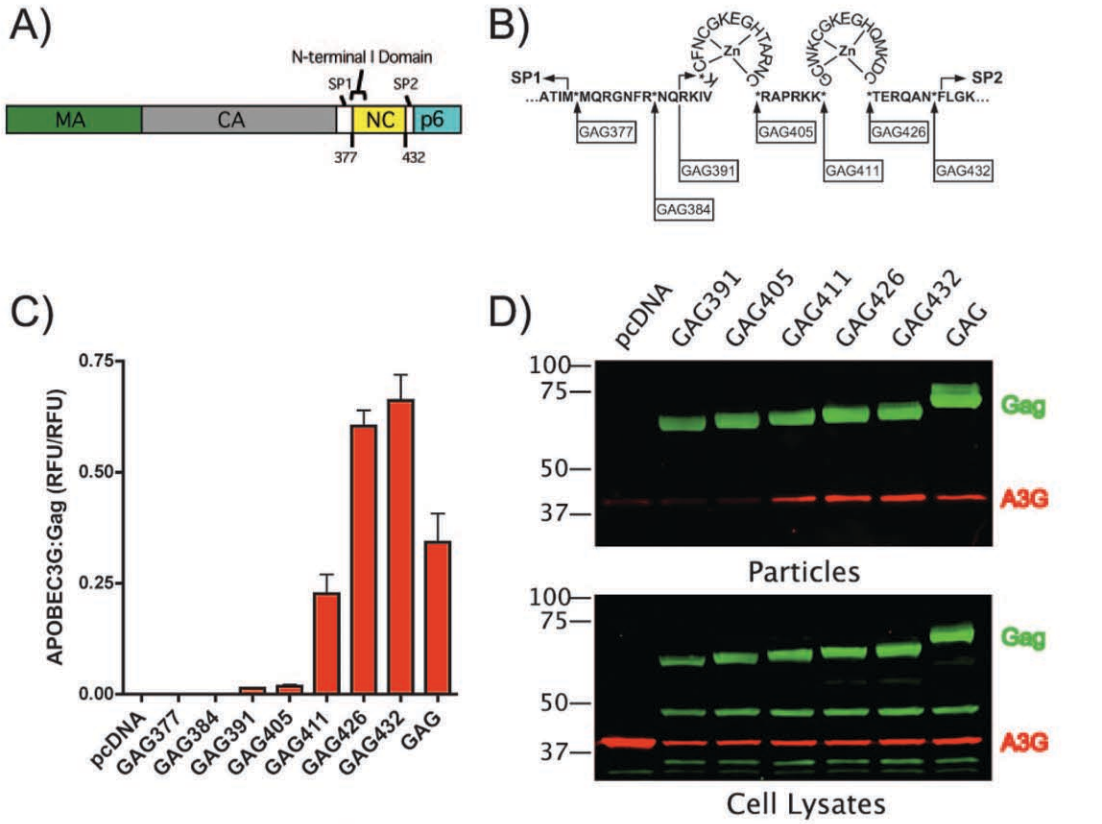

FIG. 2. Nucleocapsid determinants of APOBEC3G incorporation. (A) Schematic illustration of $Pr55^{Gag}$ and position of the N-terminal I domain and selected amino acids. (B) Schematic representation of Gag-CFP constructs subdividing HIV-1 NC. Asterisks indicate the sites of Gag truncation and CFP fusion. The number represents the C-terminal amino acid residue expressed, with the Gag initiator methionine considered residue 1. Arrows represent HIV protease cleavage sites. (C) Gag-CFP fusion constructs illustrated above were cotransfected with A3G-YFP. Supernatants were concentrated through a 20% sucrose cushion. A3G-YFP released in microvesicle contamination is estimated by the YFP fluorescence released when A3G-YFP is cotransfected with pcDNA control and represented less than 5% of the signal seen upon expression of full-length Gag. This value was subtracted, and the resulting numbers of Gag-induced relative fluorescence units (RFU) of A3G-YFP released, normalized to the amount of Gag protein present, are shown. (D) Gag-CFP fusion constructs illustrated above were cotransfected with APOBEC3G. Supernatants were concentrated through a 20% sucrose cushion. CFP fluorescence was used to normalize virus-like particle concentration. Proteins were resolved by SDS-polyacrylamide gel electrophoresis, followed by immunoblot analysis with APOBEC3G antisera and pooled HIV patient sera for Gag-CFP.

pressed as YFP relative fluorescence units (counts/s) divided by CFP relative fluorescence units (counts/s).

Gag377-CFP expresses MA, CA, and SP1 of Gag and failed to package APOBEC3G (Fig. 2C). Gag384-CFP includes the minimal "I" domain (24) yet unexpectedly also failed to package APOBEC3G. Additional constructs that did not contain the basic linker region (between amino acids 405 and 411) packaged very little APOBEC3G, despite being released into the medium in the form of VLPs. This was true for Gag405-CFP, a Gag-CFP fusion construct that includes the intact N-terminal zinc finger domain, which failed to package APOBEC3G above background levels (Fig. 2C). However, addition of the six-amino-acid basic linker region represented in Gag411-CFP produced a sharp increase in packaging efficiency. Interestingly, constructs that contain the basic linker plus the second zinc finger region but lack p6 incorporated an enhanced amount of APOBEC3G compared to that of the wild-type Gag, using this assay.

To ensure that this packaging phenotype was not an artifact of the YFP fusion construct, these experiments were repeated with an untagged APOBEC3G construct. In this experiment, the VLP pellets were normalized for loading by measuring the amount of Gag as indicated by CFP fluorescence, and the incorporated APOBEC3G protein was detected by Western blotting on a LI-COR fluorescence imaging system. Gag411-CFP, a construct containing the basic linker, demonstrated APOBEC3G packaging, as did those constructs that included the second zinc finger and the entire NC region (Fig. 2D). Together, these results confirm the dependence of APOBEC3G packaging on the nucleocapsid region and suggest that the

basic linker is required for incorporation. Strikingly, the packaging requirements of APOBEC3G were distinct from those of the "I" domain, which have been mapped more proximally to the N-terminal domain of NC (24).

RNA content of particles correlates with APOBEC3G content. Both APOBEC3G and the NC subunit of Gag are known to bind RNA. The role of RNA binding in packaging has not been completely resolved. While some investigators report RNA-dependent packaging (26, 31, 38), others have reported a direct APOBEC3G-NC interaction (1, 4). If the ability of NC to bind to cellular RNA is the prime determinant of APOBEC3G packaging into HIV VLPs, then we would expect that the amount of RNA packaged in VLPs would correlate with the quantity of APOBEC3G packaged. Furthermore, truncated Gag constructs that lack subdomains of NC may package less cellular RNA. In order to test these hypotheses, VLPs from several of the constructs shown in Fig. 2B were purified by equilibrium density sedimentation on a linear sucrose gradient. Equal fractions were collected, treated with DNase, and analyzed for protein content by CFP fluorescence and for RNA content by incorporation of the fluorescent dye RiboGreen (Molecular Probes). The RNA content of each construct, expressed as an RNA/Gag fluorescence ratio, present in the 1.16 g/ml particle peak is shown in Fig. 3A, and a representative curve demonstrating cofractionation of total RNA and Gag is shown in Fig. 3B. We found measurable RNA incorporation in constructs representing the "minimal" I domain (Fig. 3A, Gag384), which did not increase substantially when the entire N-terminal domain was included (Fig. 3A, Gag405). Inclusion of the NC basic linker substantially increased the RNA/Gag ratio (Fig. 3A, Gag411), and inclusion of full-length NC enhanced this ratio further (Fig. 3A, Gag432). The pattern of RNA incorporation that we observed closely mimicked the relative levels of incorporation of A3G-YFP (compare Fig. 3A and Fig. 2C). These data support a model in which APOBEC3G binds to the cellular RNA that is incorporated into the developing virion and indicate that the quantity of APOBEC3G incorporated is greatest in those particles with the highest RNA content, which in this experiment was the result of nonspecific interactions between NC and cellular RNA. Interestingly, the very low level of APOBEC3G packaged in the absence of the basic linker region (Fig. 2C), despite packaging of some cellular RNA by Gag384 and Gag405, argues that there may be either a specific contribution of the basic linker region of NC for packaging or a threshold level of RNA incorporation that dictates packaging.

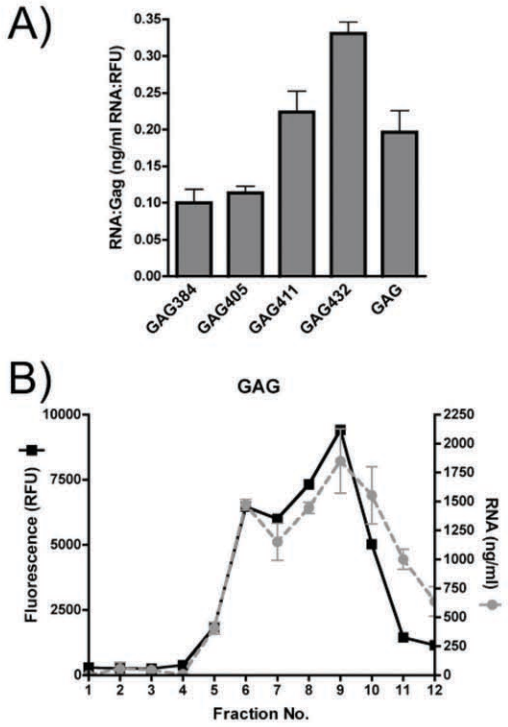

FIG. 3. RNA content of particles correlates closely with APOBEC3G content. Gag-CFP fusion constructs were transfected into 293T cells. Supernatants were purified on linear 20 to 60% sucrose gradients. Fractions were collected from the top of the gradient, treated with RQ1 DNase, stained with RiboGreen, and subjected to analysis by fluorometry. (A) RNA content of particles in peak fractions is shown normalized to Gag-CFP content (RNA:Gag ratio). RFU, relative fluorescence units. (B) Sedimentation pattern of Gag-CFP VLPs (black squares) and associated RNA (gray circles).

The NC basic linker is required for membrane recruitment of APOBEC3G. Particle budding is known to occur at the plasma membrane in both primary T cells and 293T cells. Therefore, we determined whether Gag constructs that packaged APOBEC3G also recruited it to membrane fractions. 293T cells were cotransfected with A3G-YFP and the panel of Gag-CFP truncation mutants, and membranes were isolated via flotation on iodixanol gradients. The membrane-enriched fraction was collected and assayed along with the cell lysates for APOBEC3G and Gag protein content by YFP and CFP fluorescence intensity, respectively. Results are expressed as the percentage of membrane fluorescence compared to total cell lysate fluorescence (Fig. 4). Marked recruitment of cellular APOBEC3G to cellular membranes was observed upon expression of Gag (Fig. 4A). The recruitment of APOBEC3G to the membrane fraction largely mirrored the results described above for particle incorporation: those constructs that lacked the basic linker failed to recruit APOBEC3G into membrane fractions. In parallel, we measured the membrane flotation of Gag (Fig. 4B). Remarkably, Gag membrane association did not demonstrate a requirement for the basic linker (Fig. 4B). The association of Gag constructs bearing only the N-terminal subdomain of NC with membranes is consistent with our previous description of the I domain (24) and indicates that the determinants mapped as the I domain are distinct from the packaging requirements for APOBEC3G. These data support a more specific role for the basic linker region in APOBEC3G interaction and recruitment to cellular membranes.

RNase disrupts APOBEC3G binding to NC. Indirect evidence has indicated the importance of RNA in the recruitment of APOBEC3G into Gag VLPs. To directly assess the question of RNA involvement, a glutathione *S*-transferase (GST) sedimentation assay was employed. Cell lysates expressing APOBEC3G-HA were added to each Gag subunit, fused to GST, and conjugated to glutathione Sepharose beads. After extensive washing, it was

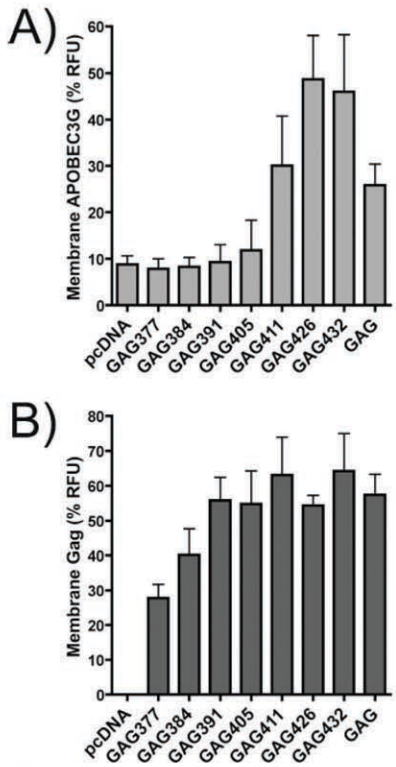

FIG. 4. Nucleocapsid determinants of APOBEC3G membrane recruitment. Gag-CFP fusion constructs illustrated in Fig. 2B were cotransfected with A3G-YFP. The protein content of membrane-enriched fractions generated by flotation on iodixanol step gradients was determined by fluorescence spectrophotometry. The percentage of protein present in the membrane fraction was calculated by dividing by the amount of protein present in the total cell lysate. (A) YFP signal was used to determine the amount of APOBEC3G present in membrane fractions for each indicated construct. RFU, relative fluorescence units. (B) CFP signal was used to determine the amount of Gag protein present in membrane fractions for each indicated construct.

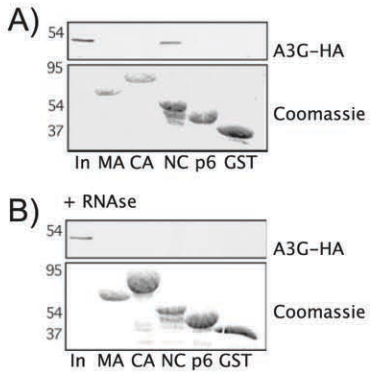

FIG. 5. RNase disrupts APOBEC3G binding to NC. (A) Cell lysates from 293T cells expressing APOBEC3G-HA were added to glutathione agarose beads containing the indicated bacterially purified Gag subunits. After extensive washing, the glutathione beads were analyzed by SDS-PAGE, followed by both Coomassie blue staining and immunoblot analysis with anti-HA for APOBEC3G-HA. In, 5% of input. (B) As described above, following the addition of RNase and DNase to the cell lysates prior to performing GST pulldown.

found that APOBEC3G-HA bound only to the NC region and not to other Gag subunits (Fig. 5A). When cell lysates were treated with nucleases, this binding was abolished (Fig. 5B). These results are consistent with those already published by several groups, further supporting an important role for RNA in particle incorporation of APOBEC3G (26, 31, 38).

APOBEC3G multimers bind to RNA in cells and particles. FRET between CFP and YFP moieties has been used to detect interactions between Gag molecules in living cells. Briefly, stimulation of a CFP molecule at 433 nm normally leads to the emission of a strong peak at 475 nm, a shoulder from 490 to 510 nm, and a broad trail from 510 to 550 nm (Fig. 6A, A3G-CFP emission spectra). YFP molecules are maximally stimulated at 514 nm; therefore, if a YFP molecule is in contact (less than 100 angstroms) from an excited CFP molecule, the overlap in CFP emission and YFP excitation will allow energy transfer from the CFP to the YFP molecule. This will lead to the YFP molecule emitting at 527 nm.

APOBEC molecules are known to dimerize when binding to RNA (14, 35). Therefore, in an effort to develop an assay to detect A3G-RNA-A3G complexes in live cells, A3G-YFP and A3G-CFP were coexpressed in 293T cells, and the emission spectra of whole cells, resuspended in PBS, were obtained with a spectrofluorometer using an excitation wavelength of 433 nm. Cells expressing A3G-YFP and A3G-CFP exhibited a curve representative of efficient fluorescence energy transfer (Fig. 6A, gray squares), as did Gag-CFP and Gag-YFP (Fig. 6A, open squares), while cells expressing A3G-CFP and a control YFP resulted in a CFP emission peak with no YFP emission peak (Fig. 6A, open circles). Identical results were obtained with YFP-A3G (results not shown). Similar levels of YFP emission were obtained upon YFP excitation for each experimental condition, indicating that the protein levels were similar (Fig. 6B).

To determine whether RNA was a necessary component of these APOBEC3G complexes, cell lysates from cells expressing A3G-YFP and A3G-CFP were prepared and treated with RNase A and DNase RQ1, while RNA in control lysates was preserved by the addition of RNase inhibitor. Control lysates expressing A3G-YFP and A3G-CFP exhibited a curve representative of efficient fluorescence energy transfer (Fig. 6C, shaded squares), while nuclease-treated lysates resulted in a CFP emission peak with no YFP emission peak (Fig. 6C, open circles). The A3G-CFP emission curve remained unchanged by nuclease treatment (Fig. 6C, closed triangles, closed diamonds). The lack of FRET in the nuclease-treated lysates was not a result of lower protein concentration or degradation since similar levels of YFP emission were obtained upon YFP excitation for each experimental condition (Fig. 6D). This establishes that FRET is an effective tool with which to measure the presence of APOBEC3G multimers bound to RNA and that RNA is required for APOBEC3G multimerization.

We next employed A3G-CFP/A3G-YFP FRET to determine whether APOBEC3G is incorporated into particles as a

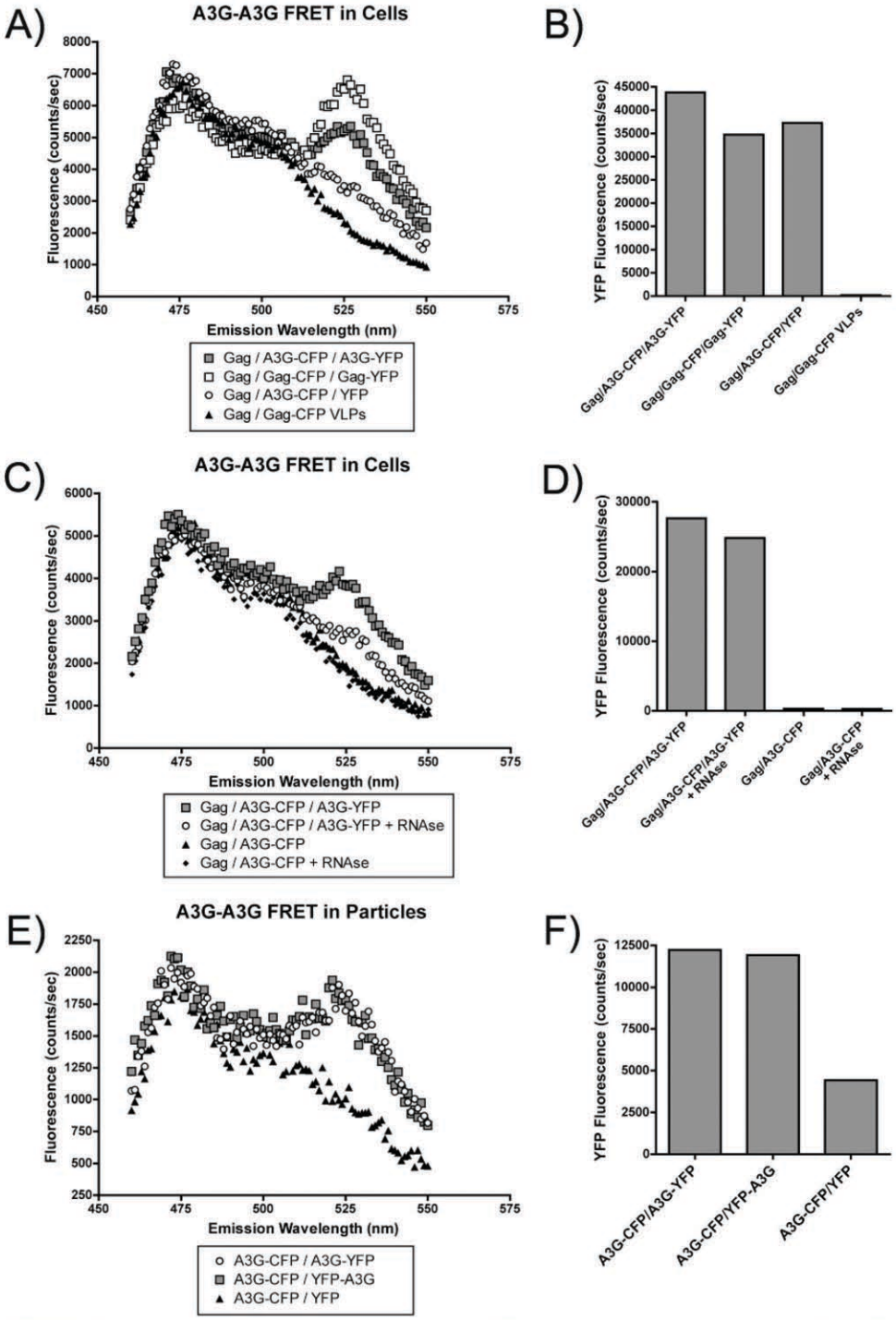

FIG. 6. APOBEC3G is packaged as multimers that interact with RNA. (A) The indicated constructs were cotransfected into 293T cells. Cells were resuspended in PBS and read directly with a scanning cuvette fluorometer. FRET was measured by stimulating the CFP fluorophore at 433 nm, and the FRET peak was observed at 527 nm. Gray squares, FRET curve for A3G-YFP/A3G-CFP and GagCFP/GagYFP (open squares). Open

multimeric complex bound to RNA. Gag VLPs were generated in cells expressing Gag, A3G-YFP, and A3G-CFP. The emission spectra of these particles were obtained with a spectrofluorometer using an excitation wavelength of 433 nm. Particles containing A3G-CFP and A3G-YFP (Fig. 6E, open circles) or A3G-CFP and YFP-A3G (Fig. 6E, gray squares) exhibited a curve representative of efficient fluorescence energy transfer. However, particles containing A3G-CFP and a control YFP resulted in a CFP emission peak with no YFP emission peak (Fig. 6E, closed triangles). Increased YFP overexpression was used in this experiment to increase the free YFP content of VLPs. We conclude that the FRET detected in Gag VLPs represents APOBEC3G multimers bound to RNA that have become incorporated in VLPs.

Lack of support for a direct Gag-APOBEC3G interaction by FRET. To further analyze the Gag-APOBEC3G interaction in living cells and particles, we asked whether we could detect a direct Gag-APOBEC3G interaction by a FRET assay. Cells expressing Gag-YFP and Gag-CFP exhibited a curve representative of efficient fluorescence energy transfer (Fig. 7A, gray circles) as a positive control. In contrast, cells expressing Gag-YFP and A3G-CFP revealed a CFP emission peak with no YFP emission peak, indicating that no FRET occurred (Fig. 7A, open squares). Results for Gag-YFP and A3G-CFP were identical to those of the negative control of Gag-YFP coexpressed with CFP (Fig. 7A, closed triangles). Similar levels of YFP emission were obtained upon YFP excitation for each experimental condition, indicating that differential protein levels did not account for the differences in positive controls and the test molecules (Fig. 7B).

Gag VLPs were then generated in cells expressing Gag, Gag-CFP, and A3G-YFP. In the same system, A3G-YFP was replaced by Gag-YFP as a FRET-positive control and YFP-Mem (Clontech) as a FRET-negative control. The emission spectra of these particles were obtained with a spectrofluorometer using an excitation wavelength of 433 nm. Particles containing Gag-CFP and Gag-YFP exhibited a curve representative of efficient fluorescence energy transfer (Fig. 7C, gray circles), while particles containing Gag-CFP and A3G-YFP resulted in a CFP emission peak with no YFP FRET peak (Fig. 7C, open squares). The lack of FRET in particles containing Gag-CFP and A3G-YFP was not due to lower concentrations of A3G-YFP in this experiment, as similar levels of YFP emission were obtained for each experimental condition (Fig. 7D). These results indicate that we were unable to detect direct interactions between Gag and APOBEC3G in cells or VLPs using this technique. Interpretation of these results must include the recognition that a negative result in a CFP-YFP FRET assay does not rule out a direct interaction, as FRET can be dependent on both the position and the orientation of the CFP and YFP molecules (9, 23).

APOBEC3G is recruited to the plasma membrane by Gag. APOBEC3G has been described as diffuse in the cytoplasm of a cell but has recently been shown to collect in dense cytoplasmic bodies identified as mRNA processing (P) bodies by Wichroski and colleagues (35). We assessed the subcellular localization of APOBEC-YFP using wide-field deconvolution fluorescence microscopy. Very bright, punctate collections of A3G-YFP were noted in the cytoplasm of most transfected cells, consistent with the report of Wichroski et al. (Fig. 8A). Under these conditions, diffusely cytoplasmic APOBEC3G could be visualized only under conditions allowing saturation of pixels in P bodies (Fig. 8B). We observed little evidence of APOBEC3G on the plasma membrane, even in these overexposed images. When Gag-CFP was coexpressed with A3G-YFP, a mixed pattern was observed. The most intense A3G-YFP signal was consistently present in P bodies, but a subset of cells demonstrated plasma membrane A3G-YFP signal (Fig. 8D to F, leftmost cell). Note that plasma membrane colocalization was not apparent in the majority of cells (Fig. 8E). When it was observed, however, the colocalization appeared in bright punctate patterns along the plasma membrane, suggestive of sites of particle assembly, as indicated in Fig. 8C (a higher magnification view of the cell shown in Fig. 8E). In many cells in which A3G-YFP was expressed, the extreme brightness of the P body did not allow assessment of potential colocalization with Gag at the plasma membrane. To better examine these cells, we performed laser photobleaching of the interior region surrounding the P bodies, followed by a longer exposure of the remaining fluorescence signal in the cell. Figure 8G to I shows one such cell in which Gag-CFP is in red, A3G-YFP is shown in green, and plasma membrane colocalization is demonstrated as yellow pixels (Fig. 8H). Little apparent colocalization of Gag was noted in the P bodies, but there appeared to be recruitment of A3G-YFP from the cytoplasm to punctate spots on the plasma membrane. We conclude from these data that, although overexpressed A3G-YFP appears most intensely in P bodies, a subset of A3G-YFP is recruited to the plasma membrane, where it colocalizes with Gag in the developing particle.

APOBEC3G-APOBEC3G interactions were observed in structures consistent with P bodies by confocal spectral analysis. The laser confocal microscope allows the spectral sepa-

circles, pEYFP coexpressed with A3G-CFP. Closed triangles, GagCFP VLPs. (B) Relative levels of cellular YFP expression are shown for the experiment whose results are depicted in panel A, as determined by peak YFP output following excitation of cell lysates at 514 nm. (C) Cell lysates prepared by treatment with hypotonic buffer and Dounce homogenization. Half of the cell lysates were treated with RNase A and DNase RQ1 prior to FRET analysis, while RNA in the control lysates was preserved with RNase inhibitor. Gray squares, FRET curve for A3G-YFP/A3G-CFP; open circles, loss of FRET in nuclease-treated A3G-YFP/A3G-CFP lysates; closed triangles, A3G-CFP curve; closed diamonds, RNase-treated A3G-CFP. (D) Relative levels of cellular YFP expression are shown for the experiment whose results are depicted in panel A, as determined by peak YFP output following excitation of cell lysates at 514 nm. (E) VLPs created by coexpressing pVRC3900Gag with the indicated constructs in 293T cells. Supernatants were concentrated through a 20% sucrose cushion, resuspended in PBS, and analyzed by scanning cuvette fluorometry. Open circles, FRET curve for A3G-CFP/A3G-YFP and for A3G-CFP/YFP-A3G (gray boxes). Closed triangles, A3G-CFP coexpressed with pEYFP. (F) Relative levels of VLP YFP content are shown for the experiment whose results are depicted in panel C, as determined by peak YFP output following excitation of VLPs at 514 nm. Note that transfection of an untagged Gag expression construct was included in each of the transfections at a constant amount.

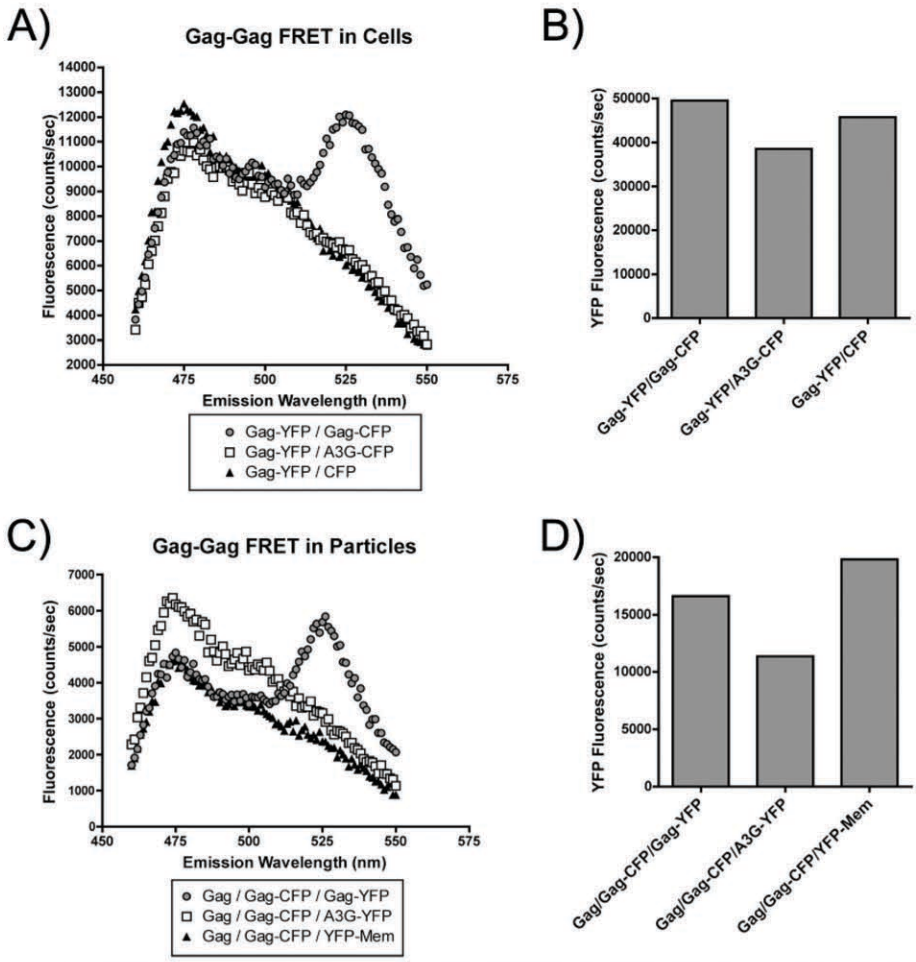

FIG. 7. Lack of FRET between APOBEC3G and Gag. (A) The indicated constructs were cotransfected into 293T cells. Cells were resuspended in PBS and read directly with a scanning cuvette fluorometer. FRET was measured by stimulating the CFP fluorophore at 433 nm, and the FRET peak was observed at 527 nm. Gray circles, FRET curve for Gag-YFP/Gag-CFP. Open squares, Gag-YFP coexpressed with A3G-CFP and pECFP (closed triangles). (B) Relative levels of cellular YFP expression are shown for the experiment whose results are depicted in panel A, as determined by peak YFP output following excitation of cell lysates at 514 nm. (C) VLPs created by coexpressing the indicated constructs in 293T cells. Supernatants were concentrated through a 20% sucrose cushion, resuspended in PBS, and analyzed by scanning cuvette fluorometry. Gray circles, FRET curve for Gag-CFP/Gag-YFP. Open squares, Gag-CFP coexpressed with A3G-YFP and pEYFP (closed triangles). (D) Relative levels of VLP YFP content are shown for the experiment whose results are depicted in panel C, as determined by peak YFP output following excitation of VLPs at 514 nm.

ration of light emitted from selected pixels when it is equipped with a multichannel detector. To further establish the presence of A3G-A3G FRET and to determine the localization of this FRET, we analyzed the emission spectra from different regions of the cell before and after photobleaching the A3G-YFP acceptor molecule. If a transfer of energy were occurring between the CFP and YFP molecules, the obliteration of YFP molecules by photobleaching would lead to retention of energy by the CFP molecules and an increase in CFP fluorescence. We had previously performed spectral analysis with a Zeiss LSM510 Meta confocal microscope to demonstrate the interaction of Gag-CFP and Gag-YFP on the plasma membrane (7). We repeated this analysis using Gag-CFP and Gag-YFP as positive controls in parallel with our APOBEC test constructs. Briefly, HeLa cells expressing Gag-CFP and Gag-YFP were imaged showing YFP localization before and after bleaching of the YFP at 514 nm (Fig. 9A and B). An emission scan of the cells shown in Fig. 9A and B was performed using excitation of CFP at 405 nm. The spectrum from a bleached section of the plasma membrane (region of interest 1 [ROI1]) revealed that after bleaching, the YFP peak at 530 nm was reduced while the CFP peak at 475 nm increased in fluorescent intensity (Fig. 9C). The emission spectra from a control region of the plasma membrane (region of interest 2) remained unchanged (Fig. 9D). This confirms the existence of FRET between Gag-CFP and Gag-YFP molecules on the plasma membrane. Next, we

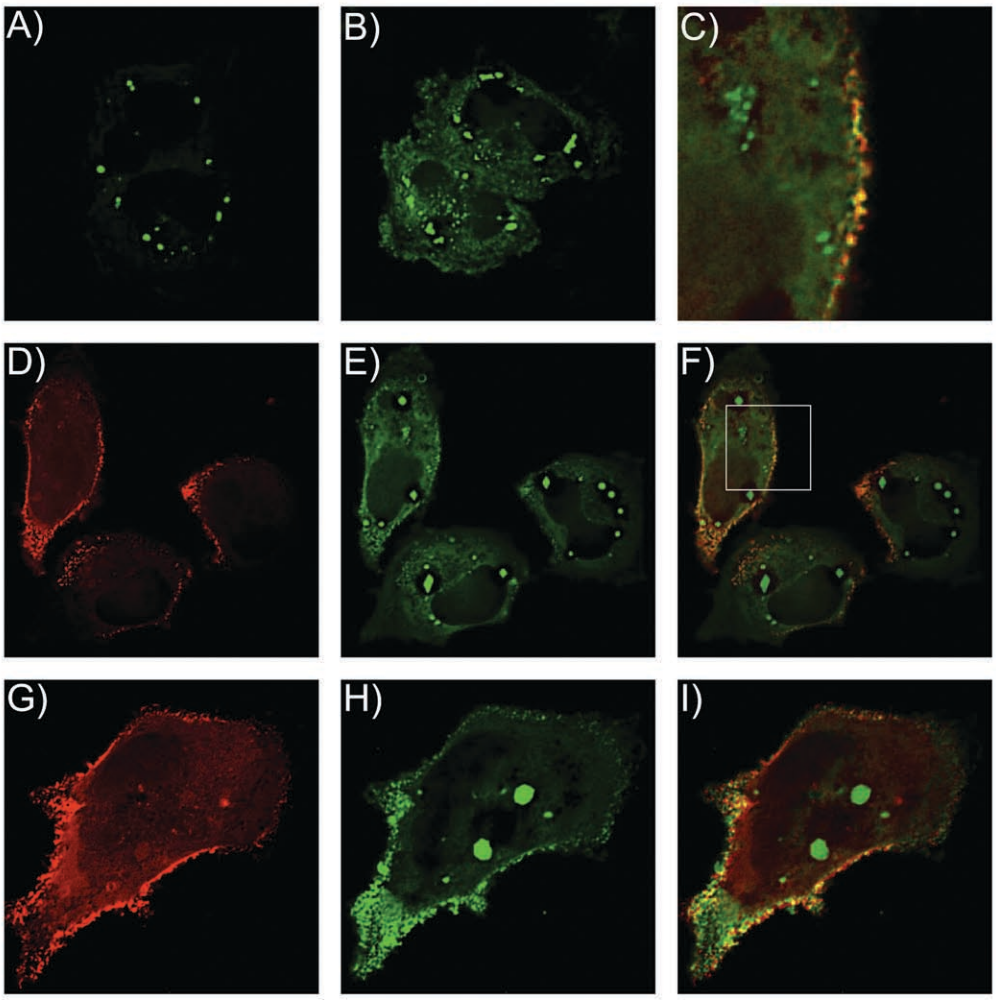

FIG. 8. Subcellular localization of Gag and A3G-YFP. A3G-YFP and Gag-CFP were expressed in HeLa cells and visualized by optical sectioning with a Nikon TE2000 microscope equipped with an automated stage and *z*-axis motor, followed by deconvolution using constrained-iterative algorithms. (A) Bright cytoplasmic collections of A3G-YFP are consistent with P body localization. (B) A longer exposure time allowing saturation of P body signal reveals a diffuse cytoplasmic A3G-YFP signal. (C) Magnified section (panel 8F, inset) showing plasma membrane colocalization of Gag (red) and A3G-YFP (green) signals. (D to F) Single-channel images and image overlay indicating Gag signal (red), and A3G-YFP signal (green). (G to I) Similar technique as in panels D to F, but bright collections of A3G-YFP in the cell interiorwere bleached with a 488-nm laser to diminish brightness and facilitate visualization of plasma membrane fluorescence.

employed this technique to determine the presence of a FRET interaction between A3G-CFP and A3G-YFP in structures consistent with P body subcellular localization. Figure 9E and F shows the localization of A3G-YFP in these cells before and after bleaching the ROI1. The emission spectra from pixels contained within the P body at ROI1 reveal that the decrease in the YFP peak following bleaching is accompanied by a significant increase in the CFP peak (Fig. 9G). P body pixels in the nearby but unbleached region of interest 2 show unchanged spectra (Fig. 9H). Bleached cytoplasmic locations close to ROI1 exhibit neither a FRET peak nor an increase in CFP fluorescence following bleaching (data not shown). This confirms that A3G-A3G interactions can be observed by FRET and occur primarily in P bodies.

APOBEC3G multimers are observed in P bodies and at the plasma membrane following Gag expression. In order to image the subcellular location of A3G-A3G interactions during Gag expression, we next employed FRET microscopy with living cells. Using distinct filter sets, we obtained individual CFP, YFP, and CFP-YFP (FRET) images and corrected each FRET image for donor bleedthrough and acceptor cross-stimulation using the algorithm described in Materials and Methods. Obtaining true FRET images using filter sets is complicated, even with the best filters and software algorithms, so we

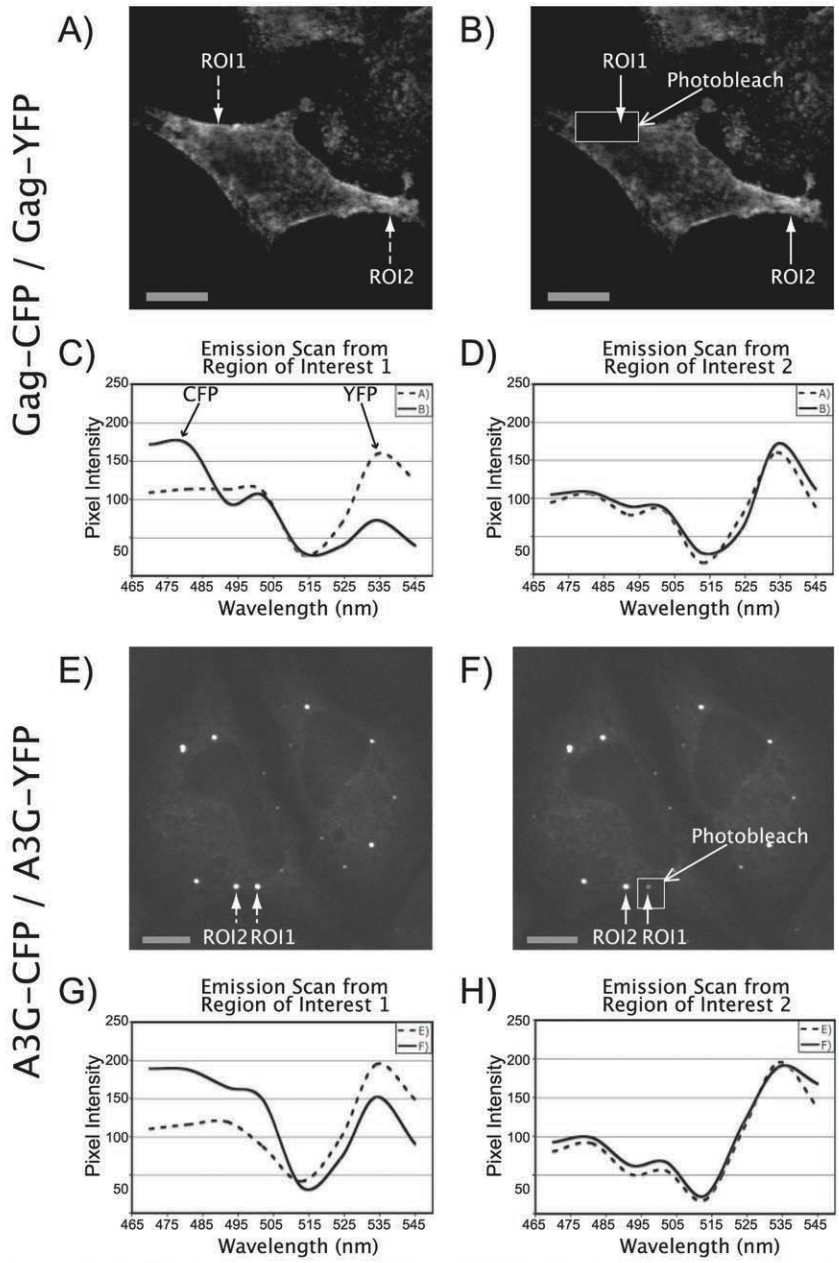

FIG. 9. Analysis of A3G-A3G interactions by confocal microscopy and fluorescence acceptor photobleaching. (A) Gag-CFP and Gag-YFP were cotransfected in HeLa cells, and images were obtained with a Zeiss LSM 510-Meta confocal microscope. The image represents YFP excitation-emission before photobleaching. The arrows indicate the selected plasma membrane region of interest to be bleached (ROI1) and the control region (ROI2). (B) The same cell as that shown in panel A is depicted following photobleaching at 514 nm in the indicated square. (C) Emission scans were obtained from region of interest 1, with excitation at 405 nm (CFP excitation), before (dashed line) and after (solid line) photobleaching of cells shown in panels A and B. (D) Emission scans were obtained from the control region of interest 2, with excitation at 405 nm, before (dashed line) and after (solid line) photobleaching of cells shown in panels A and B. (E) A3G-CFP and A3G-YFP were cotransfected in HeLa cells, and the image shows the distribution of A3G-YFP prior to bleaching. The regions of interest selected are consistent with P body localization. (F) The same cell as that shown in panel E is shown after photobleaching of the indicated square. (G) Spectra obtained from ROI1 before (dashed line) and after (solid line) photobleaching from cells shown in panels E and F. (H) Spectra obtained from ROI2 before (dashed line) and after (solid line) photobleaching from cells shown in panels E and F. Scale bar represents 10 micrometers.

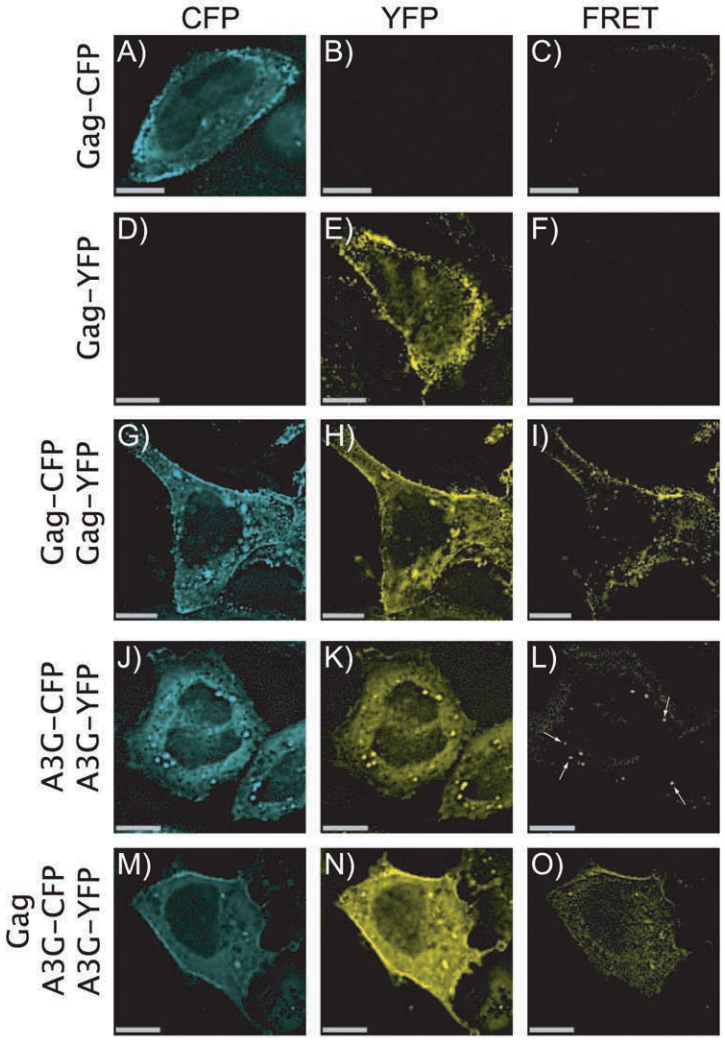

FIG. 10. Subcellular localization of A3G-CFP and A3G-YFP FRET. (A to C) CFP, YFP, and FRET images obtained from HeLa cells expressing Gag-CFP (negative control). (D to F) CFP, YFP, and FRET images from cells expressing Gag-YFP (negative control). (G to I) CFP, YFP, and FRET images from cells expressing both Gag-CFP and Gag-YFP. (J to L) CFP, YFP, and FRET images from cells expressing A3G-CFP and A3G-YFP (without Gag). Structures consistent with the subcellular localization of P bodies exhibit FRET. (M to O) CFP, YFP, and FRET images from a cell expressing Gag, A3G-CFP, and A3G-YFP. In addition to P body FRET, plasma membrane FRET and a low level of cytoplasmic FRET are shown. Scale bar represents 10 micrometers.

included known positive controls that were treated identically to the APOBEC3G expression experiments. Controls included HeLa cells expressing Gag-CFP alone (Fig. 10A to C) and cells expressing Gag-YFP alone (Fig. 10D to F). These two negative controls were critical to establish that bleedthrough and cross-stimulation from CFP and YFP, respectively, can effectively be measured and subtracted from the final FRET image. We next employed this technique to examine the location of FRET in cells expressing Gag-CFP and Gag-YFP. Consistent with the findings shown in Fig. 9A to D and our previously published findings (7) Gag-Gag FRET was detected at the plasma membrane and at distinct intracellular puncta (Fig. 10I). Finally, we employed this assay to observe the locations of A3G-A3G FRET with and without Gag expression. Consistent with the results shown in Fig. 9E to H, cells expressing A3G-CFP and A3G-YFP exhibit FRET only in the P bodies (Fig. 10J to L). However, the expression of Gag together with A3G-CFP and A3G-YFP resulted in detectable FRET signal at the plasma membrane in a subset of cells examined (Fig. 10M to O). This is consistent with a model in which Gag recruits A3G-RNA-A3G multimers to the plasma membrane.

DISCUSSION

A number of published reports have established that the NC region of Gag is necessary for APOBEC3G packaging into virions or VLPs. The majority of reports support an essential role for RNA in mediating the APOBEC-NC interaction (26, 31, 38), while some investigators have found evidence for a direct protein-protein interaction (1, 4). Our findings support an RNA-dependent incorporation of APOBEC3G into particles, using several lines of evidence. First, in vitro interactions of APOBEC3G and NC were shown to be RNase sensitive, as reported by others. Second, we found that the incorporation of APOBEC3G into a series of serially truncated Gag protein constructs correlated well with the RNA-to-Gag ratio of the released particles. Finally, data from our FRET studies provide indirect evidence for the requirement of RNA in packaging by revealing both that RNA is required for APOBEC3G-APOBEC3G interactions and that these APOBEC3G multimers are subsequently packaged into VLPs. Under the same experimental conditions in which APOBEC3G-APOBEC3G FRET was detected, and in which Gag-Gag FRET is readily detected, we failed to detect Gag-APOBEC3G FRET. Although this may be due to the fact that there is not a direct protein-protein interaction between Gag and APOBEC3G in cells or virions, we recognize that the position and orientation of the CFP and YFP tags on Gag and APOBEC3G may simply not support FRET. The presence of a flexible linker region between both proteins and the fluorescent moieties should have minimized these potential orientation effects (9, 23), but a negative result still is not definitive. Taken together, our findings support a model in which APOBEC3G multimers form on cellular RNA as part of an RNA-protein complex that is subsequently recruited into the developing particle through interactions with NC.

The N-terminal subdomain of NC has been shown to be sufficient to allow the formation of particles of normal retroviral density. The "I" domain, which is located within this region, is widely believed to contribute to Gag-Gag multimerization, mediated by NC-RNA interactions. We were surprised in this study to find that the minimal "I" domain of Gag, an essential assembly determinant, did not correspond precisely with the packaging requirements for APOBEC3G. Rather, in this study only those constructs that included the first zinc finger and basic linker packaged APOBEC3G. In contrast to our study, Luo et al. (19) showed that one Gag protein truncated proximal to the first zinc finger packaged APOBEC3G. While the reason for this discrepancy is not certain, we suggest that it reflects the fluorescence quantitation performed in our study versus the semiquantitative Western blot analysis performed in the study by Luo et al. In agreement with their results, however, we observed a minor amount of APOBEC3G in all truncated constructs (Fig. 2D). The quantitative packaging data, combined with evidence that membrane recruitment requires the same critical region, emphasizes the importance of the basic linker region for APOBEC3G interaction and packaging.

A unique aspect of the present study was the finding that Gag recruits APOBEC3G to the plasma membrane. Three lines of evidence support this finding. First, membrane flotation data indicated a redistribution of APOBEC3G to cellular membranes following Gag expression. Second, APOBEC3G colocalized with Gag at the plasma membrane. Third, APOBEC3G-RNA-APOBEC3G complexes, which were found predominantly in P bodies in the absence of Gag expression, were detected at the plasma membrane in cells cotransfected with Gag. Recruitment of APOBEC3G to the plasma membrane is somewhat intuitive, since Gag is responsible for the incorporation of RNA and APOBEC3G, and Gag must interact with membranes for intracellular trafficking and budding from the cell. It is tempting to speculate that Gag recruits APOBEC3G at early stages following translation on cytoplasmic ribosomes, in conjunction with viral genomic RNA. In this model, a Gag-RNA-APOBEC3G complex would then traffic along endosomal pathways to the plasma membrane for budding (or to the multivesicular body in the infected macrophage). We were not able to demonstrate significant colocalization of Gag and APOBEC3G within the cytoplasm of the cell, in particular in the punctate cytoplasmic collections reported by others to be P bodies (34, 35). We note that occasional faint colocalization was seen at these sites (data not shown). However, we were able to detect colocalization of Gag with APOBEC3G at the plasma membrane, especially in cells in which the intensely bright signal from P bodies was reduced by photobleaching. It is possible that the population of APOBEC3G present in the dense P bodies is itself incorporated into particles, but perhaps it is more likely that Gag recruits APOBEC3G from the cytoplasmic pool that then multimerizes on the viral RNA. Kozak et al. recently reported the binding of APOBEC3G to a pool of RNA that reversibly shuttles between polysomes and stress granules (16); it may be this pool that is packaged in the VLP in the absence of HIV genomic RNA. We note the caveat that the intensity of the signal observed in our microscopic study results from overexpression of APOBEC3G fused to YFP rather than endogenous APOBEC3G. However, these results are consistent with those of others who have reported very intense cytoplasmic (P body) collections of APOBEC3G (34, 35).

We found that multimeric APOBEC3G complexes were packaged into VLPs. Opi et al. reported a monomeric APOBEC3G mutant (C97A) that was packaged and remained catalytically active (22). However, the majority of APOBEC3G in cells is present in an RNase-sensitive multimeric form (22), and several reports have suggested that APOBEC3G binds to itself in cells (14, 35) in an RNA-dependent manner (35), producing either the head-to-tail dimers traditionally associated with APOBEC3G family members (14) or the high-molecular-mass complexes observed in activated T cells and transfected 293T cells (5, 17). We used a FRET assay to demonstrate that APOBEC3G multimers were incorporated into virions. These oligomers were also detected in cell lysates and could be disrupted by RNase treatment. These data suggest that APOBEC3G multimerizes on cellular or viral RNA, and it is APOBEC3G multimers complexed with RNA that are recruited into developing particles. It makes sense that these complexes represent the enzymatically active enzyme during the reverse transcription process, as they are recruited directly into the viral core that becomes the nucleus for reverse transcription upon infection of a cell. It is also possible that monomeric APOBEC3G is formed during the reverse transcription process as the RNA template is degraded.

In summary, our results provide strong support for the importance of RNA in mediating the incorporation of APOBEC3G into virions or VLPs. This incorporation is dependent upon re-

gions of NC that allow efficient RNA incorporation, especially the basic linker region. We suggest a model in which APOBEC3G multimerizes on RNA and the APOBEC3G-RNA complex is then recruited by Gag into the developing particle.

ACKNOWLEDGMENTS

This work was supported by R01 AI40338 and R01 AI67101.

We thank Michael Malim for providing the APOBEC3G-HA expression construct. We also thank Aaron Derdowski for help with FRET fluorometry and confocal microscopy, Jason Hammonds for help with VLP production and purification, and Kelie Reece for helpful suggestions. We thank the Winship Cancer Institute Cell Imaging and Microscopy Core for their service and assistance.

REFERENCES

1. **Alce, T. M., and W. Popik.** 2004. APOBEC3G is incorporated into virus-like particles by a direct interaction with HIV-1 Gag nucleocapsid protein. J. Biol. Chem. **279:**34083–34086.
2. **Bennett, R. P., T. D. Nelle, and J. W. Wills.** 1993. Functional chimeras of the Rous sarcoma virus and human immunodeficiency virus Gag proteins. J. Virol. **67:**6487–6498.
3. **Bowzard, J. B., R. P. Bennett, N. K. Krishna, S. M. Ernst, A. Rein, and J. W. Wills.** 1998. Importance of basic residues in the nucleocapsid sequence for retrovirus Gag assembly and complementation rescue. J. Virol. **72:**9034–9044.
4. **Cen, S., F. Guo, M. Niu, J. Saadatmand, J. Deflassieux, and L. Kleiman.** 2004. The interaction between HIV-1 Gag and APOBEC3G. J. Biol. Chem. **279:**33177–33184.
5. **Chiu, Y. L., V. B. Soros, J. F. Kreisberg, K. Stopak, W. Yonemoto, and W. C. Greene.** 2005. Cellular APOBEC3G restricts HIV-1 infection in resting CD4+ T cells. Nature **435:**108–114.
6. **Conticello, S. G., R. S. Harris, and M. S. Neuberger.** 2003. The Vif protein of HIV triggers degradation of the human antiretroviral DNA deaminase APOBEC3G. Curr. Biol. **13:**2009–2013.
7. **Derdowski, A., L. Ding, and P. Spearman.** 2004. A novel fluorescence resonance energy transfer assay demonstrates that the human immunodeficiency virus type 1 Pr55Gag I domain mediates Gag-Gag interactions. J. Virol. **78:**1230–1242.
8. **Ding, L., A. Derdowski, J. J. Wang, and P. Spearman.** 2003. Independent segregation of human immunodeficiency virus type 1 Gag protein complexes and lipid rafts. J. Virol. **77:**1916–1926.
9. **dos Remedios, C. G., and P. D. Moens.** 1995. Fluorescence resonance energy transfer spectroscopy is a reliable "ruler" for measuring structural changes in proteins. Dispelling the problem of the unknown orientation factor. J. Struct. Biol. **115:**175–185.
10. **Douaisi, M., S. Dussart, M. Courcoul, G. Bessou, R. Vigne, and E. Decroly.** 2004. HIV-1 and MLV Gag proteins are sufficient to recruit APOBEC3G into virus-like particles. Biochem. Biophys. Res. Commun. **321:**566–573.
11. **Feng, F., A. Davis, J. A. Lake, J. Carr, W. Xia, C. Burrell, and P. Li.** 2004. Ring finger protein ZIN interacts with human immunodeficiency virus type 1 Vif. J. Virol. **78:**10574–10581.
12. **Harris, R. S., K. N. Bishop, A. M. Sheehy, H. M. Craig, S. K. Petersen-Mahrt, I. N. Watt, M. S. Neuberger, and M. H. Malim.** 2003. DNA deamination mediates innate immunity to retroviral infection. Cell **113:**803–809.
13. **Huang, Y., W.-P. Kong, and G. J. Nabel.** 2001. Human immunodeficiency virus type 1-specific immunity after genetic immunization is enhanced by modification of Gag and Pol expression. J. Virol. **75:**4947–4951.
14. **Jarmuz, A., A. Chester, J. Bayliss, J. Gisbourne, I. Dunham, J. Scott, and N. Navaratnam.** 2002. An anthropoid-specific locus of orphan C to U RNA-editing enzymes on chromosome 22. Genomics **79:**285–296.
15. **Kao, S., M. A. Khan, E. Miyagi, R. Plishka, A. Buckler-White, and K. Strebel.** 2003. The human immunodeficiency virus type 1 Vif protein reduces intracellular expression and inhibits packaging of APOBEC3G (CEM15), a cellular inhibitor of virus infectivity. J. Virol. **77:**11398–11407.
16. **Kozak, S. L., M. Marin, K. M. Rose, C. Bystrom, and D. Kabat.** 2006. The Anti-HIV-1 editing enzyme APOBEC3G binds HIV-1 RNA and messenger RNAs that shuttle between polysomes and stress granules. J. Biol. Chem. **281:**29105–29119.
17. **Kreisberg, J. F., W. Yonemoto, and W. C. Greene.** 2006. Endogenous factors enhance HIV infection of tissue naive CD4 T cells by stimulating high molecular mass APOBEC3G complex formation. J. Exp. Med. **203:**865–870.
18. **Lecossier, D., F. Bouchonnet, F. Clavel, and A. J. Hance.** 2003. Hypermutation of HIV-1 DNA in the absence of the Vif protein. Science **300:**1112.
19. **Luo, K., B. Liu, Z. Xiao, Y. Yu, X. Yu, R. Gorelick, and X.-F. Yu.** 2004. Amino-terminal region of the human immunodeficiency virus type 1 nucleocapsid is required for human APOBEC3G packaging. J. Virol. **78:**11841–11852.
20. **Mangeat, B., P. Turelli, G. Caron, M. Friedli, L. Perrin, and D. Trono.** 2003. Broad antiretroviral defense by human APOBEC3G through lethal editing of nascent reverse transcripts. Nature **424:**99–103.
21. **Marin, M., K. M. Rose, S. L. Kozak, and D. Kabat.** 2003. HIV-1 Vif protein binds the editing enzyme APOBEC3G and induces its degradation. Nat. Med. **9:**1398–1403.
22. **Opi, S., H. Takeuchi, S. Kao, M. A. Khan, E. Miyagi, R. Goila-Gaur, Y. Iwatani, J. G. Levin, and K. Strebel.** 2006. Monomeric APOBEC3G is catalytically active and has antiviral activity. J. Virol. **80:**4673–4682.
23. **Patterson, G. H., D. W. Piston, and B. G. Barisas.** 2000. Forster distances between green fluorescent protein pairs. Anal. Biochem. **284:**438–440.
24. **Sandefur, S., R. M. Smith, V. Varthakavi, and P. Spearman.** 2000. Mapping and characterization of the N-terminal I domain of human immunodeficiency virus type 1 $Pr55^{Gag}$. J. Virol. **74:**7238–7249.
25. **Sandefur, S., V. Varthakavi, and P. Spearman.** 1998. The I domain is required for efficient plasma membrane binding of human immunodeficiency virus type 1 $Pr55^{Gag}$. J. Virol. **72:**2723–2732.
26. **Schafer, A., H. P. Bogerd, and B. R. Cullen.** 2004. Specific packaging of APOBEC3G into HIV-1 virions is mediated by the nucleocapsid domain of the gag polyprotein precursor. Virology **328:**163–168.
27. **Sheehy, A. M., N. C. Gaddis, J. D. Choi, and M. H. Malim.** 2002. Isolation of a human gene that inhibits HIV-1 infection and is suppressed by the viral Vif protein. Nature **418:**646–650.
28. **Sheehy, A. M., N. C. Gaddis, and M. H. Malim.** 2003. The antiretroviral enzyme APOBEC3G is degraded by the proteasome in response to HIV-1 Vif. Nat. Med. **9:**1404–1407.
29. **Stenglein, M. D., and R. S. Harris.** 2006. APOBEC3B and APOBEC3F inhibit L1 retrotransposition by a DNA deamination-independent mechanism. J. Biol. Chem. **281:**16837–16841.
30. **Stopak, K., C. de Noronha, W. Yonemoto, and W. C. Greene.** 2003. HIV-1 Vif blocks the antiviral activity of APOBEC3G by impairing both its translation and intracellular stability. Mol. Cell. **12:**591–601.
31. **Svarovskaia, E. S., H. Xu, J. L. Mbisa, R. Barr, R. J. Gorelick, A. Ono, E. O. Freed, W. S. Hu, and V. K. Pathak.** 2004. Human apolipoprotein B mRNA-editing enzyme-catalytic polypeptide-like 3G (APOBEC3G) is incorporated into HIV-1 virions through interactions with viral and nonviral RNAs. J. Biol. Chem. **279:**35822–35828.
32. **Turelli, P., B. Mangeat, S. Jost, S. Vianin, and D. Trono.** 2004. Inhibition of hepatitis B virus replication by APOBEC3G. Science **303:**1829.
33. **Weldon, R. A., Jr., C. R. Erdie, M. G. Oliver, and J. W. Wills.** 1990. Incorporation of chimeric Gag protein into retroviral particles. J. Virol. **64:**4169–4179.
34. **Wichroski, M. J., K. Ichiyama, and T. M. Rana.** 2005. Analysis of HIV-1 viral infectivity factor-mediated proteasome-dependent depletion of APOBEC3G: correlating function and subcellular localization. J. Biol. Chem. **280:**8387–8396.
35. **Wichroski, M. J., G. B. Robb, and T. M. Rana.** 2006. Human retroviral host restriction factors APOBEC3G and APOBEC3F localize to mRNA processing bodies. PLoS Pathog. **2:**e41.
36. **Yu, Q., D. Chen, R. Konig, R. Mariani, D. Unutmaz, and N. R. Landau.** 2004. APOBEC3B and APOBEC3C are potent inhibitors of simian immunodeficiency virus replication. J. Biol. Chem. **279:**53379–53386.
37. **Yu, X., Y. Yu, B. Liu, K. Luo, W. Kong, P. Mao, and X. F. Yu.** 2003. Induction of APOBEC3G ubiquitination and degradation by an HIV-1 Vif-Cul5-SCF complex. Science **302:**1056–1060.
38. **Zennou, V., D. Perez-Caballero, H. Gottlinger, and P. D. Bieniasz.** 2004. APOBEC3G incorporation into human immunodeficiency virus type 1 particles. J. Virol. **78:**12058–12061.
39. **Zhang, H., B. Yang, R. J. Pomerantz, C. Zhang, S. C. Arunachalam, and L. Gao.** 2003. The cytidine deaminase CEM15 induces hypermutation in newly synthesized HIV-1 DNA. Nature **424:**94–98.

REFERENCES

1. **Alce, T. M., and W. Popik.** 2004. APOBEC3G is incorporated into virus-like particles by a direct interaction with HIV-1 Gag nucleocapsid protein. J Biol Chem **279:**34083-6.
2. **Alkhatib, G., C. Combadiere, C. C. Broder, Y. Feng, P. E. Kennedy, P. M. Murphy, and E. A. Berger.** 1996. CC CKR5: a RANTES, MIP-1alpha, MIP-1beta receptor as a fusion cofactor for macrophage-tropic HIV-1. Science **272:**1955-8.
3. **Barre-Sinoussi, F., J. C. Chermann, F. Rey, M. T. Nugeyre, S. Chamaret, J. Gruest, C. Dauguet, C. Axler-Blin, F. Vezinet-Brun, C. Rouzioux, W. Rozenbaum, and L. Montagnier.** 1983. Isolation of a T-lymphotropic retrovirus from a patient at risk for acquired immune deficiency syndrome (AIDS). Science **220:**868-71.
4. **Basyuk, E., T. Galli, M. Mougel, J. M. Blanchard, M. Sitbon, and E. Bertrand.** 2003. Retroviral genomic RNAs are transported to the plasma membrane by endosomal vesicles. Dev Cell **5:**161-74.
5. **Benne, R., J. Van den Burg, J. P. Brakenhoff, P. Sloof, J. H. Van Boom, and M. C. Tromp.** 1986. Major transcript of the frameshifted coxII gene from trypanosome mitochondria contains four nucleotides that are not encoded in the DNA. Cell **46:**819-26.
6. **Bennett, R. P., T. D. Nelle, and J. W. Wills.** 1993. Functional chimeras of the Rous sarcoma virus and human immunodeficiency virus gag proteins. J Virol **67:**6487-98.
7. **Bertrand, E., P. Chartrand, M. Schaefer, S. M. Shenoy, R. H. Singer, and R. M. Long.** 1998. Localization of ASH1 mRNA particles in living yeast. Mol Cell **2:**437-45.
8. **Betts, L., S. Xiang, S. A. Short, R. Wolfenden, and C. W. Carter, Jr.** 1994. Cytidine deaminase. The 2.3 A crystal structure of an enzyme: transition-state analog complex. J Mol Biol **235:**635-56.
9. **Bogerd, H. P., A. Echarri, T. M. Ross, and B. R. Cullen.** 1998. Inhibition of human immunodeficiency virus Rev and human T-cell leukemia virus Rex function, but not Mason-Pfizer monkey virus constitutive transport element activity, by a mutant human nucleoporin targeted to Crm1. J Virol **72:**8627-35.
10. **Bolognesi, D. P., R. C. Montelaro, H. Frank, and W. Schafer.** 1978. Assembly of type C oncornaviruses: a model. Science **199:**183-6.
11. **Borman, A. M., C. Quillent, P. Charneau, C. Dauguet, and F. Clavel.** 1995. Human immunodeficiency virus type 1 Vif- mutant particles from restrictive cells: role of Vif in correct particle assembly and infectivity. J Virol **69:**2058-67.
12. **Boulon, S., E. Basyuk, J. M. Blanchard, E. Bertrand, and C. Verheggen.** 2002. Intra-nuclear RNA trafficking: insights from live cell imaging. Biochimie **84:**805-13.

13. **Bowerman, B., P. O. Brown, J. M. Bishop, and H. E. Varmus.** 1989. A nucleoprotein complex mediates the integration of retroviral DNA. Genes Dev **3:**469-78.
14. **Bowzard, J. B., R. P. Bennett, N. K. Krishna, S. M. Ernst, A. Rein, and J. W. Wills.** 1998. Importance of basic residues in the nucleocapsid sequence for retrovirus Gag assembly and complementation rescue. J Virol **72:**9034-44.
15. **Bratu, D. P.** 2006. Molecular beacons: Fluorescent probes for detection of endogenous mRNAs in living cells. Methods Mol Biol **319:**1-14.
16. **Briggs, J. A., M. N. Simon, I. Gross, H. G. Krausslich, S. D. Fuller, V. M. Vogt, and M. C. Johnson.** 2004. The stoichiometry of Gag protein in HIV-1. Nat Struct Mol Biol **11:**672-5.
17. **Brown, P. O., B. Bowerman, H. E. Varmus, and J. M. Bishop.** 1987. Correct integration of retroviral DNA in vitro. Cell **49:**347-56.
18. **Bryant, M., and L. Ratner.** 1990. Myristoylation-dependent replication and assembly of human immunodeficiency virus 1. Proc Natl Acad Sci U S A **87:**523-7.
19. **Burniston, M. T., A. Cimarelli, J. Colgan, S. P. Curtis, and J. Luban.** 1999. Human immunodeficiency virus type 1 Gag polyprotein multimerization requires the nucleocapsid domain and RNA and is promoted by the capsid-dimer interface and the basic region of matrix protein. J Virol **73:**8527-40.
20. **Burns, C. M., H. Chu, S. M. Rueter, L. K. Hutchinson, H. Canton, E. Sanders-Bush, and R. B. Emeson.** 1997. Regulation of serotonin-2C receptor G-protein coupling by RNA editing. Nature **387:**303-8.
21. **Campalans, A., A. Kondorosi, and M. Crespi.** 2004. Enod40, a short open reading frame-containing mRNA, induces cytoplasmic localization of a nuclear RNA binding protein in Medicago truncatula. Plant Cell **16:**1047-59.
22. **Castilletti, C., M. R. Capobianchi, S. Fais, I. Abbate, B. Ficociello, F. Ameglio, P. Cordiali Fei, S. M. Santini, and F. Dianzani.** 1995. HIV type 1 grown on interferon gamma-treated U937 cells shows selective increase in virion-associated intercellular adhesion molecule 1 and HLA-DR and enhanced infectivity for CD4-negative cells. AIDS Res Hum Retroviruses **11:**547-53.
23. **Cavrois, M., J. Neidleman, M. Bigos, and W. C. Greene.** 2004. Fluorescence resonance energy transfer-based HIV-1 virion fusion assay. Methods Mol Biol **263:**333-44.
24. **Cen, S., F. Guo, M. Niu, J. Saadatmand, J. Deflassieux, and L. Kleiman.** 2004. The interaction between HIV-1 Gag and APOBEC3G. J Biol Chem **279:**33177-84.
25. **Chen, S. H., G. Habib, C. Y. Yang, Z. W. Gu, B. R. Lee, S. A. Weng, S. R. Silberman, S. J. Cai, J. P. Deslypere, M. Rosseneu, and et al.** 1987. Apolipoprotein B-48 is the product of a messenger RNA with an organ-specific in-frame stop codon. Science **238:**363-6.
26. **Chen, Y., and G. Varani.** 2005. Protein families and RNA recognition. Febs J **272:**2088-97.
27. **Chiu, Y. L., V. B. Soros, J. F. Kreisberg, K. Stopak, W. Yonemoto, and W. C. Greene.** 2005. Cellular APOBEC3G restricts HIV-1 infection in resting CD4+ T cells. Nature **435:**108-14.

28. **Choe, H., M. Farzan, Y. Sun, N. Sullivan, B. Rollins, P. D. Ponath, L. Wu, C. R. Mackay, G. LaRosa, W. Newman, N. Gerard, C. Gerard, and J. Sodroski.** 1996. The beta-chemokine receptors CCR3 and CCR5 facilitate infection by primary HIV-1 isolates. Cell **85:**1135-48.
29. **Cimarelli, A., S. Sandin, S. Hoglund, and J. Luban.** 2000. Basic residues in human immunodeficiency virus type 1 nucleocapsid promote virion assembly via interaction with RNA. J Virol **74:**3046-57.
30. **Clark, S. J., M. S. Saag, W. D. Decker, S. Campbell-Hill, J. L. Roberson, P. J. Veldkamp, J. C. Kappes, B. H. Hahn, and G. M. Shaw.** 1991. High titers of cytopathic virus in plasma of patients with symptomatic primary HIV-1 infection. N Engl J Med **324:**954-60.
31. **Coffin, J. M.** 1992. Genetic diversity and evolution of retroviruses. Curr Top Microbiol Immunol **176:**143-64.
32. **Coffin, J. M.** 1995. HIV population dynamics in vivo: implications for genetic variation, pathogenesis, and therapy. Science **267:**483-9.
33. **Coffin, J. M.** 1996. Retroviridae and their replication, p. 1767-1848. *In* B. N. Fields (ed.), Virology. Raven Press, New York.
34. **Coffin, J. M.** 1992. Structure and classification of retroviruses, p. 19-49. *In* J. A. Levy (ed.), The retroviridae. Plenum Press, New York.
35. **Coffin, J. M., S. H. Hughes, and H. E. Varmus (ed.).** 1997. Retroviruses. Cold Sring Harbor Laboratory Press, Plainview.
36. **Conticello, S. G., R. S. Harris, and M. S. Neuberger.** 2003. The Vif protein of HIV triggers degradation of the human antiretroviral DNA deaminase APOBEC3G. Curr Biol **13:**2009-13.
37. **Courcoul, M., C. Patience, F. Rey, D. Blanc, A. Harmache, J. Sire, R. Vigne, and B. Spire.** 1995. Peripheral blood mononuclear cells produce normal amounts of defective Vif- human immunodeficiency virus type 1 particles which are restricted for the preretrotranscription steps. J Virol **69:**2068-74.
38. **Covello, P. S., and M. W. Gray.** 1989. RNA editing in plant mitochondria. Nature **341:**662-6.
39. **Craven, R. C., A. E. Leure-duPree, R. A. Weldon, Jr., and J. W. Wills.** 1995. Genetic analysis of the major homology region of the Rous sarcoma virus Gag protein. J Virol **69:**4213-27.
40. **Daar, E. S., T. Moudgil, R. D. Meyer, and D. D. Ho.** 1991. Transient high levels of viremia in patients with primary human immunodeficiency virus type 1 infection. N Engl J Med **324:**961-4.
41. **Daelemans, D., S. V. Costes, E. H. Cho, R. A. Erwin-Cohen, S. Lockett, and G. N. Pavlakis.** 2004. In vivo HIV-1 Rev multimerization in the nucleolus and cytoplasm identified by fluorescence resonance energy transfer. J Biol Chem **279:**50167-75.
42. **Dalgleish, A. G., P. C. Beverley, P. R. Clapham, D. H. Crawford, M. F. Greaves, and R. A. Weiss.** 1984. The CD4 (T4) antigen is an essential component of the receptor for the AIDS retrovirus. Nature **312:**763-7.
43. **Dannull, J., A. Surovoy, G. Jung, and K. Moelling.** 1994. Specific binding of HIV-1 nucleocapsid protein to PSI RNA in vitro requires N-terminal zinc finger and flanking basic amino acid residues. Embo J **13:**1525-33.

44. **Dayton, A. I., J. G. Sodroski, C. A. Rosen, W. C. Goh, and W. A. Haseltine.** 1986. The trans-activator gene of the human T cell lymphotropic virus type III is required for replication. Cell **44:**941-7.
45. **Debouck, C., J. G. Gorniak, J. E. Strickler, T. D. Meek, B. W. Metcalf, and M. Rosenberg.** 1987. Human immunodeficiency virus protease expressed in Escherichia coli exhibits autoprocessing and specific maturation of the gag precursor. Proc Natl Acad Sci U S A **84:**8903-6.
46. **Deng, H., R. Liu, W. Ellmeier, S. Choe, D. Unutmaz, M. Burkhart, P. Di Marzio, S. Marmon, R. E. Sutton, C. M. Hill, C. B. Davis, S. C. Peiper, T. J. Schall, D. R. Littman, and N. R. Landau.** 1996. Identification of a major co-receptor for primary isolates of HIV-1. Nature **381:**661-6.
47. **Derdowski, A., L. Ding, and P. Spearman.** 2004. A novel fluorescence resonance energy transfer assay demonstrates that the human immunodeficiency virus type 1 Pr55Gag I domain mediates Gag-Gag interactions. J Virol **78:**1230-42.
48. **Derse, D., S. A. Hill, G. Princler, P. Lloyd, and G. Heidecker.** 2007. Resistance of human T cell leukemia virus type 1 to APOBEC3G restriction is mediated by elements in nucleocapsid. Proc Natl Acad Sci U S A **104:**2915-20.
49. **Desrosiers, R. C., and N. L. Letvin.** 1987. Animal models for acquired immunodeficiency syndrome. Rev Infect Dis **9:**438-46.
50. **Dietz, H., and M. Rief.** 2006. Protein structure by mechanical triangulation. Proc Natl Acad Sci U S A **103:**1244-7.
51. **Ding, L., A. Derdowski, J. J. Wang, and P. Spearman.** 2003. Independent segregation of human immunodeficiency virus type 1 Gag protein complexes and lipid rafts. J Virol **77:**1916-26.
52. **Doehle, B. P., H. P. Bogerd, H. L. Wiegand, N. Jouvenet, P. D. Bieniasz, E. Hunter, and B. R. Cullen.** 2006. The betaretrovirus Mason-Pfizer monkey virus selectively excludes simian APOBEC3G from virion particles. J Virol **80:**12102-8.
53. **Dong, X., H. Li, A. Derdowski, L. Ding, A. Burnett, X. Chen, T. R. Peters, T. S. Dermody, E. Woodruff, J. J. Wang, and P. Spearman.** 2005. AP-3 directs the intracellular trafficking of HIV-1 Gag and plays a key role in particle assembly. Cell **120:**663-74.
54. **dos Remedios, C. G., and P. D. Moens.** 1995. Fluorescence resonance energy transfer spectroscopy is a reliable "ruler" for measuring structural changes in proteins. Dispelling the problem of the unknown orientation factor. J Struct Biol **115:**175-85.
55. **Douaisi, M., S. Dussart, M. Courcoul, G. Bessou, R. Vigne, and E. Decroly.** 2004. HIV-1 and MLV Gag proteins are sufficient to recruit APOBEC3G into virus-like particles. Biochem Biophys Res Commun **321:**566-73.
56. **Dragic, T., V. Litwin, G. P. Allaway, S. R. Martin, Y. Huang, K. A. Nagashima, C. Cayanan, P. J. Maddon, R. A. Koup, J. P. Moore, and W. A. Paxton.** 1996. HIV-1 entry into CD4+ cells is mediated by the chemokine receptor CC-CKR-5. Nature **381:**667-73.
57. **Durack, D. T.** 1981. Opportunistic infections and Kaposi's sarcoma in homosexual men. N Engl J Med **305:**1465-7.

58. **Dynes, J. L., and O. Steward.** 2007. Dynamics of bidirectional transport of Arc mRNA in neuronal dendrites. J Comp Neurol **500:**433-47.
59. **Ellison, V., H. Abrams, T. Roe, J. Lifson, and P. Brown.** 1990. Human immunodeficiency virus integration in a cell-free system. J Virol **64:**2711-5.
60. **Esnault, C., O. Heidmann, F. Delebecque, M. Dewannieux, D. Ribet, A. J. Hance, T. Heidmann, and O. Schwartz.** 2005. APOBEC3G cytidine deaminase inhibits retrotransposition of endogenous retroviruses. Nature **433:**430-3.
61. **Fan, L., and K. Peden.** 1992. Cell-free transmission of Vif mutants of HIV-1. Virology **190:**19-29.
62. **Fang, C. T., Y. Y. Chang, H. M. Hsu, S. J. Twu, K. T. Chen, C. C. Lin, L. Y. Huang, M. Y. Chen, J. S. Hwang, J. D. Wang, and C. Y. Chuang.** 2007. Life expectancy of patients with newly-diagnosed HIV infection in the era of highly active antiretroviral therapy. Qjm **100:**97-105.
63. **Farnet, C. M., and W. A. Haseltine.** 1991. Determination of viral proteins present in the human immunodeficiency virus type 1 preintegration complex. J Virol **65:**1910-5.
64. **Fauci, A. S., and H. C. Lane.** 1991. The acquired immunodeficiency syndrome (AIDS), p. 1402-1410. *In* J. D. Wilson (ed.), Harrison's principles of internal medicine, 12 ed. McGraw-Hill, New York.
65. **Feng, F., A. Davis, J. A. Lake, J. Carr, W. Xia, C. Burrell, and P. Li.** 2004. Ring finger protein ZIN interacts with human immunodeficiency virus type 1 Vif. J Virol **78:**10574-81.
66. **Feng, Y., C. C. Broder, P. E. Kennedy, and E. A. Berger.** 1996. HIV-1 entry cofactor: functional cDNA cloning of a seven-transmembrane, G protein-coupled receptor. Science **272:**872-7.
67. **Ferrer, M., A. C. Hamilton, and J. Inglese.** 2002. A PDZ domain-based detection system for enzymatic assays. Anal Biochem **301:**207-16.
68. **Fisher, A. G., M. B. Feinberg, S. F. Josephs, M. E. Harper, L. M. Marselle, G. Reyes, M. A. Gonda, A. Aldovini, C. Debouk, R. C. Gallo, and et al.** 1986. The trans-activator gene of HTLV-III is essential for virus replication. Nature **320:**367-71.
69. **Förster, V. T.** 1948. Zwischenmolekulare energiewanderung und fluoreszenz. Ann. Phys. **6:**54-75.
70. **Frankel, A. D., and J. A. Young.** 1998. HIV-1: fifteen proteins and an RNA. Annu Rev Biochem **67:**1-25.
71. **Freed, E. O.** 1998. HIV-1 gag proteins: diverse functions in the virus life cycle. Virology **251:**1-15.
72. **Freed, E. O., and M. A. Martin.** 1995. The role of human immunodeficiency virus type 1 envelope glycoproteins in virus infection. J Biol Chem **270:**23883-6.
73. **Fujino, T., N. Navaratnam, and J. Scott.** 1998. Human apolipoprotein B RNA editing deaminase gene (APOBEC1). Genomics **47:**266-75.
74. **Gabuzda, D. H., K. Lawrence, E. Langhoff, E. Terwilliger, T. Dorfman, W. A. Haseltine, and J. Sodroski.** 1992. Role of vif in replication of human immunodeficiency virus type 1 in CD4+ T lymphocytes. J Virol **66:**6489-95.
75. **Gabuzda, D. H., H. Li, K. Lawrence, B. S. Vasir, K. Crawford, and E. Langhoff.** 1994. Essential role of vif in establishing productive HIV-1 infection

in peripheral blood T lymphocytes and monocyte/macrophages. J Acquir Immune Defic Syndr **7:**908-15.

76. **Gaddis, N. C., E. Chertova, A. M. Sheehy, L. E. Henderson, and M. H. Malim.** 2003. Comprehensive investigation of the molecular defect in vif-deficient human immunodeficiency virus type 1 virions. J Virol **77:**5810-20.
77. **Gaines, H., M. A. von Sydow, L. V. von Stedingk, G. Biberfeld, B. Bottiger, L. O. Hansson, P. Lundbergh, A. B. Sonnerborg, J. Wasserman, and O. O. Strannegaard.** 1990. Immunological changes in primary HIV-1 infection. Aids **4:**995-9.
78. **Gallo, R., F. Wong-Staal, L. Montagnier, W. A. Haseltine, and M. Yoshida.** 1988. HIV/HTLV gene nomenclature. Nature **333:**504.
79. **Garrett, E. D., L. S. Tiley, and B. R. Cullen.** 1991. Rev activates expression of the human immunodeficiency virus type 1 vif and vpr gene products. J Virol **65:**1653-7.
80. **Garrus, J. E., U. K. von Schwedler, O. W. Pornillos, S. G. Morham, K. H. Zavitz, H. E. Wang, D. A. Wettstein, K. M. Stray, M. Cote, R. L. Rich, D. G. Myszka, and W. I. Sundquist.** 2001. Tsg101 and the vacuolar protein sorting pathway are essential for HIV-1 budding. Cell **107:**55-65.
81. **Gelderblom, H. R., E. H. Hausmann, M. Ozel, G. Pauli, and M. A. Koch.** 1987. Fine structure of human immunodeficiency virus (HIV) and immunolocalization of structural proteins. Virology **156:**171-6.
82. **Gerber, A. P., and W. Keller.** 1999. An adenosine deaminase that generates inosine at the wobble position of tRNAs. Science **286:**1146-9.
83. **Gerland, U., R. Bundschuh, and T. Hwa.** 2003. Mechanically probing the folding pathway of single RNA molecules. Biophys J **84:**2831-40.
84. **Gheysen, D., E. Jacobs, F. de Foresta, C. Thiriart, M. Francotte, D. Thines, and M. De Wilde.** 1989. Assembly and release of HIV-1 precursor Pr55gag virus-like particles from recombinant baculovirus-infected insect cells. Cell **59:**103-12.
85. **Goto, T., K. Ikuta, J. J. Zhang, C. Morita, K. Sano, M. Komatsu, H. Fujita, S. Kato, and M. Nakai.** 1990. The budding of defective human immunodeficiency virus type 1 (HIV-1) particles from cell clones persistently infected with HIV-1. Arch Virol **111:**87-101.
86. **Gottlieb, M. S., R. Schroff, H. M. Schanker, J. D. Weisman, P. T. Fan, R. A. Wolf, and A. Saxon.** 1981. Pneumocystis carinii pneumonia and mucosal candidiasis in previously healthy homosexual men: evidence of a new acquired cellular immunodeficiency. N Engl J Med **305:**1425-31.
87. **Gottlinger, H. G., J. G. Sodroski, and W. A. Haseltine.** 1989. Role of capsid precursor processing and myristoylation in morphogenesis and infectivity of human immunodeficiency virus type 1. Proc Natl Acad Sci U S A **86:**5781-5.
88. **Graves, M. C., J. J. Lim, E. P. Heimer, and R. A. Kramer.** 1988. An 11-kDa form of human immunodeficiency virus protease expressed in Escherichia coli is sufficient for enzymatic activity. Proc Natl Acad Sci U S A **85:**2449-53.
89. **Gu, Y., and W. I. Sundquist.** 2003. Good to CU. Nature **424:**21-2.

90. **Gualberto, J. M., L. Lamattina, G. Bonnard, J. H. Weil, and J. M. Grienenberger.** 1989. RNA editing in wheat mitochondria results in the conservation of protein sequences. Nature **341:**660-2.
91. **Hahn, B. H., G. M. Shaw, M. E. Taylor, R. R. Redfield, P. D. Markham, S. Z. Salahuddin, F. Wong-Staal, R. C. Gallo, E. S. Parks, and W. P. Parks.** 1986. Genetic variation in HTLV-III/LAV over time in patients with AIDS or at risk for AIDS. Science **232:**1548-53.
92. **Haim, H., I. Steiner, and A. Panet.** 2007. Time frames for neutralization during the human immunodeficiency virus type 1 entry phase, as monitored in synchronously infected cell cultures. J Virol **81:**3525-34.
93. **Hajduk, S. L., B. Adler, S. Madison-Antenucci, M. McManus, and R. Sabatini.** 1997. Insertional and deletional RNA editing in trypanosome mitochondria. Nucleic Acids Symp Ser**:**15-8.
94. **Hall, T. M.** 2005. Multiple modes of RNA recognition by zinc finger proteins. Curr Opin Struct Biol **15:**367-73.
95. **Hallenberger, S., V. Bosch, H. Angliker, E. Shaw, H. D. Klenk, and W. Garten.** 1992. Inhibition of furin-mediated cleavage activation of HIV-1 glycoprotein gp160. Nature **360:**358-61.
96. **Hamada, S., K. Ishiyama, S. B. Choi, C. Wang, S. Singh, N. Kawai, V. R. Franceschi, and T. W. Okita.** 2003. The transport of prolamine RNAs to prolamine protein bodies in living rice endosperm cells. Plant Cell **15:**2253-64.
97. **Handsfield, H. H.** 1982. Acquired immunodeficiency in homosexual men. AJR Am J Roentgenol **139:**832-3.
98. **Harris, R. S., K. N. Bishop, A. M. Sheehy, H. M. Craig, S. K. Petersen-Mahrt, I. N. Watt, M. S. Neuberger, and M. H. Malim.** 2003. DNA deamination mediates innate immunity to retroviral infection. Cell **113:**803-9.
99. **Hauber, J., and B. R. Cullen.** 1988. Mutational analysis of the trans-activation-responsive region of the human immunodeficiency virus type I long terminal repeat. J Virol **62:**673-9.
100. **Heath, M. J., S. S. Derebail, R. J. Gorelick, and J. J. DeStefano.** 2003. Differing roles of the N- and C-terminal zinc fingers in human immunodeficiency virus nucleocapsid protein-enhanced nucleic acid annealing. J Biol Chem **278:**30755-63.
101. **Henderson, L. E., H. C. Krutzsch, and S. Oroszlan.** 1983. Myristyl amino-terminal acylation of murine retrovirus proteins: an unusual post-translational proteins modification. Proc Natl Acad Sci U S A **80:**339-43.
102. **Hiesel, R., B. Wissinger, W. Schuster, and A. Brennicke.** 1989. RNA editing in plant mitochondria. Science **246:**1632-4.
103. **Ho, D. D., M. G. Sarngadharan, L. Resnick, F. Dimarzoveronese, T. R. Rota, and M. S. Hirsch.** 1985. Primary human T-lymphotropic virus type III infection. Ann Intern Med **103:**880-3.
104. **Huang, Y., W. P. Kong, and G. J. Nabel.** 2001. Human immunodeficiency virus type 1-specific immunity after genetic immunization is enhanced by modification of Gag and Pol expression. J Virol **75:**4947-51.

105. **Hung, M., P. Patel, S. Davis, and S. R. Green.** 1998. Importance of ribosomal frameshifting for human immunodeficiency virus type 1 particle assembly and replication. J Virol **72:**4819-24.
106. **Iwatani, Y., H. Takeuchi, K. Strebel, and J. G. Levin.** 2006. Biochemical activities of highly purified, catalytically active human APOBEC3G: correlation with antiviral effect. J Virol **80:**5992-6002.
107. **Jacobs, E., D. Gheysen, D. Thines, M. Francotte, and M. de Wilde.** 1989. The HIV-1 Gag precursor Pr55gag synthesized in yeast is myristoylated and targeted to the plasma membrane. Gene **79:**71-81.
108. **Jain, C., and J. G. Belasco.** 2001. Structural model for the cooperative assembly of HIV-1 Rev multimers on the RRE as deduced from analysis of assembly-defective mutants. Mol Cell **7:**603-14.
109. **Janke, A., and S. Paabo.** 1993. Editing of a tRNA anticodon in marsupial mitochondria changes its codon recognition. Nucleic Acids Res **21:**1523-5.
110. **Jarmuz, A., A. Chester, J. Bayliss, J. Gisbourne, I. Dunham, J. Scott, and N. Navaratnam.** 2002. An anthropoid-specific locus of orphan C to U RNA-editing enzymes on chromosome 22. Genomics **79:**285-96.
111. **Kable, M. L., S. Heidmann, and K. D. Stuart.** 1997. RNA editing: getting U into RNA. Trends Biochem Sci **22:**162-6.
112. **Kalter, D. C., H. E. Gendelman, and M. S. Meltzer.** 1991. Inhibition of human immunodeficiency virus infection in monocytes by monoclonal antibodies against leukocyte adhesion molecules. Immunol Lett **30:**219-27.
113. **Kao, S., M. A. Khan, E. Miyagi, R. Plishka, A. Buckler-White, and K. Strebel.** 2003. The human immunodeficiency virus type 1 Vif protein reduces intracellular expression and inhibits packaging of APOBEC3G (CEM15), a cellular inhibitor of virus infectivity. J Virol **77:**11398-407.
114. **Kenworthy, A. K.** 2001. Imaging protein-protein interactions using fluorescence resonance energy transfer microscopy. Methods **24:**289-96.
115. **Kjems, J., A. D. Frankel, and P. A. Sharp.** 1991. Specific regulation of mRNA splicing in vitro by a peptide from HIV-1 Rev. Cell **67:**169-78.
116. **Koup, R. A., J. T. Safrit, Y. Cao, C. A. Andrews, G. McLeod, W. Borkowsky, C. Farthing, and D. D. Ho.** 1994. Temporal association of cellular immune responses with the initial control of viremia in primary human immunodeficiency virus type 1 syndrome. J Virol **68:**4650-5.
117. **Kozak, S. L., M. Marin, K. M. Rose, C. Bystrom, and D. Kabat.** 2006. The Anti-HIV-1 Editing Enzyme APOBEC3G Binds HIV-1 RNA and Messenger RNAs That Shuttle between Polysomes and Stress Granules. J Biol Chem **281:**29105-19.
118. **Kreisberg, J. F., W. Yonemoto, and W. C. Greene.** 2006. Endogenous factors enhance HIV infection of tissue naive CD4 T cells by stimulating high molecular mass APOBEC3G complex formation. J Exp Med **203:**865-70.
119. **Larson, D. R., Y. M. Ma, V. M. Vogt, and W. W. Webb.** 2003. Direct measurement of Gag-Gag interaction during retrovirus assembly with FRET and fluorescence correlation spectroscopy. J Cell Biol **162:**1233-44.

120. **Lau, P. P., H. J. Zhu, A. Baldini, C. Charnsangavej, and L. Chan.** 1994. Dimeric structure of a human apolipoprotein B mRNA editing protein and cloning and chromosomal localization of its gene. Proc Natl Acad Sci U S A **91:**8522-6.
121. **Lecossier, D., F. Bouchonnet, F. Clavel, and A. J. Hance.** 2003. Hypermutation of HIV-1 DNA in the absence of the Vif protein. Science **300:**1112.
122. **Lemp, G. F., S. F. Payne, D. Neal, T. Temelso, and G. W. Rutherford.** 1990. Survival trends for patients with AIDS. Jama **263:**402-6.
123. **Luciw, P. A., S. J. Potter, K. Steimer, D. Dina, and J. A. Levy.** 1984. Molecular cloning of AIDS-associated retrovirus. Nature **312:**760-3.
124. **Luo, K., B. Liu, Z. Xiao, Y. Yu, X. Yu, R. Gorelick, and X. F. Yu.** 2004. Amino-terminal region of the human immunodeficiency virus type 1 nucleocapsid is required for human APOBEC3G packaging. J Virol **78:**11841-52.
125. **Macek, C.** 1982. Acquired immunodeficiency syndrome cause(s) still elusive. Jama **248:**1423-7, 1431.
126. **Mahieux, R., R. Suspene, F. Delebecque, M. Henry, O. Schwartz, S. Wain-Hobson, and J. P. Vartanian.** 2005. Extensive editing of a small fraction of human T-cell leukemia virus type 1 genomes by four APOBEC3 cytidine deaminases. J Gen Virol **86:**2489-94.
127. **Maier, B., D. Bensimon, and V. Croquette.** 2000. Replication by a single DNA polymerase of a stretched single-stranded DNA. Proc Natl Acad Sci U S A **97:**12002-7.
128. **Malek, O., K. Lattig, R. Hiesel, A. Brennicke, and V. Knoop.** 1996. RNA editing in bryophytes and a molecular phylogeny of land plants. Embo J **15:**1403-11.
129. **Malim, M. H., S. Bohnlein, J. Hauber, and B. R. Cullen.** 1989. Functional dissection of the HIV-1 Rev trans-activator--derivation of a trans-dominant repressor of Rev function. Cell **58:**205-14.
130. **Malim, M. H., and B. R. Cullen.** 1991. HIV-1 structural gene expression requires the binding of multiple Rev monomers to the viral RRE: implications for HIV-1 latency. Cell **65:**241-8.
131. **Mangeat, B., P. Turelli, G. Caron, M. Friedli, L. Perrin, and D. Trono.** 2003. Broad antiretroviral defence by human APOBEC3G through lethal editing of nascent reverse transcripts. Nature **424:**99-103.
132. **Mann, J. M., and D. J. Tarantola (ed.).** 1996. AIDS in the World II: Global Dimensions, Social Roots, and Responses: The Global Aid Policy Coalition., 2 ed. Oxford University Press.
133. **Marin, M., K. M. Rose, S. L. Kozak, and D. Kabat.** 2003. HIV-1 Vif protein binds the editing enzyme APOBEC3G and induces its degradation. Nat Med **9:**1398-403.
134. **Marras, S. A.** 2006. Selection of fluorophore and quencher pairs for fluorescent nucleic acid hybridization probes. Methods Mol Biol **335:**3-16.
135. **Marras, S. A., S. Tyagi, and F. R. Kramer.** 2006. Real-time assays with molecular beacons and other fluorescent nucleic acid hybridization probes. Clin Chim Acta **363:**48-60.
136. **Matsumoto, C., K. Hamasaki, H. Mihara, and A. Ueno.** 2000. A high-throughput screening utilizing intramolecular fluorescence resonance energy

transfer for the discovery of the molecules that bind HIV-1 TAR RNA specifically. Bioorg Med Chem Lett **10:**1857-61.

137. **Meerloo, T., M. A. Sheikh, A. C. Bloem, A. de Ronde, M. Schutten, C. A. van Els, P. J. Roholl, P. Joling, J. Goudsmit, and H. J. Schuurman.** 1993. Host cell membrane proteins on human immunodeficiency virus type 1 after in vitro infection of H9 cells and blood mononuclear cells. An immuno-electron microscopic study. J Gen Virol **74 (Pt 1):**129-35.
138. **Mehle, A., H. Wilson, C. Zhang, A. J. Brazier, M. McPike, E. Pery, and D. Gabuzda.** 2007. Identification of an APOBEC3G Binding Site in Human Immunodeficiency Virus Type 1 Vif and Inhibitors of Vif-APOBEC3G Binding. J Virol **81:**13235-41.
139. **Melcher, T., S. Maas, M. Higuchi, W. Keller, and P. H. Seeburg.** 1995. Editing of alpha-amino-3-hydroxy-5-methylisoxazole-4-propionic acid receptor GluR-B pre-mRNA in vitro reveals site-selective adenosine to inosine conversion. J Biol Chem **270:**8566-70.
140. **Menendez-Arias, L., C. Risco, P. Pinto da Silva, and S. Oroszlan.** 1992. Purification of immature cores of mouse mammary tumor virus and immunolocalization of protein domains. J Virol **66:**5615-20.
141. **Miyashiro, H., T. Kimura, M. Tomiyama, and M. Hattori.** 2000. Analysis of the RNase H activity by fluorescence resonance energy transfer. Nucleic Acids Symp Ser**:**55-6.
142. **Montanari, A., and M. Mezard.** 2001. Hairpin formation and elongation of biomolecules. Phys Rev Lett **86:**2178-81.
143. **Morikawa, Y., E. Barsov, and I. Jones.** 1993. Legitimate and illegitimate cleavage of human immunodeficiency virus glycoproteins by furin. J Virol **67:**3601-4.
144. **Muesing, M. A., D. H. Smith, and D. J. Capon.** 1987. Regulation of mRNA accumulation by a human immunodeficiency virus trans-activator protein. Cell **48:**691-701.
145. **Muramatsu, M., V. S. Sankaranand, S. Anant, M. Sugai, K. Kinoshita, N. O. Davidson, and T. Honjo.** 1999. Specific expression of activation-induced cytidine deaminase (AID), a novel member of the RNA-editing deaminase family in germinal center B cells. J Biol Chem **274:**18470-6.
146. **Muto, T., M. Muramatsu, M. Taniwaki, K. Kinoshita, and T. Honjo.** 2000. Isolation, tissue distribution, and chromosomal localization of the human activation-induced cytidine deaminase (AID) gene. Genomics **68:**85-8.
147. **Navaratnam, N., T. Fujino, J. Bayliss, A. Jarmuz, A. How, N. Richardson, A. Somasekaram, S. Bhattacharya, C. Carter, and J. Scott.** 1998. Escherichia coli cytidine deaminase provides a molecular model for ApoB RNA editing and a mechanism for RNA substrate recognition. J Mol Biol **275:**695-714.
148. **Nermut, M. V., D. J. Hockley, J. B. Jowett, I. M. Jones, M. Garreau, and D. Thomas.** 1994. Fullerene-like organization of HIV gag-protein shell in virus-like particles produced by recombinant baculovirus. Virology **198:**288-96.
149. **Ochsenbauer, C., T. Wilk, and V. Bosch.** 1997. Analysis of vif-defective human immunodeficiency virus type 1 (HIV-1) virions synthesized in 'non-permissive' T

lymphoid cells stably infected with selectable HIV-1. J Gen Virol **78 (Pt 3):**627-35.

150. **Opi, S., H. Takeuchi, S. Kao, M. A. Khan, E. Miyagi, R. Goila-Gaur, Y. Iwatani, J. G. Levin, and K. Strebel.** 2006. Monomeric APOBEC3G is catalytically active and has antiviral activity. J Virol **80:**4673-82.
151. **Ormo, M., A. B. Cubitt, K. Kallio, L. A. Gross, R. Y. Tsien, and S. J. Remington.** 1996. Crystal structure of the Aequorea victoria green fluorescent protein. Science **273:**1392-5.
152. **Pantaleo, G., C. Graziosi, and A. S. Fauci.** 1993. New concepts in the immunopathogenesis of human immunodeficiency virus infection. N Engl J Med **328:**327-35.
153. **Patterson, G. H., D. W. Piston, and B. G. Barisas.** 2000. Forster distances between green fluorescent protein pairs. Anal Biochem **284:**438-40.
154. **Peabody, D. S.** 1993. The RNA binding site of bacteriophage MS2 coat protein. Embo J **12:**595-600.
155. **Perkins, N. D., N. L. Edwards, C. S. Duckett, A. B. Agranoff, R. M. Schmid, and G. J. Nabel.** 1993. A cooperative interaction between NF-kappa B and Sp1 is required for HIV-1 enhancer activation. Embo J **12:**3551-8.
156. **Polson, A. G., H. L. Ley, 3rd, B. L. Bass, and J. L. Casey.** 1998. Hepatitis delta virus RNA editing is highly specific for the amber/W site and is suppressed by hepatitis delta antigen. Mol Cell Biol **18:**1919-26.
157. **Poon, D. T., J. Wu, and A. Aldovini.** 1996. Charged amino acid residues of human immunodeficiency virus type 1 nucleocapsid p7 protein involved in RNA packaging and infectivity. J Virol **70:**6607-16.
158. **Powell, L. M., S. C. Wallis, R. J. Pease, Y. H. Edwards, T. J. Knott, and J. Scott.** 1987. A novel form of tissue-specific RNA processing produces apolipoprotein-B48 in intestine. Cell **50:**831-40.
159. **Prochnow, C., R. Bransteitter, M. G. Klein, M. F. Goodman, and X. S. Chen.** 2007. The APOBEC-2 crystal structure and functional implications for the deaminase AID. Nature **445:**447-51.
160. **Quagliarello, V.** 1982. The Acquired Immunodeficiency Syndrome: current status. Yale J Biol Med **55:**443-52.
161. **Revy, P., T. Muto, Y. Levy, F. Geissmann, A. Plebani, O. Sanal, N. Catalan, M. Forveille, R. Dufourcq-Labelouse, A. Gennery, I. Tezcan, F. Ersoy, H. Kayserili, A. G. Ugazio, N. Brousse, M. Muramatsu, L. D. Notarangelo, K. Kinoshita, T. Honjo, A. Fischer, and A. Durandy.** 2000. Activation-induced cytidine deaminase (AID) deficiency causes the autosomal recessive form of the Hyper-IgM syndrome (HIGM2). Cell **102:**565-75.
162. **Rook, M. S., M. Lu, and K. S. Kosik.** 2000. CaMKIIalpha 3' untranslated region-directed mRNA translocation in living neurons: visualization by GFP linkage. J Neurosci **20:**6385-93.
163. **Rosen, C. A., J. G. Sodroski, and W. A. Haseltine.** 1985. The location of cis-acting regulatory sequences in the human T cell lymphotropic virus type III (HTLV-III/LAV) long terminal repeat. Cell **41:**813-23.

164. **Sandefur, S., R. M. Smith, V. Varthakavi, and P. Spearman.** 2000. Mapping and characterization of the N-terminal I domain of human immunodeficiency virus type 1 Pr55(Gag). J Virol **74:**7238-49.
165. **Sandefur, S., V. Varthakavi, and P. Spearman.** 1998. The I domain is required for efficient plasma membrane binding of human immunodeficiency virus type 1 Pr55Gag. J Virol **72:**2723-32.
166. **Santangelo, P., N. Nitin, and G. Bao.** 2006. Nanostructured probes for RNA detection in living cells. Ann Biomed Eng **34:**39-50.
167. **Sasada, A., A. Takaori-Kondo, K. Shirakawa, M. Kobayashi, A. Abudu, M. Hishizawa, K. Imada, Y. Tanaka, and T. Uchiyama.** 2005. APOBEC3G targets human T-cell leukemia virus type 1. Retrovirology **2:**32.
168. **Scarlata, S., and C. Carter.** 2003. Role of HIV-1 Gag domains in viral assembly. Biochim Biophys Acta **1614:**62-72.
169. **Schafer, A., H. P. Bogerd, and B. R. Cullen.** 2004. Specific packaging of APOBEC3G into HIV-1 virions is mediated by the nucleocapsid domain of the gag polyprotein precursor. Virology **328:**163-8.
170. **Schmalzbauer, E., B. Strack, J. Dannull, S. Guehmann, and K. Moelling.** 1996. Mutations of basic amino acids of NCp7 of human immunodeficiency virus type 1 affect RNA binding in vitro. J Virol **70:**771-7.
171. **Schultz, A. M., L. E. Henderson, and S. Oroszlan.** 1988. Fatty acylation of proteins. Annu Rev Cell Biol **4:**611-47.
172. **Schuster, W., R. Hiesel, B. Wissinger, and A. Brennicke.** 1990. RNA editing in the cytochrome b locus of the higher plant Oenothera berteriana includes a U-to-C transition. Mol Cell Biol **10:**2428-31.
173. **Schwartz, S., B. K. Felber, and G. N. Pavlakis.** 1991. Expression of human immunodeficiency virus type 1 vif and vpr mRNAs is Rev-dependent and regulated by splicing. Virology **183:**677-86.
174. **Selvin, P. R.** 2000. The renaissance of fluorescence resonance energy transfer. Nat Struct Biol **7:**730-4.
175. **Shaw, G. M., B. H. Hahn, S. K. Arya, J. E. Groopman, R. C. Gallo, and F. Wong-Staal.** 1984. Molecular characterization of human T-cell leukemia (lymphotropic) virus type III in the acquired immune deficiency syndrome. Science **226:**1165-71.
176. **Sheehy, A. M., N. C. Gaddis, J. D. Choi, and M. H. Malim.** 2002. Isolation of a human gene that inhibits HIV-1 infection and is suppressed by the viral Vif protein. Nature **418:**646-50.
177. **Sheehy, A. M., N. C. Gaddis, and M. H. Malim.** 2003. The antiretroviral enzyme APOBEC3G is degraded by the proteasome in response to HIV-1 Vif. Nat Med **9:**1404-7.
178. **Sova, P., and D. J. Volsky.** 1993. Efficiency of viral DNA synthesis during infection of permissive and nonpermissive cells with vif-negative human immunodeficiency virus type 1. J Virol **67:**6322-6.
179. **Spearman, P., J. J. Wang, N. Vander Heyden, and L. Ratner.** 1994. Identification of human immunodeficiency virus type 1 Gag protein domains essential to membrane binding and particle assembly. J Virol **68:**3232-42.

180. **Stenglein, M. D., and R. S. Harris.** 2006. APOBEC3B and APOBEC3F inhibit L1 retrotransposition by a DNA deamination-independent mechanism. J Biol Chem **281:**16837-41.
181. **Stopak, K., C. de Noronha, W. Yonemoto, and W. C. Greene.** 2003. HIV-1 Vif blocks the antiviral activity of APOBEC3G by impairing both its translation and intracellular stability. Mol Cell **12:**591-601.
182. **Svarovskaia, E. S., H. Xu, J. L. Mbisa, R. Barr, R. J. Gorelick, A. Ono, E. O. Freed, W. S. Hu, and V. K. Pathak.** 2004. Human apolipoprotein B mRNA-editing enzyme-catalytic polypeptide-like 3G (APOBEC3G) is incorporated into HIV-1 virions through interactions with viral and nonviral RNAs. J Biol Chem **279:**35822-8.
183. **Teng, B., C. F. Burant, and N. O. Davidson.** 1993. Molecular cloning of an apolipoprotein B messenger RNA editing protein. Science **260:**1816-9.
184. **Tindall, B., and D. A. Cooper.** 1991. Primary HIV infection: host responses and intervention strategies. Aids **5:**1-14.
185. **Turelli, P., B. Mangeat, S. Jost, S. Vianin, and D. Trono.** 2004. Inhibition of hepatitis B virus replication by APOBEC3G. Science **303:**1829.
186. **UNAIDS, and WHO.** 2006. 2006 Report on the global AIDS epidemic: A UNAIDS 10th anniversary special edition.
187. **VerPlank, L., F. Bouamr, T. J. LaGrassa, B. Agresta, A. Kikonyogo, J. Leis, and C. A. Carter.** 2001. Tsg101, a homologue of ubiquitin-conjugating (E2) enzymes, binds the L domain in HIV type 1 Pr55(Gag). Proc Natl Acad Sci U S A **98:**7724-9.
188. **von Schwedler, U., J. Song, C. Aiken, and D. Trono.** 1993. Vif is crucial for human immunodeficiency virus type 1 proviral DNA synthesis in infected cells. J Virol **67:**4945-55.
189. **von Schwedler, U. K., K. M. Stray, J. E. Garrus, and W. I. Sundquist.** 2003. Functional surfaces of the human immunodeficiency virus type 1 capsid protein. J Virol **77:**5439-50.
190. **Wedekind, J. E., R. Gillilan, A. Janda, J. Krucinska, J. D. Salter, R. P. Bennett, J. Raina, and H. C. Smith.** 2006. Nanostructures of APOBEC3G support a hierarchical assembly model of high molecular mass ribonucleoprotein particles from dimeric subunits. J Biol Chem **281:**38122-6.
191. **Weldon, R. A., Jr., C. R. Erdie, M. G. Oliver, and J. W. Wills.** 1990. Incorporation of chimeric gag protein into retroviral particles. J Virol **64:**4169-79.
192. **Wichroski, M. J., K. Ichiyama, and T. M. Rana.** 2005. Analysis of HIV-1 viral infectivity factor-mediated proteasome-dependent depletion of APOBEC3G: correlating function and subcellular localization. J Biol Chem **280:**8387-96.
193. **Wichroski, M. J., G. B. Robb, and T. M. Rana.** 2006. Human retroviral host restriction factors APOBEC3G and APOBEC3F localize to mRNA processing bodies. PLoS Pathog **2:**e41.
194. **Wilcox, C., J. S. Hu, and E. N. Olson.** 1987. Acylation of proteins with myristic acid occurs cotranslationally. Science **238:**1275-8.
195. **Wills, J. W., and R. C. Craven.** 1991. Form, function, and use of retroviral gag proteins [editorial]. Aids **5:**639-54.

196. **Wills, J. W., R. C. Craven, R. A. Weldon, Jr., T. D. Nelle, and C. R. Erdie.** 1991. Suppression of retroviral MA deletions by the amino-terminal membrane-binding domain of p60src. J Virol **65:**3804-12.
197. **Xu, H., E. Chertova, J. Chen, D. E. Ott, J. D. Roser, W. S. Hu, and V. K. Pathak.** 2007. Stoichiometry of the antiviral protein APOBEC3G in HIV-1 virions. Virology **360:**247-56.
198. **Yi, R., H. P. Bogerd, and B. R. Cullen.** 2002. Recruitment of the Crm1 nuclear export factor is sufficient to induce cytoplasmic expression of incompletely spliced human immunodeficiency virus mRNAs. J Virol **76:**2036-42.
199. **Yu, Q., D. Chen, R. Konig, R. Mariani, D. Unutmaz, and N. R. Landau.** 2004. APOBEC3B and APOBEC3C are potent inhibitors of simian immunodeficiency virus replication. J Biol Chem **279:**53379-86.
200. **Yu, X., Y. Yu, B. Liu, K. Luo, W. Kong, P. Mao, and X. F. Yu.** 2003. Induction of APOBEC3G ubiquitination and degradation by an HIV-1 Vif-Cul5-SCF complex. Science **302:**1056-60.
201. **Zapp, M. L., T. J. Hope, T. G. Parslow, and M. R. Green.** 1991. Oligomerization and RNA binding domains of the type 1 human immunodeficiency virus Rev protein: a dual function for an arginine-rich binding motif. Proc Natl Acad Sci U S A **88:**7734-8.
202. **Zennou, V., D. Perez-Caballero, H. Gottlinger, and P. D. Bieniasz.** 2004. APOBEC3G incorporation into human immunodeficiency virus type 1 particles. J Virol **78:**12058-61.
203. **Zhang, F., and A. E. Simon.** 2003. A novel procedure for the localization of viral RNAs in protoplasts and whole plants. Plant J **35:**665-73.
204. **Zhang, H., B. Yang, R. J. Pomerantz, C. Zhang, S. C. Arunachalam, and L. Gao.** 2003. The cytidine deaminase CEM15 induces hypermutation in newly synthesized HIV-1 DNA. Nature **424:**94-8.
205. **Zhang, K. L., B. Mangeat, M. Ortiz, V. Zoete, D. Trono, A. Telenti, and O. Michielin.** 2007. Model structure of human APOBEC3G. PLoS ONE **2:**e378.
206. **Zhou, W., and M. D. Resh.** 1996. Differential membrane binding of the human immunodeficiency virus type 1 matrix protein. J Virol **70:**8540-8.
207. **Zhu, T., B. T. Korber, A. J. Nahmias, E. Hooper, P. M. Sharp, and D. D. Ho.** 1998. An African HIV-1 sequence from 1959 and implications for the origin of the epidemic. Nature **391:**594-7.